université PARIS-SACLAY

Contribution to the study of atmospheric pressure non-thermal plasma for the treatment of biological substrates

Contribution à l'étude de plasmas froids à pression atmosphérique pour le traitement des substrats biologiques

Thèse de doctorat de l'université Paris-Saclay

École doctorale n° 575, electrical, optical, bio : physics and engineering (EOBE)
Spécialité de doctorat : Génie électrique
Graduate School : Sciences de l'ingénierie et des systèmes
Référent : CentraleSupélec

Thèse préparée dans le **Laboratoire de Génie Electrique et Electronique de Paris** (Université Paris-Saclay, CentraleSupélec, CNRS) ,
sous la direction de **Emmanuel ODIC**, Professor à CentraleSupélec,
le co-encadrement de **Michael Kirkpatrick**, Maître de Conférences à CentraleSupélec,
le co-encadrement de **Michael DUBOW**, Professeur à l'université Paris-Saclay

Thèse soutenue à Paris-Saclay, le 10 Mai 2022, par

Chih-Min CHEN

Composition du Jury

Stéphane PASQUIERS Directeur de Recherche, CNRS & Université Paris-Saclay	Président
Zdenko MACHALA Associate Professor, Comenius University	Rapporteur & Examinateur
Nofel MERBAHI Professeur, Université Paul Sabatier	Rapporteur & Examinateur
Emmanuel ODIC Professeur, CentraleSupélec	Directeur de thèse

THESE DE DOCTORAT

NNT : 2022UPAST048

"To my father who advanced to get off during my PhD program."

Chien-Jung Chen

1960 - 2018

Acknowledgments

Firstly, I would like to express my deepest appreciation to my supervisors for the comments on not only my thesis but also my life in France. Thank you Prof. Michael Dubow for all the comments on biology. I will remember you. Thank you Prof. Emmanuel Odic for everything you did for me. I will not forget that you always encourage me when I felt unconfident. And you never give me up even though I faced a lot of troubles in my research or in my personal life. Thank you Prof. Michael Kirkpatrick for your physical comments and English correction. You never give my Taiwanese English cold shoulder. I also enjoyed talking politics with you at lunchtime. Thanks to director of GEEPs, Claude Marchand and director of I2BC, Frédéric Boccard for accepting me to join your laboratories. I would like to thank my research colleagues Djinthana Dufour in I2BC for the microorganism preparation and Jennifer Arthur Ataam in Hôpital Marie Lannelongue for the preparation of cancer cell culture. Also, thank you Zuzana Kovalová. Your manuscript helped a lot in my research, and I was very happy to know you attend to my oral defense. It is also important to mention that I cannot finish my program without a scholarship from the Ministry of Education in Taiwan and Université Paris-Saclay and financial support from CentraleSupélec. In the final part of my PhD program, the comments from all the jury members were very valuable, thanks to president of jury, Mr. Stéphane Pasquiers, two referee, Prof. Zdenko Machala and Prof. Nofel Merbahi, and invited examiner, Prof. Jenn-Wei Chen. And many thanks go to my colleague in my group Giacomo Galli, Robert Szilágyi, and Vladimir Pineda for your concerns and for sharing their different cultures. Thank you to the members in Hemeris, my bosses Steven Deves-Girain and Flore Vandier in particular. Your invitation to join you gave me high confidence in my research. Besides, thank you Yi-Ling Kuo (郭以琳), you always company with me for these years as well as in the future. Thanks to all the members in Eglise Passage National and in Arbre de Vie especially Ljavaus Pakaleva (翁亞暄). All your prays during such years gave me much power. My friends in Taiwan also gave me the strong help from their concerns to Taiwanese food, thank you Chun-Hao Cho (卓俊豪), Hung-Chieh Su (蘇泓傑), Kuo-Feng Chiu (丘國鋒), Po-Sheng Chiu (邱博聖), Chiao-Peng Hsu (許皦朋), Chia-Hsaing Huang (黃家祥), Shu-Pei Weng (翁淑珮), and Silver Hsieh (謝銀子). Lastly, I am grateful to my father Chien-Jung Chen (陳健榮) who passed away in the second year of my PhD program, my mother Hsiu-Hui Wei (魏秀惠), my sister Ching-I Chen (陳景怡), and my cousins Yin-Ling Wei (魏吟玲) and Chi-Chou Wei (魏啟州) spending a lot of time to have a conversation with me, especially during the lock-down of Covid-19. I cannot list everyone who ever helped me during my PhD program here, so I give thanks to God for bringing me to France.

université PARIS-SACLAY | ÉCOLE DOCTORALE Physique et ingénierie : électrons, photons, sciences du vivant (EOBE)

Titre : Contribution à l'étude de plasmas froids à pression atmosphérique pour le traitement des substrats biologiques

Mots clés : plasma froid, décharge sur barrière diélectrique, plasma médecine, cellules cancéreuses, décontamination de surface, bactériophage

Résumé : L'objectif de ces travaux était d'étudier l'interaction entre des plasmas froids à pression atmosphérique et des milieux biologiques en vue d'application de ce type de technologie au secteur biomédical.

Dans un premier temps, des sources plasma ont été conçues, réalisées et caractérisées. Il s'agissait de réacteurs mettant en œuvre des décharges sur barrière diélectrique dans différents gaz en flux (air synthétique, argon, avec ou sans apport de vapeur d'eau). L'utilisation de l'argon a permis de sélectionner des conditions dans lesquelles le plasma demeurait confiné dans la zone inter-électrodes (humidité relative supérieure à 95% à température ambiante) ou au contraire se propageait soit en atmosphère libre, soit guidé dans un tube isolant dans lequel circulait le gaz (argon sec). Dans ce dernier cas, le phénomène de propagation a été examiné par des mesures électriques résolues dans le temps et les résultats ont été discutés à l'aide des travaux antérieurs disponibles dans la littérature. Le choix de l'air comme gaz plasmagène a également été considéré en raison des contraintes d'application ne permettant pas systématiquement l'utilisation d'un autre gaz.

Deux études spécifiques ont été conduites, l'une susceptible de trouver des applications dans le domaine de la « plasma médecine », l'autre dans le domaine de la lutte contre les épidémies virales.

Dans ce dernier cas, les travaux ont porté sur l'inactivation de virus bactériens, ou bactériophages, infectant Escherichia coli. Il s'agissait du phage T4, phage à ADN double brin, et du phage MS2, phage à ARN simple brin. Les suspensions de phages ont été diluées dans différentes solutions tampons et déposées sur un substrat de papier hydrosoluble pour être exposées aux différents traitements par plasma froid. L'utilisation originale de ce substrat a permis de résoudre le problème difficile de la récupération des particules de phage après traitement. Ce substrat correspond également à une situation d'application défavorable à ce type de traitement (surface complexe avec diffusion en volume de la suspension, au contraire d'une surface lisse non-adsorbante telle qu'une lamelle de verre), conduisant à obtenir des résultats plus réalistes et transposables à une application réelle. L'inactivation des phages a été quantifiée par comptage de plages de lyse sur culture de E. coli. Ainsi, des taux d'inactivation compris entre 0,66 log/min et 2 log/min ont été mesurés suivant le type de phage, la nature de la solution tampon et le type de traitement. L'influence de la température imposée au substrat a également été examinée.

Dans le cadre de l'application en plasma médecine, des cellules d'adénocarcinome humain (cancer du poumon) provenant de cinq patients ont été traitées in-vitro à l'aide du réacteur à barrière diélectrique dans deux conditions de fonctionnement déterminées par la composition du gaz d'alimentation : jet de plasma avec de l'argon sec et source d'espèces oxydantes avec de l'argon saturé en vapeur d'eau à température ambiante. A l'issue d'une exposition de 5 minutes au traitement par décharge d'argon humide, 65% des cellules étaient dans un état apoptotique/nécrotique. Pour le traitement par plasma d'argon sec, les tests globaux de prolifération et d'apoptose n'ont pas montré une grande efficacité. Toutefois, le jet de plasma d'argon sec a présenté un effet rapide et localisé sur les cellules cancéreuses, induisant une inhibition de la capacité des cellules à proliférer et à migrer. Ces deux conditions de fonctionnement sont d'intérêt pour l'application clinique, permettant d'avoir un seul dispositif plasma capable de délivrer un traitement très localisé des cellules (jet plasma) ou de transférer des espèces oxydantes sur une plus grande surface conduisant à des mécanismes d'apoptose (décharge d'argon humide).

Title : Contribution to the study of atmospheric pressure non-thermal plasma for the treatment of biological substrates

Keywords : Non-thermal plasma, dielectric barrier discharge, plasma medicine, cancer cells, surface decontamination, bacteriophage

Abstract : The objective of this work was to study the interaction between non-thermal plasmas at atmospheric pressure and biological media in perspective of the application of this type of technology to the biomedical sector.

In a first step, plasma sources were designed, realized, and characterized. These reactors implement dielectric barrier discharges in various gases in flow (synthetic air, argon, with or without water vapor admixture). The use of argon allowed the selection of conditions in which the plasma remained confined in the inter-electrode zone (relative humidity higher than 95% at room temperature) or on the contrary propagated either in free atmosphere or guided in an insulating tube in which the gas was flowing (dry argon). In the latter case, the propagation phenomenon was examined by time-resolved electrical measurements and the results were discussed with the help of previous works available in the literature. The choice of air as reactor feed-gas was also considered because of the application constraints that do not systematically allow the use of another gas.

Two specific studies were conducted, one likely to find applications in the field of "plasma medicine", the other in the field of control of viral epidemics.

In the latter case, the work focused on the inactivation of bacterial viruses, bacteriophages, infecting Escherichia coli. These were phage T4, a double-stranded DNA phage, and phage MS2, a single-stranded RNA phage. The phage suspensions were diluted in different buffer solutions and deposited on a water-soluble paper substrate to be exposed to different non-thermal plasma treatments. The original use of this substrate solved the difficult problem of phage particle recovery after treatment. This substrate also corresponds to an unfavorable application situation for this type of treatment (complex surface with volume diffusion of the suspension, as opposed to a smooth non-adsorbent surface such as a glass slide), leading to more realistic results that can be transposed to a real application.

Phage inactivation was quantified by counting lysis plaques on E. coli culture. Thus, inactivation rates ranging from 0.66 log/min to 2 log/min were measured depending on the type of phage, the nature of the buffer solution and the type of treatment. The influence of the temperature imposed on the substrate was also examined.

For the plasma medicine application, human adenocarcinoma cells (lung cancer) from five patients were treated in-vitro using the dielectric barrier reactor under two operating conditions determined by the composition of the feed-gas: plasma jet with dry argon and reactive oxidizing species (ROS) source with argon saturated with water vapor at room temperature. After a 5-minute exposure to the humid argon discharge treatment, 65% of the cells were in an apoptotic/necrotic state. For the dry argon plasma treatment, the overall proliferation and apoptosis assays did not show much efficacy. However, the dry argon plasma jet exhibited a rapid and localized effect on the cancer cells, inducing inhibition of the cells' ability to proliferate and migrate. These two operating conditions are of interest for clinical application, allowing to have a single plasma device able to deliver a very localized treatment of cells (plasma jet) or to transfer ROS on a larger surface leading to apoptosis mechanisms (humid argon discharge).

CONTENT

Content I
List of figures IV
List of tables X
Introduction 1
1 Background and motivation 5
1.1 Cross-infection diseases 7
1.1.1 Nosocomial infections 7
1.1.2 Conventional sterilization methods 8
1.1.2.1 Heat sterilization 8
1.1.2.2 Low temperature chemical treatment 10
1.1.2.3 Radiation sterilization 12
1.1.3 Upcoming sterilization technologies 14
1.2 Cancer 18
1.2.1 Various types of cancer 18
1.2.2 Main treatments 19
1.2.2.1 Surgery 19
1.2.2.2 Radiotherapy 20
1.2.2.3 Chemotherapy 23
1.2.2.4 Immunotherapy 24
1.2.3 Upcoming technologies 26
1.2.3.1 Electroporations 26
1.2.3.2 Gene therapy 28
1.2.3.3 Virus therapy 29
1.2.3.4 Non-thermal plasma 30
2 Nonthermal plasma for biomedical applications 31
2.1 Theoretical background of non-thermal plasmas 31
2.1.1 Electron avalanche 31
2.1.2 Pachen's law 32
2.2 Non-thermal plasma generators 33
2.2.1 Glow discharges 33
2.2.2 Corona discharges 34
2.2.3 Dielectric barrier discharges (DBD) 35
2.3 Application to micoorganism decontamination 42
2.3.1 Comparison of plasma sources for decontamination 42
2.3.2 Brief description of biological assay techniques 44

2.3.3 Planktonic bacteria versus biofilm 46
2.3.4 Virus deactivation 47
2.4 Plasma medicine 53
2.4.1 Introduction to applications 53
2.4.2 Cancer cure induced by non-thermal plasma 56
2.4.2.1 Mechanisms of anti-cancerous components 56
2.4.2.2 Treatment assay 59
2.4.2.3 Different procedures of NTP treatment 60
2.4.2.4 Studies of PAM treatment (indirect treatment) 61
2.4.2.5 Investigation of direct NTP treatment 68
3 Dielectric barrier discharges 80
3.1 Introduction 80
3.2 Materials and methods 81
3.2.1 DBD configuration setup 81
3.2.2 Configurations of plasma propagation 84
3.3 Results and discussions 87
3.3.1 Comparison of electrical and chemical measurements of different DBD configurations 87
3.3.2 Plasma propagation in tubes 90
3.4 Summary 103
4 Surface decontamination 105
4.1 Introduction 105
4.2 Materials and methods 106
4.2.1 Preparation of phage stock 107
4.2.2 Bacteriophage spotting and recovery on solid substrate 107
4.2.3 Treatment exposure and recovery 109
4.2.4 Paque assay 110
4.2.5 Plasma treatment 111
4.2.6 TEM Observation 114
4.3 Results 115
4.3.1 Phage stability on water-soluble paper 116
4.3.2 Exposure to plasma treatment 118
4.4 Summary 129
5 Human adenocarcinoma cells treatment 132
5.1 Introduction 132
5.2 Materials and methods 132
5.2.1 Plasma generation 132
5.2.2 Tumor cell culture 133

5.2.3 Treatment process 133
5.2.4 Assays 135
5.3 Results and discussions 135
5.3.1 Proliferation 135
5.3.2 Apoptosis 137
5.3.3 Migration 138
5.4 Summary 141
6 Conclusion 143
6.1 Investigation of DBD non-thermal plasma 143
6.2 Surface decontamination 144
6.3 *In-vitro* human adenocarcinoma (lung cancer) cell treatment 146
6.4 Perspectives for future work 146
Reference 148

LIST OF FIGURES

FIGURE 1.1 THE RANK OF DEATH CAUSE IN 2017. 5
FIGURE 1.2 THE INCREASE OF OVERALL CANCER DEATH IN WORLDWIDE POPULATION FROM 1990 TO 2017 5
FIGURE 1.3 THE AUTOCLAVE AND STERILIZED ITEMS (MEDIUM) 9
FIGURE 1.4 THE MACHINE OF DRY HEAT STERILIZATION 10
FIGURE 1.5 THE ETHYLENE OXIDE STERILIZATION CHAMBER 10
FIGURE 1.6 THE PROCESS OF EO STERILIZATION 11
FIGURE 1.7 THE VAPORIZED HYDROGEN PEROXIDE STERILIZER 11
FIGURE 1.8 THE PROCESS OF H_2O_2 STERILIZATION IN CHAMBER 12
FIGURE 1.9 CELL CULTURE HOOD WITH UV LIGHT 12
FIGURE 1.10 THE PRODUCTS ON CAROUSEL ARE TRANSPORTED TO ELECTRON SHOWER / THE GAMMA RADIATION SOURCE (UPPER BLUE LIGHT) AND THE PRODUCTS 14
FIGURE 1.11 THE FE-SEM IMAGES OF STAPHYLOCOCCUS AUREUS INTERACTION WITH GRAPHENE NANOPLATES. THE DAMAGE ON CELL MEMBRANE BY SHARP EDGE OF 2D, 1D, AND MIXING OF 1D AND 2D NANOMATERIALS 15
FIGURE 1.12 THE DOSE DECAY OF E-BEAM (10 MEV), GAMMA RADIATION (100 KEV), AND X-RAY (5 AND 7 MEV) (PROPORTION OF THE DOSE AT GIVEN DEPTH TO THAT AT SURFACE) VERSUS THE MASS DEPTH IN MATERIAL 17
FIGURE 1.13 NON-THERMAL PLASMA STERILIZER TYPICALLY UNDER LOW PRESSURE OF 10^{-3} ATM / NON-THERMAL PLASMA JET TREATMENT ON *STAPHYLOCOCCUS AUREUS* UNDER ATMOSPHERIC PRESSURE 17
FIGURE 1.14 PATIENT BEING TREATED BY RADIOTHERAPY 21
FIGURE 1.15 PROSTATE GLAND TREATMENT USING CATHETERS TO DELIVER THE RADIATION SOURCE, UNDER ULTRASOUND PROBE MONITORING 21
FIGURE 1.16 PATIENT BEING TREATED BY PROTON BEAM THERAPY 22
FIGURE 1.17 THE PATIENT IS RECEIVED CHEMOTHERAPY THROUGH CHEMOPORT ON THE CHEST AND INJECTION IN A VEIN ON THE HAND 23
FIGURE 1.18 PD-L1 AND PD-1 ARE THE CHECKPOINT OF ANTICANCER. IN IMMUNOTHERAPY, ANTI-PD-L1 AND ANTI-PD-1 ARE USED FOR IMMUNE CELLS TO DIAGNOSIS THE TUMOR CELLS 25
FIGURE 1.19 ELECTRODE TOUCHING AND INSERTED TISSUE NEAR TUMOR; ELECTRIC FIELD DISTRIBUTION SHOWED (EREV AND EIRREV: ELECTRIC FIELD OF REVERSIBLE AND IRREVERSIBLE ELECTROPORATION LIMITS RESPECTIVELY) 27
FIGURE 1.20 THE DIFFERENT MECHANISMS OF ELECTROPORATION CANCER THERAPY: ELECTROCHEMOTHERAPY AND IRREVERSIBLE ELECTROPORATION. 28

Figure 1.21 Adenovirus vector bringing modified DNA through cancer cell membrane and injecting gene in cell nucleus 29
Figure 1.22 Cancer-killing process of oncolytic virotherapy 30
Figure 2.1 Electric avalanche by electron-neutral particle collision 32
Figure 2.2 Paschen's curves 33
Figure 2.3 The simple DBD configuration 35
Figure 2.4 Several kinds of DBD in tube scheme.. 36
Figure 2.5 Photos of plasma plume are taken by Cannon camera and ICCD 37
Figure 2.6 Configuration of Boeuf's demonstration. / Parameter of given voltage where V_M=1kV, V_M=4kV, and t=50ns. / The ionization rate distribution. 38
Figure 2.7 This demonstration electron distribution 39
Figure 2.8 Relation between plasma plume length and gas flow rate and Reynolds number in three sizes (3 mm, 6mm, and 8 mm) of tube 40
Figure 2.9 The shapes of plasma plume change under different He flow rate 40
Figure 2.10 Waveforms of current peak and onset voltage for three different raising time 41
Figure 2.11 The plasma plume length for different power supply frequencies on different applied voltage. Argon flow rate: 8.3 $Lmin^{-1}$ 41
Figure 2.12 The *E. faecalis* structure changes imaged by TEM after plasma treatment 47
Figure 2.13 The plasma etching on *C. albicans* biofilm in both vertical and horizontal direction. 47
Figure 2.14 T4 phages attach on *E. Coli* and penetrate the membranes 48
Figure 2.15 The untreated and treated MS2 sample under SEM. 49
Figure 2.16 The inactivation mechanisms of plasma producing ROS and RNS 49
Figure 2.17 The blood coagulation on mouse 53
Figure 2.18 The concentration of prothrombin raising after plasma treatment 54
Figure 2.19 Wound area changes after He plasma treatment on non-diabetic or diabetic rats 54
Figure 2.20 The recovery of eyelid after 6^{TH} air plasma treatment 55
Figure 2.21 The figures show the E. *coli* and L. *casei* before and after 0.9s/mm^2 plasma treatment 55
Figure 2.22 The process of cell apoptosis induced by ROS and RNS 57
Figure 2.23 Schematic representation of ROS transfers in cancer cell and normal cell 58
Figure 2.24 Flow chart of necrosis and apoptosis process 60
Figure 2.25 Procedure of direct treatment and plasma activated medium 61
Figure 2.26 Apoptosis comparisons between argon activated medium (Ar-AM) and

PAM in four gene types of ovarian cancer. Effect of apoptosis strongly depended on gene type 62
Figure 2.27 The real photo and statistical results of cancer cell migration 63
Figure 2.28 Glioblastoma cell viability measured after 24 hours of chemical compounds and PAM treatment. H_2O_2 and NO_2^- has the same concentration as that in PAM. 64
Figure 2.29 The schedule of PAM treatment and the evolution (arrowhead shown the first death of mouse.) of animal survival ratio in pancreatic cancer mouse trials 65
Figure 2.30 Lactated ringer's solution (control) and plasma activated lactated ringer's solution (PAL) treating pancreatic cancer mice. Tumors are bright due to luciferin staining, and the color is luminosity of fluorescence 66
Figure 2.31 Treated spots shown after NTP treatment. Scale bar are 200 μM 68
Figure 2.32 The value of cell viability after direct and indirect NTP treatment ... 69
Figure 2.33 The edge between healthy cells and dead cells formed after long and short term treatment. 70
Figure 2.34 The dead and alive lung cancer cell staining after giving exposure time and assay delay 70
Figure 2.35 Figures and statistics of 3D lung cancer cell matrix treated by 15 s NTP treatment with a day assay delay 71
Figure 2.36 Survival ratio of oral cancer cells after the exposure of O_2 plasma and air plasma in giving irradiation period 71
Figure 2.37 The life-death assay of collected detached cells at 1 and 24 hours after NTP treatment 72
Figure 2.38 The comparable result of cell viability assay in two gene types of prostate cancer LNCaP and PC3 and normal prostate cell 72
Figure 2.39 The evolution of breast tumor size and survival ratio of treated mice in 24 days after helium plasma treatment and drug treatment 75
Figure 2.40 *In vivo* NTP treatment on mouse skin. /The concentration of colorectal cancer-specific antigen guanylyl cyclase C (GUCY2C) after plasma or/and vaccine treatment 75
Figure 3.1 Scheme of rod system installed in chamber. 81
Figure 3.2 The experimental setup for the measurement of H_2O_2 at the reactor outlet, the plasma generator (mesh block) can be either of the following two arrangements: simple two-ring system or Teflon-tube-insulated HV two-ring system. 82
Figure 3.3 Experimental setup of the two ring DBD system. A_1 is the homemade current probe, A_2 and A_3 are CT-2 current probes. /A photograph of plasma

propagation in the tube. 85
Figure 3.4 The scheme of RS plasma generator for streamer propagation in a silicon tube. 86
Figure 3.5 The experimental setup of the TR DBD propagating within a thin and long silicon tube. 87
Figure 3.6 The discharge power as a function of peak-to-peak input voltage in the RS and TR systems. 88
Figure 3.7 The quite comparison between RS plasma plume and TR plasma plume. The cameras and the resolutions were different. 89
Figure 3.8 The concentrations of hydrogen peroxide increased with plasma exposure duration. 89
Figure 3.9 The propagation length and the power of discharges under such applied voltage in Teflon-tube-insulated HV TR system . 91
Figure 3.10 Input voltage measured for the given streamer length for each constant current. 92
Figure 3.11 Conductivity calculation with assumption of streamer geometry: single streamer and multiple streamers. 92
Figure 3.12 Oscilloscope traces for the current measurement at downstream wire (A_3) with the input voltage of 10 kV. The tip of wire was moved to every 2 cm from 4 to 16 cm away from the counter electrode. 93
Figure 3.13 Average streamer velocity at various input voltages in different propagation length. 94
Figure 3.14 The instantaneous streamer velocity at every position with input voltage from 7 to 13 kV. 95
Figure 3.15 Oscilloscope traces of voltage (black) and three current signals: at the HV electrode (A_1-red), counter electrode (A_2-blue), and downstream electrode (A_3-green). Grounded downstream electrode located at 10 cm away from the grounded ring. 95
Figure 3.16 The RS plasma propagation in 100 cm length thin silicon tube.. 97
Figure 3.17 The RS plasma propagation length versus pulse amplitude with given argon mass flow rate 98
Figure 3.18 The RS plasma propagation length versus pulse amplitude with given pulse widths 99
Figure 3.19 The RS plasma propagation length versus pulse width at fixed pulse amplitude. 99
Figure 3.20 The plasma generated by the Teflon-tube insulated HV two-ring system propagated in a silicon tube (50 cm) inserted into the treatment chamber. 100

Figure 3.21 The TR plasma propagation length versus pulse amplitude with given argon gas flow rate 101
Figure 3.22 The TR plasma propagation length versus pulse amplitude with given pulse widths. 101
Figure 3.23 The TR plasma propagation length versus pulse width at fixed pulse amplitude. 102
Figure 4.1 Overnight incubation Petri dishes of *E. coli* after dry argon flow only and argon plasma treatment..... 105
Figure 4.2 Transmission electron microscopy images of T4 and MS2 106
Figure 4.3 Water-soluble paper spotting test: 1 µL of λ-dil buffer solution containing red and blue dye..... 109
Figure 4.4 The three paper disc samples spotted with the same stock dilution: control of dilution, treatment sample, and bench sample..... 110
Figure 4.5 Illustration of the Gratia method for plaque assay. 111
Figure 4.6 Control of dilution. Plaques of T4 bacteriophages (109 plaques) and MS2 bacteriophages (120 plaques). MS2 phage had much larger plaques. According to the dilution (here 10^{-2}), the concentration of phage particles was $5.45x10^5$ PFU/mL and $6x10^5$ PFU/mL for T4 and MS2 respectively. 111
Figure 4.7 Scheme of plasma system for bacteriophage treatment on WSP sample. 112
Figure 4.8 Typical input voltage and discharges current waveforms..... 113
Figure 4.9 Temperature measurement at the sample location when submitted to humid air post-discharge..... 113
Figure 4.10 The solid (RNA contains) gas flow blown phages and the empty (RNA lost) plasma treated phages are shown..... 115
Figure 4.11 Survival fraction of T4 phage diluted in SM, λ-dil, Mu and M9 buffer solutions at 4°C with and without 10%Vol. glycerol admixture..... 117
Figure 4.12 Survival fraction of T4 phage diluted in SM, λ-dil, Mu and M9 buffer solutions at room temperature with and without 10%Vol. glycerol admixture..... 117
Figure 4.13 Survival fraction of MS2 phage diluted in SM, λ-dil, Mu and M9 buffer solutions at room temperature with and without 10%Vol. glycerol admixture..... 118
Figure 4.14 MS2 phage (λ-dil buffer solution) PFU on paper vs. exposure time to air (dry and humid) and argon (dry and humid) plasma treatment..... 119
Figure 4.15 FTIR absorption spectra obtained in both conditions dry and humid air (95%RH at room temperature and atmospheric pressure). 2 L/min gas flow rate, 3 W input power..... 120

Figure 4.16 T4 phage PFU on paper vs. exposure time on the bench, to gas flow-only, to warm gas flow-only, to humid air plasma treatment. 122
Figure 4.17 Survival fraction of T4 phage after different treatments: on the bench, exposed to gas flow-only, exposed to warm gas flow-only, exposed to humid air plasma treatment. 122
Figure 4.18 MS2 phage PFU on paper vs. exposure time on the bench, to gas flow-only, to warm gas flow-only, to humid air plasma treatment. 124
Figure 4.19 Survival fraction of MS2 phage after different treatments: on the bench, exposed to gas flow-only, exposed to warm gas flow-only, exposed to humid air plasma treatment. 124
Figure 4.20 TEM micro-figures of MS2 stock, on bench for 4 min, 4 min. humid air flow exposure, and 4 min humid air post-discharge exposure. 129
Figure 5.1 Images of the lung cancer cell cultures from two patients after 48 hours of incubation; the images were taken by charge-coupled device camera under an inverted microscope 133
Figure 5.2 Schematic description and photograph of the experimental set-up ... 134
Figure 5.3 Treatment zones in Petri dish sample and photograph of a sample being treated by dry argon plasma plume. 134
Figure 5.4 The plasma treatment result of proliferation with feeding gas: dry argon and humid argon 136
Figure 5.5 The plasma treatment result of apoptosis with feeding gas: dry or humid argon. 137
Figure 5.6 Micrographs of the treatment zone. First row: humid argon treatment. Second row: dry argon treatment. Third row: dry argon control. For all the three rows, the first column is for imagery made immediately after treatment, second column for 24 h delay after treatment and third column for 48 h delay after treatment. 139
Figure 5.7 Statistics Quantification of the normalized area of treated spots measured after dry orhumid argon plasma treatment. 140

LIST OF TABLES

TABLE 2.1 THE FIRST IONIZATION ENERGY OF SOME GAS SPECIES 33
TABLE 2.2 THE PREVIOUS STUDIES OF DBD PLASMA DECONTAMINATION. 50
TABLE 2.3 THE RESULTS OF CELL VIABILITY, PROLIFERATION, AND APOPTOSIS ASSAYS IN DIFFERENT CANCER TRIALS. 62
TABLE 2.4 THE RESULT OF GROWTH OF TUMOR SIZE OR NUMBER, METASTASIS, AND ALIVE RATIO IN PAM-TREATED MOUSE TRIALS. 64
TABLE 2.5 THE PARAMETER OF PAM GENERATION *IN VITRO* TREATMENT. 67
TABLE 2.6 NTP TREATMENT RESULTS (CELL VIABILITY, PROLIFERATION, AND APOPTOSIS) OF VARIOUS CANCER. 68
TABLE 2.7 THE RESULTS OF DIRECT NTP TREATMENT *IN VIVO*. 73
TABLE 2.8 THE PARAMETER OF DIRECT NTP TREATMENT *IN VITRO*. 76
TABLE 2.9 THE PARAMETER OF DIRECT NTP TREATMENT *IN VIVO* 78
TABLE 4.1: PLASMA SYSTEM OPERATING CONDITIONS FOR BACTERIOPHAGE TREATMENT ON WSP SAMPLE 114
TABLE 4.2 CONCENTRATION (PPM) OF IDENTIFIED SPECIES IN DRY AND HUMID AIR (95%RH À ROOM TEMPERATURE AND ATMOSPHERIC PRESSURE) USING UV AND FTIR ABSORPTION SPECTROSCOPY. 2 L/MIN GAS FLOW RATE, 3 W INPUT POWER. 119
TABLE 4.3 SOLUTION PH VALUE FOR 4 MIN. EXPOSURE TIME TO PLASMA TREATMENT. 2 L/MIN GAS FLOW RATE, 3 W INPUT POWER. 121
TABLE 4.4 BACTERIOPHAGE INACTIVATION RATES (LOG/MIN) FOR DIFFERENT TREATMENTS. 127

INTRODUCTION

In the top ten cause of death all over the world, cancer and respiratory infections ranked two and four respectively in 2017 [1]. Several approaches were developed for cancer treatment (e.g. surgery, radiotherapy, chemotherapy, *etc.*) and for surface bio-decontamination (e.g. dry heat treatment, wet heat treatment - autoclave, chemical treatment, radiation, *etc.*). However, these technical approaches have major drawbacks. In cancer treatment, surgery causes risks of metastasis [2], radiotherapy might induce secondary malignant tumors [3], and chemotherapy has impact on normal cells and results in some side effects on patients [4]. On the other hand, in the field of bio-decontamination, thermal processing (autoclave and dry heat treatment) can lead to degradation and deformation of heat-sensitive materials [5], the residues in chemical treatment can lead to persistent toxicity for operators and patients [5], and exposure to ionizing radiation presents risks for human cells and even DNA in case of careless operation [5]. Therefore, it is still eager to design and develop new and safe technical on cancer treatment and surface decontamination. Non-thermal plasma (NTP) technology is one of the options.

Dielectric barrier discharges (DBD) is widely applied for the generation of NTP. Coaxial cylinder geometry consisting in a high voltage (HV) metal rod electrode inserted in a dielectric tube whose external face is partially covered with a ground electrode has been investigated as a plasma source for a long time [6]. An alternative geometry consisting in a two-ring configuration (both HV and ground electrodes are attached outside the tube) was developed. In this manuscript, we will compare these two configurations from physical and chemical points of view. Moreover, the plasma propagation is worth to be investigated if the sample is placed far away from plasma generation region (e.g. inside the human body cavity). Several fundamental studies describe the plasma motion in long tube. However, in the systems under investigation, plasma motion was still not clear. In our studies, we propagated plasma in a 60 cm long quartz tube, and a downstream wire was used to measure several properties such as voltage drop, conductivity, streamer velocity, and to analyzed the waveform on oscilloscope. As a model of endoscopy to insert cavity, the plasma generator will be connected to a small and soft silicon tube. And the plasma parameter will be further investigated.

Non-thermal plasma (NTP) can be also applied for the surface inactivation of viruses. Bacteriophage was used as a surrogate model of the human infectious virus. Previous works on phage treatment by means of non-thermal plasma techniques were investigated in aerosol [7, 8] or in liquid phase [8, 9, 10]. In this study, we provide experimental results of bacteriophage inactivation on porous surface when submitted to direct or indirect interaction with atmospheric pressure plasma. We thus wished to propose a realistic model of complex surface (fiber) contaminated with saliva droplets. In the same objective, we focused on air as a feed gas, where reactive oxygen species (ROS) and reactive nitrogen species (RNS) are the main agents for the inactivation of microorganisms and viruses [11]. Heat transportation and desiccation effect were controlled or investigated for the phage inactivation mechanisms. DNA phage T4 and RNA phage MS2 were the treated target particles and inactivation results were compared and discussed.

NTP were also investigated for tumor cells treatment. When plasma interacts with water vapor or oxygen, reactive oxygen species (ROS) are produced, and an apoptosis processing can be triggered [12]. There is also evidence of selective effect between cancer cells and normal (non-cancerous) cells [12]. Charged particles and electric fields could induce cell membrane electro permeabilization [13] allowing for ROS to penetrate into the cytoplasm and initiate complex mechanism leading to cell apoptosis and/or necrosis. Electrical discharges are also source of UVB radiation which could induce nuclear condensation and fragmentation and eventually lead to cell apoptosis [14]. Currently, direct and indirect NTP exposure has been widely applied on cancer treatment in various cancer *in vitro* or *in vivo* (see in Table 2.5 and Table 2.8). In our work, dry and humid argon NTP was investigated and compared in application of *in vitro* treatment on lung tumor cells.

The manuscript is organized in two distinct parts. The first part consists in a selected state of the art and theoretical background, including cancer therapy and microorganism decontamination in Chapter 1, and in Chapter 2, the theory of non-thermal plasma and the introduction to bio-decontamination and plasma medicine. The second part presents our experimental results: the physical and chemical comparison of rod-system and two-ring-system dielectric barrier discharge (DBD) plasma and the characteristics of plasma propagation will be discussed in Chapter 3. Chapter 4 and Chapter 5 describe the biological application on bacteriophage inactivation and lung cancer cell

treatment. In Chapter 6, we give the general conclusion of our work, including the reviews of experimental results and future work.

Part I

Theoretical background

1 BACKGROUND AND MOTIVATION

As the development of technology, the average of human age is longer and longer, however, no one can escape from death. Nevertheless, a constant effort is made to fight the disease. Cardiovascular disease remains the leading cause of death in the world [1].

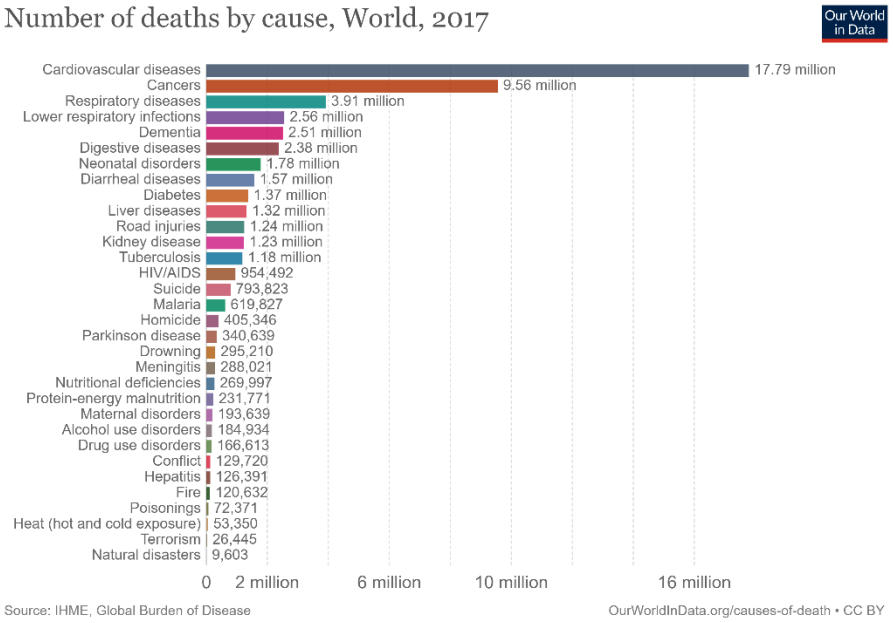

Figure 1.1 The rank of death cause in 2017 [1].

The second leading cause of death is cancer. In 2017, over nine million people died from cancer. In past 30 years, the number of cancer deaths increased from 5.75 million in 1990 to 9.56 million in 2017. Among various type of cancer, the respiratory-related cancer was responsible for the majority of deaths [15]. In some developed countries, for example Taiwan, cancer death was the first leading cause of death in 2018 [16].

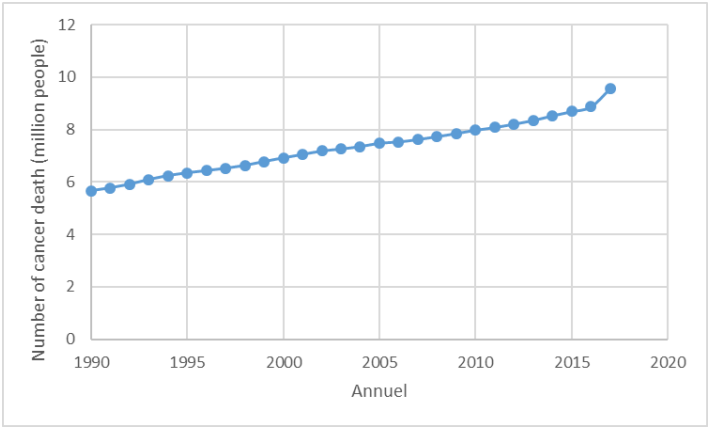

Figure 1.2 The increase of overall cancer death in worldwide population from 1990 to 2017 [3].

It is also worth mentioning that the number of respiratory infection deaths is high. For the past 20 years, respiratory infections have been the fourth leading cause of death in the world [1]. Even though infection happens frequently, it is usually neglected. But many infections can lead to lethal diseases, and emerging solutions are still needed in the perspective of prevention and treatment.

The main cause of cancer-related death is the metastasis (about 90%) [17, 18]. The mechanism of cancer metastasis is still unclear, but scientists believed that it is significantly depended on extracellular matrix structure, growth factors, chemokines, and matrix metalloproteinases [18], and the metastasis could happen spontaneously [19]. Also, the metastasis could be induced by the surgery [2] or radiation therapy [20] of cancer. After these kinds of therapy, the main tumor can be smaller or removed, however, there is residue of tumor fraction spreading by circulation (blood and lymphatic vessels) and moving to other organ. The metastasis process could be separated in four steps, detachment, migration, invasion and adhesion, and strongly affected by tumor microenvironment [18]. Metastasis with the secondary organ exhaustion and malignant consumption of nutrition causes patient go into die. Overall, the better and various types of cancer treatment and prevention of metastasis are urgently requested for saving more people from cancer.

Cancer patients could be infected in hospital, however, infection does not only appear on cancer patients. In fact, infection disease is always ranked in the leading 10 cause of death in the world [1]. Everyone and everywhere even outside the hospital has a chance to contact with the pathogens, such as bacteria, virus, and fungi. Normally, people have immune system strong enough to fight with these infective agents. However, some people such as elders, children, and lower immunity population have less capability of resistance. Better decontamination can help these groups away from the attack of pathogens and keep healthy.

Nowadays, there are several types of cancer treatment and bacterial disinfection, for example, surgery, chemotherapy, radiation therapy, and immune therapy for cancer, and UV light, hydrogen peroxide, autoclave, and else for decontamination. However, each method has its own suitable working conditions. In this thesis, the new method of cancer treatment which is non-thermal plasma is introduced. Also, the solution of infection is investigated in

the same method. In the following sections, we will present a short state of the art on cross-infection diseases and cancer.

1.1 Cross-infection diseases

Cross-infection is narrowly defined as transmission of pathogenic specious in hospital [21]. In general, cross-infection is taking place everywhere people can arrive and touch. For example, in kitchen, bacteria can transmit from the fresh meat to the cooked meat if there is no distinguished knife or chopping board. Also, on mass transit, virus of influenza is easier to transport due to the high population density. Cross-infection is a conventional event in our life.

The infectious agents can be bacteria, viruses, fungal parasites [22], and fungi [23]. Burn wound patients have high risk of bacterial infection and infected death, the most frequently found specious are *Staphylococcus aureus*, *Klebsiella pneumoniae* and coagulase negative *Staphylococci* [23]. Moreover, in 2020, corona virus of COVID-19 infected more than 250 million people and killed over 5 million people [24]. This virus came from China and cross-infected in airplanes, trains, subways, even ships. Besides, the most frequent skin diseases are induced by the infection of fungi [25]. Even though fungi infection seldom leads patients die, it may deeply affect the life quality (flavor, outlook…) of patients. These infectious agents are too small to see and hard to avoid touching them.

The access of transportation of the pathogens can be human to human during their physical interaction, instrument to human (such as dental treatment [21], mobile phone transmission [26]), animals (pets) to human [27].

1.1.1 Nosocomial infections

WHO estimated about 15% patients suffering from infection in hospital [22], especially in the surgical and intensive care units [28]. The infection has three kinds of spreading paths.

Firstly, the infectious agents are transporting from human to human. In 2020, COVID-19 virus widely spread in the healthcare workers [29],and consequently to patients. Then, the virus spread. Endogenous infections could also happen, such as *Candida* infections [22].

Secondly, instrument or material of therapy would bring infectious pathogens

to patients. For instance, blood transfusion provides the risk of infection. A research shows the secondary bacterial infection in sepsis patients whose immune depression in previous infection [30]. Moreover, endoscopy and bronchoscopy would insert and bring bacteria inside human body [31]. The bacteria can form biofilm on the tube walls, and then they grow, spread and infect the patients.

Thirdly, basic, everyday human activities such as drinking (biofilms can be found in drinking water [32]) or using the telephone (possible vector [26]) constitute a risk of contamination in the hospital.

Besides, cross-infection is also the cause of cancer patient death in hospital. Cancer patients have higher probability to go to these units and get infection due to the treatment and disease progress. At the same time, their immunity is reduced because of the stress of the environmental condition or situation (quality of life) [33]. As a result, cancer patients is easier to be killed by the infection.

The pathogens of nosocomial infection are bacteria (such as *Streptococcus spp*., *Acinetobacter spp*., *Enterococci*, *Pseudomonas aeruginosa*, coagulase-negative *Staphylococci*, *Staphylococcus aureus*, *Bacillus cereus*, *Legionella*, *Proteus mirablis*, *Klebsiella pneumonia*, *Escherichia coli*, and *Serratia marcescen* [34]), virus (such as influenza A and B, RSV A and B, coronavirus, parainfluenza, human metapneumovirus, adenovirus, rhinovirus, and enterovirus [35]), and fungi (such as *Candida spp*., *Aspergillus spp*., *Mucorales*, *Fusarium spp*., and *Scedosporium spp*. [36]). In this thesis, we will focus on decontamination of virus.

1.1.2 Conventional sterilization methods

In hospital, patients have lower function of immune systems, and they are easier infected and killed by the pathogens. To avoid the cross-infection, all the items for medical use need to be sterilized as clean as possible. These items are made of several kinds of the materials they have different sterilization conditions. Therefore, the various sterilization systems are developed. These systems are introduced and compared as follows:

1.1.2.1 Heat sterilization

Autoclave (steam sterilization)

The autoclave, which is also called steam sterilization, was invented in 19th

century. The working conditions of autoclave are 120-135˚ C and 1.02 atm. For the 120˚ C, the working time is 15-20 min, and high percentage of microorganisms are destroyed depended on the structure of sterilized items. The benefits of autoclave are nontoxic and friendly to environment. However, the most drawbacks of autoclave that the moisture sensitive and low melting or boiling point materials (such as PLGA, nylon, polystyrene, and else) could be degraded in autoclave sterilization [5]. Also, powder and oil could not be decontaminated in autoclave (humid sterilization). The autoclave can be applied on decontamination of medical waste [37] and surgical instruments [38].

Figure 1.3 The autoclave and sterilized items (medium) [39].

Dry heat sterilization(DHS)

Compared to the steam sterilization of autoclave, there is also dry heat sterilization. DHS works under 163˚ C for two hours or 190.5˚ C for six to 12 min [40], and it can sterilize dry powders and other materials having the impact of moisture. It also does not generate toxic substance. However, the same as the autoclave, DHS cannot sterilize the items with low melting or boiling point. DHS can be used on disinfection of health care products, medical devices, equipment, components or bulk active pharmaceutical ingredients.

Figure 1.4 The machine of dry heat sterilization [41].

1.1.2.2 Low temperature chemical treatment

Ethylene oxide

Figure 1.5 The ethylene oxide sterilization chamber [42].

Ethylene oxide (EO) is a chemical method and the widest (50% occupied in the US [43]) use of industrial disinfection. It is useful for decontamination of the heat- or radiation-sensitive medical items, such as endotracheal tubes, plastic syringes, hemodialysis tubes [44], and even electronic devices, but no embedded batteries because of the vacuum during the process [5]. EO sterilization can work in low temperature (compared with room temperature) due to it boiling point of only 10.4˚C [5]. The main mechanism of EO decontamination is alkylation of DNA or RNA of microorganisms. Then, metabolism of these organisms is changed, and directly affects the growth of microbes [45]. Nevertheless, EO is a flammable gas and a carcinogen, and it may provide the irreversible toxic effect for human when they contact the chemical

residue on the items [5]

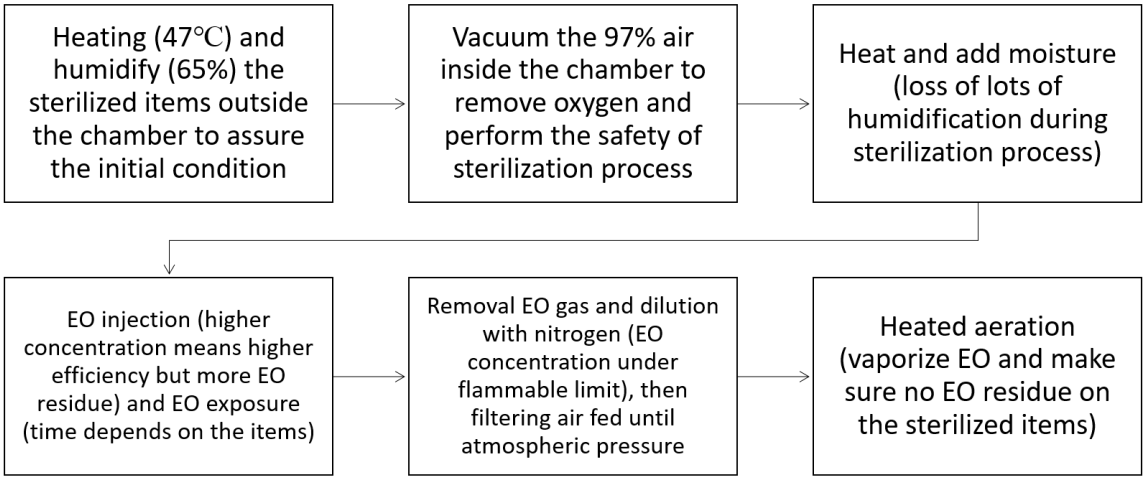

Figure 1.6 The process of EO sterilization [5, 46].

Hydrogen peroxide

Figure 1.7 The Vaporized Hydrogen peroxide sterilizer [47].

Hydrogen peroxide (H_2O_2) is a strong oxidant, which can degrade the cell membrane and DNA of microorganisms in order to decontaminate. H_2O_2 has the benefits of safety and materials compatibility, and it is used as antiseptic to clean wounds with low concentration (3%). However, high concentration (>10%) of H_2O_2 will hurt human skin. In hospital, H_2O_2 is utilized on tooth bleaching [48] and medical devices decontamination. It is expected that H_2O_2 vapor plays a role of decontamination in room after patients left [49]. Moreover, H_2O_2 vapor is also combined with the plasma to generate more radical species. The method

is utilized for polymer decontamination, but the vacuum condition and high radiofrequency power make a problem for the devices with the embedded electronics [5].

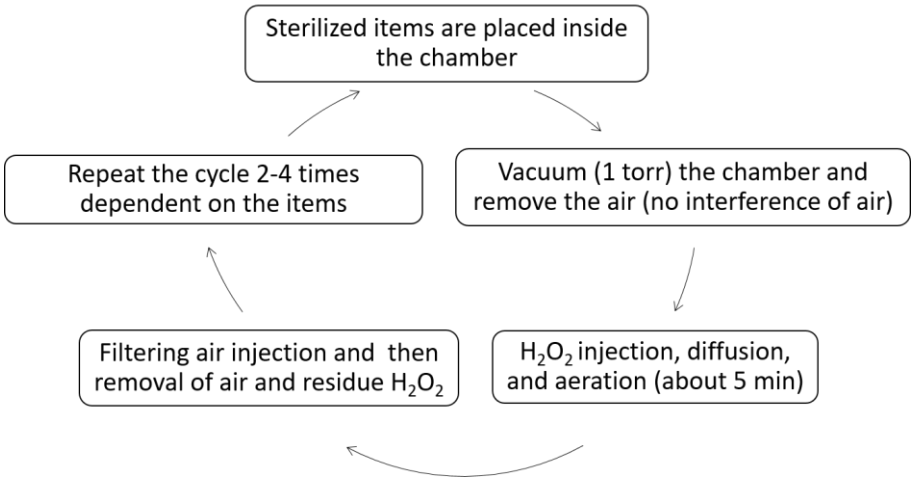

Figure 1.8 The process of H_2O_2 sterilization in chamber [5, 50, 51].

1.1.2.3 Radiation sterilization

Ultraviolet

The radiation with various wavelengths is applied for pathogen decontamination. The longer wavelength of the radiation is ultraviolet (UV) spectrum. UV light is currently generated by mercury lamp and applied for sterilization of laboratorial hood surface, and the same idea could be used in operation room with decontamination of atmosphere [52].

Figure 1.9 Cell culture hood with UV light [53].

Also, UV is used on water decontamination [5]. The mechanisms of UV

decontamination are the break of DNA and damage of cell membrane [54]. However, the danger of UV light depends on the familiar degree of the user. UV light with different wavelength can be separated in four groups, UVA, UVB, UVC, and VUV. The wavelength of UVA is 315-400 nm which has the lowest energy among these four types of UV. UVA could age the skin cells and also cause indirect hurt on DNA of skin cells [55]. UVB wavelength ranged from 280 to 315 nm has slightly high energy than UVA. UVB could induce sunburns and it damages the DNA of skin cells directly, and UVB is the main cause of skin cancer [55]. UVC has much higher energy with wavelength 200-280 nm. Normally, UVC cannot go through atmosphere and reach ground, so human do not get hurt from natural UVC. UVC still exists in human society for sterilization with man-made UV source. The main UV sterilization is applied with UVC. The wavelength of vacuum ultraviolet (VUV) is ranged from 100 to 200 nm shorter than UVC. The researches show that VUV which is produced by the plasma is also effective in the bacterial decontamination [56] and killing of spores [57]. But VUV cannot be operated under atmosphere due the strong absorption of atmospheric oxygen. Overall, the advantage of UV light is that it could do air [52], water, and surface decontamination without toxic residue, but it will hurt human skin with careless operation.

Gamma radiation and electron beam

Besides UV light, there is another use of radiation sterilization with the shortest wavelength, which is gamma radiation. The decontamination with gamma radiation occupies about 40.5% in industrial medicine in the US [43], including pharmaceuticals [58], surgical items [43] and polymer tools [5]. However, the high costs and strict conditions governing the use of ionizing radiation result in its use being restricted to the industrial sector. The source of gamma radiation in sterilization use is the radiation emission of Co-60 [58, 5, 43]. Sterilization of gamma radiation is usually parallel to that of electron beam (e-beam) whose source is accelerating electrons [5]. But it only occupies 4.5% of industrial sterilization. E-beam can sterilize the similar items with gamma radiation. The decontaminated duration of gamma radiation in certain dose is from few minutes to hours. E-beam is much shorter in a few seconds but only works in small area [59]. Like UV light, gamma ray and e-beam can make a damage of DNA. Moreover, they can form free radicals in air, and these radical species also help to kill microorganisms [5] The advantages of these sterilization are their significant penetration [5] and substantially less toxicity [59] compared with EO sterilization. For sterilization of pharmaceutical drug, high energy irradiation is

better choice than dry heat or autoclave, but requires strict protection preventing from radiation leakage.

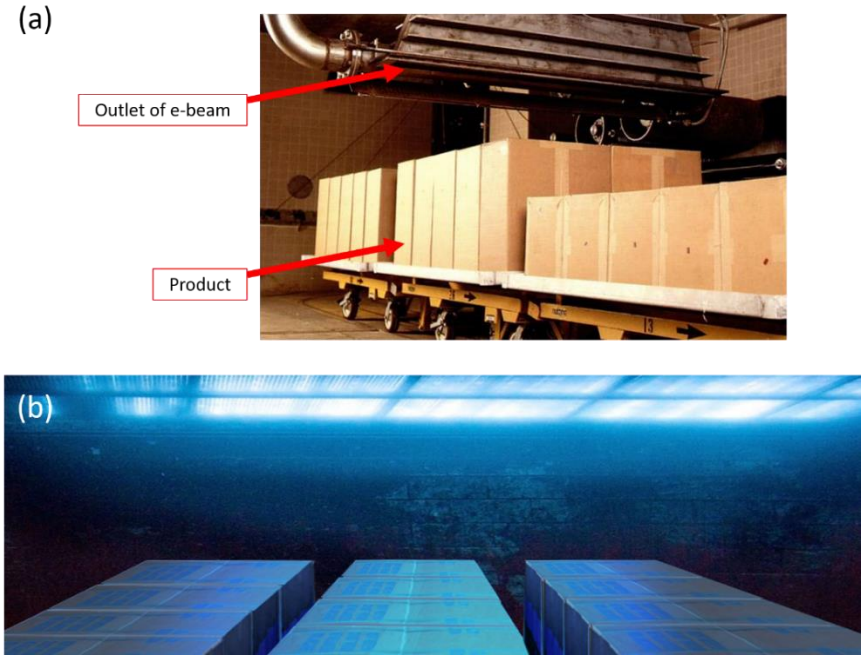

Figure 1.10 (a) The products on carousel are transported to electron shower [60]. (b) The Gamma radiation source (upper blue light) and the products [61].

1.1.3 Upcoming sterilization technologies

Because of the various operation conditions and the use of new medical items, as well as the development of antibiotic resistance, the current sterilization methods are not enough for the decontamination in medical care, surgery, and else in hospital. Some sterilized technologies continue to be invented and developed, for example ozone is working in gas phase, nanoparticles as solid phase, and wave-induced decontaminations microwave and non-thermal atmospheric plasma. An overview of these methods is proposed in the following paragraphs.

Ozone

Ozone has existed in high atmosphere of earth for few hundred million years, and it protects terrestrial organisms from UV light from the sun. Ozone in our atmosphere comes from splitting oxygen. When oxygen is excited with discharges or extreme ultraviolet (wavelength of 10-120 nm), the oxygen molecule could be split in two monatomic oxygen. The monatomic oxygen reacts with the oxygen molecule and then ozone appears [5, 62]. Due to the strong oxidizing capability of ozone, it has considered for decontaminations.

For instance, before placing the implantable biomaterial (Poly(Lactide-co-Glycolide) nanofiber) scaffolds in human body, the sterilization is the important process. But most of the decontaminated methods will change the characteristics of the scaffolds, and a research shows that ozone sterilization of 2-8 exposures (each 20 min exposure) can maintain the properties of scaffolds [63]. Ozone can keep the biomaterial characteristics, however, ozone could change the mechanical and electrical properties of the polymers due to oxidized reactions [64]. Furthermore, if people are exposure 0.1 mg/m^3, it could stimulate human noses. When the concentration is over 2 mg/m^3, it will induce pulmonary edema, and continuous long time exposure will cause human hypoxia and damage of DNA. Overall, the careful use of ozone sterilization is still expected.

Nanomaterial

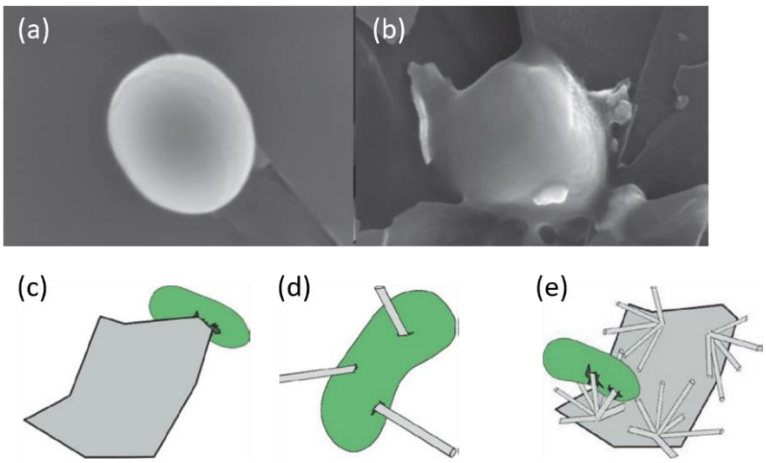

Figure 1.11 The FE-SEM images of (a) Staphylococcus aureus and (b) interaction with graphene nanoplates. The damage on cell membrane by sharp edge of (c) 2D, (d) 1D, and (e) mixing of 1D and 2D nanomaterials [65].

The decontamination effect of nanomaterial (such as graphene nanoplatelets, zinc-oxide nanoparticles, zinc-oxide microrods, and else) was found due to the nanostructure which can provide physical damage of cell membrane of microorganisms [65]. Also, a research shows that mixture of the graphene nanoplates and the dental adhesive has the inhabitation capability of adhesion and growth of biofilm on teeth *in vitro* [66]. Moreover, there is a risk of antibiotic resistance on the microorganism survived under low concentration chemical treatments such as hydrogen peroxide and else [67], but the pathogens do not show resistance with nanomaterials sterilization [65]. However, there are disadvantages of nanomaterials. Although a paper shows that the human immortal keratinocyte cell (HaCaT) and breast cancer cell (MCF-7) have no significant effect after incubation of over 24 hours with zinc oxide nanorods in

liquid phase [68], the nano-size particles in the air are probably inhaled into human lung, and it cause some respiratory tract problems [69, 70]. Therefore, like chemical sterilization, nanomaterial only could be used for medical device sterilization with secure protection.

Microwave

Microwave sterilization works with 2.45 GHz, water molecules resonate in this frequency and produce heat. The sterilization is because of the heat and also the non-thermal lethal effect of ion shifts across membranes and reorientation of long-chain molecules [62, 71]. Currently, microwave is used for medical waste sterilization in some countries (such as Brazil, Canada, Japan, Korea, Philippines, Saudi Arabia, UK and US) [72]. Metal items also can be sterilized by microwave, but certain precautions must be required. Compared with the autoclave, microwave consumes less energy for sterilization. However, microwave strongly works with water, if water contains microorganisms, it is still less efficient for the solid dry items. The control of water content is the important point in the investigation of microwave sterilization [73]. Some authors claim that microwave technique could be applied for sterilization of medical devices [62] (such as contact lenses, dental instruments, dentures, and urinary catheters) [73].

X-ray sterilization

Currently, UV light and gamma radiation are used to decontaminate, and X-ray with the intermediate wavelength of 0.01-10 nm is potential sterilization method with the best penetration compared with gamma radiation and e-beam [74]. The source of X-ray for medical use is the collision of energetic electron beam and tungsten [75]. However, during the energy transition, only 7.6% energy is converted to X-ray, and else is loss in cooling water. Compared with X-ray, gamma radiation sterilization is safer and easier control [76]. The researches show the decontamination effect of X-ray on bacteria (dose of 1000 Gy provides over 6log reduction of *Salmonella enterica* on shell egg) [77] and bacterial spores (dose of 130 Gy provides 1.5log reduction of *Bacillus pumilus* spore) [78]. Benefit of X-ray sterilization is like that of UV light, gamma radiation, and e-beam with less toxicity, but these radiation users also need to carefully generate it and avoid from the risk of radiation leakage. The mechanism of X-ray decontamination is still unclear, and the interaction between microorganism and X-ray should be deeper investigated [78].

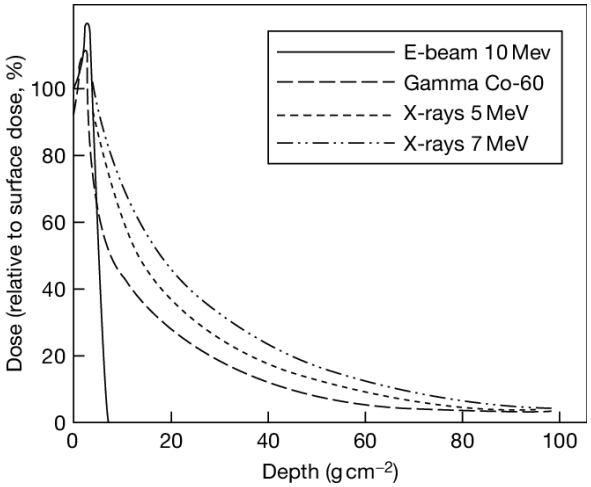

Figure 1.12 Dose decay of e-beam (10 MeV), Gamma radiation (100 keV), and X-ray (5 and 7 MeV) with depth in material [79].

Non-thermal plasmas (NTPs)

Nowadays, the biocide resistance is increasingly common, and single sterilization is less efficient for decontamination of microorganisms [80]. Non-thermal plasma, which is ionized gas providing multiple factors of sterilization, such as electric field, charged particles, reactive oxygen or nitrogen species (ROS or RNS), and UV emission [81]. NTP processes can be operated under various gas pressure and composition.

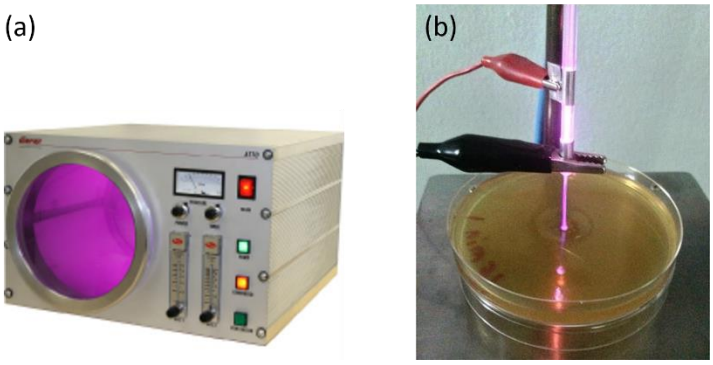

Figure 1.13 (a) Non-thermal plasma sterilizer typically under low pressure of 10^{-3} atm [82] (b) Non-thermal plasma jet treatment on *Staphylococcus aureus* under atmospheric pressure [83].

Compared with the sterilization of gamma radiation or autoclave, plasma treatment has less penetration, and NTPs is more focused on the use of surface treatments [81]. Overall, NTP is one of the potential surface sterilization method, and more detail of NTPs will be discussed in next chapter.

1.2 Cancer

Cancer, which is also called malignant neoplasm, is one of the most potential threat in modern society. As the development of technology, some lethal disease (such as smallpox) were isolated from human society, and cancer became one of the main cause of human mortality. Even though many patients fortunately escape from the death, they may face some symptoms including of cough, pain, weight loss, body shape deforms, change of social function, and else [84]. Due to these reasons, there are two objectives of cancer treatment: one is to remove the tumors (including the metastasis) and the other is improving patients' suitability.

Tumor is result of the abnormal situation that the speed of cell divide is higher than the cell died [85]. The tumor could be malignant and benign. The cells in benign tumor are noncancerous and they do not invade the near normal cells and metastasize to second location [86]. The risk of benign tumor is that the tumor can grow very large to pressure nearby tissue or organ and block the vessel. It should be removed by surgery if it is located at specific position such as in brain [86]. The common benign tumors are fibroids in the uterus and lipomas [87]. The cells in malignant tumor are cancerous and aggressive (invade the nearby tissue), and they can metastasize to other location through the circulation systems. The malignant tumor could appear everywhere in the body, including breast, intestines, lungs, *etc*. Under the microscope, the cells in benign tumor look normal, but the cells in malignant tumor have abnormal chromosomes and DNA in their darker nuclei (darker is due to cancer cell contains more DNA) [86]. Although the benign tumors have no threat in short time, they may transfer to be the malignant tumors with time [88].

1.2.1 Various types of cancer

According to the location and formation of cancer cells, the malignant tumor is separated into two groups. Liquid tumor which is known as blood cancer exists in blood vessel, lymph gland, or bone marrow. This kind of cancer has no clear shape of tumor [89]. It could be detected by blood laboratory test [90]. Lymphoma and leukemia belong to this group. Another is solid tumor, including most of cancer with tumor shape. The solid tumor is localized and could be removed with surgery, but there is still the risk of metastasis. There are five main techniques for solid tumor imaging: X-ray, computed tomography (CT), magnetic resonance imaging (MRI), ultrasound (US), and positron emission

tomography (PET). Among them, only X-ray, MRI, CT, and PET can build three-dimensional imaging [91].

The number of species of cancer is over one hundred, and tumors in different tissue or organ have various characteristics. The most common cancer types in 2018 are lung cancer, breast cancer, colorectal cancer, prostate cancer, skin cancer, stomach cancer, and liver cancer [92]. The lung cancer is induced by cigarette smoking and air pollution [93]. The breast cancer is related to the estrogens [94] and heredity [95]. The colorectal cancer frequently occurs on the elder [96] and people who have bad eating habits (consumption of red and processed meat) [97]. Age and heredity are regarded as the major cause of prostate cancer [98]. Long time exposure to ultraviolet radiation is the major cause of skin cancer [99]. Bacteria, virus or fungi could also induce cancer. Infection of *Helicobacter pylori* is a high risk of suffering from stomach cancer; high intake of salt and dietary nitrite is also the cause of stomach cancer [100]. Human papillomavirus (HPV) is the most viral infection of the cervix, and almost all the cervical cancers are related to HPV [101]. The main causes of liver cancer are hepatitis B and C viruses, and it estimates over 75% of liver cancer patients due to these viruses [102]. Absorption of fungal toxin of *Aspergillus flavus* on food (such as peanuts) and excessive absorption of alcohol would also result in liver cancer [103]. The diversity of carcinogen agents which we cannot thoroughly avoid in our lives in addition to the increase in the average lifespan of the world's population makes the probability of developing cancer high. Most of these cancers have structure of solid tumor. Therefore, there is a need for a wide range of treatments for these tumors. We will discuss the current and upcoming treatment in the following sections.

1.2.2 Main treatments

Due to specific characteristics and location of tumors, various cancer therapies are developed. They could be classified in surgery, radiation therapy, chemotherapy, and immunotherapy. The detail of these therapies is introduced in the following paragraphs.

1.2.2.1 Surgery

Surgery is the most fundamental treatment of tumor removal. It provides a chance to thoroughly remove tumors. Surgical treatment is also used in incurable patients. This treatment at the last stage helps patient feel more comfortable and have better shape by removal of tumors [103]. However, the

main disadvantage of surgery is the increase in risk of metastasis. After the surgery, the fraction of tumor tissue may transport to the circulation, and incontrollable metastasis appears. The inflammatory response due to the wound of surgery accelerates the growths of metastatic cancer [2]. For the eradication of tumor, the surgeons will not only remove the tumor but also the nearby healthy tissues and lymph nodes [104]. Surgery is useful for most solid tumor, but it is dangerous to operate in some position, in brain for example.

1.2.2.2 Radiotherapy

Photon radiation

Similar to the effect of sterilization, X-ray and Gamma radiation could make DNA damage of cancer cells. The DNA broken cells will stop dividing and die [105, 106]. X-ray for cancer therapy is generated by excited electrons in cathode ray tubes and linear accelerators. The emission of gamma radiation is from cobalt-60, radium or cesium. The efficiency of radiation therapy depends on the exposure dose. The typical therapy is advised daily 1.5-3 Gy for several weeks [106]. The advantages of this therapy are that X-ray and Gamma radiation allow for localized treatment and have a deep penetration into the tissue. Moreover, the research shows that normal cells have better recovery capability than cancer cells after treatment [106]. Nevertheless, like surgery, the residue of tumor is also the risk of cancer metastasis after radiation treatment [20]. The secondary malignant tumor also should be considered. It is estimated that about 10 % secondary malignant tumors is induced by radiotherapy [3], and in calculation, 1.7% radiation received patients suffer from the fatal cancer [107]. Moreover, the response to radiation therapy is depended on gender. Increase of dose of each Gy makes the risk of secondary solid tumor 35% higher in male and 58% higher in female [3]. X-ray and gamma radiation therapy could be used for several kinds of cancers, such as skin cancer, prostate cancer, lung cancer, breast cancer, and else. Some of them could have good efficiency by radiation treatment only, and others require multiple therapies [106].

Figure 1.14 Patient being treated by radiotherapy [108].

Curietherapy

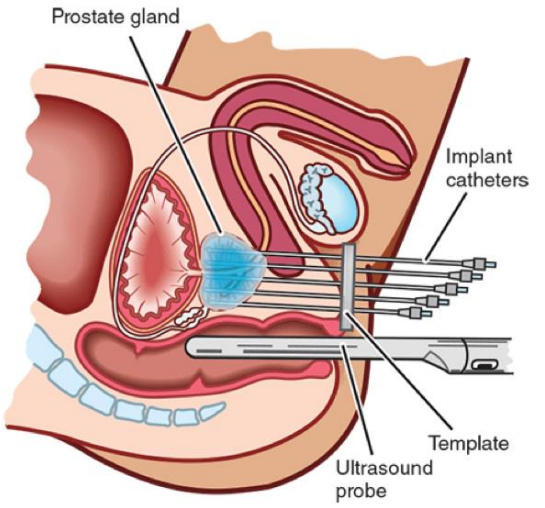

Figure 1.15 Prostate gland treatment using catheters to deliver the radiation source, under ultrasound probe monitoring [109].

Curietherapy differs from the latter technique in terms of radiation source location. In Curietherapy, also called brachytherapy (BT), the radiation source is in or near the tumor. Curietherapy was invented more than one century ago, but its development is not based on power and precision as for external radiation therapy. Recently, the techniques improved, BT source can be placed more precisely and it is still investigated [110]. Cs-137 and Ra-226 [111] are the source of BT; these radiative materials are supplied through the catheter or applicator [111]. The duration of treatment is a few minutes, a few days, or even the rest of patient's life. Nowadays, compared to external radiation therapy, BT is more precise and release higher dose to the tumor. Nearby tissue withstands less damage under treatment [110]. However, it is not good for pregnant

women or children to be treated with BT due to the radiation substance in body. Even though patients finish with the temporal treatment, they still give off radiation from their bodies for a while [112]. Curietherapy can be applied for prostate cancer, cervical cancer, head and neck cancer, gynecological cancers, *etc.* [110].

Particles radiation

Besides electromagnetic wave, particles radiation (such as electron, proton, neutron, and heavy ion beam) also could be used to break DNA and kill cancer cells. These particles radiation can be generated by cyclotrons and synchrotrons. Compared to X-ray and gamma ray, the electron beam has less penetration, and it cannot interact with the deeply tissue. Therefore, the electron beams only operate the near surface treatment [106]. Moreover, due to the Bragg's peak (the largest dissipation of energy of positive particles just before they stop), the proton beams less damage the normal cells on the route and beyond the target [106, 113]. However, the penetration depth is dependent on the initial energy. If the tumor is deep under the skin, the particles energy should be higher, and the risk is the skin break [114]. The neutrons and positive charged particles beam have higher linear energy transfer than photon radiation, and these particles radiation shows better results on radio-resistant cancer, such as renal cell carcinomas, melanomas and glioblastoma [106]. Many clinical studies combining charged particles therapy with photon radiotherapy were conducted [114].

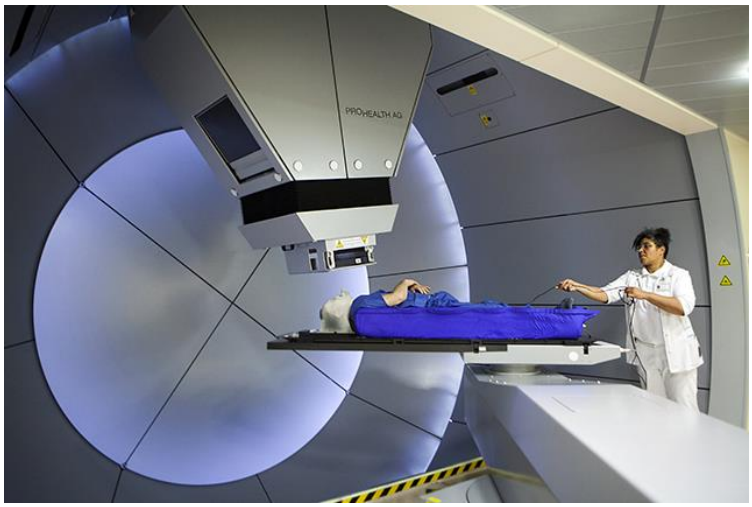

Figure 1.16 Patient being treated by proton beam therapy [115].

1.2.2.3 Chemotherapy

Chemotherapy

When metastasis occurs, surgery and radiation therapy are no longer to be used, and chemotherapy plays an important role in this situation. The effect of chemotherapy is systemic [116], and the function of that is depended on the cancer type and the drugs, but the main objective is to stop the cancer cells from growing and breeding, or directly lead these cells to apoptosis [117]. The chemotherapy is not only applied for metastasis but also for the treatment of larger size tumors (breast tumor > 10 mm) [116] or of tumors located close to lymph nodes [118] om order to increase the survival ratio. The mechanisms of chemotherapy are various, but basically, the active agents are cytotoxic [117]. Because this mechanism also affects part of normal cells, there are some side effects on patients, such as pain, fatigue, mouth and throat sores, diarrhea, nausea and vomiting, constipation, blood disorders, memorize problem, hair loss [4]. During the chemotherapy, there are several routes of drug administration, for example, intravenous injection with duration ranging from a few minutes to a few hours, sometimes artery injection, muscle or under skin injection, oral drugs administration (e.g. daily for four weeks), cream type chemotherapy applied to patients' skin [117]. Chemotherapy is widely used for cancer treatment; the main drawback is the existence of side effect due to its systemic behavior.

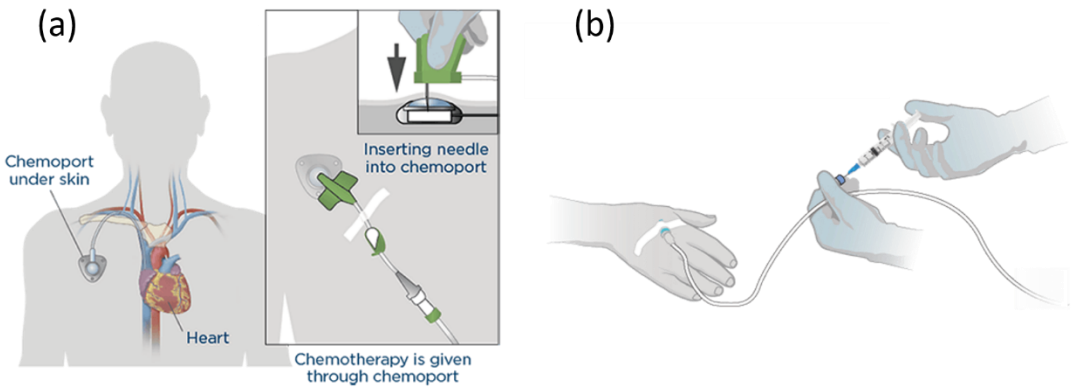

Figure 1.17 The patient is received chemotherapy through (a) chemoport on the chest and (b) injection in a vein on the hand [119].

Targeted therapy

To avoid the systemic effect, a targeted chemical treatment therapy is developed. The chemical of targeted therapy could affect the specific protein

existing in cancer cells rather than normal cells. When the protein interacts with the chemical, it will block the signals of growing and dividing, shorten cancer cells lifespan compared to normal cells, or destroy cancer cells [120, 121]. There are two forms of targeted therapy. Some active agent molecules are small enough to enter the cell membrane and directly operate [121]. Some others play the role of angiogenesis inhibitor, so they can cut the nutrient transportation by the inhibition of blood vessel [120, 121]. Both of them allow for oral administration. Targeted therapy could also use monoclonal antibodies as for immunotherapy (further described). These antibodies are injected in a blood and mark the cancer cells in order to be destroyed by the immune system; others can directly damage the targeted cells and/or induce apoptosis [121]. However, the targeted therapy does not always work successfully. For example, several types of cancer cells have no target to be treated. Even though a type of cancer has target, the effect of the therapy may not significant or may not work due to the appearance of resistance mechanism. Therefore, the targeted therapy could follow chemotherapy or radiotherapy [120, 121]. Also, the targeted therapy has some side effects (skin, hair, nail, eye problems) but different from chemotherapy [120]. Currently, the targeted therapies are applied for breast cancer, colorectal cancer, lung cancer, lymphoma, and melanoma [120].

Hormone therapy

Hormone therapy, also called endocrine therapy is applied on the hormone-caused cancer, such as breast cancer (female only) or prostate cancer. The two directions of hormone therapy are adding the hormone and inducing hormonal production in human body. Before surgery or radiation therapy, the hormone therapy usually helps to smaller the tumor size. Also, the therapy could lower the risk of cancer recurrence after other therapies [122]. There are some side effects due to the control of hormone, including hot flashes, diarrhea, nausea, fatigue, low interest in sex. Especially, for prostate cancer patients, the therapy makes them weaken bone and larger the breast, and vaginal dryness for women with breast cancer [122]. The forms of hormone therapy could be pills and injection. Also, the removal of organ with surgery could help, for instance, the ovaries for breast cancer and the testicles for prostate cancer [122].

1.2.2.4 Immunotherapy

Immunotherapy is more natural cancer treatment with patient's own immune system including white blood cells and organs of the lymph system [123]. In

normal situation, immune system can detect the abnormal cells and attach or destroy them. However, in other situations, the cancer cells could escape from the immune system. Moreover, the cancer cells could produce some kinds of protein on the cell membranes, and the protein would turn off the function of immune cells. Cancer cells could also change the nearby normal cells and perturb the response of immune systems. Immunotherapy is developed to solve these problems. Immune checkpoint (controller of the immune response) is inhibited by the therapy, and immune cells would more operate on the cancer cells.

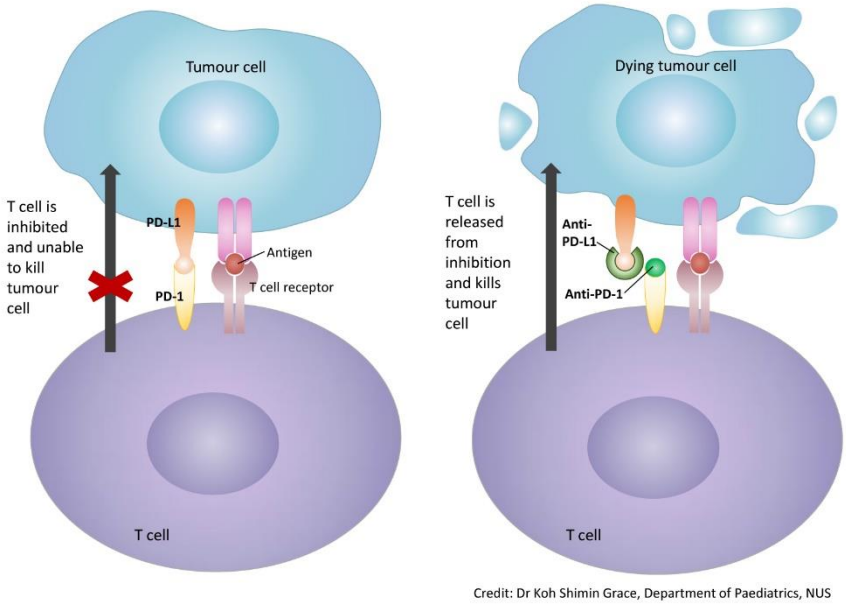

Figure 1.18 PD-L1 and PD-1 are the checkpoint of anticancer. In immunotherapy, anti-PD-L1 and anti-PD-1 are used for immune cells to diagnosis the tumor cells [124].

In T-cell transfer therapy, the immune cells are separated from the tumors. After cultivation in laboratory, these cells are injected in a vein to attack the cancer cells. Monoclonal antibodies which is introduced in targeted therapy is another kind of immunotherapy. These antibodies could mark the cancer cells, and immune systems could distinguish them through the mark. Besides, treatment vaccine differing from prevent vaccine is used to increase the capability of immune system to kill more cancer cells. There are also immune system modulators applied for enhancement of immune response [123]. However, sometimes the over exited immune response would attack the normal cells or tissues. The side effects of immunotherapy are inflammation response or flu-like symptoms [125]. The substance of immunotherapy could be injected in a vein, made into pills or capsules, or rubbed on the skin surface like cream [123]. Moreover, the immunotherapy could work directly in a bladder. A catheter is

inserted into the bladder through the urethra, and the drugs is injected into bladder. The intravesical therapy can avoid the systemic effects of oral and injection treatment [126]. Immunotherapy is currently applied for varies cancers, including breast cancer, colorectal cancer, kidney cancer, lung cancer, melanoma, prostate cancer and else [127]. This most natural therapy with oneself immune systems is still under development to treat wider range of cancers.

1.2.3 Upcoming technologies

Even though there are the various of current cancer treatments, the number of cancer death is still high. The cancer therapies with higher efficiency of tumor cells removal and less side effects are urgently developed.

1.2.3.1 Electroporations

Electroporation is combination of pulse electric field application with chemical molecule or biological gene admixture. In normal situation, these substances are too large to permeate the cancer cell membrane. The characteristic pulse electric field propagated by the current induces transient pores formation in the cell membrane due to intracellular electrophoretic mechanism and allows for molecules entering the cell [128].

Electrochemotherapy

Electrochemotherapy (ECT) is one of the application of electroporation. Through the electroporation, the cytotoxic drug can flow into the tumor cells and destroy them. Typical operating conditions correspond to an electric field generated under the condition of 8 square pulse of 100 μs with repetition frequency of 1 Hz [128, 129]. The given voltage is depended on the number and the shape (needle or rod) of electrodes, and the local electric field on the tumor is about 400 V/cm [129].The treatment process of ECT can be described as follows. Firstly, the systemic or intratumoral drug is injected in patient's body or directly into the tumor. Once drug is in direct contact with the tumor, a pulsed electric field is applied to the tumor thanks to electrodes which are touching or inserting the tumor, so creating temporal tunnels for drug. Finally, the voltage source is turned off, the tunnels close, and drug remains in the tumor cells. The whole procedure of ECT is about 25 to 30 minutes duration [128]. With such an electrode arrangement, ECT technique is limited to the treatment of tumors located close to the skin surface, such as melanomas, sarcomas, and other types of skin cancer, cervix leiomyosarcoma, and breast cancer [128]. Studies show a

control of melanoma tumor size after ECT for more than 70% of treated patients even two years after treatment [130, 131]. The side effect of ECT is minor, and the patient receiving ECT got painful in low ratio. ECT also could be used on metastasis tumor, and on the contrary to radiation therapy, patients can withstand repeatedly ECT [128]. Due to the electricity and the needle inserting, the patients holding cardiac pacemakers and/or receiving anticoagulant treatment are not suitable for ECT. Today, ECT is still under development for the treatment of tumors located deeper in patient's body.

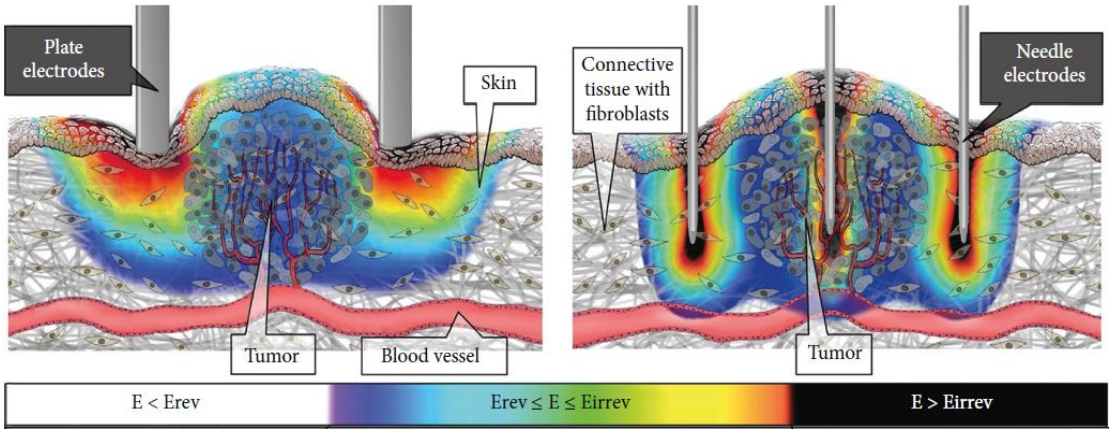

Figure 1.19 Electrode touching (left) and inserted (right) tissue near tumor; electric field distribution showed (Erev and Eirrev: electric field of reversible and irreversible electroporation limits respectively) [129].

Irreversible electroporation

Besides the application of reversible electroporation (RE), irreversible electroporation (IRE) which can induce non-thermal tissue ablation is also developed for cancer treatment. The main mechanism of IRE is to make nanopores on cell membranes, break the cancer cells balance, and lead to cells death [132]. Collagenous and other protein and/or lipid-based tissue can be preserved during IRE treatment, and it means that IRE is suitable for the cancer treatment near critical blood vessel [132]. The pulse electric field of IRE is 2500 V/cm with 10 pulse widths of 100 μs, and electric field is rotated with angle of 90° with frequency of 1 Hz. The next round will start after 45 s [133]. The tumor cells lose the cells balance and go into apoptosis in minutes to hours after IRE treatment. Apoptosis of cancer cells would induce immune response [132]. Studies provide that immune system has higher efficacy due to the faster T-cell proliferation after IRE, and it also reduces the risk of metastasis [134]. Currently, IRE has positive results on lung, kidney, brain, prostate, pancreas, and other organ systems [132].

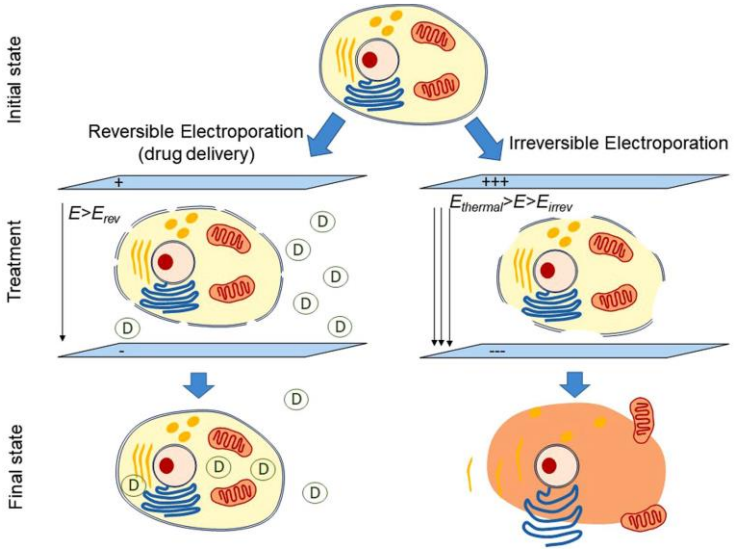

Figure 1.20 The different mechanisms of electroporation cancer therapy: electrochemotherapy (left) and irreversible electroporation (right) [135].

1.2.3.2 Gene therapy

Gene therapy aims to modify the DNA or mRNA of cancer cells to achieve the objective of cell apoptosis through various mechanisms. The methods of gene modification are divided into viral carriers (e.g. adenovirus, AAV, Herpes simplex virus) and non-viral gene delivery (e.g. electroporation, micro-injection, gene gun, tattooing, laser and ultrasound) [128]. There are five directions of gene cancer treatment as further detailed: suicide gene therapy, DNA vaccine, gene silencing, transcription factor-targeted oligodeoxynucleotide (ODN) decoy therapy, and gene correction therapy [136].

In suicide gene therapy, the DNA expression of cancer cell is modified by viral vectors or electroporation [128], and the cells will convert the nontoxic drug into toxic metabolites. These toxic products will lead cancer cells to apoptosis. Suicide gene therapy is suggested to treat head and neck squamous cell carcinoma, ovarian, and endometrial cancer [136]. The other direction of gene therapy is DNA vaccine. The principle of vaccine is to inject DNA modified plasmid in normal cells to increase the protection capability of immune system. DNA vaccine is transmitted in normal cells through the tunnel of electroporation [128]. Therefore, DNA vaccine treatment can inhibit but also prevent from cancer growth. A study on mice shows that DNA vaccine successfully protects from tumor cells attack and spread, so it is hopeful for the metastasis treatment [136]. Currently, DNA vaccine could be applied on breast cancer, prostate cancer, melanoma, and cervical cancer for mice experiments

[128]. Gene silencing is also one of the gene therapy research field. In gene silencing treatment, small interfering RNA (siRNA) is used to interfere the specific gene expression and makes the messenger RNA (mRNA) degrade. Gene silencing reduces the abnormal gene expression (e.g. cancer growth, spread, survival, and therapy resistance) in cancer cells [136], but gene silencing would not completely eliminate the gene expression and it would leave necessary gene expression which could maintain cell working. Currently, gene silencing is tested on mice squamous cell carcinoma, lung cancer, and mammary cancer [136]. Transcription factor-targeted ODN decoy therapy is another type of gene therapy. ODNs are used to inhibit the activity of transcription factor (the controller of cell growth and breeding) of cancer cells. This therapy was successfully tested on mice lung cancer, and human trials on head and neck cancer also show positive results [136]. Gene correction therapy aims to fix the broken tumor suppressor gene in cancer cells. Tumor suppressor gene is related to apoptosis pathway. Gene correction therapy makes the primary and metastasis tumors of squamous cell carcinoma, lung, thyroid, colon, head and neck, thymoma, vaginal cancer stable on human trial [137, 138] Overall, metastasis treatment and the selective effect bring the expectation of various gene therapies.

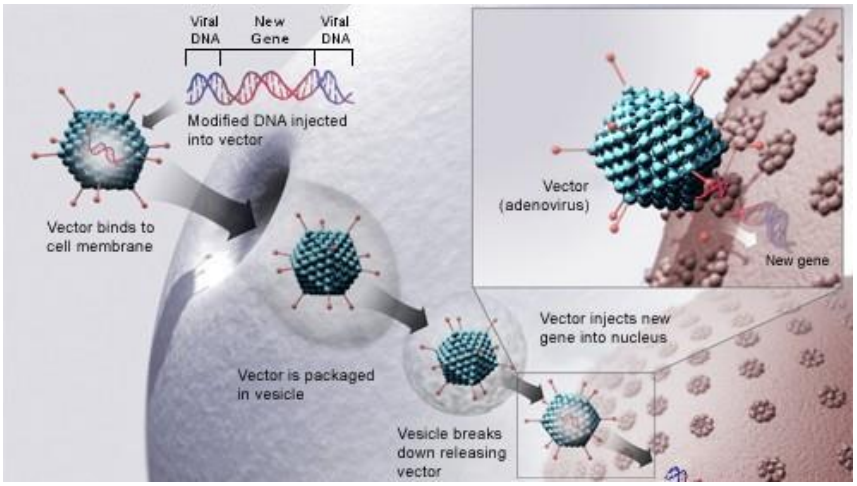

Figure 1.21 Adenovirus vector bringing modified DNA through cancer cell membrane and injecting gene in cell nucleus [139].

1.2.3.3 Virus therapy

Oncolytic virotherapy

Incidentally, cancer patients have been found to go into remission following a viral infection. Indeed, some viruses (e.g. measles, reovirus, Newcastle disease virus, and adenoviruses) have oncolytic or cancer-killing properties [136, 140]. Virus is not always human's enemy; it is expected to help for cancer treatment

in the future. Then, thanks to the development of genetic engineering, viruses can be modified to increase their lethal potential on cancer cells. The virus is injected into the patient, infects cancer cells, and kills them. The process will induce the immune response, and in turn the immune systems attacks tumor cells. The antitumor effect is systemic, and it can also kill homologous metastatic tumor cells [140]. When oncolytic virotherapy is combined with genetic modification (e.g. gene of immunostimulator) or virus-resistance drug (e.g. anti-viral immune response reducer), the efficacy of therapy is enhanced. Studies provide that oncolytic virotherapy has efficacy on lung cancer, head and neck cancer, metastatic colorectal cancer, cervical cancer, prostate cancer [140].

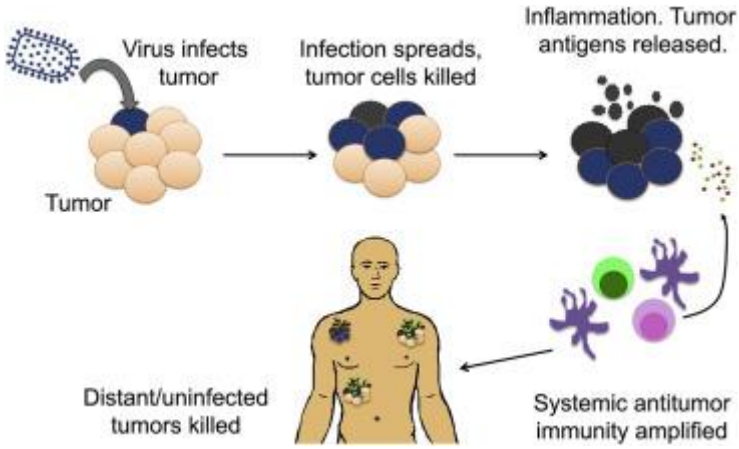

Figure 1.22 Cancer-killing process of oncolytic virotherapy [141].

1.2.3.4 Non-thermal plasma

Non-thermal plasmas (NTPs) are expected for not only surface decontamination but also cancer treatments. The first paper describing the use of NTP under atmospheric pressure for the treatment of cancer was published in 2007 [142], and then, until 2016, there are over 100 papers were published and over 20 kinds of cancer trials, including brain cancer, skin cancer, breast cancer, colorectal cancer, lung cancer, cervical cancer, leukemia, hepatoma, head and neck cancer, *etc* [12]. More detail about NTP treatment will be introduced in next chapter.

2 NONTHERMAL PLASMA FOR BIOMEDICAL APPLICATIONS

2.1 Theoretical background of non-thermal plasmas

A plasma is a gas which is either partially or fully ionized. Sometimes referred to as a 4th state of matter, it may be noted that more than 99% of matter in the universe exists in the form of plasma (because the matter in stars is ionized, and much interstellar gas also exists in the ionized state). These types of plasma are ionized either by collisions at high temperatures as in the case of stars, or by radiation as for the case of interstellar gas. In the laboratory, plasma may be created by the use of electrical discharges. The following sections describe the basic physics of an electrical discharge, and some of the methods used to create them in a laboratory setting.

2.1.1 Electron avalanche

The basic physics of an electrical discharge was first described by J.S. Townsend at the end of the 19th century. Townsend's theory seeks to explain the mechanism for a breakdown in the insulating properties of a gas between a positively polarized anode and negatively polarized cathode. Depending on the electric potential applied between these electrodes, the distance between the electrodes, and also the shape of the electrodes, the electric field present in the gas may be sufficient to lead to an *electron avalanche*. The theory therefore presupposes the presence of an electron in the gas-filled region between the electrodes, a so-called seed electron. There are various possible sources for seed electrons including ionizing radiation from either terrestrial or cosmic sources, as depicted in Figure 2.1. When one of these seed electrons is accelerated by the electric field, it acquires an amount of energy proportional to the electric field and to the distance over which this acceleration occurs. The average value of this distance is often referred to as the mean free path of the electron in a gas, and depends on the gas density: at low gas density (or pressure), a particle will travel a greater distance before encountering another particle. If the energy acquired by the electron is superior to the ionization energy of the bulk gas, the collision may result in the ionization of the bulk gas molecule or atom, thereby creating a positive-ion electron pair. This process may repeat itself and result in an exponential increase in the population of free electrons in the gas gap.

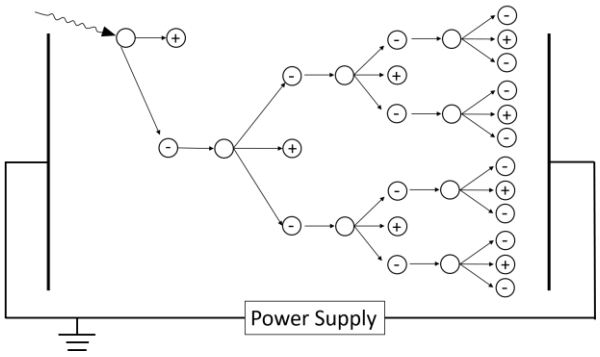

Figure 2.1 Electric avalanche by electron-neutral particle collision

The kinetic energy of seed electron is therefore determined by the applied voltage, electrode spacing, and the mean free path of the gas. For a fixed separation distance between the two electrodes, a higher applied voltage provides a higher electric field. Seed electrons can therefore obtain adequate energy for ionization over a shorter distance. More neutral gas can therefore be ionized. The mean free path may be thought of as the particle acceleration length before collision. The length is related to density of gas particles

$$l \propto (\sigma n)^{-1}$$

where l is mean free path, σ is the ionization cross section, and n is the particle density which may be found from a first approximation from the ideal gas equation:

$$PV = nKT$$

where P is pressure, V is volume, K is Boltzmann constant, and T is the temperature. If the mean free path is short, or in the other words, if the gas density or pressure in the system is high, then a seed electron may not be accelerated up to the point of having sufficient kinetic energy for ionization. On the other hand, if the mean free path is very long, the seed electron may reach the electrode before collision. This situation is the case of vacuum insulation.

2.1.2 Pachen's law

Paschen's law describes the relation between onset voltage of discharge or arc, the feeding gas pressure, and the gap length of cathode and anode.

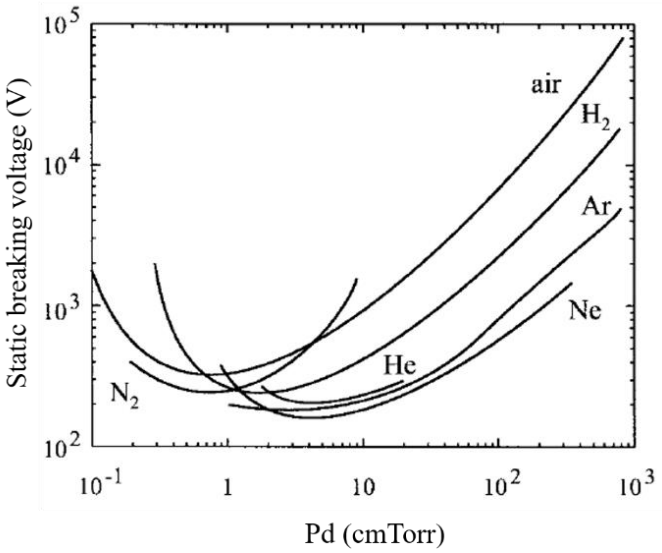

Figure 2.2 Paschen's curves [143].

Figure 2.2 shows the Paschen's curve of different kinds of gases. On the right side of the figure, for conditions near atmospheric pressure (760 Torr), and for distances on the order of millimeters or higher, nitrogen gas has the highest breakdown voltage and that of noble gases (He, Ne, Ar) are lower.

Table 2.1 The first ionization energy of some gas species [144].

	N_2	O_2	H_2	He	Ne	Ar
First ionization energy (kJ/mole)	1503	1175	1488	2373	2080	1520

2.2 Non-thermal plasma generators

Electrical discharges may appear in many different situations, and have different characteristics depending on the electrode nature and arrangement, the nature and density of the gas milieu in which the discharge develops, and also on whether the electrodes are separated by a solid insulator. This section will present and discuss several categories of electrical discharges: glow discharges, corona discharges, and dielectric barrier discharges.

2.2.1 Glow discharges

Glow discharges get their name from the diffuse emission of light which is seen to emanate from the plasma region. While the history and background of this category of electrical discharges is vast and beyond the scope of this manuscript, some general comments may be made here. work under the low pressure condition with noble or molecular gas and commonly seen in the plasma in fluorescent light bulbs. This kind of discharge can be powered by DC, AC, or RF

sources and requires lower input voltage (according to Paschen's curve). When the discharges appear, the positive ions are accelerated in the direction of the cathode. The impact of these ions on the cathode surface leads to the creation of secondary electrons, which in turn are and accelerated by the electric field to excite other gas particles, leading to a self-sustaining discharge. This type of electrical discharge leads to a homogeneous plasma throughout the gas volume. Much of the energy input into this type of system is ultimately released in the form of visible and ultra-violet radiation (via the release of photons from excited states or from radiative recombination of electron-ion pairs), and hence the name glow discharge. Glow discharges are currently applied on industrial scales for etching, deposition of thin films, lasers, lamp, and display [145].

2.2.2 Corona discharges

Corona discharges get their name from the fact that they appear to extend from sharp points in the shape of a crown. They can be generated in air at atmospheric pressure in proximity to the edges or corners of conductors at high electric fields. They were even observed in antiquity at the top of ship's masts at sea due to the electric field created by the Earth's natural electric field, and given the name St. Elmo's fire. In the laboratory, corona discharges may be created between two electrodes, one of which may be a point or a wire, the other typically being the wall of a tube or some other planar counter-electrode. The electrodes, separated by a gas gap, may be polarized in alternating, continuous, or pulsed regimes. At atmospheric pressure, the breakdown electric field is about 3kV/mm as mentioned before, but in the case of an sharp point or this wire electrode, field enhancement can lead to the situation where the breakdown field strength is attained only in the vicinity of the high field strength electrode. In the case when the field enhancement happens at the anode, an electron avalanche may occur in the high field zone; the light, high mobility electrons are transported by the field to the anode, leaving behind a zone of positively charged ions. This so-called space charge creates its own local electric field, and therefore in a way acts as an extension of the anode. An electrical discharge which propagates in this manner is referred to as a streamer. During streamer propagation, photoionization plays an important role to provide new electrons. The high electric field and the new electrons cause the new avalanches, and so on. Previous research shows that lower electric field of 5kV/cm is enough for the new avalanche and propagation the streamer [146]. It can be noted that an inconvenient feature of this type of discharge when applied in a practical way is that, if the streamer propagates all the way to the

cathode, a conductive path now exists between anode and cathode. The voltage between electrodes then drops abruptly, the current increases greatly, and an electric arc is formed. There are different methods to avoid the formation of an arc; the simplest is to keep the voltage low enough and the electrodes distanced enough to where the streamer propagation does not reach the cathode.

Nowadays, corona discharges are widely applied in industry, for example, for the modification of the surface structure of fibers to adapt printing [147], for ozone generator when the feeding gas is air or oxygen [148], for the removal of toxicity in the air [149], and for surface decontamination [150], etc.

2.2.3 Dielectric barrier discharges (DBD)

A convenient and simple way to prevent the formation of an electric arc between electrodes is to place an electrical insulator between them, a dielectric barrier. A dielectric barrier discharge (DBD) is the name given to a discharge in this kind of electrode geometry, depicted in Figure 2.3. The application of DBD is similar to that of corona discharges, such as surface decontamination [6], water purification [151], etc. As the main plasma generation configuration in the thesis, a detailed description of DBD is made in this section.

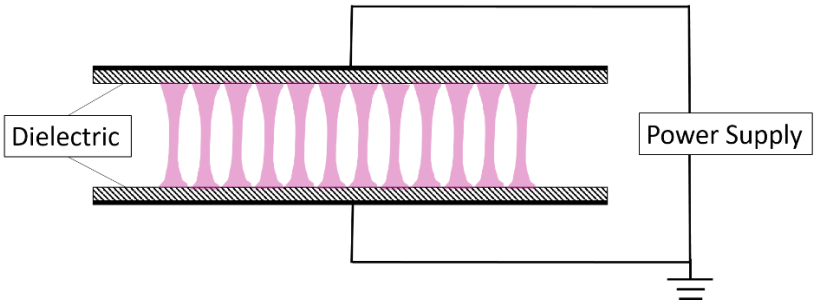

Figure 2.3 The simple DBD configuration

An example of a DBD configuration consists of two electrodes playing roles of the high voltage and ground, separated by either one or two dielectric barriers. Working gas flows in the space between dielectric barriers. Different gases have different onset voltages according to Paschen's law. When high voltage is applied to the electrodes, plasma is generated by Townsend discharges. The structure of dielectric barrier ensures that the arcing will not occur. It may be added that, with the protection afforded by a dielectric barrier, biological samples are at lower risk of exposure to dangerous currents. This reasoning may be extended to the case of a living organism or even a human patient in the case of medical applications of electrical discharges.

A tubular arrangement scheme of DBD is used for the generation of a propagating form of plasma sometimes referred to as a plasma bullet or plasma jet. The feeding gas flows inside the tube and provides the region for gas excitation and ionization. The propagation of plasma has specific direction which follows the gas flow and the electric field. The tube plasma generator is showed in Figure 2.4 :

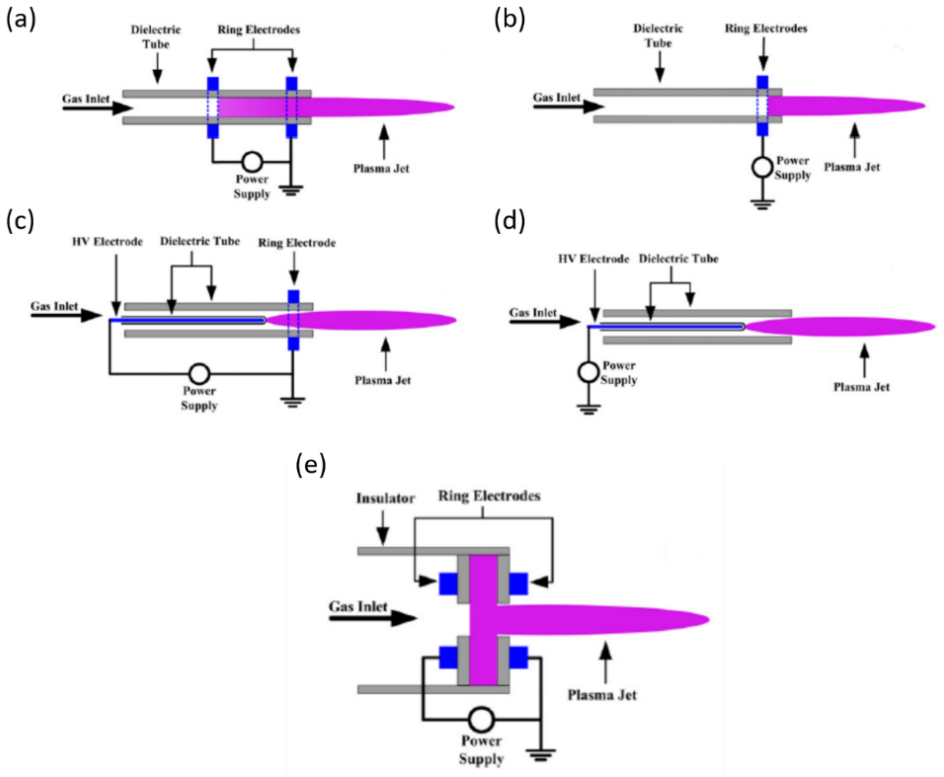

Figure 2.4 Several kinds of DBD in tube scheme [152]. Figure (a), (b) and (c) are the rings electrodes, and (c) and (d) are the configuration of rod electrode for high voltage. Among these different arrangements, the grounded electrode is absent in (b) and (d).

Plasma bullet is generated in the high electric field region inside the tube. There are several kinds of applied high voltage, such as pulse signal or sinusoidal voltage. No matter which voltage is applied, the discharges in DBD are related to Townsend's discharges. The generation of plasma bullet can be separated in three processes: displacement current and charge accumulation, Townsend's discharges, and charge saturation.

A precise description of the mechanism of the propagation of plasma bullets is still needed. To the naked eye, the zone where plasma bullets occur appear as continuous plasma plume, however, the discrete bullet shape is observed by high speed camera.

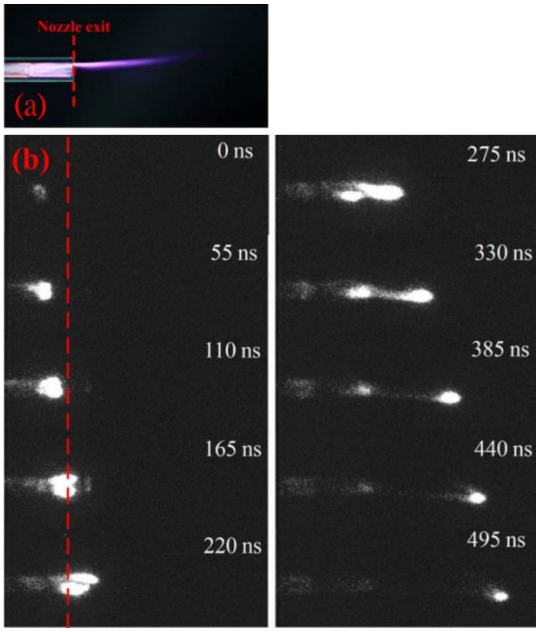

Figure 2.5 Photos of plasma plume are taken by (a) Cannon camera and (b) ICCD(intensified charge coupled device) [153].

According to experimental results, the change of voltage pulse width impacts the length of plasma plume. The plasma bullet is not really like a "bullet", but two zones may be delineated: a luminous channel and a dark channel. The luminous part is the ionization wave which produces its own electric field at the tip of the plasma plume. The motion of ionization wave can be regarded as a fluid containing charged particles which are caused to move along the electric field lines by Coulombic forces, but also by the diffusion of particles moving from the higher to the lower particle density region [154]. Also, the high field created by the charged particles in the ionization wave lead to a simultaneous streamer-like mechanism: electrons produced by photoionization which is a type of photo-electron interaction [155] can be accelerated and collide with other ground state atom or molecule like the Townsend's discharge. This also makes the avalanche in front of the streamer tip and the ionization wave move. The mechanism was demonstrated by Prof. Boeuf in University of Toulouse, and the trend of demonstration result is consistent with the experiment. Also, along the streamer path, deposition of positive charges on the inner wall of the tube has been observed by Mussard *et al* in 2013 [156].

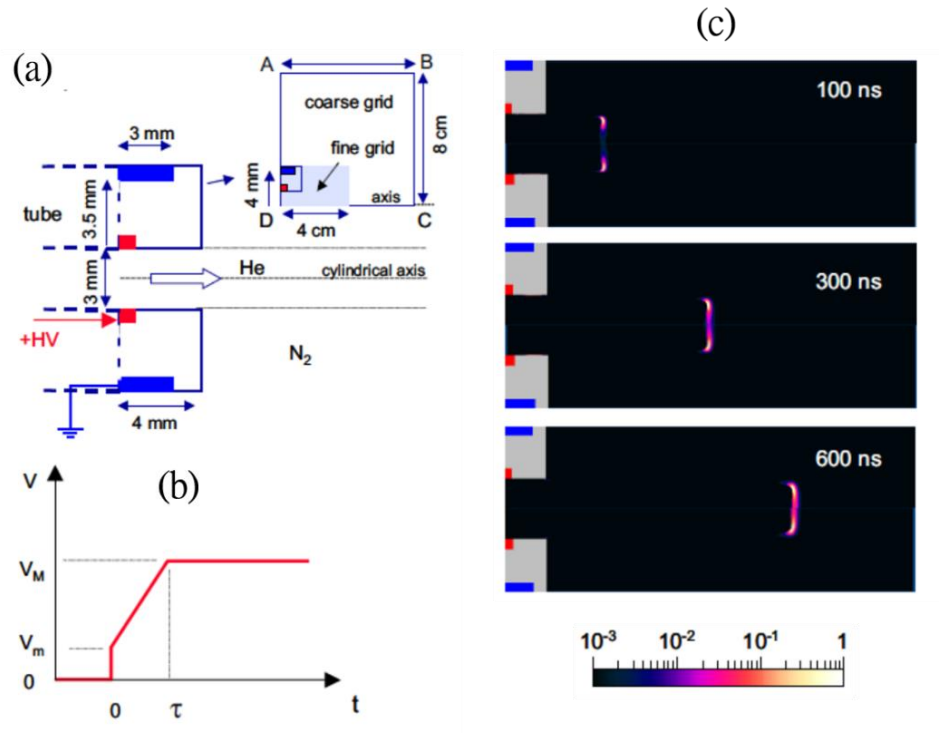

Figure 2.6 (a) Configuration of Boeuf's demonstration. (b) Parameter of given voltage where V_m=1kV, V_M=4kV, and τ=50ns. (c) The ionization rate distribution. The units of the figures are 2.5×10^{21} $cm^{-3}s^{-1}$, 0.4×10^{21} $cm^{-3}s^{-1}$, 0.15×10^{21} $cm^{-3}s^{-1}$ at 100 ns, 300 ns and 600 ns.

In Figure 2.6(c), the plasma bullet is demonstrated in Helium jet (He tube). The region of higher ionization rate looks like a ring shape where is the interface of He and N_2. It matches Vladimirov's prediction that discharges appear at the interface of two media [157]. The ring shape is also explained by Penning effect.

$$He_m + N_2 \rightarrow He + N_2^+ + e^-$$
$$k = 7 \times 10^{-11} cm^{-3} s^{-1}$$

Due to the Penning effect, the free electron for acceleration and collision can be generated near the edge of a He tube [158]. The dark channel connected the tip of streamer (plasma bullet) and the high voltage electrode. There is a low but continuous current carried by electron flow. The electron distribution is demonstrated by Prof. Beouf [154].

Figure 2.7 This demonstration electron distribution used the same configuration as Figure 2.6. The units of the electron density are 5 × 10^{13} cm^{-3}, 3 × 10^{13} cm^{-3}, 2 × 10^{13} cm^{-3} at 100 ns, 300 ns and 600 ns [154].

The electron flow is near the edge of helium tube, this region is also the route of the ionization wave. After the ionization wave (plasma bullet) passes, positive charges remain [156]. The accumulation of positive charge on the inner wall of tube attracts with electrons, so the electron flow has its own hollow shape (shown in Figure 2.7). The electron flow in dark channel follows the Ohm's law because the conductivity of plasma is finite. The energy loss (voltage drop) is also related with the resistance of this part of plasma. The length of plasma is directly corresponding to the critical voltage for ionization.

The voltage plays a most important role on ignition and propagation of plasma bullet. Even though, plasma bullet is not exactly the same as corona discharges, ionization waves can propagate from high voltage electrodes over some distance depending on the energy imparted by the electric field. The velocity of plasma plume can be measured by two current probes placed at grounded copper rings at positions along the bullet's path [156]. The propagation is due to the electric field in front of plume and strongly dependent on input voltage. The length of plasma plume extends as the increase of flow rate of noble gas until its critical value, and then the length shortens. Chen *et al* [159] provided the relation between the Reynolds number of argon gas flow and the plasma

plume length. In the case of high gas flow rate, the plasma becomes unstable due to turbulence, and the plasma propagation length decreases [160].

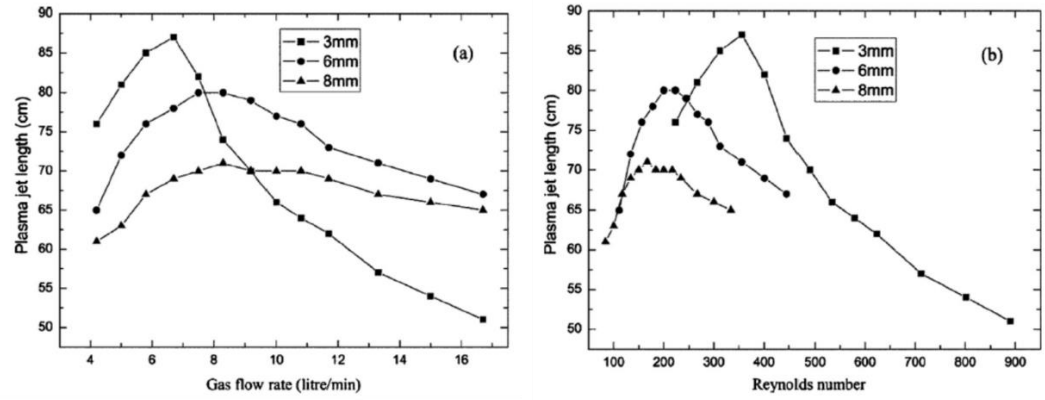

Figure 2.8 Relation between plasma plume length and (a) gas flow rate and (b) Reynolds number in three sizes (3 mm, 6mm, and 8 mm) of tube [159].

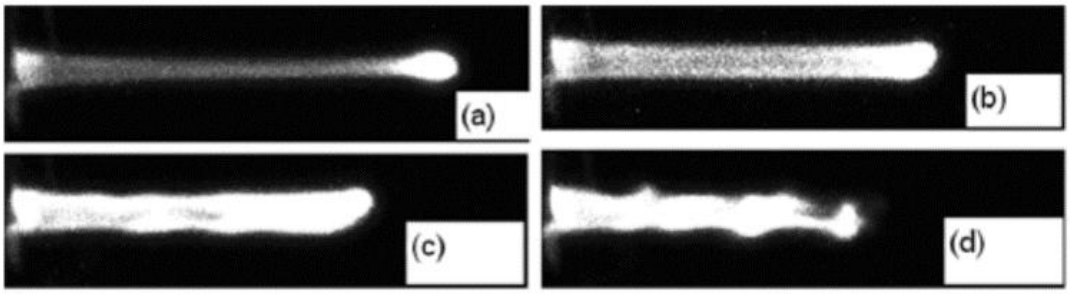

Figure 2.9 The shapes of plasma plume change under different He flow rate which are (a) 6.6 $Lmin^{-1}$, (b) 8.8 $Lmin^{-1}$, (c) 11 $Lmin^{-1}$ and (d) 13.2 $Lmin^{-1}$ and applied voltage V = 5 kV [160].

The width of voltage pulse is related to the energy supply of plasma bullet. When the width increases from several hundred nanoseconds to about one thousand nanoseconds, the propagation of plasma bullet elongates [160]. There is a critical width around one thousand nanoseconds, and then the length of plasma plume goes into saturation. The voltage rise duration also influences the onset voltage. The two rings system can be regarded as a capacitor, and this capacitor is charged during the voltage rise. When the charges in the capacitor result in an electric field sufficient to start a discharge, the gas inside the tube starts to be ionized. However, if the duration of the rise time is too short to charge enough in capacitor, the onset voltage will be higher [154]. At the same time, the discharge current is higher and plasma plume is longer [161].

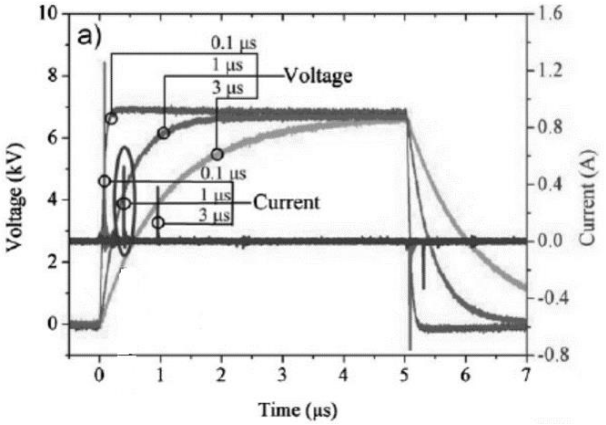

Figure 2.10 Waveforms of current peak and onset voltage for three different raising time [161].

In the work of Mericam-Bourdet [160], a relation between pulse frequency and plasma propagation has been demonstrated. The frequency may need to be controlled simply to adjust the power of the process for a given application. When the period between two plasma bullet is shortened (high frequency), the energy dissipation will have less time to take place before the next ionization waves arrives. Therefore, the energy gain and the energy loss have a new balance; this new balance leads the plasma bullet to propagate farther.

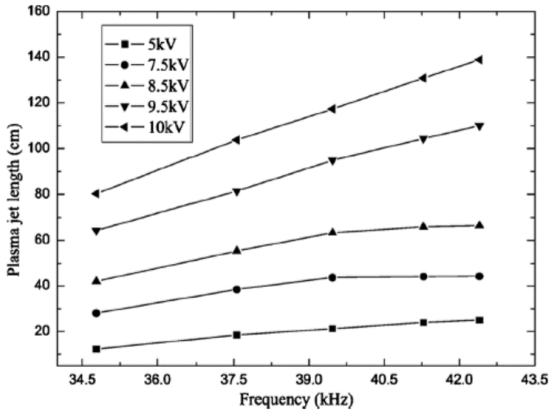

Figure 2.11 The plasma plume length for different power supply frequencies on different applied voltage. Argon flow rate: 8.3 $Lmin^{-1}$ [159].

Here it may be noted that electrical discharges, when used for applications in the healthcare sector, and especially if envisaged for use on human patients, should be subject to strict safety requirements. The presence of a dielectric barrier is therefore a must in order to minimize the risk of short circuiting between the electrical energy source and the patient. Other precautions may also be taken, for example in the design of the electrical energy source such that, in the event the compromise of the dielectric material, that the resulting rise in current will cause a large and rapid drop in the applied voltage. It is

important to realize that this may be done by both active (current detection and control loop response in the case of a rapid current rise beyond some pre-determined threshold) and passive (simply increasing the output impedance of the source using high value resistors) elements in the power supply.

The next two sections of this chapter will deal with the application of electrical discharges to surface decontamination and to plasma medicine.

2.3 Application to micoorganism decontamination

Non-thermal plasma (NTP) generated by various sources has been applied on microorganism decontamination for decades. Due to its non-toxicity, low temperature, and safety, NTP is suitable for decontamination of thermally sensitive materials [162]. NTPs are widely used for microbial agent decontamination, including virus (T4 Phage [9], MS2 Phage [9, 7, 8, 10], Potato Virus Y [163]), planktonic bacteria (*E. faecalis* [164], *S. aureus* [164], *E. Coli* [165, 166, 6, 167], *Listeria monocytogenes* [165, 167], *W. confusa* [168], *Salmonella Typhimurium* [167]), biofilm (*E. faecalis* [164, 169], *P. agglomerans* [170], *C. albicans* [171, 172], *S. aureus* [173], *W. confuse* [168], *Salmonella* [174], *P. aeruginosa* [175]), spores (*G. stearothermophilus* [162], *Bacillus subtilis* [176]), *etc*.

Assays are applied to determine the efficiency of plasma treatment: colony counting for bacteria and plaque assay for phages. Colony counting quantifies the number of viable colony forming units (CFU): the overnight viable microbial number on Petri dishes, and the microbial structure can be observed by fluorescence microscopy or transmission electron microscopy (TEM). A plaque assay similarly quantifies the number of plaque forming units (PFU) for the case of phages. The specific procedures involved with these assays will be described in the next chapter.

2.3.1 Comparison of plasma sources for decontamination

Low pressure plasma (glow discharges):

The main expected anti-microbial effects of low pressure plasma for decontamination are UV/VUV light, radical species, and etching by the impact of charged particles. UV light can interact with the DNA of bacteria or viruses, resulting in photochemical lesions which then lead to microbe death or mutation. Low pressure plasma has been used as a UV source for water sterilization [177]. A study provided by Lerouge *et al* (2000) shows that the

membranes of bacterial spores can resist UV light, but not VUV light generated by low pressure plasma [178]. The chemical products of low pressure plasma are dependent on the gas inside the reaction chamber. If the feeding gas is air, reactive oxygen and nitrogen species are produced (O and OH radicals, H and N atoms, O_3, HO_2, NO, N_2O, NO_2, N_2O_5, and HNO_x molecules) [179]. Among these, the radical species O and OH have high efficiency for sterilization, as does ozone. Hayashi *et al* (2006) found that the number of *Bacillus stearothermophilus* spores is reduced 78% or 88% after 5 min exposure to air or oxygen plasma chemical products [179]. The authors state that the spore membranes are penetrated due to etching. The etching can damage the protein of the membrane and provide a channel for reactive species to reach the core [178]. Low pressure plasma has high efficiency for decontamination, but there are still some disadvantages: The UV/VUV emission can damage not only bacteria or viruses but human cells, the etching process will damage the surface of materials or instruments, and the pressure is too low for convenient usage.

Corona discharges

Literature may also be found on the use of corona discharges for microbial decontamination. Corona discharges also create pathways for the inactivation of microorganisms, such as thermal effects, radical species, charged particles, and UV light [180]. Usually, corona discharge devices use a geometry of either point to plane of wire to concentric cylinder to create an inhomogeneous electric field, in atmospheric pressure air. Studies of corona discharges on surface decontamination have been done in numerous kinds of strains: *Pseudomonas aeruginosa* [180], *E. coli* [180, 181, 182], *Streptococci* [183], *C. albicans* [184, 182], *S. epidermidis* [182] etc. Even though corona discharges are widely used and convenient, there are some drawbacks to it. If the input voltage is too high, corona discharges transform to sparks. Also, the uninsulated electrode represents a risk for a sample or a human to become connected with high voltage directly. Therefore, the dielectric barrier electrode is developed.

Dielectric barrier discharges (DBD)

As the name of DBD implies, the electrodes are separated by dielectric material, which adds a level of safety vis-à-vis prevention of full breakdown for the treatment of biological systems. Moreover, in the case of plasma propagation along the length of tubes, the treated region can be 1 m away from the high voltage electrode. Therefore, the sample can be *in vitro* or *in vivo*.

The various ways that DBD plasma may act on biological systems, which are similar to those of glow discharges and corona discharges, are via chemical reactions with reactive species created in the plasma, by the impact of charged particles, by thermal effects, and via irradiation by UV light (dependent on feeding gas). Plasma treatment can be roughly divided into direct and indirect effects on biological systems. Indirect treatment refers to the situation in which a medium such as water is "activated" by plasma and then put into contact with the biological sample, while direct treatment is where a plasma is in either direct contact or in the immediate vicinity of the treated biological system.

A DBD generator may be used either to treat a sample directly on the dielectric surface, or on a remote surface in the case of a propagating plasma jet. These two configurations differ in that the surface plasma can treat the sample over a larger area, but the sample should be closer to plasma generator. The plasma jet configuration may be more convenient and safe, especially for the treatment of a patient. The following sections will give an overview of some of the previous studies of DBD plasma treatment on planktonic bacteria, biofilms, and viruses; a summary of this overview is provided in Table 2.2.

2.3.2 Brief description of biological assay techniques

Colony forming units (CFU) counting

CFU counting is used to quantify the concentration of bacteria in a sample. Petri dishes are filled with a medium such as agar (e.g. LB agar) at a temperature slightly above ambient, and then left to cool so that the medium solidifies. The bacteria samples in liquid phase are diluted several times with another sterilized medium (e.g. LB broth). Then, the dilutions are uniformly spread on the agar-filled Petri dishes, which are then incubated at 37˚ C. After a period of 12-48 hours (dependent on the bacterial strain), the number of colonies on the Petri dishes (which are visible to the naked eye after this amount of time) are counted and the original undiluted sample's bacterial concentration may then be calculated.

Fluorescence microscopy

Fluorescence microscopy is usually used to determine the live/dead ratio of bacteria. Two stains of propidium iodide (PI) and SYTO9 can be used to dye the nucleic acid in the cell. SYTO9 is a green staining which can penetrate the membrane of both the live and dead cells. The other staining, PI, is a membrane impermeant dye which only cannot penetrate live cell's membranes and

therefore only stains the cells with damaged membranes, thus revealing the dead cells. PI has the higher affinity for nucleic acid than SYTO9, and therefore, the dead cells under fluorescence microscopy emit more red light [185]. On the other hand, the live cells appear green. After the counting and calculation, the live/dead ratio is obtained.

Biomass measurement

Crystal violet (CV) is used for biomass measurement and is able to detect both surface-adhering cells and the extracellular matrix of biofilm. CV can stain the negative charged surface molecules and polysaccharides in the matrix [186]. In our experiments, CV is used to quantify the removal of biomass by plasma etching.

Plaque assay

Plaque assay can be thought of as the viral version of CFU counting for the measurement of the concentration of viruses in solution. Bacteria (e.g. *E. coli*) are grown on Petri dishes to form uniform lawn on the surface of LB agar. If some of the *E. coli* are infected by phages and become unviable, the infected bacteria are no longer able to reproduce and the lawn of bacteria which would otherwise have been uniform, instead forms visible spots called plaques. Each plaque then corresponds to an individual phage, and may be used to quantify the original concentration of phage or virus. Both the double-layer agar and Gratia methods are commonly applied for this kind of assay [187].

The basic procedure of a plaque assay is done as follows: Firstly, the hard medium agar is poured into sterilized Petri dishes. Secondly, liquid soft medium agar is prepared in heating blocks at 45˚ C as is uninfected bacteria culture (e.g. *E. coli*) in incubator at 37˚ C. Thirdly, the virus-containing solution is serially diluted with sterilized medium. Fourthly, these dilutions are mixed with bacteria culture and soft agar, and poured onto the hard agar plate. The Petri dishes are then incubated at 37˚ C incubator for 16 hours. The number of plaques is counted and the concentration of initial virus solution may then be calculated.

Transmission electron microscopy (TEM)

When the size of microbes is too small (e.g. nanometer region: MS2 phage) for imagery to be made using optical microscopy, due to the long wavelength (hundreds of nanometers), the short wavelength electron beam is useful. TEM has been proven to work well for the analysis of all the cellular components,

including the cytoskeleton, membrane systems, organelles, cilia, etc [188]. Some limitations of TEM are small number of cell samples due to high magnification and fact that the sample must be elaborately prepared for the vacuum environment of the electron microscope chamber (the microbes are therefore necessarily dead when imaged). For the sample preparation, the sample is fixed and stained with glutaraldehyde and osmium tetroxide (osmium tetroxide is dangerous) [188]. Then, the sample is moved to electron beam and imaged. In our experiment, TEM is applied to confirm the capsid and the tail damage on phage sample, and to quantify the treatment effect.

2.3.3 Planktonic bacteria versus biofilm

Microbes, such as the following bacteria strains: *E. coli*, *Salmonella spp.*, *P. aeruginosa*, *A. pyogenes*, *S. aureus*, *S. hyicus* [189] usually survive in liquid phase ecosystems by constructing biofilms in order to reduce the impact from environmental changes [190]. The three dimensional structure of biofilm including pores, channels, and mushroom-shaped protuberances are made of extracellular polymeric substances (EPS) which are produced by the microorganisms themselves. Biofilm has high resistance to many currently known bactericidal agents, such as heavy metals, chemical antimicrobial agents [190], UV light [191] etc. The resistance of bacteria in biofilm to toxic agents is up to 1000 times than that of planktonic bacteria [192]. The various mechanisms by which biofilms are able to protect the bacteria inside include: increased number of persistent cells, quorum sensing systems, biosorption, gene expression response, and efflux systems [190]. Therefore, the decontamination of bacteria in biofilm is not only concerned with the inactivation of bacteria as in the case of the treatment of planktonic bacteria but also with removal of the matrix.

The main mechanism of decontamination of planktonic bacteria by plasma treatment is damage caused by the products of plasma to the bacterial membrane. A study by Cao *et al* in 2011 described the structural changes in the case of *E. faecalis* after exposure to plasma treatment [164]. In Figure 2.12 (a), the complete structure of *E. faecalis* is shown in the sample without any treatment. After 2 and 4 minutes of treatment, the cell shell is rough, and the bacteria is gradually swelling. In Figure 2.12 (d), after 8min treatment, the cell ruptures and the cytoplasm is released into the medium. The cell wall damage is due to the interaction of plasma chemical products and the chemical components of the cell wall, such as peptidoglycan, proteins, and lipids [193].

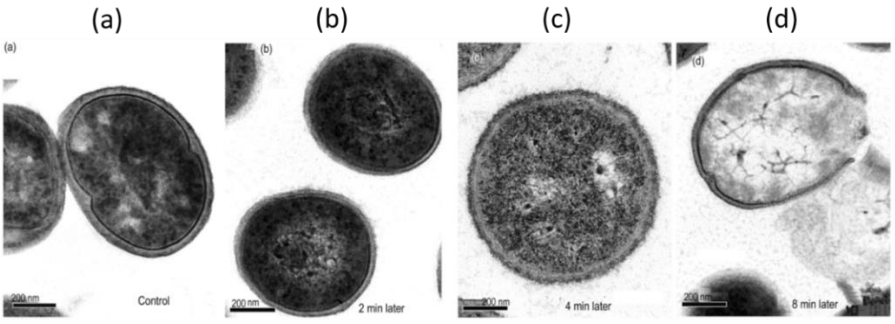

Figure 2.12 The *E. faecalis* structure changes imaged by TEM after (a) 0, (b) 2, (c) 4, and (d) 8min plasma treatment [164].

In biofilm decontamination, the removal of biofilm matrix is an important topic. Studies have shown that the removal effect of plasma not only occurs in a vertical direction but horizontal direction [171]. The mechanisms of plasma etching on biofilm could be that: The plasma exited atoms/molecules or the radical products may break the bond of hydrocarbon compounds. Also, the modification and damage of open bonds on bacteria membrane induces the cell releasing molecular fragments and volatile compounds, and therefore, deformation appears on bacteria until they are dead [171].

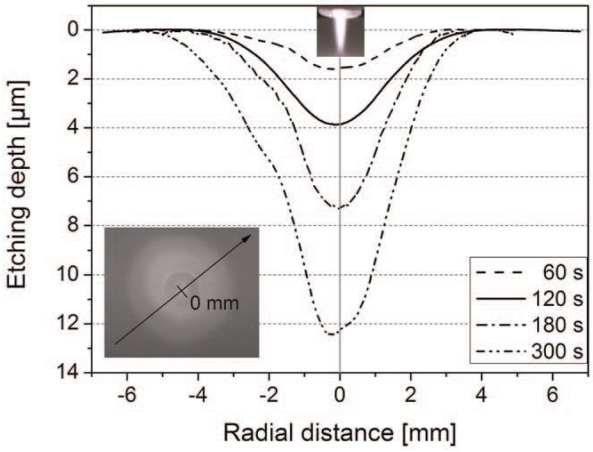

Figure 2.13 The plasma etching on *C. albicans* biofilm in both vertical and horizontal direction.

2.3.4 Virus deactivation

Compared to bacteria, the structure of a virus is simpler and much smaller, including the enveloping protein shell, the genome-containing capsid, the genome itself, and enzymes. The viral genome inside the capsid can be DNA, e.g. T4 phage, adenoviruses, the herpes viruses, and the poxviruses [194], or RNA, e.g. MS2 phage, Orthomyxoviruses, Hepatitis C Virus, and corona viruses [195]. The size of DNA virus is usually larger than that of RNA virus. DNA viruses can contain up to 305,000 nucleotides, but RNA viruses typically have only up

to 31,000 nucleotides. The bonds of molecules in RNA is weaker than DNA. Therefore, the size of RNA is limited, and also RNA has more possibility of mutations [196].

The overall goal of virus decontamination is to eliminate the ability of the virus to infect a new host. This may be done by damaging the virus in one or more different ways. One way is for reactive chemical species to be transported through the holes on broken capsid and degrade the viral genomes inside [197]. However, there are other ways to prevent a virus from infecting a host than direct damage to the genome itself. For example, some viruses use tail-like structures to transport their genome inside the uninfected cells. For example, T4 phages are known to attach themselves to the cell wall of *E. coli* by their own baseplate, and then transmit their genome through the tails [198]. Therefore, if the tail is compromised, the phage is no longer to infect *E. coli*.

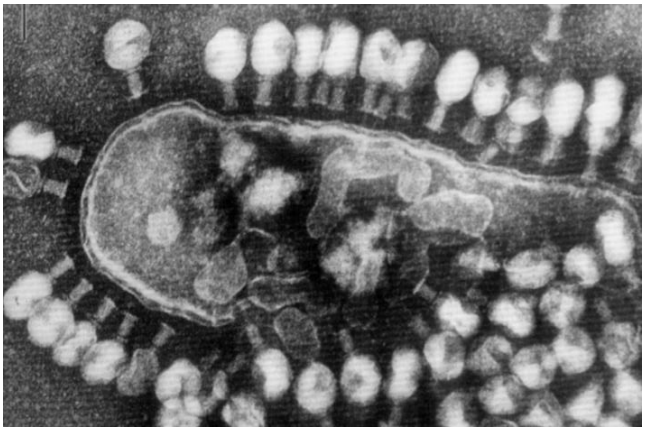

Figure 2.14 T4 phages attach on *E. Coli* and penetrate the membranes [198].

In our studies, we have focused on phage decontamination, T4 and MS2 phages in particular. To our best knowledge, current published studies of phage treatment by plasma are about the phages carried by aerosol [7, 8] or phages in liquid phase [9, 8, 10]. The studies by Wu *et al* in 2015 described the damage of surface proteins on MS2 after plasma treatment, and there were obviously more phage fragments in treated samples than untreated ones; the phages in the untreated samples are observed by SEM to maintain more rounded morphology as shown in Figure 2.15 [8]. Moreover, the other group, Guo *et al*, state that the results that the plasma producing reactive oxygen and nitrogen species can damage the capsid of T4 phages and induce the T4 phage tails aggregation [9].

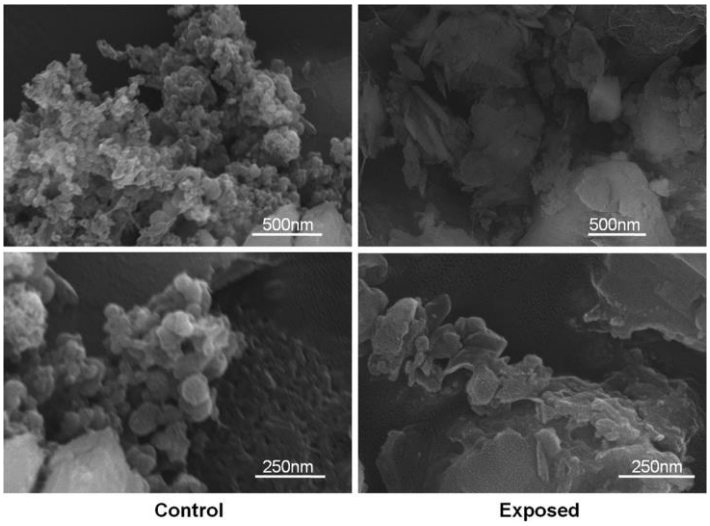

Figure 2.15 The untreated (left) and treated (right) MS2 sample under SEM [8].

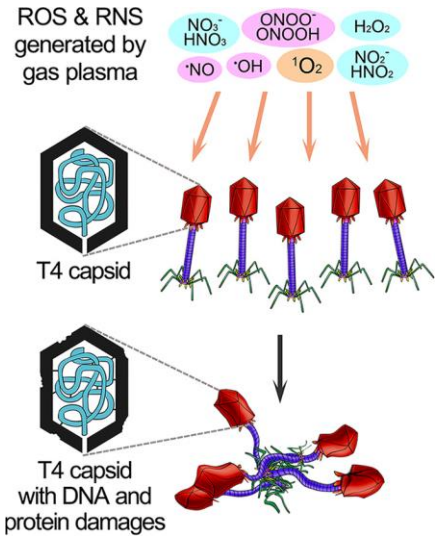

Figure 2.16 The inactivation mechanisms of plasma producing ROS and RNS [9].

Different from the previous studies of phage treatment in aerosol or in liquid phase, our work is to decontaminate phages on solid substrate.

Table 2.2 The previous studies of DBD plasma decontamination.

Plasma source	Sample strain	Method	Results	Ref.
Plasma jet He/air	*Escherichia coli* planktonic on agar	CFU counting	Reduction of over 2.5log in 120s with 220V input voltage	[166]
Surface plasma He/O_2	*Pantoea agglomerans* 12h and 24h biofilm	CFU counting	Reduction of 1.2log on 24h biofilm in 10min then stable, and 2log on 12h biofilm then keep decreasing	[170]
Plasma jet $Ar/1\%O_2$ and surface plamsma Ar	*Candida albicans* ATCC 10231 48h biofilm	CFU counting and SEM	Reduction of 0.55log by plasma jet and 5.22log by surface plasma in 10min	[172]
Plasma jet Ar	*Pseudomonas aeruginosa* strain PA103 (Pa) and *Burkholderia cenocepacia* (Bc) strain Bc 46 72h biofilm	Live/dead cell viability assay for Pa and CFU counting for Bc	Survival ratio is 0.005-2% in Bc by CFU counting by 5min plasma and plasma-treated Pa has higher dead ratio in cell viability assay	[175]
Plasma jet $He/2\%O_2$	*Enterococcus faecalis* ATCC 29212 48h biofim and *Staphylococcus aureus* ATCC 25923 planktonic on agar	CFU counting and SEM	Planktonic *E. faecalis* inhibition diameter is 8.16cm after 15min treatment and 2log decrease in E. faecalis biofilm after 10min treatment	[164]
Plasma jet $Ar/1\%O_2$	*Candida albicans* ATCC 10231 7days biofilm	Light microscope and surface profilometry	The etched area and depth are 35μm^2 and 12μm after 5min treatment	[171]

Plasma jet air	*Weissella confusa* LBAE C39.2 planktonic and 48h biofilm	CFU counting and Live/dead cell viability assay	Reduction of over 3 log in 15min and then keep stable for adherent bacteria, and less than 10% live bacteria after 15min treatment and then keep stable for biofilm	[168]
Plasma jet dry air	*Salmonella, S. Anatum* F4317, *S. Stanley* H0558, and *S. Enteritidis* PT30 24-72h biofilm	CFU counting	Maximum reduction of 1.57 log, 1.82 log, and 2.13 log after 5, 10, an 15s short treatment	[174]
Plasma jet air	*Escherichia coli* O157:H7 and *Listeria monocytogenes* on pork	CFU counting	Reduction of 1.5 log for *E. coli* and 1.0log for *L. monocytogenes* after 120s treatment on pork	[165]
Plasma jet Ar/2%O_2	*Bacillus aureus* planktonic on agar and *Enterococcus faecalis 7days biofilm*	CFU counting and Confocal Scanning Laser Microscopy	No *B. aureus* found on agar 7 log reduction and everyone dead of *E. faecalis* after 10min treatment	[169]
Surface plasma air	*E. coli* O157:H7 ATCC 43894, *L. monocytogenes* KCTC 3569 and *S. Typhimurium* KCTC 1925 planktonic on agar and cheese	CFU counting	Reduction of 8.9 log, 10.3log, 7.5 log for *E. coli*, *L. monocytogenes*, and *S. Typhimurium* after 4min, 10min, and 75s treatment on agar	[167]
Plasma jet He/<=1%O_2	MS2 phage in liquid phase	Plaque assy (double-layer method)	Reduction of 3log in viability after 3min treatment, and >7log in viability after 9min	[10]

Plasma jet air, He/2%O_2, Ar/2%O_2	MS2 phage in aerosol and liquid phase	Plaque assy (double-layer method) and SEM	Reduction of1.3log in viability of aerosol MS2 after 0.12s air plasma exposure, and >0.69log decrease of waterborne MS2 viability after >30s treatment	[8]
Surface plasma Ar/1% artificial air and PAW	T4, Φ174, and MS2 phage in liquid phase	Plaque assy and SEM	T4 phages are aggregation after 60s plasma or PAW treatment. Reduction of over 10log in viability of 3 kinds of phages after 120s treatment	[9]
Surface plasma air	MS2 phage in aerosol	plaque assays and RT-qPCR	Reduction of 2log in MS2 viability after 0.25s exposure	[7]

2.4 Plasma medicine

Currently, the scope of advancement in medical technology is vast. New and innovative medical methods are under study, and non-thermal plasma (NTP) is one of them. Currently, NTPs and are being actively investigated for medical applications such as blood coagulation, wound healing, skin pathologies, infectious diseases, dental cavities, etc.

2.4.1 Introduction to applications

Blood coagulation

Hemorrhaging is involved in 35% of the mortality related to bodily injury [199], and also increases the risk of infection [200]. It is highly desired to develop new and improved techniques to promote blood coagulation in wounds. Research on plasma blood coagulation started about 30 years ago. One study showed that thermal and electric field effects can be negligible, and that changes in the pH value or Ca^{+} concentration are not necessary for plasma promotion of coagulation [201]. Another study described the result that the plasma treatment induces production of coagulation factor at an even faster rate than the natural situation [202].

Figure 2.17 The blood coagulation on mouse [203].

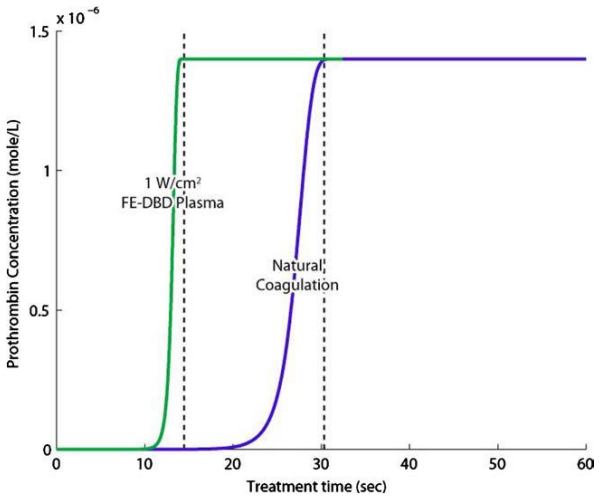

Figure 2.18 The concentration of prothrombin raising after plasma treatment [202].

Wound healing

Some studies have shown that non-thermal plasma (NTP) and its derivatives (e.g. chemical products, radicals species, UV light, charged particles, electric field) can cause microbes decontamination and cell healing [204]. Oxidative stress from plasma products induces biochemical reactions or cytoskeleton damage to trigger cell evolution [205]. Another study showed that He plasma improves the wound healing on normal rats, and significantly increases the wound healing on diabetic rats [206].

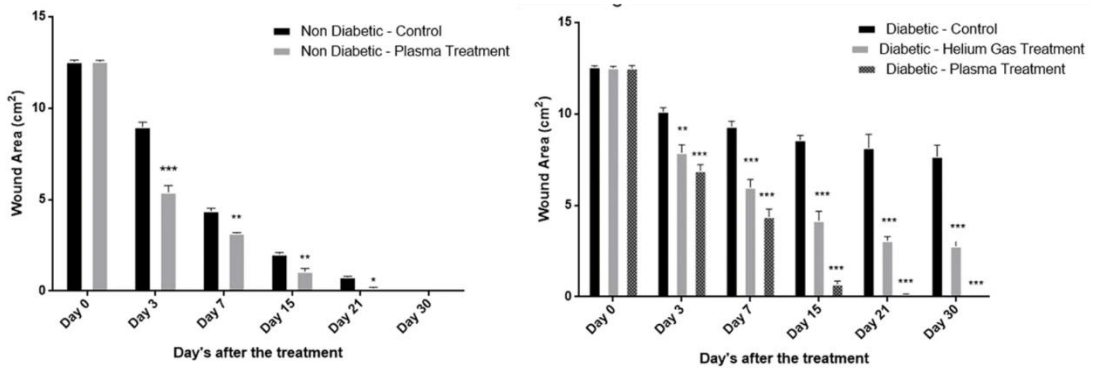

Figure 2.19 Wound area changes after He plasma treatment on non-diabetic (left) or diabetic (right) rats [206].

Skin pathology

NTP can be applied for local treatment of skin disease due to the inactivation of micro-organisms and promotion of wound healing. One study showed that NTP treatment resulted in improvements for patients with complicated ulcerous eyelid wounds [207]. Necrotic phlegm on eyelids were treated by 5s air plasma once every few days, and the edema and inflammation were reduced after the

5th treatment. The figure shows the patient after 6th treatment in Figure 2.20.

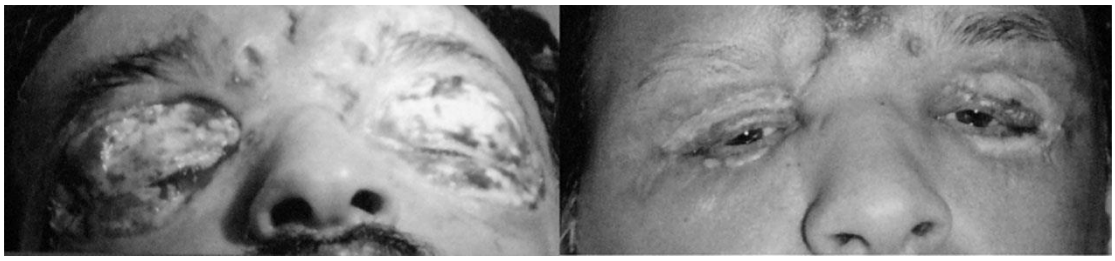

Figure 2.20 The recovery of eyelid after 6th air plasma treatment [207].

Dental cavities

NTPs can also applied for decontamination in the field of dentistry. NTPs are able to adapt to the complex structure of surfaces such as teeth. Different from the classical method, NTPs can treat dental cavities without drilling. For example, a small plasma jet system was designed to generate NTPs in root canals [208]. Rupf *et al* in 2010 showed that planktonic E. *coli* and L. *casei* on dentin slices are deformed after 18s plasma treatment using scanning electron microscopy [209].

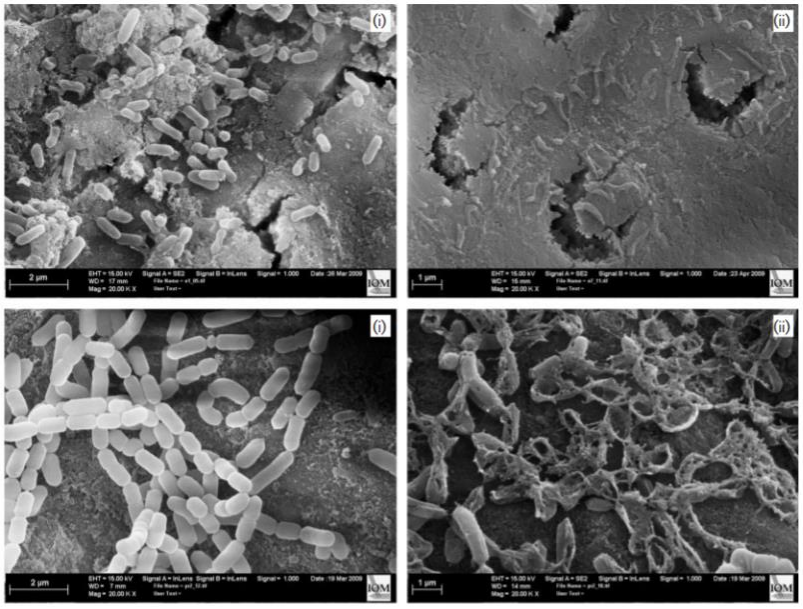

Figure 2.21 The figures show the E. *coli* (upper row) and L. *casei* (bottom row) (i) before and (ii) after 0.9s/mm^2 plasma treatment [209].

Cancer treatment

The application of plasma medicine has also been investigated for cancer treatment. Various cancer trials are studied, including brain cancer, skin cancer, breast cancer, colorectal cancer, lung cancer, cervical cancer, leukemia, hepatoma, head and neck cancer, *etc* [12]. In the next section, the mechanisms of plasma cancer treatment and current research will be reviewed.

2.4.2 Cancer cure induced by non-thermal plasma

Application of non-thermal plasmas (NTPs) on cancer treatment has been investigated over one decade since 2007 [142]. Most of studies focus on the treatment of solid tumors, including brain cancer, skin cancer, breast cancer, colorectal cancer, lung cancer, cervical cancer, hepatoma, head and neck cancer, etc. [210]. A limited number of studies have focused on liquid tumor (e.g. leukemia) treatment *in vitro* [211]. In this section, we will discuss the details of NTP treatment for solid tumor.

Some kinds of cell phenomena are used to determine the treatment efficiency: Proliferation gives the information of cell breeding capability, cell viability shows the number of viable cells, apoptosis is one of cell death process without inflammatory response, migration is the important process of cancer metastasis, and selective effect tells us normal cell could be ignored by NTP treatment.

2.4.2.1 Mechanisms of anti-cancerous components

<u>Electropermeabilization due to charged particles and electric field</u>

When charged particles (mainly ions) reaches cells or tissues, and the charge particles carrying would be deposited on the surface of cell membrane, and the difference of electric potential could induce electric field (electric force) on membrane. Under specific field conditions of plasma, including pulsed strength, pulse duration, and pulse frequency, the electrostatic force is enough to overcome the tensor of cell membrane and make it rupture [13]. The process would lead the temporary increase of permeability, induce ion leakage and escape of metabolites, and more drugs are uptake. It is also the so-called "electroporation" we discussed in the previous section. When gradient of electric potential on the membrane reaches 200 mV reversible local disorganization and transient breakdown occur, and there is more permeability for molecules to move inside cell membrane [212].

<u>UV emission</u>

UVB emission is generated during plasma process. Although the cancer cell surrounding is humid and UVB would be absorbed by water, part of UVB would reach cancer cell culture. When the intensity of UVB is high enough, UVB would induce nuclear condensation and fragmentation which are the evidence of apoptosis [14]. Then, the apoptosis ratio is higher as the increase of UVB intensity.

Apoptosis due to ROS and RNS

ROS and RNS are the main anti-cancerous products during plasma-gas (nitrogen, oxygen, water vapor, *etc*) and plasma liquid (water) interaction [210]. In fact, not only NTP treatment but radiotherapy and chemotherapy are producing and using some ROS to kill cancer cells [213].

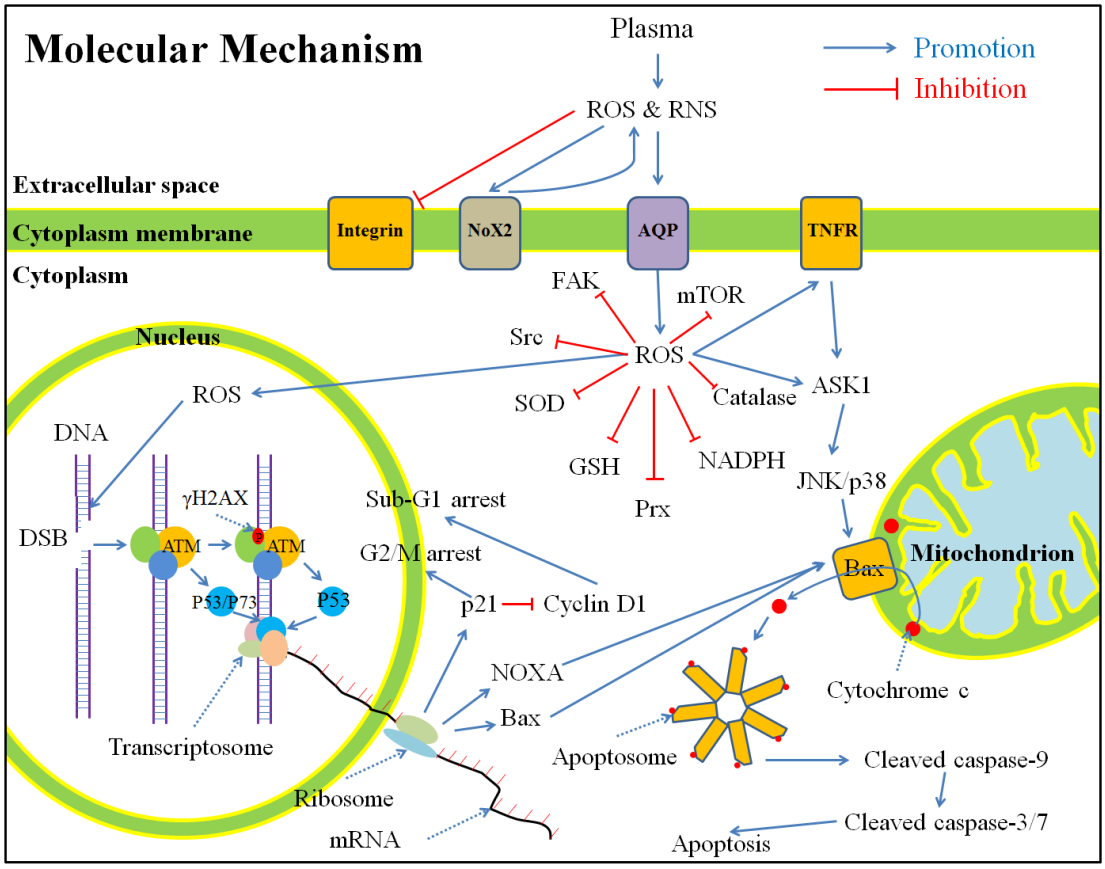

Figure 2.22 The process of cell apoptosis induced by ROS and RNS [210].

When the plasma activated medium (PAM) is brought into contact with the medium to be treated, ROS and RNS interact with cell membrane and increase the concentration of intracellular ROS through the channels of aquaporins (AQP) and reduce nicotinamide adenine dinucleotide phosphate (NADPH) oxides (NOX2); NOX2 is also regarded as the source of secondary ROS [214]. Some of intracellular ROS can face ROS inhibitors, such as focal adhesion kinase (FAK), Src kinase (Src), superoxide dismutase (SOD), glutathione (GSH), peroxiredoxin (Prx), NADPH, and mechanistic target of rapamycin (mTOR), and then the concentration of ROS is reduced. Some ROS could react with tumor necrosis factor receptor (TNFR), and apoptosis signal-regulating kinase 1 (ASK1) is produced. Besides, ROS could also directly break DNA and make double strand

break (DSB) which induces DNA repair in nucleus. Ataxia telangiectasia mutated (ATM) appears in DNA repair, and γH2AX, p53, and transcriptome are produced. In transcriptome, there are ribosome and mRNA, and NOXA (a pro-apoptotic member) is released. Finally, ASK1 and NOXA with Bcl-2-associated X protein (BAX) in mitochondrion make cell apoptosis [210].

Selective anti-tumor effect

Selective anti-tumor effect was observed in PAM experiment [215, 216, 217, 218]. Even though it is still lack of direct evidence, some studies show that it is due to the number of AQP channels and antioxidant enzymes. Compared with normal cell, there are more AQPs and less enzymes in cancer cell [219, 220]. A higher number of AQPs in cell membrane leads to an increased ROS concentration in the intracellular medium. In addition, these species are facing a lower antioxidant enzymes (catalase) concentration. As a result, cancer cells are facing higher increase in ROS and higher ratio of cell apoptosis is observed [210].

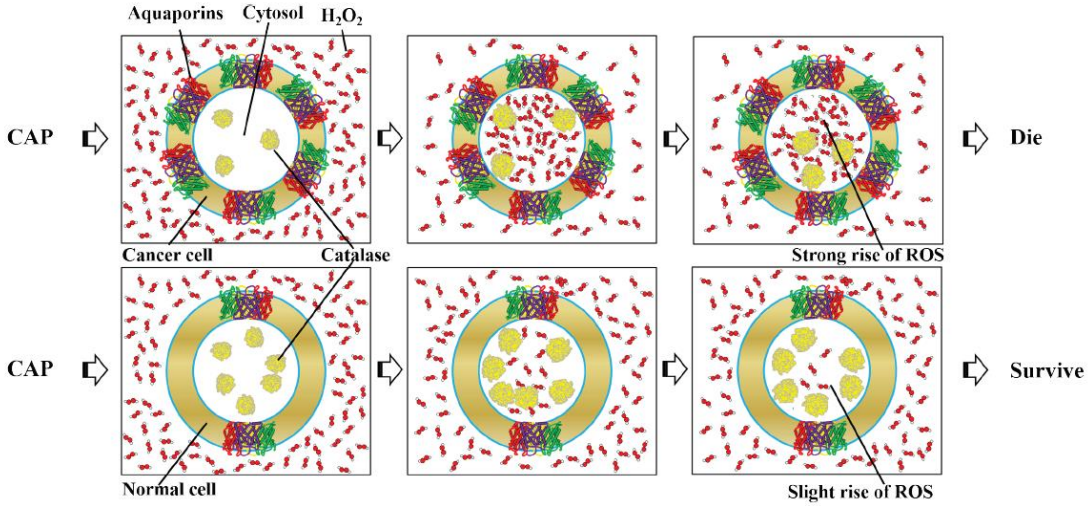

Figure 2.23 Schematic representation of ROS transfers in cancer cell (upper) and normal cell (down) [210].

NTP induced immune response

After *in vitro* direct NTP cancer treatment, the dead cells are injected in mice trial one before the cancer cells injection, and researchers found that the dead cancer cells have the property of immunogenic cell death (ICD) which provides dangerous signals for immune system against dead cell antigens [221]. It is also found that even NTP surface treatment on mice trail directly, ICD is still generated and helps eliminate tumor grows. Moreover, the immune system shows selective effect and specific attacks the targeted cancer cells but not

normal cells [221]. The more ICD mechanism is still investigated.

2.4.2.2 Treatment assay

Proliferation assay

Cell proliferation is the fact that cells multiply rapidly and abundantly. Cells reproduce by mitosis, i.e. by dividing themselves. The mechanism is thus including cell division and cell death. One of cancer cell characteristics is the abnormal increase of cell number. Therefore, proliferation measurement is an important diagnosis target. Proliferation assay can be conducted *in vitro* or *in vivo*: *In vitro* assays provide information of cell cytotoxicity and apoptosis, and *in vivo* assays express the pathology of cancerous tissues [222].

Viability assay

Cell viability could be described by cell proliferation, cytotoxic effects of compounds, and viable cell number [223]. The purpose of cell viability is to understand the cause of cell death, including damage of cell membrane, prevention of protein synthesis, irreversible interaction with receptors, enzymatic reactions, *etc.* [224].

Apoptosis assay

Apoptosis is usually compared with necrosis. Both are the process of cell death with different properties. In cell apoptosis, cell shrinks, nucleus condense, membrane blebs, they are breaking into apoptotic bodies, and finally they induce phagocytosis (process of living cells ingest or engulf nearby particles) [225]. In cell necrosis, cell membrane is damaged first, and cell swells. Then, the cytoplast leaks into extracellular space, and finally karyolysis (dissolution of cell nucleus) appears [225]. Apoptosis could be divided into early apoptosis and late apoptosis. Early apoptotic cell has complete cell membrane, but membrane of late apoptotic cell has been broken [226]. Moreover, necrosis process would induce inflammatory response, but apoptosis not [223].

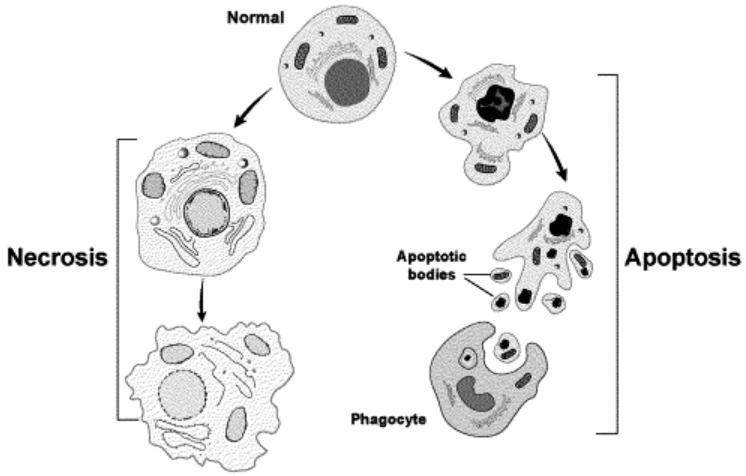

Figure 2.24 Flow chart of necrosis (left) and apoptosis (right) process [225].

Migration assay

Cells migration is linked to cancer metastasis. The first step of metastasis is invasion of cancer cells in nearby tissues and circulation system. Migration is the main mechanism of cancer invasion [227]. As a consequence, migration assay provides qualifies the treatment effect on preventing from metastasis.

Selectivity assay

Selectivity is also the important point of cancer treatment. During the real therapy, it may affect the nearby normal cells and change cell expression. The change could be cell membrane damage, cell death, and even gene mutation (e.g. secondary cancer induced by radiotherapy [3]). They would be potential problem of cancer treatment.

In vivo assay

In vivo treatment, there is more complicated system of sample surrounding. It usually counts the tumor size (volume or weight) and the number of tumor, and they present the metastasis and cancer evolution. Moreover, the most problem patient concern is the survival ratio. The survival ratio could show that NTP treatment helps patient lives extend or not.

2.4.2.3 Different procedures of NTP treatment

Non-thermal plasma applied to cancer therapy is divided into indirect and direct treatment. In indirect NTP treatment, the cell cultures and/or tissues are not directly treated by the plasma jet. The plasma jet first interacts with distilled water or medium, and the so called plasma activated water (PAW) or plasma activated medium (PAM) is then added in cells culture or injected in tissues [210].

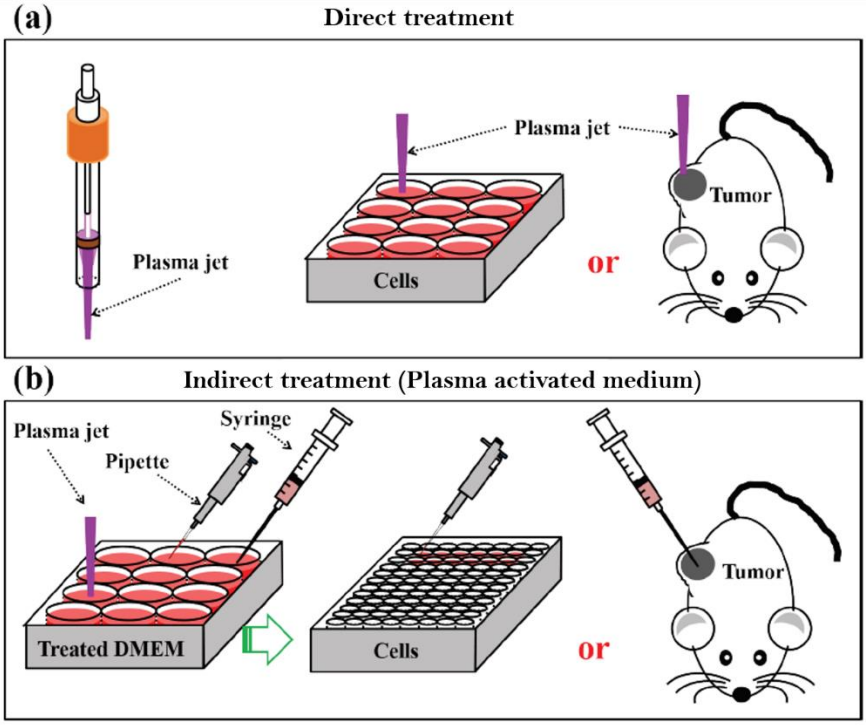

Figure 2.25 Procedure of (a) direct treatment and (b) plasma activated medium [210].

Most important of anti-cancerous components contain in PAM treatment is ROS and RNS due to the separated procedures: plasma-medium chemical reaction and PAM-samples mixing. In direct treatment, the multiple components play role of cancer cell killers: charged particles, electric field, UV emission, heat transportation, and reactive species.

2.4.2.4 Studies of PAM treatment (indirect treatment)

In a real patient, tumors are always surrounded by liquid, such as blood and interstitial fluid. Therefore, both of direct and indirect treatment would produce PAM, and PAM treatment is long-time effect (over 24 hours) even though the plasma source has been removed [216]. The most mechanism of PAM treatment is ROS or RNS inducing cell apoptosis, and ROS provides selective expression [210]. In this treatment, there is no risk of high voltage and increase of temperature on cell culture, and therefore, most of PAM is made by DBD plasma which could provide higher area and higher power (compared with plasma jet).

In vitro

PAM treatment has been applied on several kinds of cancer trial *in vitro,* including melanoma, breast cancer, pancreatic cancer [216, 228], liver cancer [215], ovarian cancer [217], glioblastoma [218], *etc*. In *vitro* treatment, cells were

cultured and moved in well with constant number of cells. Then, PAM is added in the wells for giving duration. After PAM treatment, cell viability [216, 217, 218], proliferation assay [217, 228], apoptosis assay [228, 229], migration measurement [9], and selective effect [215, 216, 217, 218].

Most PAM is generated using DBD plasma (DBD could have higher power and larger surface than plasma jet) in air, argon, oxygen, or their mixture with flow ranging from 0.5 to 15 L/min. Different volume medium (3-6 mL) is exposed under plasma in duration ranged from 0.5 to 10 minutes. However, these papers do not provide the delay between plasma exposure and samples treatment. Then, the cell culture is mixing of PAM, and the assay would be done on one and two days after. The parameter of PAM generation is provided in Table 2.5.

Table 2.3 The results of cell viability, proliferation, and apoptosis assays in different cancer trials.

Cell culture	Treatment duration	Cell viability	Proliferation	Apoptosis
Pancreatic cancer [216]	24 hours	About 20%	X	X
Ovarian cancer [217]	24 hours	About 20%	No effect	X
Glioblastoma [218]	24 hours	About 10%	X	X
Melanoma [228]	48 hours	About 20%	No effect	No effect
Pancreatic cancer [228]	48 hours	About 60%	No effect	3*control
Ovarian cancer [229]	24 hours	X	About 10%	3-65%

These studies provide that PAM has high efficiency for the decrease in cancer cell viability, however, in cell proliferation assay, there are different expressions. Moreover, it shows less cell migration of ovarian cancer in artificial wound in 6-well plate [217].

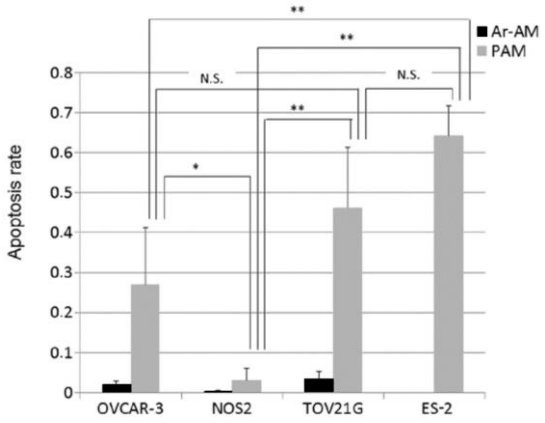

Figure 2.26 Apoptosis comparisons between argon activated medium (Ar-AM) and PAM in four gene types of ovarian cancer (OVCAR-3, NOS2, TOV21G, and ES2). Effect of apoptosis strongly depended on gene type [229]. *P<0.05, **P<0.01. N.S., not significant.

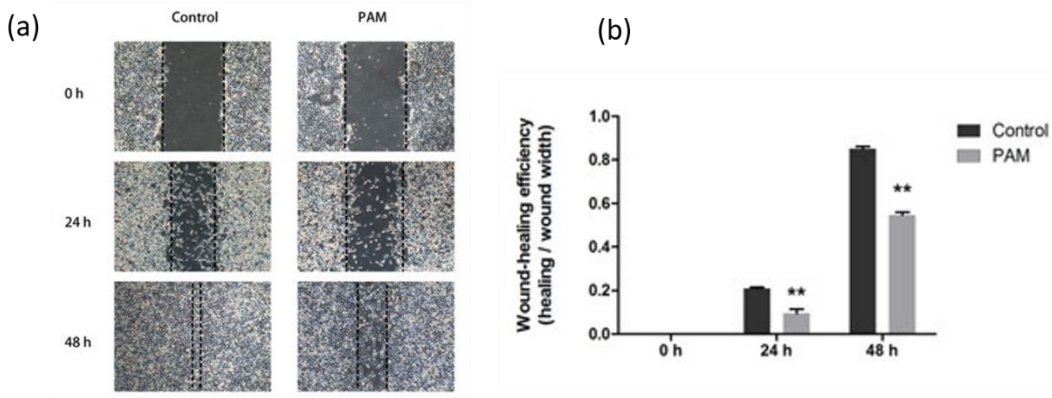

Figure 2.27 (a) The real photo and (b) statistical results of cancer cell migration [217].

Selective effect is shown in the cell viability results: After treatment, the cell viability of pancreatic cancer is about 20%, while that of normal cell is about 60% [216]. PAM reduces the cell viability of ovarian cancer over 80% but only 20% for normal cell [217]. There is also comparison between glioblastoma cell and normal cell in cell viability assay, the value is about 10% in cancer cell and 90% in normal cell after PAM treatment [218]. PAM is also shown selective effect on apoptosis assay, ovarian cancer cells have higher apoptosis ratio (25-65%) than normal cells (few %) [229]. Overall, PAM provides efficiency on cell viability decrease, increase of apoptosis and also shows selective effect on it *in vitro*.

A comparison between two pancreatic studies, PAM is generated in ambient air (not air flow) in Ref. [216] and in 0.5 L/min oxygen flow in Ref. [228]. The chemical measurements in concentration are: H_2O_2 of 12 μM and NO_2^- of 300 μM in PAM of Ref. [216] and H_2O_2 of 180 μM in PAM of Ref. [228]. The loss of cell viability is about 80% in Ref. [216] and only 40% in Ref. [228]. It is hard to say that H_2O_2 or NO_2^- has higher efficiency, but it is obviously that higher concentration of ROS and RNS is better for cancer treatment [230].

In ovarian cancer ES2 cell treatment, Ref. [217] and Ref. [229], it seems to provide contrary result in proliferation assay. Actually, in Ref. [229], proliferation assay is done just after PAM treatment in 24 hours, and it decreases over 90% proliferation ratio (compared with control) under initial number of 2500 cells per well; in Ref. [217], after 24 hours PAM mixing, the PAM is replaced to normal medium, proliferation is measured every day for 4 days, and there is no significant effect on proliferation under initial number of 1000 cells per well. From these two results, PAM immediately lowers cell proliferation, but no long term effect after PAM replacement. Moreover, when the apoptosis assay result

(65% apoptosis) of Ref. [229] (which is shown in Figure 2.26) is considered, only survival cells can proliferate and the proliferation ratio is significantly influenced by apoptosis. Therefore, PAM may only induce cell apoptosis and much less affect cell proliferation.

The effect of ROS and RNS is also the interesting part of the experiment. In Ref. [218], the same concentration (made by chemical process) of H_2O_2 and NO_2^- as that in PAM is submitted on cancer cell sample. The result provides: After PAM treatment, glioblastoma cell viability is lower than 10 %; it is almost no effective on killing glioblastoma cell with NO_2^- alone; and there is about 70% reduction of cell viability with H_2O_2 alone; moreover, when the two components are mixture and treat glioblastoma cell together, the cell viability is slightly decrease again but still higher than that after PAM treatment. It could be shortly concluded that NO_2^- has no effect on glioblastoma treatment, and PAM includes more anti-cancerous agents besides H_2O_2 and NO_2^-.

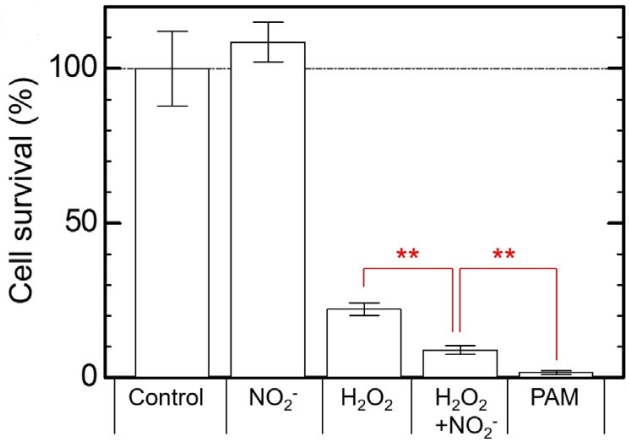

Figure 2.28 Glioblastoma cell viability measured after 24 hours of chemical compounds and PAM treatment [218]. H_2O_2 and NO_2^- has the same concentration as that in PAM. **P<0.01.

In vivo

Compared with direct treatment, it is more convenient to use PAM in vivo experiment (e.g. mouse trial) due to the high voltage and the tube of plasma jet. The main objectives of in vivo treatment are as follows: the growth of tumor size or number, metastasis, and the life time of samples. Currently, in vivo PAM experiment only done for mouse trials, including ovarian cancer [217], gastric cancer [231], colon cancer [232], pancreatic cancer [233, 234].

Table 2.4 Selected results of PAM-treated mouse trials.

Cell culture	Duration	Tumor growth	Metastasis	Survival ratio
Ovarian cancer [218]	3 days	Slower	Less	40% (90^{th} day)

Gastric cancer [231]	8 days	Slower	Less	X
Pancreatic cancer [233]	35 days	Decrease 31%	X	25% (70th day)
Pancreatic cancer [234]	7 days	2 tumors (15th day)	X	X

PAM *in vivo* treatment expresses anti-tumor effects. In ovarian cancer, once PAM a day for three days helps to reduce the growth of tumor size and leads to less metastasis [217]. In gastric cancer, weekly four times PAM for two weeks maintains tumor size in 15 days and prevents peritoneal metastasis formation [231]. In two studies of pancreatic cancer, continuous 36 daily increases survival ratio of PAM mice from control of 7% to the treated of 25% [232], and mice treated 3 plus 4 days PAM grow 2 tumors (per mouse) compared with control 14 tumors (per mouse) [234].

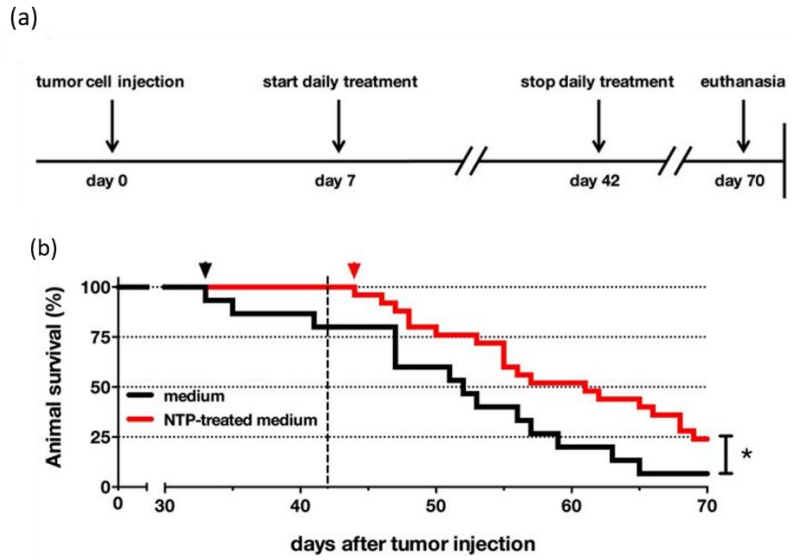

Figure 2.29 (a) The schedule of PAM treatment and (b) the evolution (arrowhead shown the first death of mouse.) of animal survival ratio in pancreatic cancer mouse trials [233]. (Dash line is the end of treatment.)

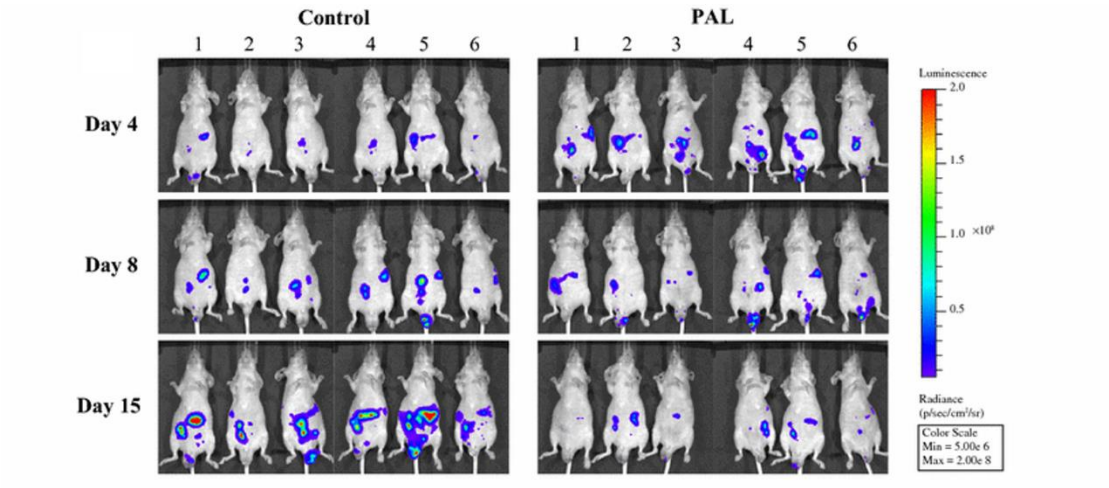

Figure 2.30 Lactated ringer's solution (control) and plasma activated lactated ringer's solution (PAL) treating pancreatic cancer mice. Tumors are bright due to luciferin staining, and the color is luminosity of fluorescence [234].

Mice infected with pancreatic cancer cell are investigated in Ref. [233] and Ref. [234]. In Ref. [234], mice are injected PAL from second day to forth day and from eighth day to eleventh day, 7 days in total. The tumor images (Figure 2.30) are taken on fourth, eighth and fifteenth day. From these figures, PAL plays an important role on elimination of tumor grows and even reduce the tumors size [234]. The longer investigation is provided in Ref. [233], mice are treated by PAM for continuously 35 days (on 7^{th} to 42^{nd} day), and there is no systemic side effect is observed after 21 consecutive injections. The first mouse death in control group is on 33^{rd} day during treatment, and that of PAM group is on 44^{th} day out of treatment duration. Until 70^{th} day, the survival ratio of PAM nice is about 20% higher than that of control mice [233]. Overall, the plasma activated solution may help mice not only reduce the tumor size but also prolong their lives.

Table 2.5 The parameter of PAM generation *in vitro* treatment.

Cell culture	Ratio (Vol PAM/Vol supernatant)	Contact time (hours)	Time delay (between plasma activation and mixing)	Exposure time (medium to plasma)	Medium composition	P (W) or SIE (J/L)	Feed gas	Discharge type
Pancreatic cancer [216]	30uL PAM /70 uL 3000 cells	24,48 hours	X	X	Saline Solutions	18W	Air	DBD
Ovarian cancer [217]	5.5 mL PAM (dilute in 1/4-1/512)	24 hours	X	10 min in 5.5 mL	RPMI-1640 medium	12000J/2L *10 min	Ar	DBD
Glioblastoma [218]	1 mL PAM on sample	24 hours	X	0.5-5 min in 3mL	DMEM	12000J/15L *0.5-5 min	1%O_2+Ar	DBD
Melanoma [228]	X	24,48 hours	X	1 or 3 min	glucose	177~573J/ 0.5L* 3min	Air or O_2	DBD
Pancreatic cancer [228]	X	24,48 hours	X	1 or 3 min	glucose	177~573J/ 0.5L*3min	Air or O_2	DBD
Ovarian cancer [229]	X	24 hours	X	0-8 min in 6 mL	RPMI-1640 medium	12000J/2L *0-8 min	Ar	DBD

2.4.2.5 Investigation of direct NTP treatment

In indirect NTP treatment, PAM or PAW could be injected at deep located organ, which is not possible for direct NTP treatment. But reactive agents in direct NTP treatment are much more various; besides ROS and RNS, charged particles, UV emission, local heating, and electric field, can affect cancer cells.

In vitro

The most difference of *in vitro* treatment between PAM and direct NTP treatments the is the treated spot. Although PAM treatment reduces adherent cells in vitro [231], direct NTP treatment can provide a clear treated spot.

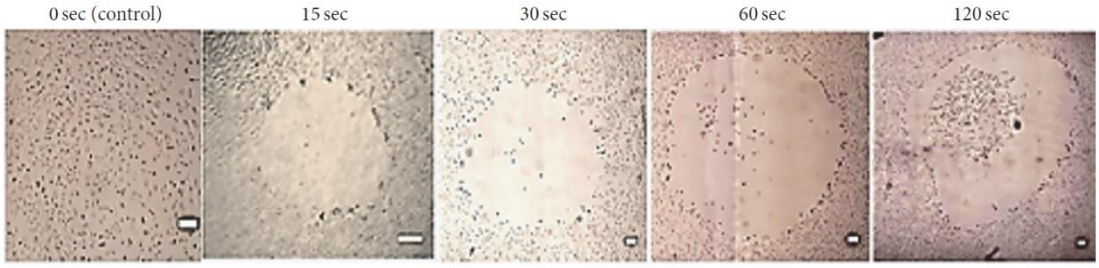

Figure 2.31 Treated spots shown after 0-120 second NTP treatment [235]. Scale bars are 200 μm.

Nowadays, NTP *in vitro* has been widely investigated in various cancer types, in this thesis, we will introduce the application on colon cancer, melanoma, brain cancer, breast cancer, pancreatic cancer hypopharyngeal cancer, squamous cancer, oral cancer, prostate cancer, and lung cancer.

Table 2.6 NTP treatment results (cell viability, proliferation, and apoptosis) of various cancer.

Cell culture	**Cell viability**	**Proliferation**	**Apoptosis**
Colon cancer [236]	50 % (15 min)	X	X
Melanoma [237]	X	X	35.8 % (60 s)
Brain cancer [238]	20% (120 s)	X	X
Breast cancer [238]	30% (120 s)	X	X
Brain cancer [239]	X	0% (23.5 J/cm^2)	65% (20 J/cm^2)
Colon cancer [239]	X	0% (23.5 J/cm^2)	X
Pancreatic cancer [240]	X	30% (90 s)	X
Colon cancer [240]	X	10% (90 s)	X
Hypopharyngeal [240]	X	25% (90 s)	X
Squamous cell [240]	X	20% (90 s)	X
Melanoma [240]	X	7% (90 s)	X
Melanoma [241]	4% (60 s)	X	X

Oral cancer [242]	X	40%(60s O_2) 0%(60s Air)	X
Prostate cancer [243]	X	No growth(5 days)	X
Prostate cancer [244]	25% (120 s)	X	X
Breast cancer [245]	X	X	88% (60 s)
Lung cancer [235]	52% (120 s)	X	48.08% (120 s)
Lung cancer (matrix) [246]	36% (120 s)	X	99% (120 s)

From the results of these studies, it obviously provides that NTP could play a role on cancer therapy. Cancer cell viability is reduced about or over 50% after certain duration of plasma exposure. Proliferation ratio of treated samples is about 40% or much less than the control group. Apoptosis ratio is also high, especially in local treated region, the apoptosis can be up to 99% [246].

A comparison of efficiency between indirect and direct brain cancer NTP treatment was made with the same dose as shown in Figure 2.32 [239]. For indirect treatment, cells were mixed with PAM immediately after plasma treated. The efficiencies of both treatments are similar, and twice dose gives over twice larger reduction of cell viability.

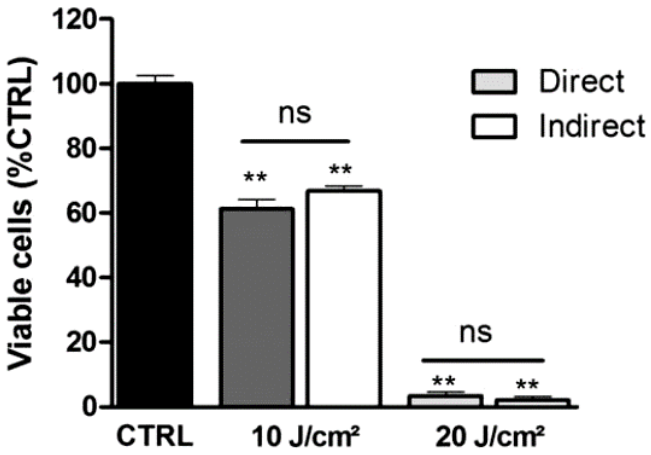

Figure 2.32 The value of cell viability after (a) direct and (b) indirect NTP treatment with dose of 10 and 20 J/cm^2 [239]. ns, no significant.

After direct NTP treatment, spots can be observed. In short term (15 s in Figure 2.31) lung cancer treatment, a single circle (cell-free zone) is forming, resulting from cell detachment attributed to ROS interacting with the adherent molecules [235]. With increasing treatment time (60 and 120 s in Figure 2.31), a second concentric circle is created, containing dead cells (Figure 2.33(a)). The

melanoma cells after 5 s treatment in treated region shrink and form the apoptotic shape shown in Figure 2.33(b). The clear edge between treated and untreated region expresses the precise treatment of NTP [237].

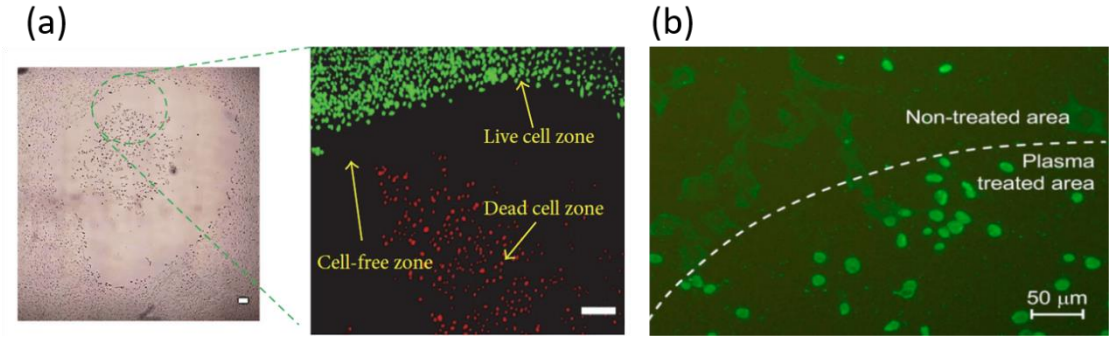

Figure 2.33 Optical analysis of the direct NTP spot after (a) long treatment (lung cancer cells, 12 kV amplitude 10 μs width pulses at 1000 Hz in ambient air) [235] and (b) short treatment (melanoma cells, helium plasma at 6 $kV_{peak-peak}$, 36 kHz) [237].

Different delay post NTP treatment assays show that plasma exposure has long term effects [246]. Lung cancer cells mixed with collagen and form three-dimensional cell matrix. The matrix was treated by 0 (control), 15, 30, 60, 120 s NTP treatment. The cell death assay was done immediately after treatment and after a 24-hour delay time after treatment. Just after the 120 s exposure, the dead cell ratio was counted about 33%; 24 hours after, the dead ratio reach over 99% (shown in Figure 2.34). Furthermore, the with 3D cell matrix allowed for investigation of the treatment depth. In Figure 2.35, the effective depth for 15 s treatment was about 250 μm. The affected area was seen to be reduced as the depth increased, [246].

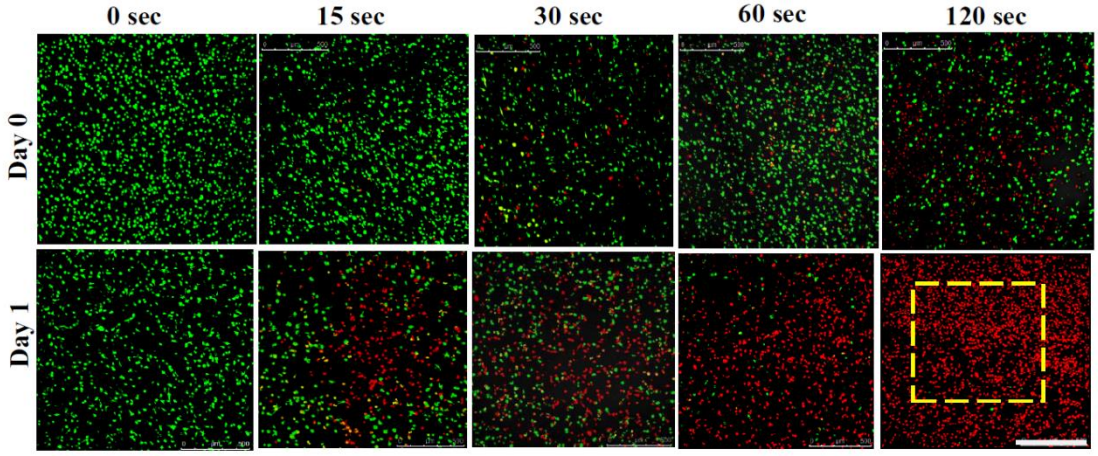

Figure 2.34 Dead (red) and live (green) lung cancer cell staining after selected exposure time (0, 15, 30, 60 ,120 s) to plasma (12 kV amplitude 4 μs pulse width at 1000 Hz in ambient air) and delay assay (0, 1 day) [246]. Scale bar: 500 μm, yellow square is the counting region (1

mm^2).

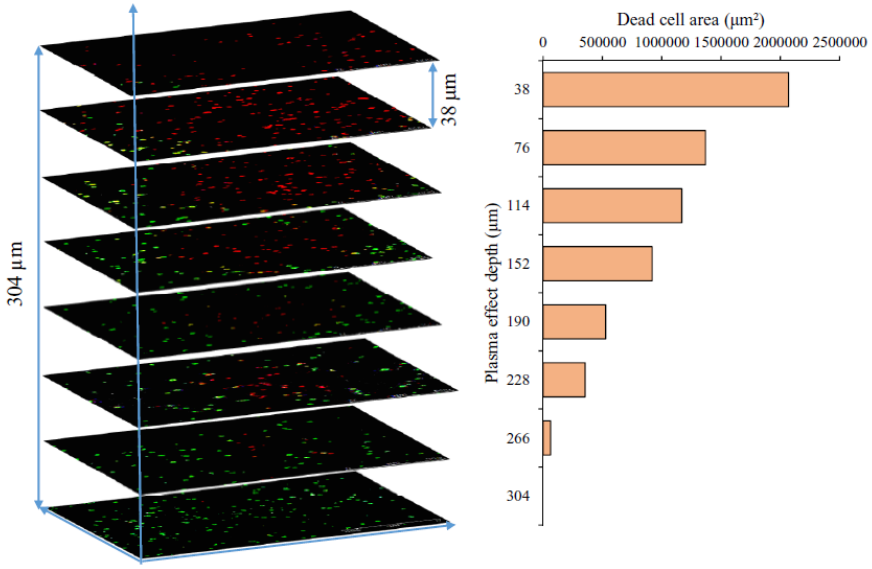

Figure 2.35 Figures (left) and statistics (right) of 3D lung cancer cell matrix treated by 15 s NTP treatment with a day assay delay.

Oral cancer cell survival ratios after humid O_2 plasma and humid air plasma were compared. For 40 s and 60 s exposure samples, air plasma was seen to be much more effective in cell inactivation (shown in Figure 2.36). Production of NO_2^- and NO_3^- production in liquid phase was invoked to explain such a result [242].

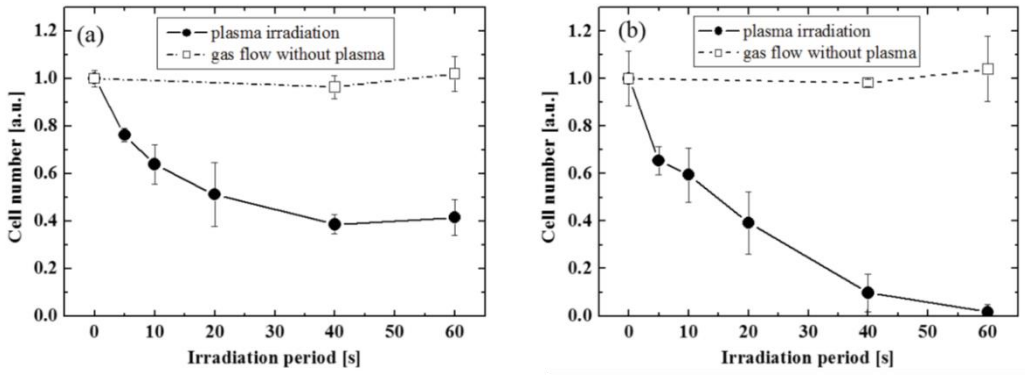

Figure 2.36 Survival curves of oral cancer cells after the exposure of (a) O_2 plasma and (b) air plasma [242].

During treatment process, part of cells in treated region detached from the plates It is important to note that over half of detached cells are still alive [235]; this may present the risk of metastasis in real therapy.

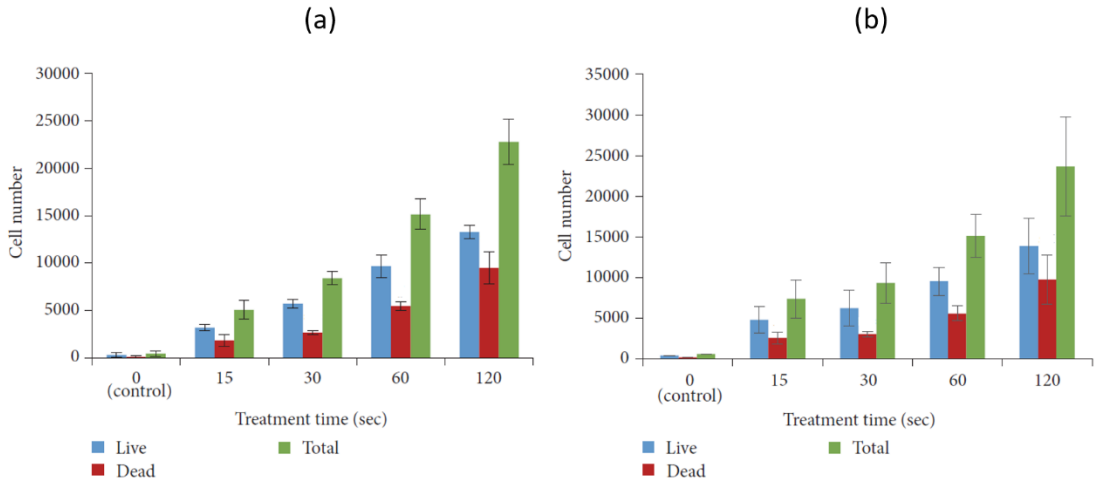

Figure 2.37 The life-death assay of collected detached cells at (a) 1 and (b) 24 hours after NTP treatment.

Selective effects are also present in *in vitro* direct NTP treatments. For example, two gene type of prostate cancer LNCaP and PC3 were investigated [244]. The cell viability assay was done at 72 hours after NTP treatment (shown in Figure 2.38). The cell viability of cancer cell after 120 s NTP treatment was reduced to 25% or less, however, normal cell submitted to the same treatment could maintain over 60% viability.

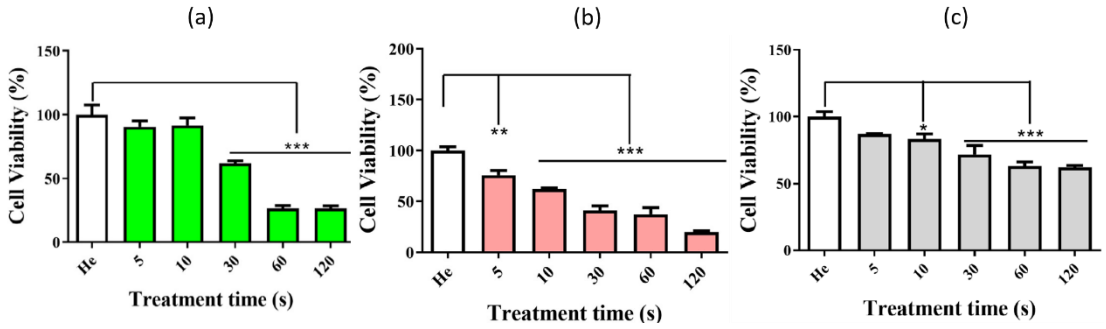

Figure 2.38 The comparable result of cell viability assay in two gene types of prostate cancer (a) LNCaP and (b) PC3 and (c) normal prostate cell [244].

In vivo

There are two forms of *in vivo* NTP treatments: tumor treatment across skin and plasma propagation in a tube inserted in trial body through a hole made in the skin. The configuration of plasma generator depends on the treated region. When the treatment is done on the skin surface, the plasma could be generated by both DBD [239] and plasma jet systems [240]. Otherwise, the tumor under skin only could be treated by plasma jet guided by a tube through a hole on

the skin, so that plasma directly interacts with the tumor [245].

In vivo NTP treatment should be operated under specific conditions adapted to a patient or an animal model. High voltage electrodes should be well insulated and/or away from the patient. Gas flow and stable plasma products should not interact with healthy tissue [245]. Noble gases are commonly used as plasma feed-gas to avoid the production of harmful reactive species (e.g. ozone) and to propagate the jet onto the tumor.

Table 2.7 Selected results of *in vivo* direct NTP treatment.

Cell culture	Duration	Tumor growth	Survival ratio
Brain cancer [239]	5 days	39.4% (control 100%)	X
Head and neck cancer [247]	1-12 months	Progressive disease (3/6) Partial remission (2/6)	1 (total 6) person survival (8 months)
Melanoma [240]	3 weeks	41.4% (control 100%)	X
Colorectal Cancer [221]	26 days	48.9% (control 100%)	X
Breast cancer [245]	24 days	About 10 % (control 100%)	40% survival

The velocity of tumor growths after NTP treatment was seen to be over 50% less than that with no treatment (control) in mouse trial [221, 239, 240, 245]. Plasma treatment has been tried for patients having head and neck cancer at the last stage. After one year, no patient survived. The results were inconclusive, particularly because of the late stage of the disease [247]. Nevertheless, during this year, the social functions and life quality of these patients was improved. From the observer's point of view, the odor of tumor region was reduced after NTP treatment. This may be due to the wound disinfection induced by plasma exposure [247]. It was also observed that the demand for pain management has been reduced, reflecting the relief of patients. [247].

The dose effect was also investigated in animal *in vivo* studies. The same total dose with various procedures was seen to produce slightly different results. Melanoma in mouse trial was treated by total 125 s per week NTP [240]. For single dose group, mice were treated once 125 s NTP a week; for five doses group, mice were submitted to 25 s NTP on five days a week. Results showed that single dose had slightly higher efficiency (47.3% remanent tumor volume for single dose and 61.6% for five doses) on reduction of tumor growth [240].

Author invoke a possible mechanism of cancer cell resistance induced by multiple low dose NTP treatments.

NTP treatment is compared with chemotherapy (doxorubicin) in reduction of tumor growth and extension of mouse life [245]. Although the dose between them is incomparable (different units), NTP can have the similar efficiency on elimination of cancer growth with drug of chemotherapy (in Figure 2.39(a)). The survival ratios are 40% in NTP and 60% in drug, actually only a mouse trial difference [245]. Overall, NTP is a potential treatment to replace chemotherapy for local therapy.

NTP treatment is found to induce immunogenic cell death (ICD) in recent years [221], ICD is described that dead cell in creature body would stimulate immune response against dead cell antigen. In Ref. [221], it shows that ICD could be induced *in vitro* and *in vivo*. *In vitro*, ICD is produced in plasma-treated culture cell culture, and then ICD with medium is injected in left flank of mice (which is plasma-treated group). After immune response of 7 days, challenged cancer cells are injected at another side flank. At the same time, plasma is replaced as pure medium and chemotherapy drug for control and drug group. Among these three conditions, tumors slowest grow in plasma-treated group. Even 30% of the mice did not find the tumor on 19th day after challenged cancer cell injection, and it provides that ICD induced by NTP *in vitro* would have the property of vaccine [221]; *In vivo* test, NTP is treating on seven days old tumors covered by naked skin once a day for five days. However, under the less dose which would not damage skin, there is no difference in tumor shape. Even the dose is higher, both of skin and tumor only have inflammatory response due to thermal effect. Although it looks less effective on tumor side, in another perspective, immune system is detected by the stain of leukocytes, antigen-presenting cells, and else. By the way, if NTP treatment is combined with vaccine of cancer, the number of T cell (which will attack cancer cell) is more than that without NTP [221].

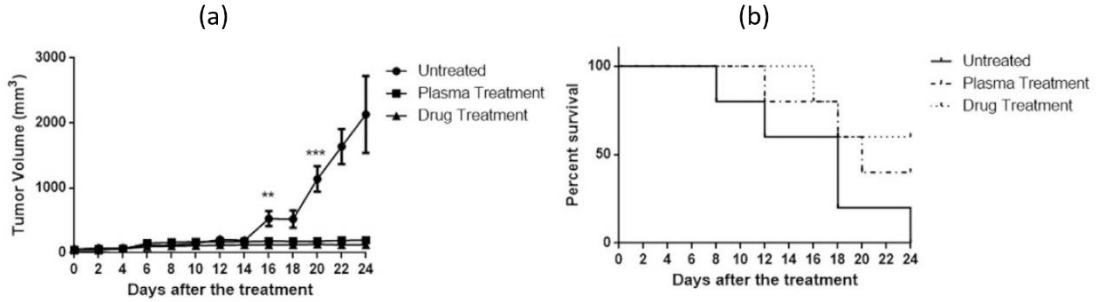

Figure 2.39 Breast tumor growth (a) and (b) survival ratio of treated mice in 24 days after helium plasma treatment (4 kV, 6 kHz (duty cycle 20%)) and drug treatment [245].

(a) (b)

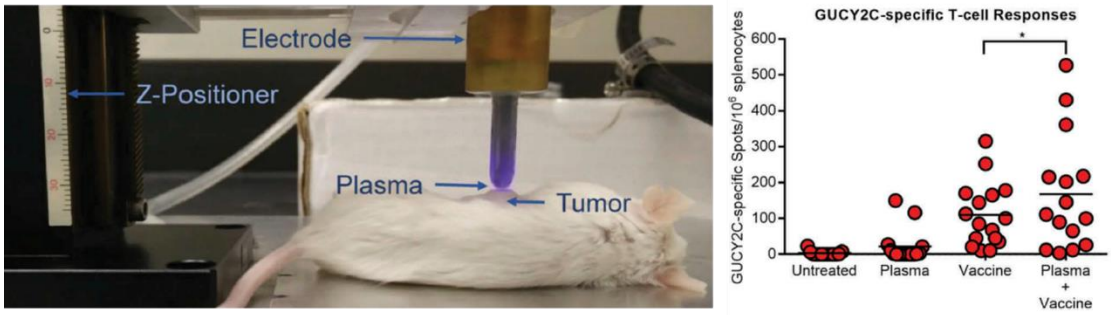

Figure 2.40 (a) *In vivo* NTP treatment on mouse skin. (b) The concentration of colorectal cancer-specific antigen guanylyl cyclase C (GUCY2C) after plasma or/and vaccine treatment [221].

Table 2.8 The parameter of direct NTP treatment *in vitro*.

Cell culture	Exposure time	Treated area (diameter)	Assay delay	Sample humidity (dry or humid)	Electrode material	Input voltage	P (W) or SIE (J/L)	Feed gas	Discharge type (DBD , Jet, …)
Colon cancer [236]	5,10,15 min	3.5 cm	24 hours	Humid	Silver	1.16 kV 22 kHz	3.25 W	N_2 1.5 L/min	DBD
Melanoma [237]	2,5s *12positions	0.25 mm *12	24 hours	Quasi-dry	Copper ring	6 kV 35 kHz AC	X	He 0.15 L/min	Plasma jet
Brain cancer [238]	5-120 s	0.275 mm	24,48 hours	Humid	Copper needle +Copper ring	8 kV 16 kHz AC	X	He 0.2 L/min	Plasma jet
Breast cancer [238]									
Glioblastoma [239]	15 s	0.78 cm^2	24 hours	Humid	X	23 kV 2 kHz Pulse voltage	0.52 W	Ar	DBD
Colon cancer [239]									
Pancreatic cancer [240]	10-90 s	3.1 mm	24 hours	Humid	Signal metal ring	1.15 kV 1 MHz AC and modulated with 487 kHz and 800 μs width	0.5-3 W	98%Ne+2%Ar 3 L/min	Plasma jet
Colon cancer [240]									
Hypopharyngeal [240]									

Squamous cell [240] Melanoma [240]	10-90 s	3.1 mm	24 hours	Humid	Signal metal ring	1.15 kV 1 MHz AC and modulated with 487 kHz and 800 μs width	0.5-3 W	98%Ne+2%Ar 3 L/min	Plasma jet
Melanoma [241]	10-60 s	3.5 mm	24 hours	Humid	Two+one stainless	7 kV AC 19.8 kHz	X	He 3.46 m/s	Plasma jet
Oral cancer [242]	5-60s	4 mm	0.5 & 24 hours	Quasi-dry	Stainless mesh electrode	4.16 kV AC 10 kHz	X	Air or O_2 with 70% vapor	Plasma jet
Prostate cancer [243]	10 s	X	1-5 days	Humid	Pin-type electrode	1.8 kV AC 1.1MHz	X	Ar 3 L/min	Plasma jet
Prostate cancer [244]	0-120s	6 mm	3 days	Humid	Inner copper ring	5-8 kV 20kHz pulse	X	He 5 L/min	Plasma jet
Breast cancer [245]	1 min	0.25 mm	24 hours	X	Copper wire	4 kV 6kHz pulse	X	He 0.5 L/min	Plasma jet
Lung cancer [235]	0-120 s	6 mm	24 hours	Humid	Copper (Covered)	12 kV 1 kHz	X	Ambient air	Micro DBD
Lung cancer [246]	0-120 s	6 mm	24 hours	Humid	Copper (Covered)	12 kV 1 kHz	X	Ambient air	Micro DBD

Table 2.9 The parameter of direct NTP treatment *in vivo*.

Cell culture	Exposure time11	Treated area (diameter)	Treated location	Electrode material	Input voltage	P (W) or SIE (J/L)	Feed gas	Discharge type (DBD, plume, Jet, …)
Brain cancer [239]	Daily 6min 5days	X	2mm above tumor	X	23 kV 200Hz	120J/cm^2/day	Ar	DBD
Head and neck cancer [247]	30min three times/week and rest one week	30 cm^2	8 mm above tumor	Pin-type electrode	2-3kV AC 1 MHz duty cycle 1:1 2.5kHz	X	Ar 5 L/min	Plasma jet
Melanoma [240]	125 s/week for 3 weeks	Entire tumor + 0.5 cm edge	1-2mm above skin	Signal metal ring	1.15 kV 1MHz AC 487kHz 800μs width	0.5-3 W	98%Ne+2%Ar 3 L/min	Plamsa jet
Colorectal Cancer [221]	Daily 10-50 s 5 days	X	Above naked skin (1mm away tumor)	Barrier electrode	X	7.5-37.5 J	X	DBD
Breast cancer [245]	3 min	X	Directly on tumor	Copper wire	4 kV 6kHz pulse	X	He 0.5 L/min	Plasma jet

Part II Experimental part

This work is separated in a physical analysis and two biological applications: Studies of DBD plasma, plasma surface decontamination, and plasma treatment on tumor cells. The investigations of characteristics of DBD plasma and plasma propagation were supported by Group of Electrical Engineering – Paris (GeePs) in Gif-sur-Yvette in France. The studies of surface decontamination were carried out in two laboratories Group of Electrical Engineering – Paris (GeePs) and Institute of Biology Intégrative De La Cellule (I2BC) in Gif-sur-Yvette in France. And the other cooperation (tumor treatment) was between Group of Electrical Engineering – Paris (GeePs) in Gif-sur-Yvette in France and Hôpital Marie Lannelongue in Le Plessis-Robinson in France.

In this manuscript, the non-thermal plasma configuration and plasma bullet propagation in long tube will be investigated to deeper understand the plasma motion. On the other hand, one plasma configuration will be used for two biological applications, surface decontamination focusing on bacteriophage inactivation and plasma medicine of lung cancer cell treatment.

3 DIELECTRIC BARRIER DISCHARGES

3.1 Introduction

As discussed in the previous chapter, studies found in the scientific literature have considered non-thermal plasma (NTP) generated by various electrode arrangements for the investigation of surface decontamination [166, 172, 164, 6] and cancer treatment [238, 243]. One common type of system is the dielectric barrier discharge (DBD). In this work, two types of DBD system have been used, both based on the use of a quartz tube. In the first version, a high voltage electrode, in the form of a stainless steel rod, is placed inside the quartz tube, and the grounded counter-electrode, is placed on the outer surface of the quartz tube. This system will be referred to as the rod system (RS) in this manuscript. The second DBD system considered here has both the high voltage and the grounded electrode placed on the outer surface of the quartz tube, and will be referred to as the two ring (TR) system in the text.

The RS type DBD system has the disadvantage that the high voltage electrode represents a risk for an *in vivo* sample due to the possibility of an electrical connection via the plasma channel between the high voltage electrode and living tissue. Therefore, the TR DBD system, whose electrodes were both outside the tube was developed. In this chapter, both the RS and TR configurations will be first discussed in detail. The production of H_2O_2 from RS plasma and TR plasma is compared. In the next few chapters, both TR and RS plasma were applied for surface decontamination and plasma medicine. The RS plasma is shown to exhibit an inactivation effect on bacteriophages in Chapter 4 and a removal effect on lung cancer cells in Chapter 5.

In the second part, plasma propagation along the inner surface of a tube made from insulating material (either quartz or silicone) was investigated for both the RS and the TR systems. Although there are some models [154, 158] to describe the plasma bullet propagation in tubes, some aspects related to the streamer propagation are still unclear, for example the streamer velocity and the electrical conductivity of the plasma. On the other hand, for medical applications, the plasma bullet can move through an endoscope inside human body and treat the affected region, and in this case, the high voltage power source will be far away from the patient. Therefore, the increased propagation distance of plasma

inside tubes made from insulating materials such as silicone is of high interest to investigate.

3.2 Materials and methods

In the first part of this section, the two kinds of plasma generator setup and the measurement methods are introduced. The electrical setups for the investigation of plasma propagation are provided in the second part.

3.2.1 DBD configuration setup

Electrical setup of RS DBD system

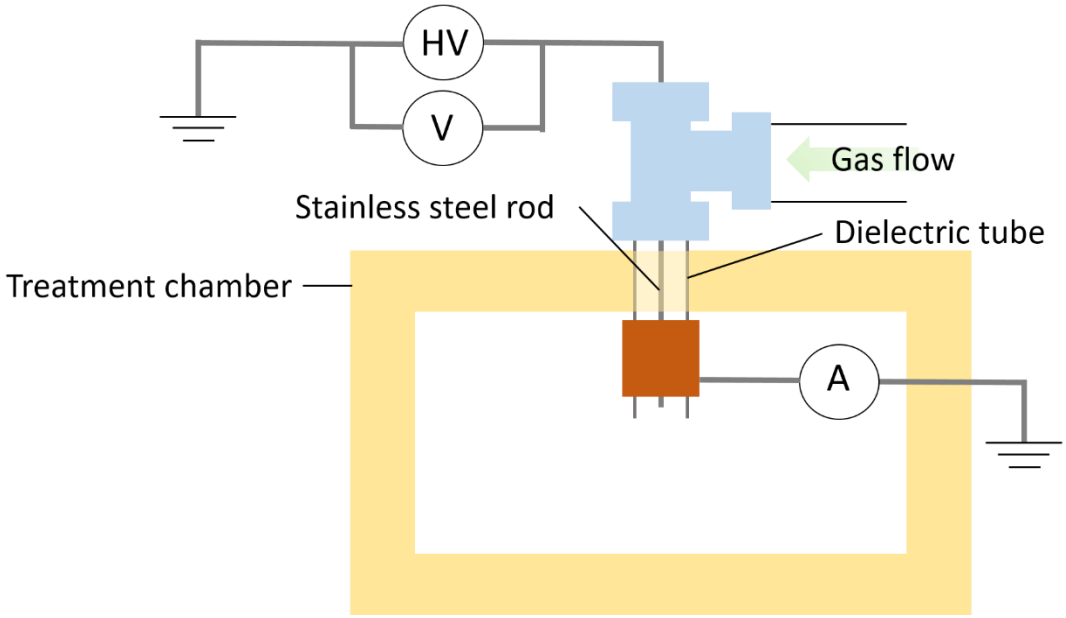

Figure 3.1 Scheme of rod system installed in chamber.

The rod system (RS) is one of the two DBD plasma generator designs considered in this manuscript. As implied by its name, the RS configuration included a metal rod connected to a HV power supply. This 2 mm outer diameter stainless steel rod was inserted into a dielectric tube with a 4 mm inner and 6 mm outer diameter, and a 24 mm long copper foil counter electrode was attached on the outer wall of the tube. The dielectric tube was made of quartz (outer diameter 6mm and inner diameter 4 mm). The feeding gas at a flow rate of 2 L/min was dry/humid argon/air depending on our experimental targets. Humid gas flow refers to the case when the totality of the gas flow was made to flow through a gas bubbler apparatus which very nearly saturated the gas with water at room temperature, or in other words, the gas was very close to100% relative humidity at ambient temperature. The gas (e.g. argon) from gas cylinders, flowed through the mass flow controller then transited a gas sparger bottle containing distilled

water.

The high voltage (HV) power supply provided an AC voltage with a variable frequency of from 10 kHz to 30 kHz. This power supply consisted of a commercial 60V/30A DC power supply coupled with a homemade H-bridge inverter and a high voltage transformer. The output voltage could be varied using this system from 7 kV to 16 kV. As shown in Figure 3.1, a voltage probe (Tektronix P6015) was used to measure the voltage at the HV electrode, and a current probe (Tektronix CT-2) was connected on the conductor which connected the counter-electrode to ground. The power was determined by integrating the product of the voltage and current. The rod DBD reactor system was installed in a treatment chamber as shown in Figure 3.1, which served to hold the reactor in place above the sample location, and to prevent ambient air from entering the system and interacting with the plasma or with the biological samples. This configuration was also applied for plasma generation in Chapter 4 and Chapter 5.

Electrical setup of TR system

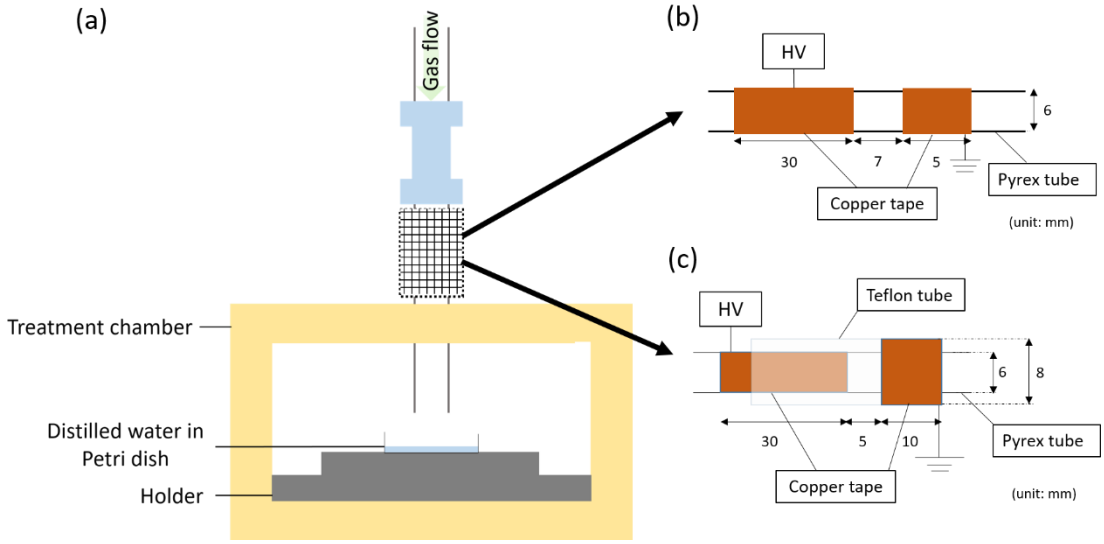

Figure 3.2 (a) The experimental setup for the measurement of H_2O_2 at the reactor outlet, the plasma generator (mesh block) can be either of the following two arrangements: (b) simple two-ring system or (c) Teflon-tube-insulated HV two-ring system.

The two-ring system (TR) was used in two different configurations for plasma generation. First, a simple TR configuration (shown in Figure 3.2(b)) consisted of two pieces of copper tape (30 mm and 5 mm) (the longer copper tape with larger capacitance for HV electrode was found to make the plasma propagate further than a smaller copper tape HV electrode, presumably due to a higher

quantity of charge at a given applied voltage leading to a more stable force) attached to a quartz tube (inner and outer diameter were 4 mm and 6 mm) with a 7 mm gap between them. The longer tape connected to the HV power supply and shorter one was grounded. These two electrodes were covered by Teflon tape in order to prevent discharges between them on the outside of the quartz tube; the breakdown voltage outside the tube was at about 15 kV. This voltage was not sufficient for the plasma to propagate over a long distance (over 20 cm) inside the tube. Therefore, the Teflon-tube-insulated HV configuration was developed. The Teflon-tube-insulated HV TR configuration consisted of a 30 mm copper tape as a HV electrode directly attached on the quartz tube and covered by a Teflon tube (inner and outer diameter were 6 and 8 mm) and a 10 mm length of copper tape grounded and attached on the outside of the Teflon tube at a distance of 5 mm along the tube from the grounded electrode (as shown in Figure 3.2(c)). This arrangement meant that the total distance for a surface discharge on the outside of the tube to bridge the gap would be on the order of 20mm, and so this configuration could operate without discharges on the outside of the tube at voltage differences over 20 kV. Either of these two configurations could be installed on the treatment chamber. The power measurement was the same as that in RS configuration. The simple TR DBD setup was connected to the AC voltage power supply with frequency of 15 kHz with argon flow rate of 2 L/min for power measurements. In addition, the Teflon-tube-insulated TR setup was connected to the pulsed voltage power supply for measurement of H_2O_2 production (detailed in the next section, H_2O_2 measurement).

H_2O_2 measurement

H_2O_2 is one of the reactive species produced during plasma-water interaction. The measurement of H_2O_2 was done in the liquid phase by optical absorption spectroscopy. Under an acidic environment (dipicolinic acid, distilled water, sulfuric acid), H_2O_2 reacts with ammonium vanadate to form yellow vanadium oxide complex. The maximum absorption of this solution was at 430 nm and was measured using a Perkin Elmer Lambda 15 UV/Vis absorption spectrometer [248]. A linear relation between H_2O_2 concentration and absorption value (Abs_{430nm}) was found:

$$[H_2O_2]_{mg/l} = Abs_{430nm} \times 642$$

The H_2O_2 production efficiency of the RS system was compared with that of simple TR system; the results of these measurements will be presented in a

subsequent section. The electrical conditions for the RS system were the following: AC voltage with frequency of 15 kHz, peak to peak voltage of 8.4 kV, and power of 1.3 W. As for the simple TR system, a fast pulse voltage arrangement (the higher voltage required for TR plasma was not easily reached using the AC power supply) was used consisting of a DC high voltage power supply (TECHNIX SR30.P.300 30 kV, 10 mA), a 1.6nF storage capacitor, and a fast high voltage (HV) switch (BEHLKE HTS 301-03-GSM). The control for the HV switch was made using a pulse generator (TTi TGP110 10MHz Pulse Generator). For the measurement of H_2O_2, TR plasma was generated at pulse voltage of 11.4 kV with frequency of 1500 Hz, pulse width of 900 ns, and power of 0.44 W. An oscillogram of the voltage waveform will be presented in a subsequent section concerning the propagation of the discharge within the insulating tube and downstream from the two ring electrodes. To collect the H_2O_2 produced in the discharge, a glass Petri dish containing 3 mL distilled water was placed at a distance of 10 mm from the tube outlet (RS or TR system) inside the treatment chamber with the experimental chamber window closed (this setup was shown in Figure 3.2 (a)). Dry argon was made to flow in the chamber for 5 min to purge the chamber (reduce the air concentration in the chamber). Next, the plasma system was turned on to treat the water in the Petri dish. The plasma exposure duration was varied from 5 to 40 min. After the exposure, 0.3 mL of the treated water was diluted with 2.7 mL of hydrogen peroxide reagent solution and put in spectrometer cuvettes for the measurement of optical absorption at 430 nm.

3.2.2 Configurations of plasma propagation

Electrical setup for the investigation of plasma propagation in quartz tube

In these studies, the same two-ring electrode DBD system that was previously described and represented in Figure 3.3, was utilized. The system, as shown in Figure 3.2, consisted of a 30 mm copper tape connecting to a high voltage (HV) power supply (pulse voltage system described in section 3.2.1) on the outside wall of a quartz tube (outer and inner diameter: 6 mm and 4 mm; length: 600 mm). The HV tape was covered by a longer Teflon tube (outer and inner diameter: 8 mm and 6 mm; length: 50 mm). Another shorter copper tape of 10 mm to be a counter electrode was attached on the outside wall of Teflon tube at 5 mm away from the HV tape. In addition to the measurement of the voltage as previously described, several different current measurements were also made. Firstly, as depicted in Figure 3.3, a home-made current probe (A_1) which was able to be used on high voltage lines, was used to measure the total current from the HV power source. Two Tektronix CT-2 current probes were also placed

on the conductors used to connect the counter electrode (A_2) and a downstream copper wire inserted into the quartz tube (A_3) to ground. The feeding gas was argon (from CentraleSupélec building gas system) with a flow rate of 2 L/min. In addition, marks were made every 2 cm from the end of grounded ring on the quartz tube in order to facilitate measurement of the propagation length.

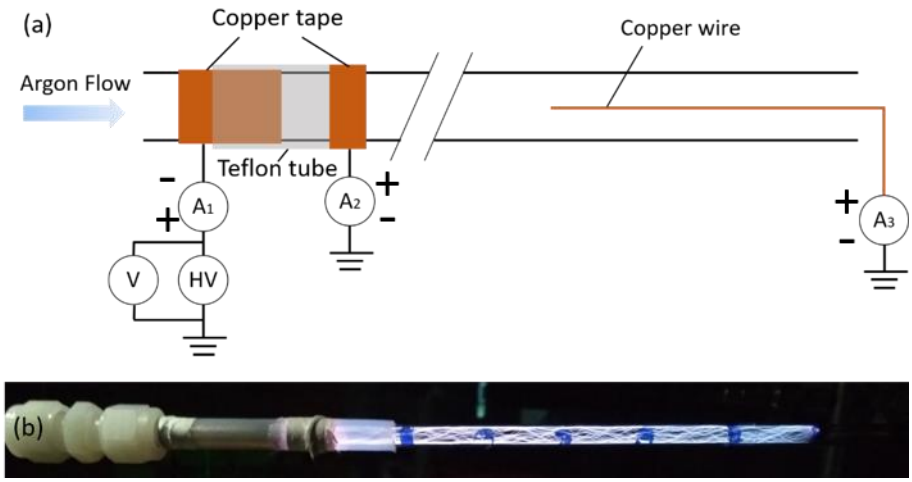

Figure 3.3 (a) Experimental setup of the two ring DBD system. A_1 is the homemade current probe, A_2 and A_3 are CT-2 current probes. (b) A photograph of plasma propagation in the tube.

For the measurement of discharge propagation distance versus applied voltage, the pulse frequency and pulse width were fixed at 500 Hz (the propagation length did not depend on frequency, but the average current was in proportion to the frequency and was lowered compared to other experiments made at 1500 Hz) and 900 ns (the streamer length increased with pulse width until 900 ns, and then, the length went into saturation), respectively. In this experiment, the propagation distance of the discharge was measured with the counter electrode placed at the tube outlet (without inserting the copper wire as in Figure 3.3). The input voltages were recorded for corresponding propagation lengths at every 2 cm from positions along the tube starting at 10 up to 28 cm.

Another type of experiment was made by inserting the external downstream wire with a current probe and measuring the discharge current conducted in the counter electrode. The pulse frequency and width were also 500 Hz and 900 ns. Measurements of input voltage were done when the current peak was measured by A_3 (Figure 3.3) fixed at 500, 1000, 1500, or 2000 mA. This was done while placing the tip of the counter electrode wire inserted into the tube at

every 2 cm starting from 2 cm (away from the edge of the ring counter electrode). Using the results of these measurements, the effective conductivity for each plasma current was then calculated by Ohm's law.

The velocity of plasma propagation was calculated by the various propagation distances and the corresponding time delay from the beginning of propagation, determined by the measurement of a current pulse at the HV electrode to the end of the propagation which corresponded to the arrival of the discharge current at the inserted counter-electrode. The velocity was measured with the input voltage ranging from 7 to 13 kV. For each value of applied voltage, the tip of the inserted wire was moved every 2 cm, starting from position of 2 cm and up to 28 cm, and the time point of the current peak was recorded. Then, the average velocity between every two points were calculated.

Electrical setup of RS plasma or TR plasma propagation in small silicon tube

diameter of 1 mm), and soft insulting silicon tubes, the stainless steel rod high voltage electrode was replaced by a tungsten needle (diameter less than 1 mm). In addition, an additional solid insulating layer was used, which consisted of a Teflon tube into which the silicon tube was placed. The grounded copper ring was replaced by a grounded copper wire (which acted to extend propagation and avoided incidental damage from handling) twisted along the entire length of the outside of the protective Teflon tube as shown in Figure 3.4. The principal function of the protective Teflon tube was the inhibition of arcing between the grounded wire and the inner silicon tube.

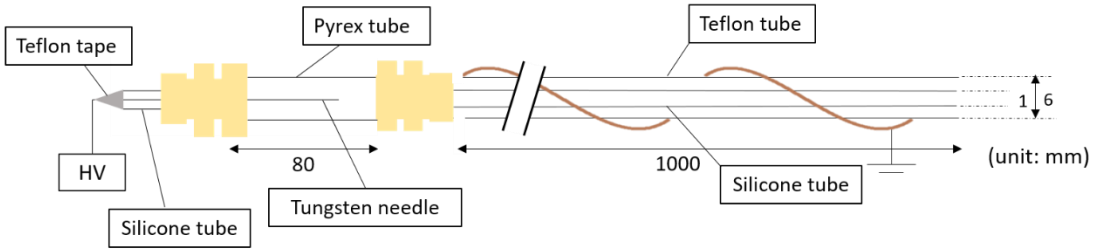

Figure 3.4 The scheme of RS plasma generator for streamer propagation in a silicon tube.

For these experiments investigating the discharge propagation, the tungsten needle was connected to a fast pulse voltage (detailed in Section 3.2.1 part of H_2O_2 measurement). For a given applied voltage and argon gas flow rate, the propagation of the plasma could be modified simply by changing the pulse width. For this system, the system variables which could be modified were the high voltage pulse width (from 420 ns to 1260 ns), the input voltage (from 10

kV to 20kV), and the argon gas flow rate (from 0.18 L/min to 0.89 L/min).

The high voltage tungsten needle electrode could be replaced by the Teflon-tube-insulated HV TR configuration to investigate the TR plasma propagation in a small silicon tube (see in Figure 3.5). The investigating plasma parameters were the same as those in the RS tungsten system.

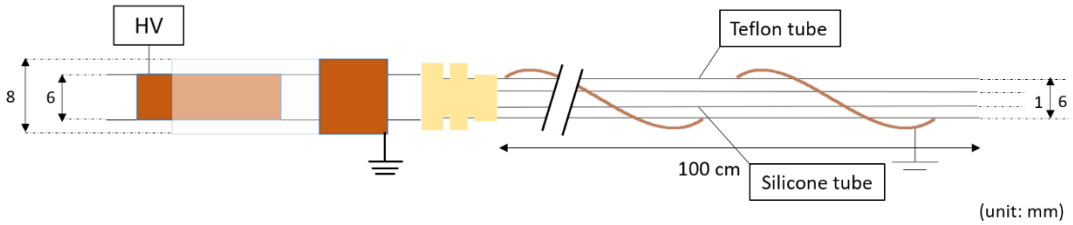

Figure 3.5 The experimental setup of the TR DBD propagating within a thin and long silicon tube.

3.3 Results and discussions

This section is divided into subsections as follows: first, a subsection will compare electrical measurements made in the two cases of the rod system (RS) and two ring (TR) DBD systems. This subsection also contains measurements of the production of hydrogen peroxide for the two systems and comparison of the energy efficiency of H_2O_2 production. Next, a subsection is dedicated to the propagation of the discharge in the interior of tubes made of insulating materials. This section contains both original work and a comparison with studies found in the literature.

3.3.1 Comparison of electrical and chemical measurements of different DBD configurations

Power measurement

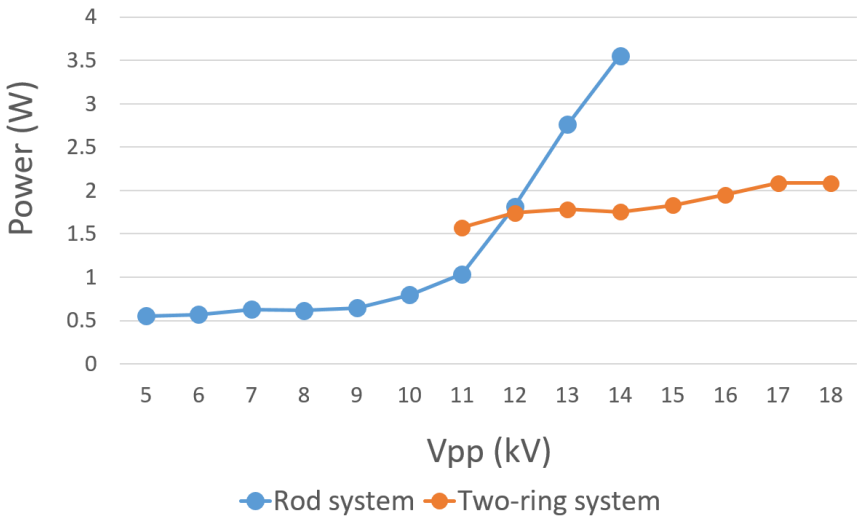

Figure 3.6 The discharge power as a function of peak-to-peak input voltage in the RS and TR systems (dry argon flow: 2L/min, AC frequency: 15 kHz).

The onset voltage of our RS configuration with dry argon feeding gas was at peak to peak voltage V_{pp} of 5 kV. V_{pp} could be increased from 5 kV to 9 kV with no significant rise in power; this stationary phase with power of around 0.5 W was followed by a sharp rise in power with peak voltage (shown in Figure 3.6 blue line). When the input voltage was over 10 kV, the power was measured to increase from 0.8 W at 10 kV to 3.6 W at 14 kV. To the naked eye, from 5 kV to 8 kV, there was no plasma plume or it was discontinuous (only a local light emission near the HV electrode tip could be discerned), and above 8kV, the plasma plume was clearly visible and stable. This may be seen to suggest that the plasma plume dissipated more power during the propagating phase than the stationary phase where it remained confined to the near vicinity of the high voltage rod electrode

The power measurement of plasma generated by the simple TR configuration is shown in Figure 3.6, orange symbols. The onset voltage was at about 11 kV with power of 1.6 W. As the input voltage rose, the power slightly increased from 1.6 W at 11 kV to 2.1 W at 18 kV.

It should be emphasized that the discharge onset voltage for RS plasma was at about 5 kV, while the onset voltage for TR was at 11 kV, over twice higher than RS plasma. This difference was on one hand due to the fact that the sharp tungsten needle electrode had a high aspect ratio, leading to a high local electric field for relatively low applied voltage. On the other hand, the physical

structure of the TR system meant that higher applied voltage was needed in order to create a high enough electric field within the quartz tube for the initiation of a discharge. Therefore, the RS plasma can work under much less applied input voltage.

It was observed that there was a difference between the plasma plumes at the tube outlet created by the two systems. Compared to the RS plasma plume, which was concentrated at one side on the tube, the TR plasma was more homogeneously spreading on the inner wall, probably due to the uniform electrode configuration.

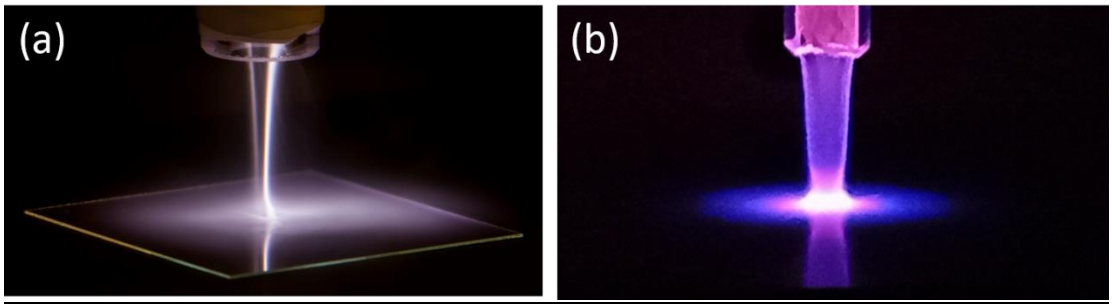

Figure 3.7 The quite comparison between (a) RS plasma plume (argon plasma, 8.1 $kV_{peak-peak}$, 1.3 W) [249] and (b) TR plasma plume (argon plasma, 15 kV, 1500 Hz, pulse width 900 ns) (photo by author). The cameras and the resolutions were different.

H_2O_2 measurement

This section will present the measurement of H_2O_2 produced by the plasma (two-ring or rod system) and absorbed by downstream distilled water. The measurement was made by optical absorption spectrometry as described earlier.

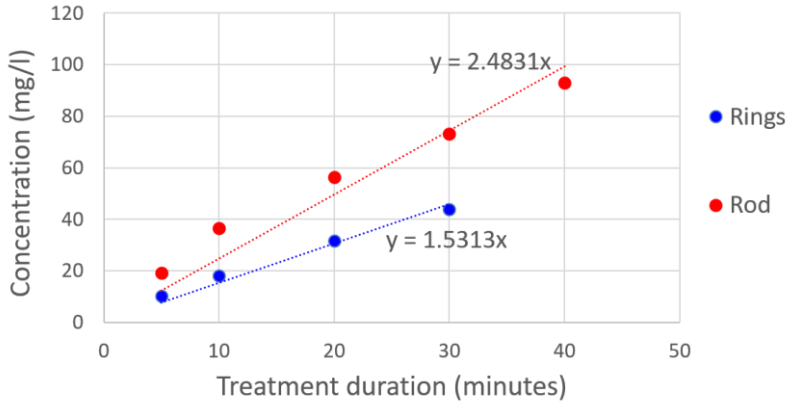

Figure 3.8 The concentrations of hydrogen peroxide increased with plasma exposure duration.

As illustrated in Figure 3.8, the RS system generated plasma (power of 1.3 W) provided the H_2O_2 concentration 19 ppm (mg/l) and 73 ppm at 5 min and 30

min exposure, respectively. The plasma created by the electrical discharge in the Teflon-tube-insulated HV TR system (power of 0.44 W) gave 10 ppm and 44 ppm H_2O_2 in 3 mL distilled water in 5 min and 30 min exposure. If these data are analyzed using linear regression, the H_2O_2 concentration rate of increase was 2.5 ppm/min for RS plasma and 1.5 ppm/min for TR plasma. This result was due to the higher power of RS plasma and perhaps related also to the absence of a barrier between HV electrode and ground in the RS plasma. The hydrogen peroxide production efficiency was calculated by H_2O_2 increasing rate, solution volume, and plasma power. The efficiency of H_2O_2 production was 0.34 g/kW·hr for RS plasma and 0.63 g/kW·hr for TR plasma.

The higher H_2O_2 production efficiency could be related to the larger cross-section of the plasma plume in TR system (see in Figure 3.7). The larger cross-section of relatively diffuse plasma plume of the TR system compared to the more filamentary discharge in the case of the RS DBD plasma may have meant that more liquid phase would be in contact with the plume, and as a result, more H_2O_2 would be absorbed by the water layer, and therefore the calculated H_2O_2 production efficiency would be higher. Alternatively, if the local temperature of the more filamentary RS discharge were higher than the more diffuse TR system, there could have been more thermal degradation of the formed hydrogen peroxide in that case, also leading to decreased energy efficiency. Further work may be done to determine the exact cause of the difference in energy efficiency for H_2O_2 production between the two systems.
Because of limitations of input voltage and power for the TR system, only the RS system was used for studies on surface decontamination (Chapter 4) and cancer cell treatment (Chapter 5). From the perspectives of medical application perspective, the TR plasma is considered to be a safer plasma source because of the additional dielectric barrier separating the high voltage source and the patient. The TR system may also provide higher plasma-substrate interaction area and the higher ROS production per input energy will be advantageous for application to plasma medicine in the future.

3.3.2 Plasma propagation in tubes

Plasma propagation in quartz tube

In this section, the Teflon-tube-insulated HV TR system connected to a 60 cm quartz tube was applied for the generation and propagation of plasma created by an electrical discharge. The measurement results showed that both the propagation length and the power increased with increasing applied voltage. In

Figure 3.9, the propagation length versus the voltage followed a nearly linear growth curve, however, the power versus the voltage was observed to increase in a more exponential fashion. This can be interpreted as an increasing energy cost for propagation, presumably because of increasing losses at more energetic discharge regimes. Because the voltage at the tip of streamer is presumably decreasing during the propagation, the propagation stopped when the voltage was less than the onset voltage for new avalanches. The voltage drop along the plasma channel during plasma propagation is an important aspect of this system, and it is for this reason that relevant measurement results on the voltage gradient are presented later in this section.

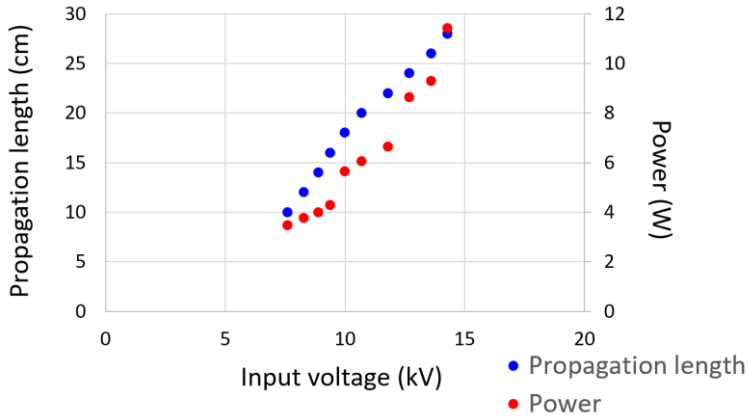

Figure 3.9 Propagation length of the discharge in Teflon-tube-insulated HV TR system and corresponding mean input power as a function of pulsed voltage amplitude (900 ns pulse width, 1500 Hz).

Discussion of plasma propagation in quartz tube

The streamer propagated from the inner surface of the quartz tube near the high voltage electrode (ion deposition on inner wall of tube and nearby free electron) and grounded downstream wire (luminous channel) [154]. In previous studies, the voltage gradient of the propagating plasma channel from a HV tungsten needle placed inside the tube was measured [250]. The results from this work showed electric fields of 520 V/cm for dry argon plasma and 590 V/cm for humid argon plasma (water vapor 760ppm) when the current peak was fixed to 550 mA. In our two-ring system results, a value of 217 V/cm electric field was calculated from the measurements made at 500 mA with feeding gas of dry argon. Further measurements were done for four constant currents. Figure 3.10 shows that higher current resulted in higher voltage drops as may be expected: 217 V/cm for 500 mA, 288 V/cm for 1000 mA, 389 V/cm for 1500 mA, and 413 V/cm for 2000 mA.

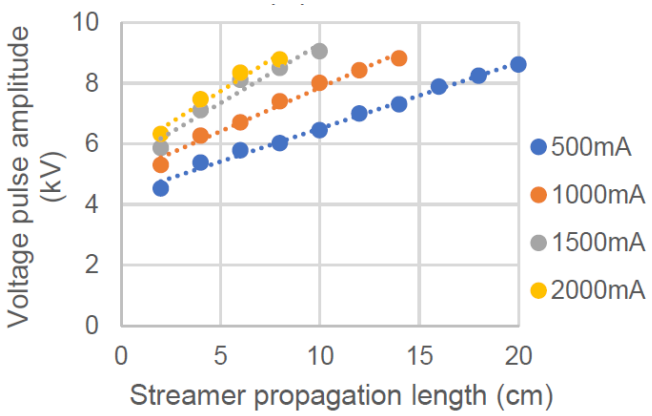

Figure 3.10 Pulse voltage amplitude (900 ns pulse width, 1500 Hz) as a function of discharge propagation length for given current pulse amplitude.

Considering the Ohm's Law calculation as proposed in Ref. [154], and assuming either single streamer with constant diameter of 30 µm or multiple streamers constructing a donut distribution on the inner wall with thickness of 30 µm, the conductivity of the plasma was calculated using the simple relation:

$$\vec{J} = \sigma\vec{E}$$

Where $\vec{J}$ is current density, σ conductivity, and E electric field (voltage gradient). Results are presented in Figure 3.11. As expected, higher current pulses result from both higher charged particles density and drift velocity, and plasma conductivity therefore increases with discharge current. Between these two geometric assumptions, the one with multiple streamers (Figure 3.11(b)) were consistent with the simulation result in previous literature [251].

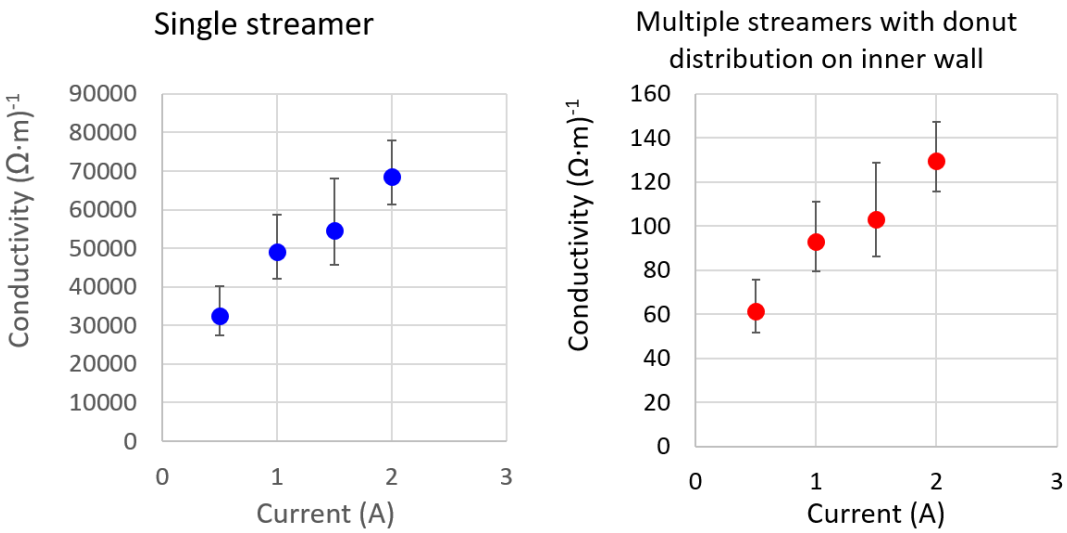

Figure 3.11 Conductivity calculation with assumption of streamer geometry: (a) single streamer and (b) multiple streamers.

Nevertheless, the voltage measurement made using the probe at HV side did

not really represent the voltage inside the tube (the above calculations were made assuming this was the case). The voltage reached on the inner surface of the quartz tube near the HV electrode is important because it is this voltage which corresponds to the actual electric field which the gas on the inside of the tube is exposed to. In order to estimate this voltage using the known applied voltage at the copper ring on the outside of the tube, it is necessary to know the capacitance of the TR system and then it will be possible to correct the voltage distribution in the gas gap between the two rings.

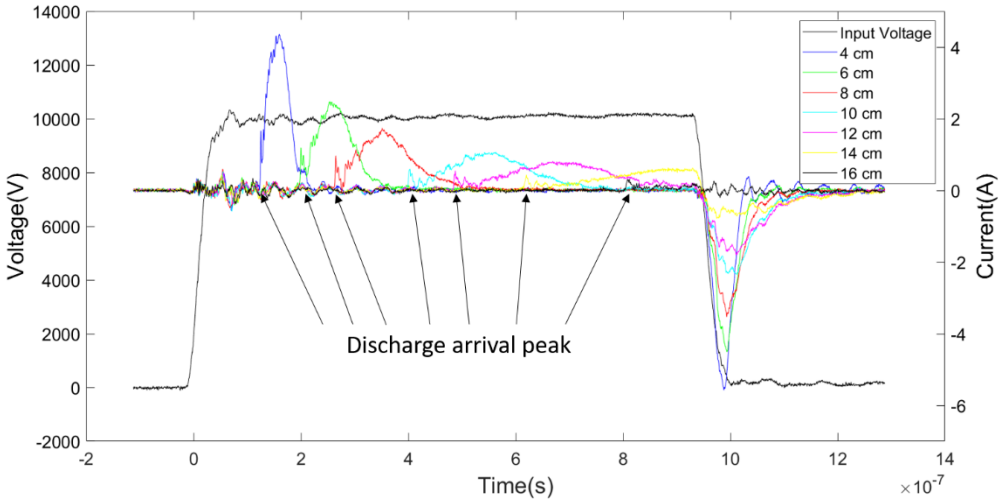

Figure 3.12 Oscilloscope traces for the current measurement at downstream wire (A_3) with the input voltage of 10 kV. The tip of wire was moved to every 2 cm from 4 to 16 cm away from the counter electrode (the distance between HV electrode and the edge of counter electrode was 1.5 cm).

The velocity of plasma propagation was also measured in previous studies of pulsed corona configuration [250]. With the feeding gas of dry argon, the streamer velocities were 5.0×10^5 m/s near the beginning of the propagation (at a position of 13.5 cm in the tube) and 2.3×10^5 m/s at a point in the propagation further downstream (47.5 cm) at 23.3 kV. In our Teflon-tube-insulated HV TR system with dry argon condition and with the input voltage ranging from 7 kV to 13 kV, the total propagation length was up to 27.5 cm downstream of the HV electrode. The arrival time data were recorded when the streamer was reaching every 2 cm from 3.5 cm to 27.5 cm. The average velocity of the propagation was calculated and shown in Figure 3.13. In the case of input voltage at 13 kV, the average velocity was 5.48×10^5 m/s at 9.5 cm of propagation and 2.87×10^5 m/s at 27.5 cm of propagation, and the therefore the results matched the prediction in Ref. [250].

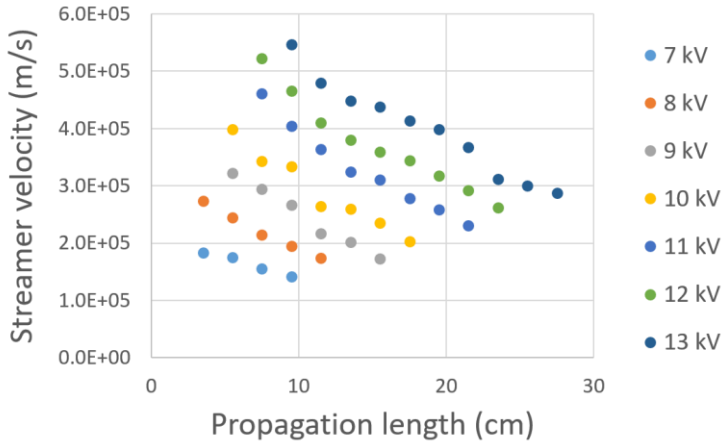

Figure 3.13 Average streamer velocity at various input voltages in different propagation length.

Furthermore, if it may be assumed that the change in the electric field distribution was negligible in the case when the downstream wire was moved in 2 cm increments, the instantaneous streamer velocity can be calculated, for example the instantaneous velocity $V_{4.5m}$ at 4.5 cm:

$$V_{4.5cm} = \frac{2 \ \text{(cm)}}{t_{5.5cm} - t_{3.5cm}}$$

The results of this calculation are shown in Figure 3.14 For an input voltage of 8 kV, the streamer velocity at 4.5 cm was 2.21×10^5 m/s and at 10.5 cm, it was 1.21×10^5 m/s. For applied voltage of 13kV, the streamer velocity at 10.5 cm was 3.21×10^5 m/s and decreased to 1.89×10^5 m/s at 26.5 cm. The higher voltage of course creates a stronger electric field, and therefore induces more acceleration on free electrons during avalanches, resulting in faster drift velocity. Even though the tip of downstream electrode was located at different distance from the HV electrode, the "return" discharges (the discharge observed immediately after the annulation of the voltage pulse) happened very rapidly after the voltage drop (shown in Figure 3.12 at t=1000 ns).

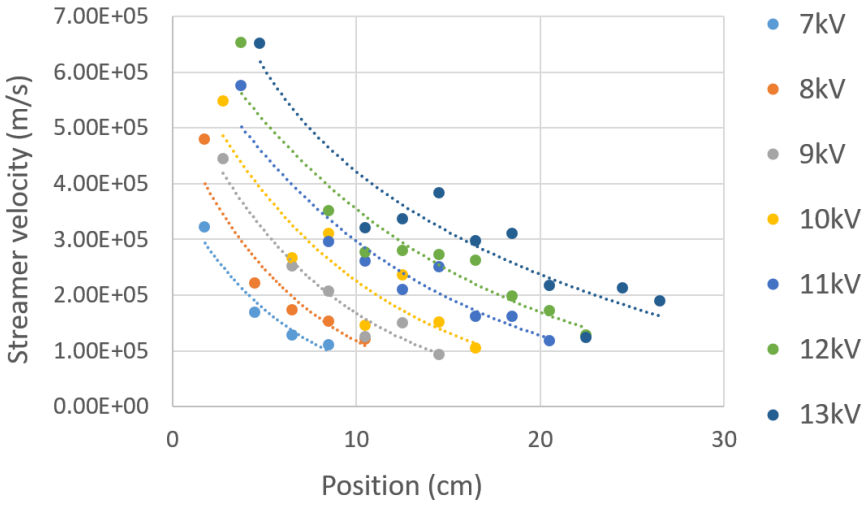

Figure 3.14 The instantaneous streamer velocity at every position with input voltage from 7 to 13 kV.

Analysis of electrical waveform

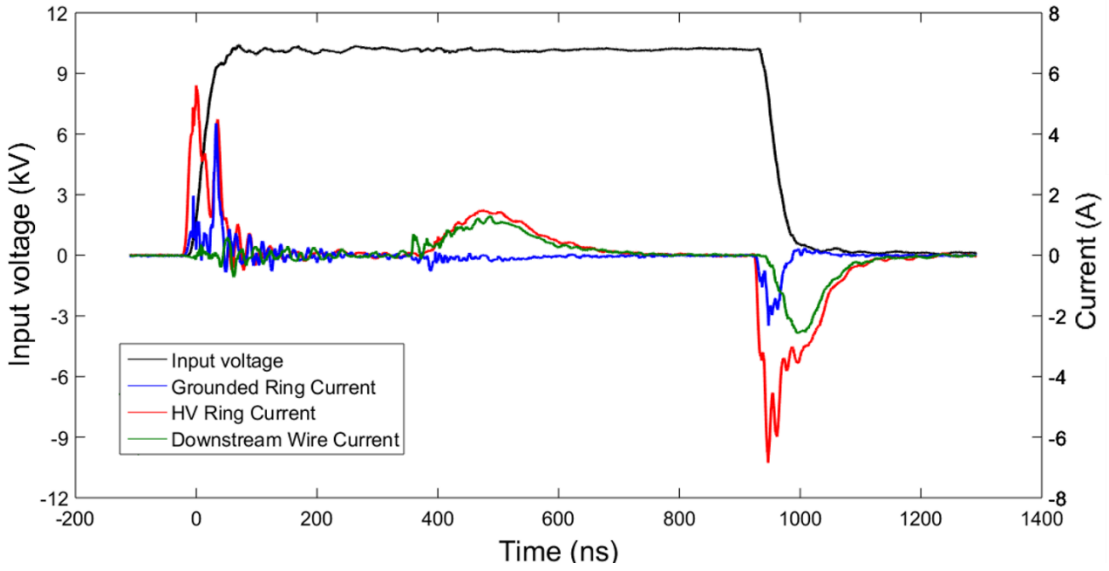

Figure 3.15 Oscilloscope traces of voltage (black) and three current signals: at the HV electrode (A_1-red), counter electrode (A_2-blue), and downstream electrode (A_3-green) (see Figure 3.3). Grounded downstream electrode located at 10 cm away from the grounded ring.

During the streamer propagation, the current signal was simultaneously recorded at three different locations: at HV electrode (A_1), grounded ring (A_2), and downstream side (A_3) (as illustrated in Figure 3.3). These current signals are shown in Figure 3.15 for a pulse width of 900 ns.

The two-ring system may be thought of simply as a capacitor, including two electrodes of copper tape, and a mix of dielectric materials consisting of quartz and Teflon tube barriers, and a gas gap. At the beginning of a voltage pulse, the

input voltage increased and displacement currents appeared. The high displacement current in A_1 corresponds to the combined capacitance of the two-ring arrangement and the capacitance of the HV probe itself. When the voltage reached the inception voltage of the two-ring system, the discharge was generated inside the tube in the high electric field region confined on the inner surface of the quartz tube between the two ring-electrodes. At this moment, very similar signals were measured by current probes A_1 and A_2. Then, due to the free electrons, photoionization, and new avalanches, the streamer propagated from the inner surface of the quartz tube near the grounded ring and propagated toward the downstream wire. When the streamer reached the electrode, a small positive pulse signal followed by a large current pulse (at 400 ns in Figure 3.15) was measured by the downstream current probe A_3. The HV current probe simultaneously measured a very similar current pulse, but the grounded ring probe only measured a low amplitude negative current pulse (no large positive current pulse detected). These observations suggest that the current flowed from DBD plasma source and also a bit from the counter electrode to the downstream wire through the propagated plasma channel. During this phase, a charge build-up takes place on the quartz tube inner surface, resulting in a progressive decrease of the local electric field along the tube length. As a consequence, the discharge current progressively decreases, reaching a zero value at 750 ns. At the instant when the applied voltage drops at the end of the voltage pulse, a displacement current was detected by A_1 at HV and A_2 at the grounded ring. Then, due to the voltage change in the tube, the negative current measured by A_3 flowed back to A_1 (negative current) and A_2 (positive current).

Thus, the system may be summarized into five phases as follows: 1) the fast rise of the voltage causes a large displacement current, 2) the resulting large electric field inside the tube initiates a plasma in the zone on the inner surface of the tube delineated by the two electrodes, 3) the resulting charge accumulation on the inside of the tube near the grounded ring electrode causes a discharge which propagates down the tube, reaching the downstream grounded wire electrode, and the associated current is seen by both probes A_1 and A_3, 4) the annulation of the applied voltage causes a new displacement current, and finally 5) the charges accumulated along the tube length are evacuated via a back discharge under the influence of their own electric field. Some questions remain, such as why the small positive signal occurs (at about t=380 ns in Figure 3.15) as measured by A_3 (perhaps corresponding to current induced by the

approaching streamer head?), and the reason for the shape and duration of the large current peak (measured by both A_1 and A_3 between 400 and 600 ns). Further studies should be done with optical emission spectroscopy to better understand the different phases of plasma propagation in this system.

Plasma propagation in a thin silicon tube

A 100 cm long plasma propagation was achieved in a thin silicone tube when using the rod system (RS) DBD configuration (shown in Figure 3.16). Such a propagating discharge could be envisaged to be used on medical devices such as endoscopes, or even inside the human body in the future. A parametric study of the discharge propagating inside the small diameter silicon tube was done and will be presented here.

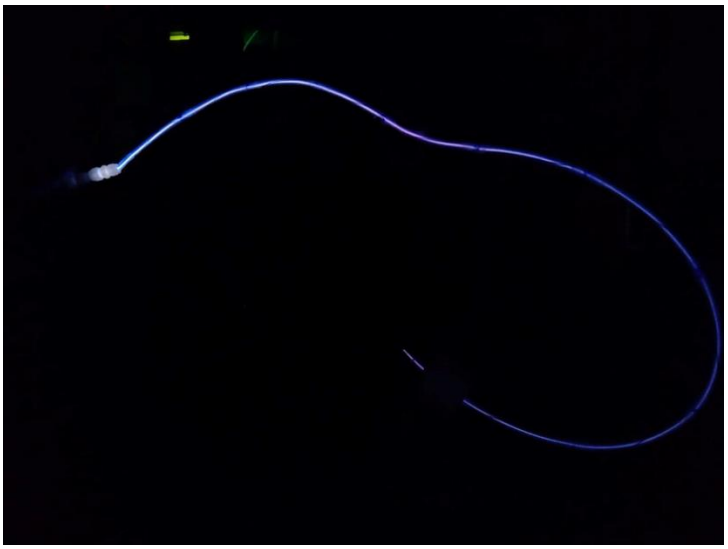

Figure 3.16 The RS plasma propagation in 100 cm length thin silicon tube. (pulse amplitude:20 kV, width: 1000 ns, frequency: 500Hz, feeding gas: dry argon and mass flow rate: 0.41 L/min).

Because the cross-section of the silicon tube (1 mm inner diameter) was much smaller than the quartz tube (inner diameter 4 mm) used before, the mass flow rate was reduced to have similar flowing velocity and pressure drop to other experiments. Figure 3.17 presents the plasma propagation length (as seen by eye in a dark room) as a function of the pulsed voltage amplitude and for different gas flow rates with pulse width 900 ns. The gas flow rate of 0.06 L/min gave the shortest propagation length under the same pulse amplitude, but the propagation length was similar for the other flow rates as seen in the figure. The mass flow rate helping the plasma propagate over the longest distance was in the region between 0.30 and 0.59 L/min. An intermediate value for the mass flow rate of 0.41 L/min was chosen for further investigation.

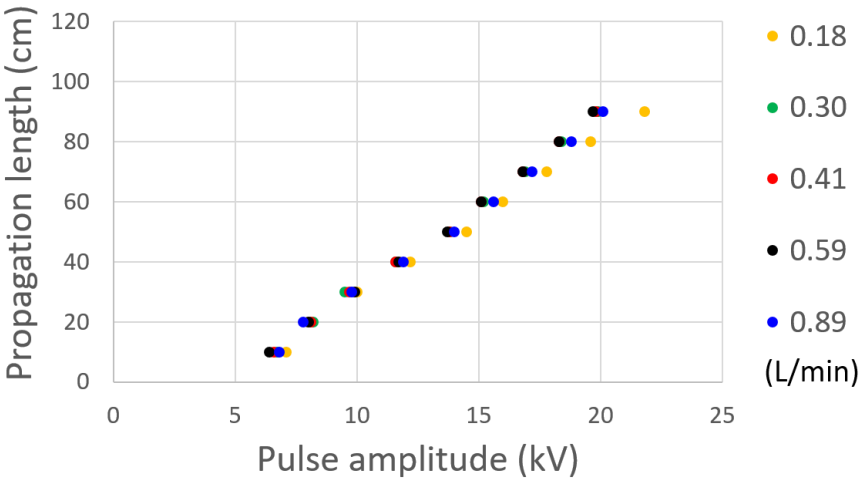

Figure 3.17 The RS plasma propagation length versus pulse amplitude with given argon mass flow rate (pulse width: 900ns and frequency: 265 Hz).

Besides the mass flow rate of feeding gas, the pulse width was another variable to control the plasma propagation length. Figure 3.18 presents the propagation length, again as a function of pulsed voltage amplitude, for different pulse widths. For a given pulse amplitude, the shortest pulse width of 420 ns caused the plasma to propagate over the shortest distance as might be expected. In other words, propagation distance increases with pulse width for a given applied pulse amplitude. One way of representing this is shown in Figure 3.18: for a given propagation distance, for example 90 cm propagation length, case of a discharge created by an applied voltage pulse with pulse width of 420 ns required 22.4 kV, 630 ns needed 20.6 kV, 840 ns needed 19.8 kV, 1050 ns needed 19.6 kV, and 1260 ns needed 19.4 kV. However, as shown in Figure 3.19 (fixed pulse amplitude with various pulse widths), the propagation length stopped increasing or went into a saturation phase (longer pulse widths no longer leading to further propagation) when the pulse width was longer than 900 ns, for all measured applied pulse amplitudes.

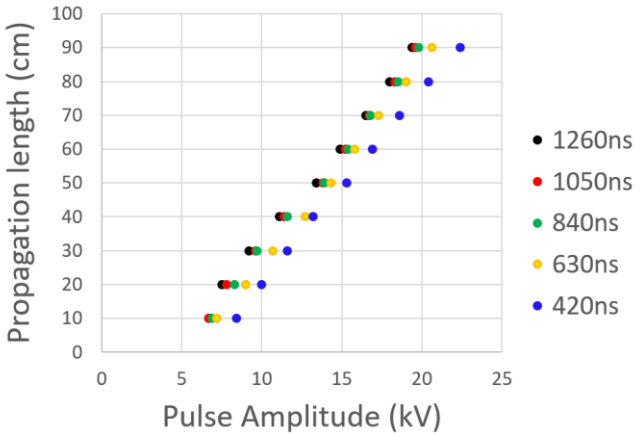

Figure 3.18 The RS plasma propagation length versus pulse amplitude with given pulse widths (argon mass flow rate: 0.41 L/min and pulse frequency: 265 Hz).

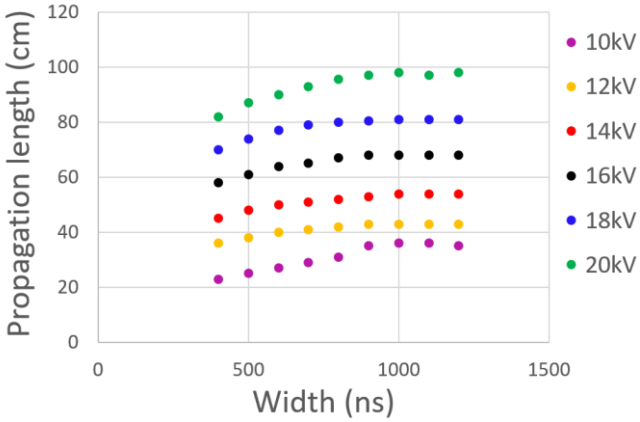

Figure 3.19 The RS plasma propagation length versus pulse width at fixed pulse amplitude (argon mass flow rate: 0.41 L/min and pulse frequency: 265 Hz).

This saturation phase for propagation stagnating above a certain value of applied voltage pulse width has also been previously observed. In reference [160], it is hypothesized that the width of the voltage pulse is related to the energy supply to the plasma bullet. When the width increases from several hundred nanoseconds to about one thousand nanoseconds, the propagation of plasma bullet was reported to elongate [160]. There is a critical pulse width value around one thousand nanoseconds, above which the length of plasma propagation was reported to go into saturation, much as observed in our work.

It can be noted that, from the point of view of possible medical applications, the shortest pulse width with longest plasma propagation should be chosen to avoid a galvanic high voltage connection between the tungsten needle and sample at the tube outlet via the plasma channel inside the silicon tube. A photograph of the TR plasma propagation in a 40 cm silicon tube inserted in

the treatment chamber is shown in Figure 3.20. In this configuration, the plasma propagation at the silicon tube outlet could be touched with the finger without the sensation of electric shock

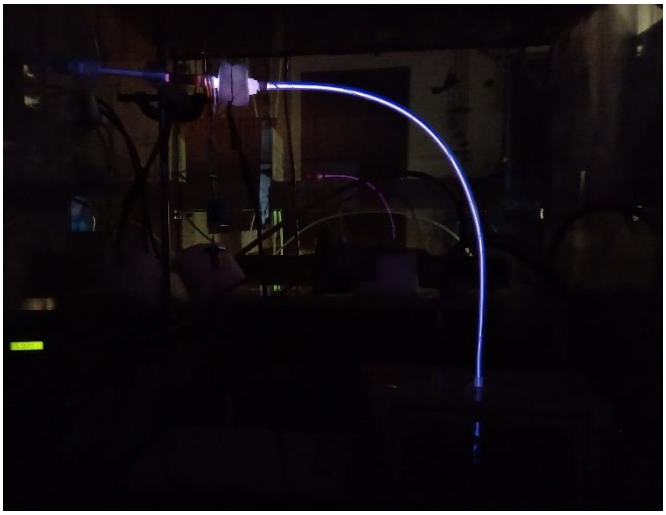

Figure 3.20 The plasma generated by the Teflon-tube insulated HV two-ring system propagated in a silicon tube (50 cm) inserted into the treatment chamber. (Pulse amplitude: 18.2 kV, frequency: 2000 Hz, and width: 8200 ns dry argon mass flow rate: 0.6L/min)

Due to the smaller diameter of the silicon tube (the same reason in TR silicon tube system), a different mass flow rate of feeding gas was tested than for other experiments with larger diameter tubes. From the propagation length measurement shown in Figure 3.21, increasing gas flow rate over 2 L/min helped modestly to propagate the plasma further along the tube. The input voltage (V_{36}) for the streamer length of 36 cm varied from16.5 kV with gas flow rate of 2.4 L/min to 16.3 kV with 3.3 L/min. This difference of V_{36} between the two cases being small, the lower gas flow rate (2.4 L/min) was chosen for further measurements. The result was in contrast to the result of RS plasma, for which the optimal gas flow rate was less than 2 L/min. In TR plasma, the better gas flow rates were higher than 2 L/min. The major difference between the RS configuration and the TR configuration as far as gas flow is concerned was that the tungsten needle inserted in the tube for the RS system may have perturbed the gas flow, causing turbulence.

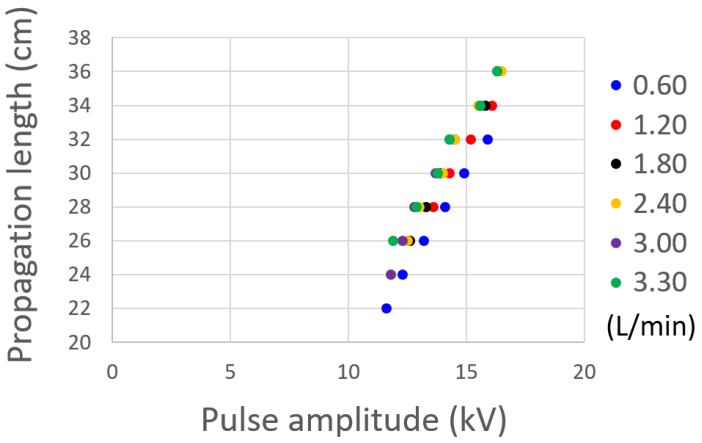

Figure 3.21 The TR plasma propagation length versus pulse amplitude with given argon gas flow rate (pulse width: 1500ns and frequency: 265 Hz).

In Figure 3.22, the plasma propagated farther with rising pulse amplitude for a given pulse width fixed from 420 ns to 1500 ns. Under the same pulsed voltage amplitude, a streamer propagated furthest with the width of 1500 ns (from 11.8 kV for 24 cm to 16.5 kV for 36 cm). The saturation phase of pulse width was again observed, as shown in Figure 3.23, with gas flow rate of 2.4 L/min and fixed input voltage, the plasma propagation length stopped increasing when the pulse width was raised over 2000 ns (compared to RS plasma at 900 ns)..

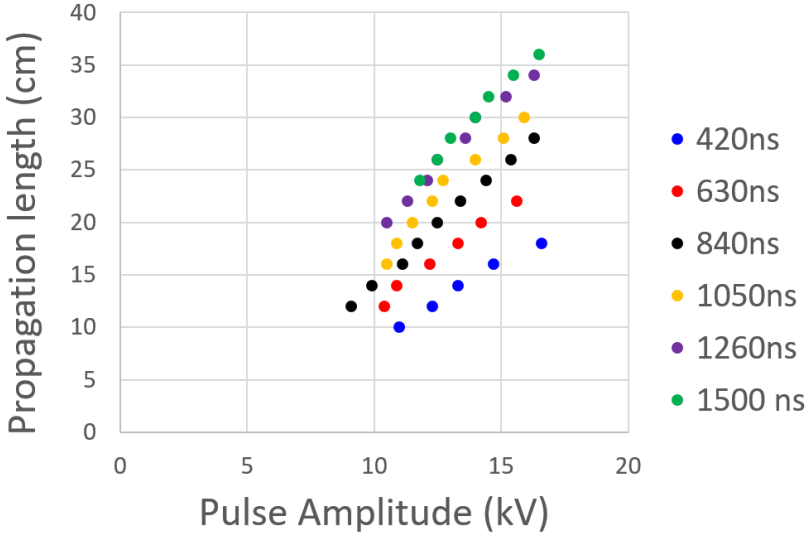

x

Figure 3.22 The TR plasma propagation length versus pulse amplitude with given pulse widths (argon mass flow rate: 2.4 L/min and pulse frequency: 265 Hz).

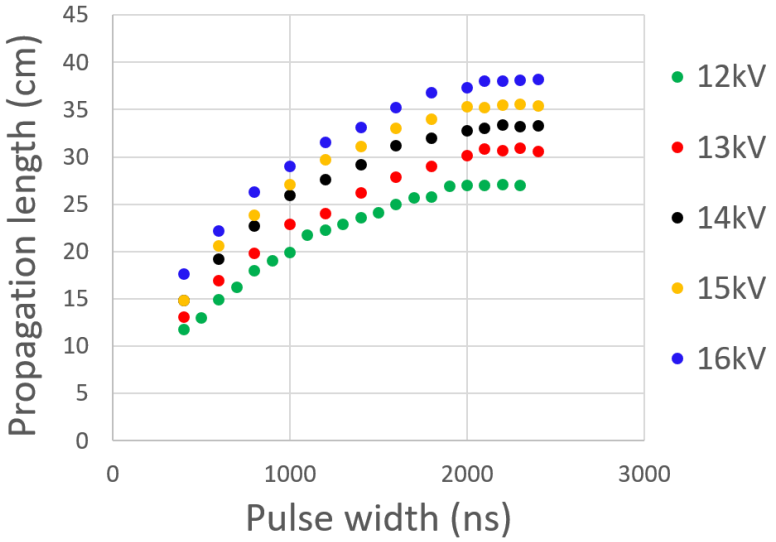

Figure 3.23 The TR plasma propagation length versus pulse width at fixed pulse amplitude (argon mass flow rate: 2.4 L/min and pulse frequency: 265 Hz).

In this section, plasma parameter for reaching the longest propagation has been found, however, the conditions for this long propagation would not be suitable for the experiments on bio-samples. The gas velocity of the gas at a flow rate of 2.4 L/min in a small silicon tube was very high and caused mechanical pressure on sample. Therefore, a much longer pulse width and much smaller gas flow rate was used to make the photo of plasma propagation for the future treatment shown in Figure 3.20.

From the measurement result, the RS plasma propagation length can easily exceed 90 cm at 20kV, while the TR plasma only can only propagate to a distance of about 50 cm. It might be due to the different voltage distributions in the two configurations. In the RS configuration, the HV electrode was a bare conductor inside the tube whereas in the TR configuration, the "electrode" was actually the inner surface of the insulating quartz tube, the high electric field was therefore along the inner surface of the quartz tube between the two copper rings. Therefore, the two systems had some fundamental differences and the propagation length of the TR plasma was observed to be shorter than RS plasma in general. Alternatively, the shorter propagation distance in the RS system could have simply been due to turbulence created by the presence of the tungsten needle high voltage electrode, an effect which is found in the literature.

3.4 Summary

The characteristics of RS and TR system plasma were measured and discussed in this chapter. In the power measurement of the rod system (RS) DBD dry argon plasma, there was a stationary phase where the power remained at about 0.5 W with applied AC voltage of 5 to 9 kV and an increasing phase where the power significantly rose from 0.8 W at 10 kV to 3.6 W at 14 kV. The power of the discharges generated by the simple two ring (TR) configuration was measured to increase from 1.6 W at 11 kV to 2.1 W at 18 kV; the power in this case increased linearly rather than the exponential increase observed in the RS configuration. The different discharge onset voltages between the RS DBD plasma system and the TR DBD plasma system was due to the higher local electric field of the high aspect ratio rod structure.

Chemical measurements were made on the systems, notably the H_2O_2 production from RS plasma and from TR plasma were compared. RS plasma under the power of 1.33 W produced 2.48 ppm/min H_2O_2 in 3 ml distilled water, and TR plasma produced 1.53 ppm/min under the plasma power of 0.44 W in the same volume of water. To compare the two systems, the production efficiency of the TR plasma (0.63 g/kw·hr) was higher than that of RS plasma (0.34 g/kw·hr). The difference in efficiency might be explained by the more diffuse nature of the plasma plume in TR plasma system compared to the RS plasma system. The larger area of plasma-liquid phase interaction with plasma generated by TR system compared to the RS plasma as well as its higher level of safety led to the choice of the TR system for future application.

The propagation of the electrical discharge DBD plasma along the inner surface of tubes made from insulating materials was studied in a modified two ring system, the Teflon-tube-insulated TR HV system. The length of the streamer was observed to be extended by an increase in the applied input voltage. When an external downstream wire with a current probe was inserted in the tube to measure the current of streamer (It should be noted that the presence of the inserted grounded electrode changed the electric field inside the tube and therefore the propagation), the voltage gradient was calculated at fixed current. Through Ohm's law, the conductivity calculated by an assumption of multiple streamers was obtained and consistent with literature. For increasing discharge current, the conductivity of the plasma channel was calculated to be increase. Furthermore, the downstream wire was also used to measure the velocity of

propagation. Under fixed input voltage, the velocity decreased with increasing propagation length. At the same propagating position, the velocity was faster with higher input voltage. Different phases of plasma development and propagation including displacement current, discharges, plasma propagation, charged particle deposition, and "return" or "back" discharges were identified using oscillograms of the current in three different locations in the system. Future work is recommended on optical emission spectroscopy, to be applied to further investigate plasma propagation.

In addition, a smaller RS configuration was used and connected to a 100 cm length, 1 mm inner diameter silicon tube to investigate plasma propagation. This system was able to cause plasma propagation over 100 cm inside the silicon tube. The gas flow rate of the feeding gas was lowered to 0.41 L/min for the experiments with the thin tube, thus maintaining a similar gas velocity compared to the larger diameter quartz tube used in other experiments. The propagation length was observed to enter a saturation phase (the length was not dependent on pulse width anymore) when the pulse width was longer than 900 ns.

Furthermore, the TR configuration was also able to be connected to a downstream silicon tube. The optimum gas flow rate of over 2 L/min in TR configuration was in contrast to that observed for the RS configuration. The saturation phase of pulse width was at 2000 ns, longer than the one in RS configuration (900 ns). Under the same pulse voltage, the propagation length in TR configuration was much shorter than that in RS configuration due to the starting voltage in the tube. Even though we can generate a plasma propagating over 35 cm in a small silicon tube by TR system, the high flow rate would give high mechanical pressure on the sample in the future medical application. Therefore, optimized plasma parameters are still under investigation. For example, as in Figure 3.20, the TR plasma is shown to propagate over 50 cm in a small silicon tube with low flow rate and large pulse width.

4 SURFACE DECONTAMINATION

4.1 Introduction

Newly emerging viruses such as SARS-CoV-2, the cause of Covid-19, are affecting the entire way of life of human society on Earth. In 2020, this disease swept all over the world, until today, there are over 418 million people being or been infected [252]. It is eager to have a surface decontamination method with high efficiency on virus deactivation. Non-thermal plasma is one of the options (detailed in Section 2.3).

Many DBD systems for plasma generation have been investigated for surface decontamination [6, 166, 168], and provided promising results for inactivation of bacteria. The systems under study in this work were also tested in this perspective. An example of result is given in Figure 4.1. Planktonic samples were directly treated in Petri dishes by the two-ring plasmas system. Just before treatment, 100 mL of bacteria culture (*Escherichia coli* MG1655 - 10^8 CFU/ml in LB broth) was spread on LB agar Petri dish. The Petri dish with *E. coli* culture was inserted into the treatment chamber 10 mm under the tube outlet ("X" marker facing the tube outlet). After flushing the chamber with dry argon (5 min.), the sample was submitted to a 5 min. dry argon (2 L/min) plasma treatment. After treatment, the samples were incubated at 37˚C overnight. A 15 mm diameter area without any colony or lawn around the treated point was observed, attesting to the decontaminating effect of such a treatment.

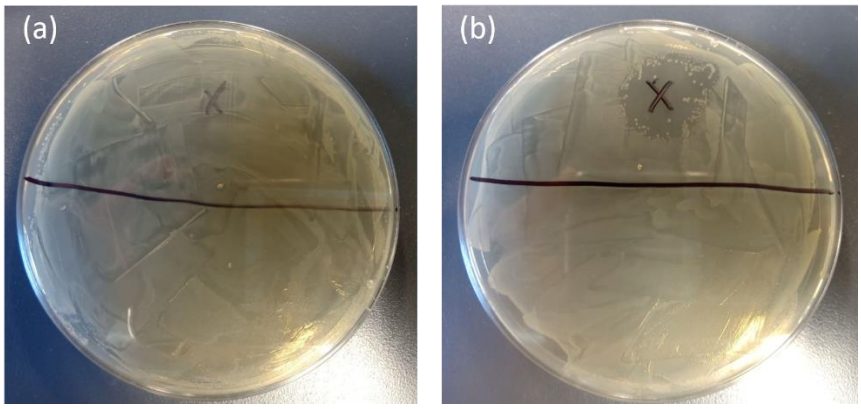

Figure 4.1 Overnight incubation Petri dishes of *E. coli* after (a) 5 min. dry argon flow only and (b) 5. min argon plasma treatment (two-ring system 0.45 W).

It was then decided to conduct a study on the inactivation of viruses carried by a surface using such non-thermal plasma sources at atmospheric pressure.

It is worth noting that the inactivation of the surface-borne SARS-COV-2 virus using a non-thermal plasma device (argon-helium jet plasma) has already resulted in a study with promising results in terms of effectiveness [253]. More recently, argon jet plasma was tested for inactivation of SARS-CoV-2 like viruses and for different SARS-CoV-2 variants. A 3 log reduction in viability of Delta variant was obtained for 5 min exposure to treatment [254]. However, the authors indicate that this encouraging result should motivate further research and it is with this objective that the present study was conducted. As we did not have the environment to manipulate human viruses, we have chosen to use bacteriophages as surrogate models to corona virus. Two different kinds of bacteriophages were examined (Figure 4.2):
Bacteriophage T4 is a virus that infects Escherichia coli bacteria. It is a double-stranded DNA virus in the subfamily Tevenvirinae from the family Myoviridae. T4 is a large size virus: 125 nm including capsid and tail.

Bacteriophage MS2 (*Emesvirus zinderi*) is also a virus that infects the bacterium *Escherichia coli. It is* a single-stranded RNA. MS2 is a small size virus (25nm) with a round shape.
Hereafter, T4 and MS2 will refer to Bacteriophage T4 and Bacteriophage MS2 respectively.

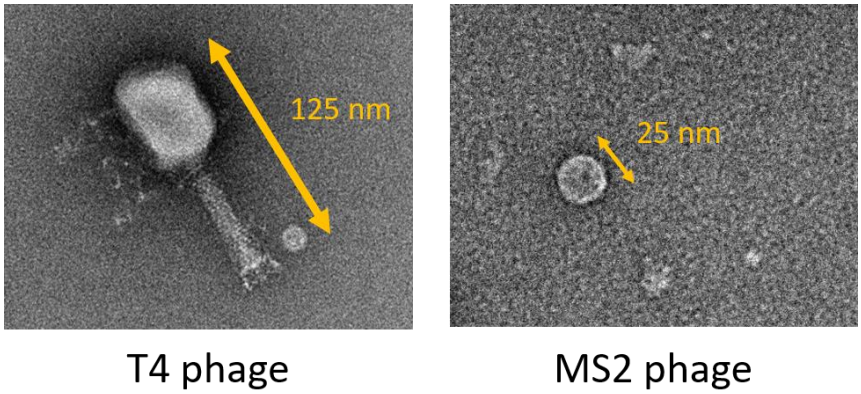

Figure 4.2 Transmission electron microscopy images of T4 (left) and MS2 (right).

RNA bacteriophage MS2 will be considered as a surrogate model to SARS-CoV-2. Obtained results will be compared and discussed with those observed for DNA bacteriophage T4 treatment.

4.2 Materials and methods

Bacteriophage culture, spotting, exposure, recovery, and assay

Bacteriophage T4 and MS2, and host bacteria, *E. coli* MG1655, and *E. coli* MG1655 F+, were provided by INRAE (Jouy-en-Josas, France)

4.2.1 Preparation of phage stock

The process of preparing phage stock was similar to double-layer agar method of plaque assay (detailed in Section 4.2.4). One day before preparing the phage stock, the liquid phase of bottom agar (LB broth or NB broth with 1.25% agar) with 1 mM $CaCl_2$ were poured in Petri dishes. Note that LB and NB broth solutions were used for T4 and MS2 respectively. These Petri dishes were incubated at 37°C for 24 hours to dry the surface of agar (to reduce the spreading area of plaque). On the exact day of new stock making, the liquid phase of top agar (LB broth or NB broth with 0.5% agar) with 1 mM $CaCl_2$ was stored in glass tubes (2.5 mL per tube) in the heating block at 50°C. Overnight culture of host bacteria was 10% resuspended in medium (LB broth or NB broth) and the resuspension solution was incubated at 37°C for one hour. After an hour incubation, 100 µL of host bacteria culture and the proper number of phage particles (to end up with 10 000 PFU – Plaque Forming Unit - per plate) from the old phage stock was poured in the glass tubes with top agar. The tubes were vortexed and then the suspension was poured on the 24-hour-old bottom agar plate. When the top agar solidified, Petri dishes were moved to an incubator at 37°C. Multiple rounds of phage infection and lysis was processing during the incubation of 20 hours. On the second day, 5 mL of LB broth or NB broth was added in the Petri dishes, and then the plates were stored at 4°C for about 7 hours; the plates were occasionally swirled during this period. The fluid in the plates was collected by pipetting and deposited in Eppendorf tubes for centrifugation (3 345 x g) to separate bacteria or agar fraction from the phage suspension. The supernatant was filtered with a 0.2 µm syringe. The filtrate was collected in a glass bottle, and the phage lysate was tittered.

4.2.2 Bacteriophage spotting and recovery on solid substrate

The chosen surface material for phage spotting was water-soluble paper (WSP) (Aquasol ASW-35 sodium carboxyl methyl cellulose and wood pulp; 35 µm thick). This material fully dissolves in most aqueous solutions. The use of this support material solves the problem of phage suspension collection after treatment. Furthermore, previous work on SARS-CoV-2 showed that inactivation efficacy was primarily a factor of surface absorptivity : the higher the absorptivity of the surface, the lower the plasma treatment efficacy [253]. This result also motivated the choice of WSP, highly absorbent, as a

contaminated surface, considering unfavorable conditions and supposedly representatives of a cross contamination *via* a surface.

T4 and MS2 bacteriophages on WSP were facing environmental stress factors, such as desiccation and interaction with fibers. The stability of bacteriophages was tested using four buffer solutions:

- SM: 50mM Tris.HCl, pH7.5, 100mM NaCl, 8mM $MgSO_4$
- λ-dil: 10 mM Tris-HCl, pH 7.4, 10 mM $MgCl_2$
- M9: 18.7 mM NH_4Cl, pH 7.4, 48 mM Na_2HPO_4, 22 mM KH_2PO_4, 8,56 mM NaCl
- Mu: 20 mM Tris-HCl, pH 7.5, 200 mM NaCl, 2 mM $CaCl_2$, and 20 mM $MgSO_4$

To limit desiccation, the effect of glycerol (highly hygroscopic and often used to keep moisture) addition in buffer solutions on phage stability was also examined.

Note that an addition of 5–10% glycerol to the phage suspension is known to guarantee safe viability and infectivity for 30 days at −20°C or −70°C (prevents formation of the crystal structure of ice which may cause destruction of phages). [255].

Furthermore, it is assumed that viruses spread in the environment from infected hosts to surfaces *via* saliva droplets. Saliva consists in a complex aqueous (more than 99% Vol. water) solution of electrolytes, mucopolysaccharides, enzymes, nucleic acids, and cells [256]. The viscosity of saliva is about 1.4 mPa·s [257] and can be compared to the viscosity of 10% Vol. glycerol solution in distilled water which is 1.56 mPa·s at 20°C (decreasing to 1.02 mPa·s at 40 °C) [258]. In terms of viscosity, the experimental model was thus consistent with a realistic situation of surface contamination by the saliva of an infected host.

The four buffer solutions with or without 10% Vol. glycerol were then used to dilute phage stock from 10^{11} to 10^9 PFU/mL in Eppendorf tubes (10 µL phage suspension in 990 µL buffer solution).

Paper discs of 6 mm diameter perforated in a WSP sheet were used as support. 1 µL (10^6 PFU) of the solution from the Eppendorf tube was spotted on the WSP discs. The phage suspension spotted area occupied about a quarter of the disc are shown in Figure 4.3. The WSP fully adsorbed the spotted volume. This was

done by holding the paper disc in the air (without contact with a solid support) using sterilized clip (making sure that the deposit did not contact with the clip). Clip and paper were placed in a sterile Petri dish for 15 min maximum duration. The paper sample was then immersed (1 mL) in LB for T4 or NB for MS2. After 3 minutes, the paper was fully dissolved in medium. However, fibers could sometimes be distinguished. The viability of phage in solution was measured by plaque assay.

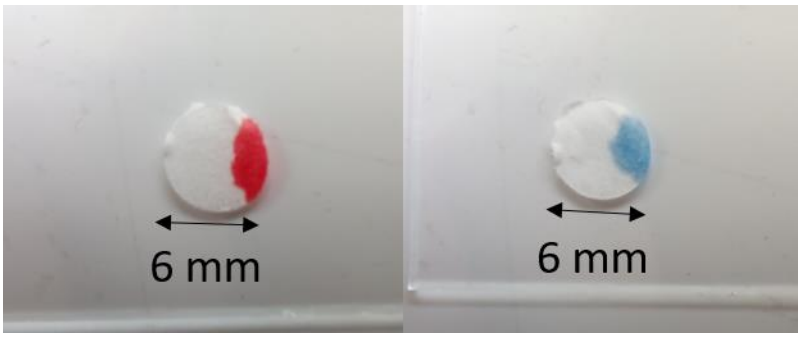

Figure 4.3 Water-soluble paper spotting test: 1 µL of λ-dil buffer solution containing red and blue dye.

4.2.3 Treatment exposure and recovery

Phage stock was diluted 1% (10 µL stock with 990 µL suspension medium) in λ-dil with or with 10% Vol. glycerol in a 1.5 mL Eppendorf tube. Three 6 mm diameter WSP discs were spotted 1 µL (10^6 PFU) of diluted suspension (procedure detailed above): one for control of dilution sample, one for bench sample, and one for treatment sample. The treatment sample and the bench sample were placed on a glass slide (one for each) and the non-spotted area was covered by another glass slide to be fixed. Immediately, the paper sample of control of dilution was put in 1 mL LB for T4 or in 1 mL NB for MS2. The control of dilution was also regarded as the no treated sample or 0 min treatment sample. Then, the treatment sample was introduced in the chamber to be exposed to the treatment for a given duration (ranging from 1 to 4 minutes): bench without any operation, water vapor saturated air flow (water vapor content detailed in Section 3.2.1 (87% relative humidity (RH) at 20˚ C at 2 cm away from tube outlet), warm humid air flow (37% RH at 34˚ C at 2 cm away from tube outlet), and humid air plasma. Simultaneously, the bench sample covered by a top of Petri dish (to avoid contaminating from ambient air) was placed on table. After the treatment, both paper samples were put in 1 mL LB or NB (one for each). After waiting 3 minutes to obtain a complete dissolution, plaque assay of the dissolving solutions was performed.

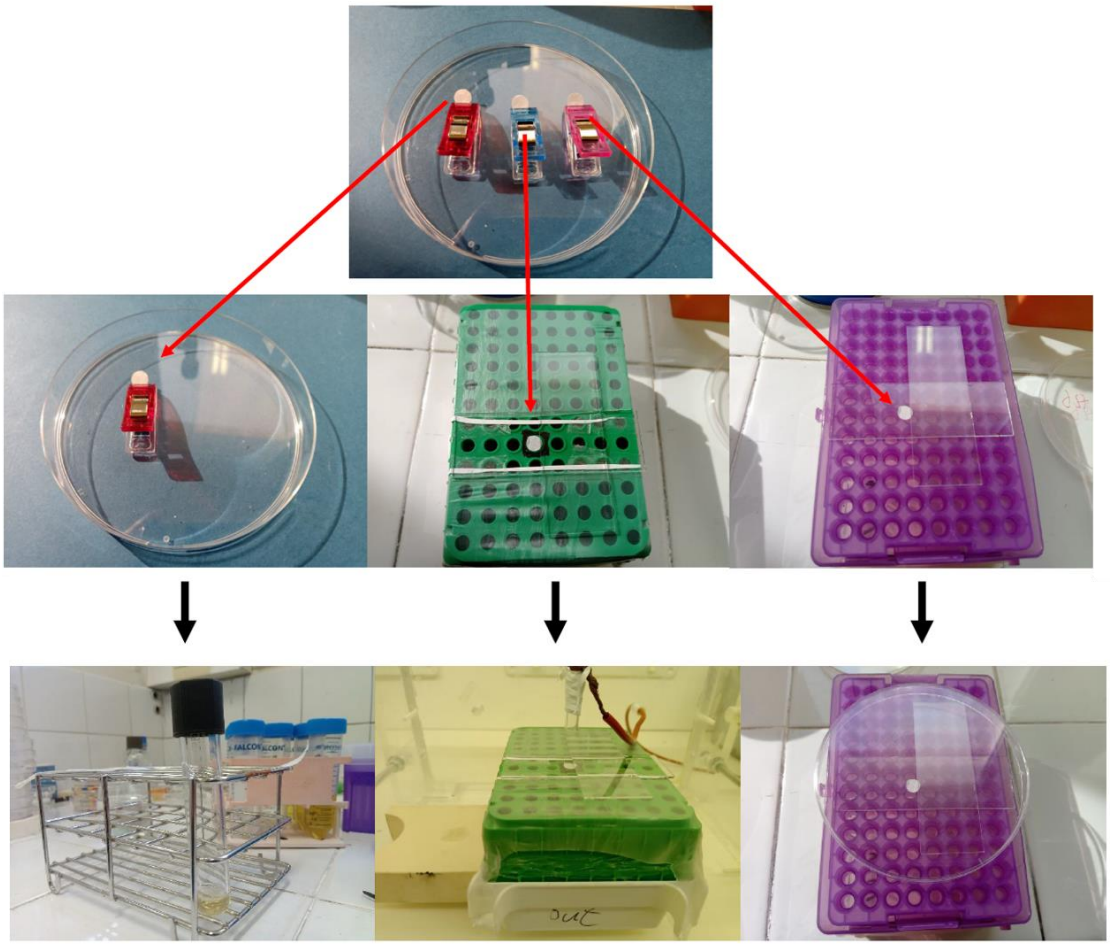

Figure 4.4 The three paper disc samples spotted with the same stock dilution (top row): control of dilution (left column), treatment sample (center column), and bench sample (right column). In the bottom row, the three samples were individually: directly dissolved for control of dilution (left column), submitted to treatment for a given duration (center column), stored on the bench for the corresponding duration (right column).

4.2.4 Paque assay

For the plaque assay, the double-layer agar method with Gratia method [259] was applied for the procedure of the assay. Petri dishes with bottom agar (NB or LB+ 1.25% agar) were prepared (pre-incubation of bottom agar at 37˚ C to dry the surface of agar) 24/48 hours before assay. On the day of treatment, the top agar (NB or LB + 0.5% agar) was heated, poured 2.5 mL in test tubes, and kept at 45˚ C in block heater. The overnight *E. coli* culture was resuspended in LB or NB (1 Vol. E. coli culture in 9 Vol. LB or NB) and incubated for 60 min (for T4 phages) or 90 min (for MS2 phages) at 37°C. Serial 10% Vol. dilutions of the treated suspension (4 µL phage-spotted paper dissolved in NB or LB + 36 µL medium) were performed according to the expected concentration of phage. 20 µL of diluted suspension and 100 µL of *E. coli* culture were added in the test

tube containing top agar (2.5 mL) and mixed using vortex shaker. Then, obtained suspension was poured on the 24 hours old bottom agar (MS2) or on the 48 hours old bottom agar (T4). When the top agar solidified, Petri dishes were incubated at 37˚ C for 16 hours. The number of plaques was then counted after incubation, and the concentration of the treated suspension was calculated. For plaque counting, only a number of plaques higher or equal to 3 per plate (which corresponds to 150 PFU/ml if there is no serial dilution) was taken into account. This process is illustrated in Figure 4.5 and Figure 4.6 shows an example of plaque counting for T4 and MS2.

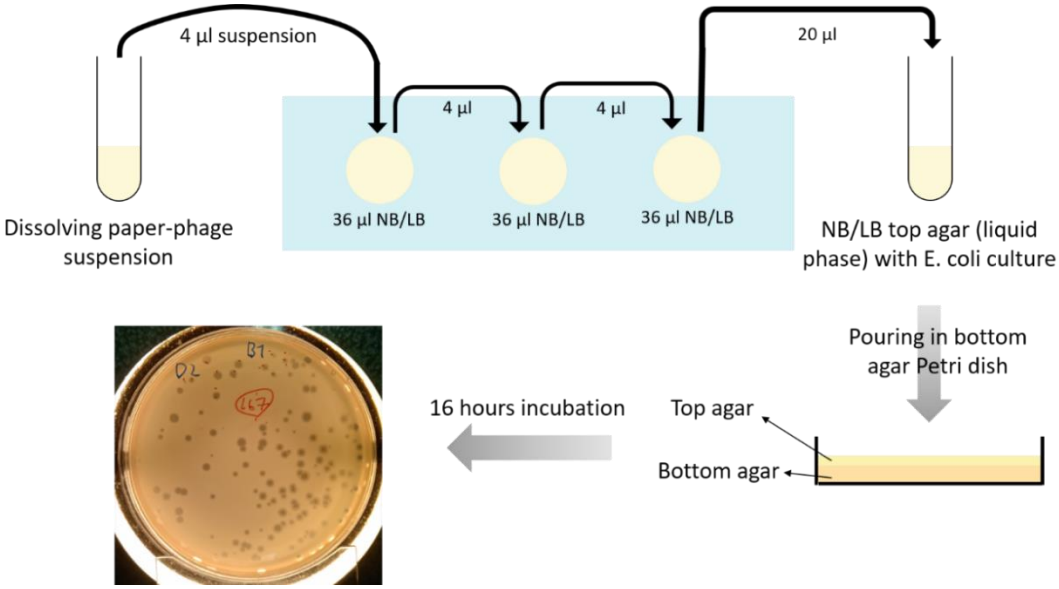

Figure 4.5 Illustration of the Gratia method for plaque assay.

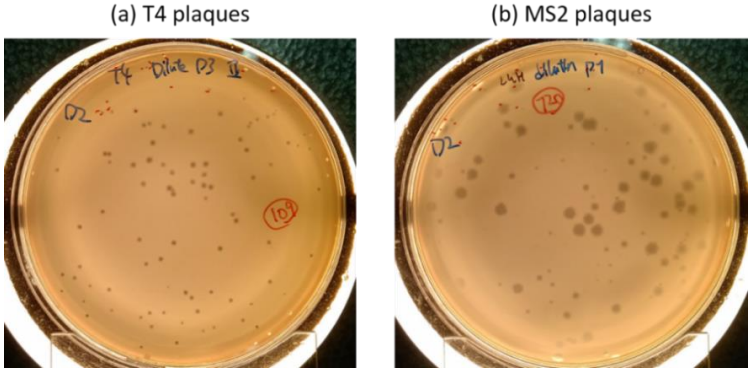

Figure 4.6 Control of dilution. Plaques of (a) T4 bacteriophages (109 plaques) and (b) MS2 bacteriophages (120 plaques). MS2 phage had much larger plaques. According to the dilution (here 10^{-2}), the concentration of phage particles was 5.45×10^5 PFU/mL and 6×10^5 PFU/mL for T4 and MS2 respectively.

4.2.5 Plasma treatment

The water-soluble paper (WSP) discs on which the bacteriophage suspension

was deposited were exposed to a plasma treatment in a chamber open to the ambient atmosphere. The plasma source consisted in a DBD reactor in a cylinder geometry. A stainless steel 2 mm diameter rod electrode was centered in a borosilicate tube (6 mm outer diameter and 4 mm inner diameter). A 24 mm copper ring electrode was placed on the tube external surface 20 mm from its outlet. The rod electrode was connected to an AC high voltage power supply. Voltage applied to the rod electrode was measured using a high voltage probe (Tektronix P6015A, 1 V: 1000 V, 4 ns rise time, 75 MHz band width). The ring electrode was connected to ground through a fast current transformer (Tektronix CT-2, 1 mV: 1 mA, 500 ps rise time, 1.2 kHz-200 MHz bandwidth). Signals were recorded with a digital oscilloscope (Tektronix MSO54 – 500 MHz bandwidth – 6.25 GS/s). Using the current x voltage instantaneous product, mean discharge input power was calculated. WSP disc samples to be treated were facing the dielectric tube outlet and the distance was fixed to 20 mm (see Figure 4.7). Reactor feed-gas was flowing at atmospheric pressure in the dielectric tube at constant flow rate 2 L/min.

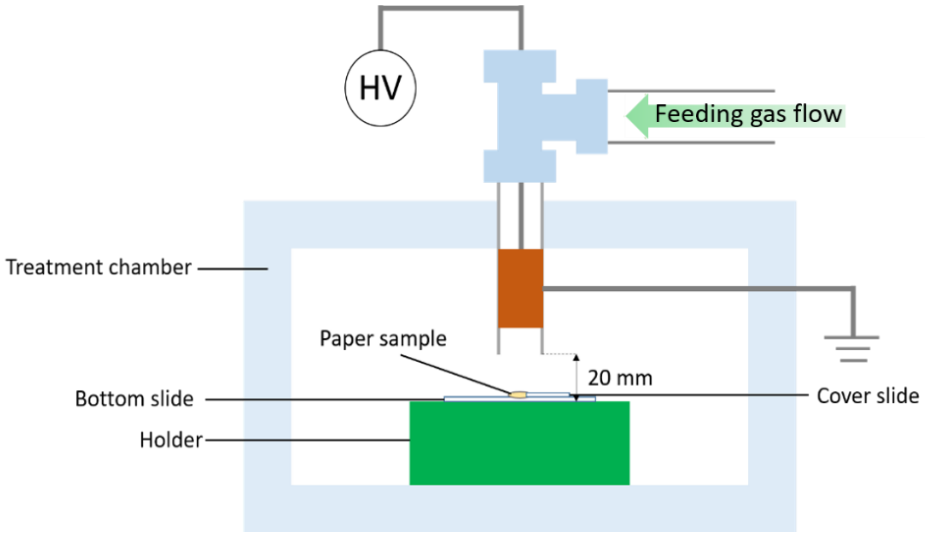

Figure 4.7 Scheme of plasma system for bacteriophage treatment on WSP sample.

Four different feed gas were tested:

- water vapor saturated synthetic air (water vapor content detailed in Section 3.2.1)
- dry synthetic air
- water vapor saturated argon
- dry argon

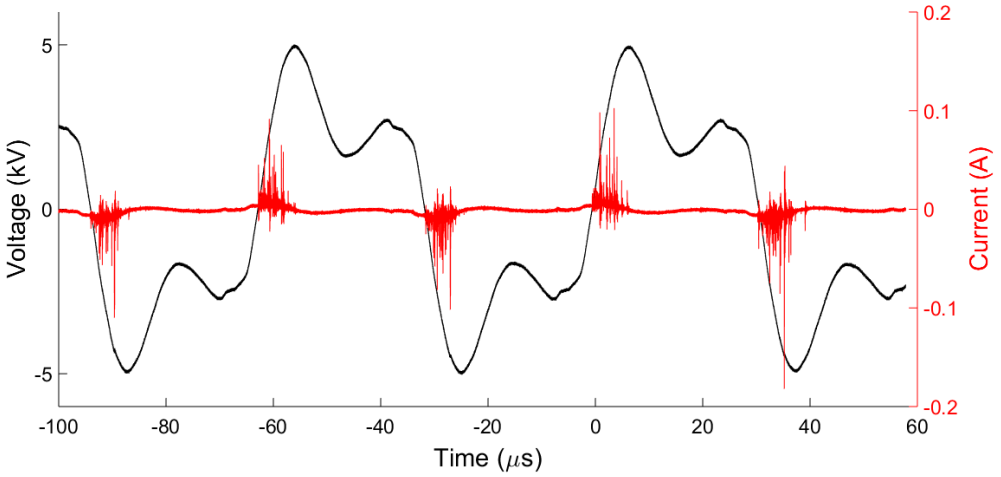

Figure 4.8 Typical input voltage and discharges current waveforms. (Feed-gas: humid air 2L/min, Vpp: 10 kV, frequency: 16 kHz, mean input power: 3 W.)

Temperature measurements at the sample exposure location were performed either by replacing the sample with the probe of an alcohol thermometer or by placing a thermocouple (K type) under the glass slide exposed to the treatment (using heat transfer paste). An example is presented for humid air in Figure 4.9.

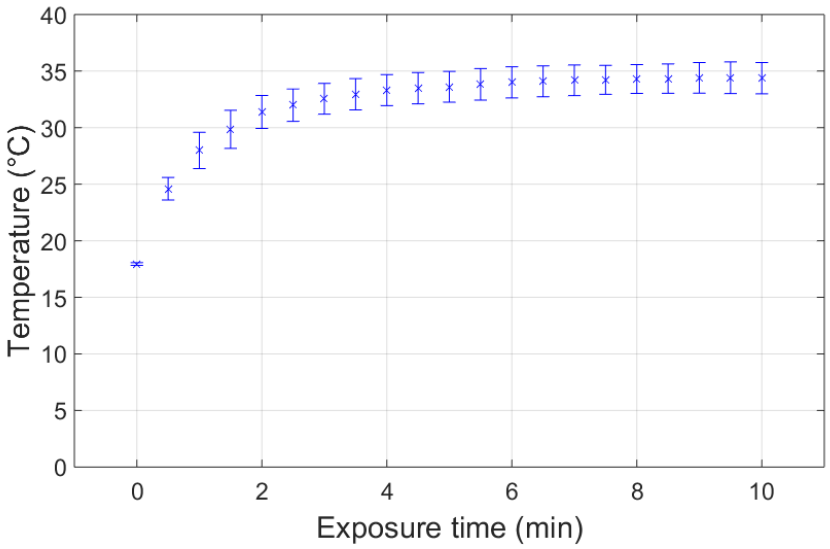

Figure 4.9 Temperature measurement at the sample location when submitted to humid air post-discharge (K-type thermocouple under the glass slide exposed to the treatment - 3 W, 2 L/min gas flow).

For 3 W input power in the discharge, the maximum surface temperature at the sample location did not exceed 35°C (measured by alcohol thermal meter in steady state). The operating conditions that ensure a maximum temperature increase of 14°C after 4 min. exposure were chosen for each gas (Table 4.1).

Table 4.1: Plasma system operating conditions for bacteriophage treatment on WSP sample

	Humid air	Dry air	Humid argon	Dry argon
HV frequency (kHz)	15.9	12.3	16.1	26.6
HV peak voltage (kV)	9.8	11	9.2	9.1
Mean discharge input power (W)	3	3	3	3.2
Sample location temperature (°C)*	34	34	34	34

*measured with a 20˚C room temperature

In complementary experiments, a water bath heat exchanger allowing to heat the gas flowing in a tube was implemented in order to obtain at the sample level the same temperature increase as during the plasma treatments with identical gas flow.

4.2.6 TEM Observation

Preparation of phage stock for TEM observation

The procedure for preparing phage suspensions for transmission electron microscopy (TEM) observation was the same as for the treatments. The protocol of MS2 stock making for TEM observation was similar to the previous stock making process. The most different manipulation started from the phage resuspension from the NB top agar plate. In the previous process, the resuspension medium was NB broth, but here 5 mL pure λ-dil buffer (lower the background noise under TEM) was chosen and added in the Petri dishes. Then the plates were also stored at 4°C for about 20 hours. The fluid in the plates was collected by pipetting and deposited in Eppendorf tubes for centrifugation (3345 x g) to separate bacteria or agar fraction from the phage suspension. The supernatant was filtered with a 0.2 µm syringe. Then, the filtrate was submitted to ultracentrifugation (92 635 x g) to increase phage concentration, from 25000 µL (collected from 10 Petri dishes) to 30 µL. The suspension was collected, and the phage lysate was tittered.

Plasma treatment for TEM observation

Phages were also treated on water-soluble paper. A 1 µL drop of phage stock was spotted on paper and submitted to different treatments for4 minutes. Then, the paper sheet was dissolved in pure λ-dil buffer under gentle shaking. The paper fiber in the λ-dil suspension was separated by centrifugation (3345 x g). The supernatant of the suspension was collected for the TEM observation.

TEM observation

A 1 µl suspension (phages and λ-dil buffer) was spotted on a 400-mesh carbon-coated copper grid and stained with 2 % (w/v) uranyl-acetate solution which is a negative staining (i.e. stain will absorb electron beam and will appear dark under TEM). TEM magnification was 3710 pixels for 850 nm. Assuming a homogeneous suspension, about 20-200 phages could be observed per mesh (active bacteriophage concentration at about 10^{12} PFU/mL). In TEM observations, the capsid was always light because not subjected to stain accumulation. In "healthy" phages, the stain cannot accumulate inside the capsid, so RNA can be distinguished inside the capsid, and the color of RNA was close to the capsid one (shown in Figure 4.10(a)). However, if the capsid was broken or RNA lost, the staining chemicals accumulate inside the capsid and appear dark (shown in Figure 4.10(b)). Therefore, if a dark region appeared inside the phages, they were regarded as empty (or on the way to be emptied).

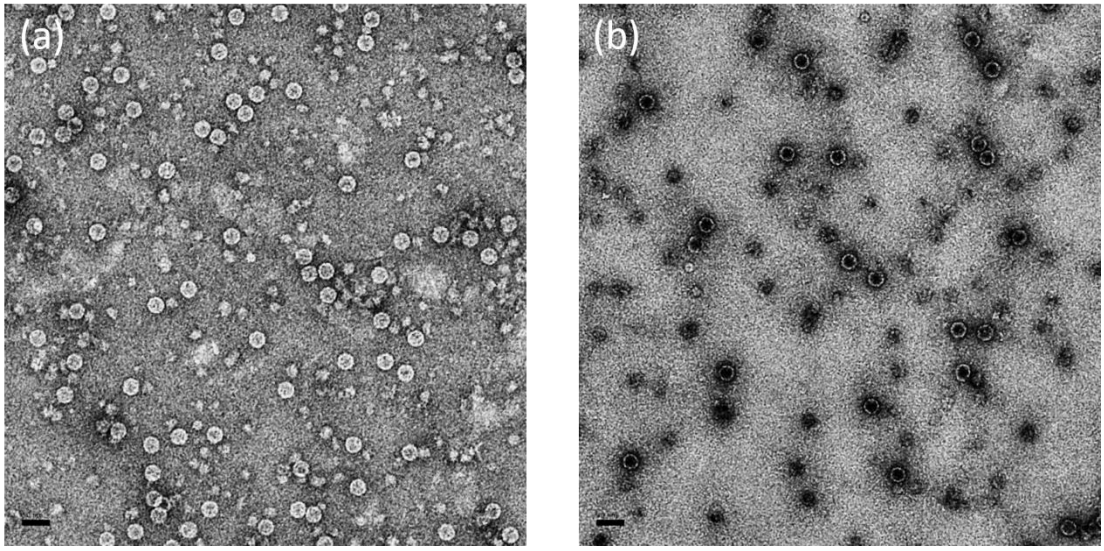

Figure 4.10 The solid (RNA contains) gas flow blown phages and the empty (RNA lost) plasma treated phages are shown.

4.3 Results

All results presented in the following sections were obtained by 3 replicates of each experiment. Results are presented in terms of number of phages (PFU) on water-soluble paper as a function of exposure time or in terms of survival fraction as a function of exposure time, i.e. ratio of the number of phages (PFU) on paper at t by the initial number of phages (PFU) on paper at t_0=0 min.

4.3.1 Phage stability on water-soluble paper

The stability of T4 and MS2 phages in 1 µL buffer droplet spotted on water-soluble paper (10^6 PFU) was tested on the bench at room temperature (and 4°C for T4). Four buffer solutions (detailed in the section 4.2.2) were tested with or without glycerol admixture (10% Vol.) for phage suspension.

At 4°C (Figure 4.11), a constant inactivation rate of 0.01 log/min over 45 minutes was observed for T4 diluted λ-dil buffer solution. T4 inactivation rate was higher for SM, M9 and Mu buffer solutions over the 15 first minutes and tended to increase from 15 min in the case of Mu and 30 minutes for both SM and M9. With 10%Vol. glycerol admixture, inactivation rate was higher than without glycerol for the first 30 minutes and then dropped drastically afterwards (up to 45 minutes).

At room temperature (Figure 4.12), T4 inactivation rates were much higher (from 4 to 6 times higher than at 4°C) for all buffer solutions. Limit of detection for PFU counting was reached after 30 minutes for SM, λ-dil and M9 buffers, and after 45 minutes for Mu buffer. As for 4°C tests, 10%Vol. glycerol admixture was seen to increase inactivation rate (e.g. 3 times higher than without glycerol for λ-dil) for the 15 first minutes and then dropped drastically afterwards (up to 45 minutes).

At room temperature, MS2 phage was much more stable. On a 15-minute time scale, the inactivation rates observed for MS2 at room temperature were comparable to those obtained with T4 at 4°C. In contrast to T4, the addition of glycerol helped stabilize the MS2 phage within the first few minutes. And as with T4, the buffer solution in which MS2 was most stable (this time on a 15-minute time scale) was λ-dil (Figure 4.13).

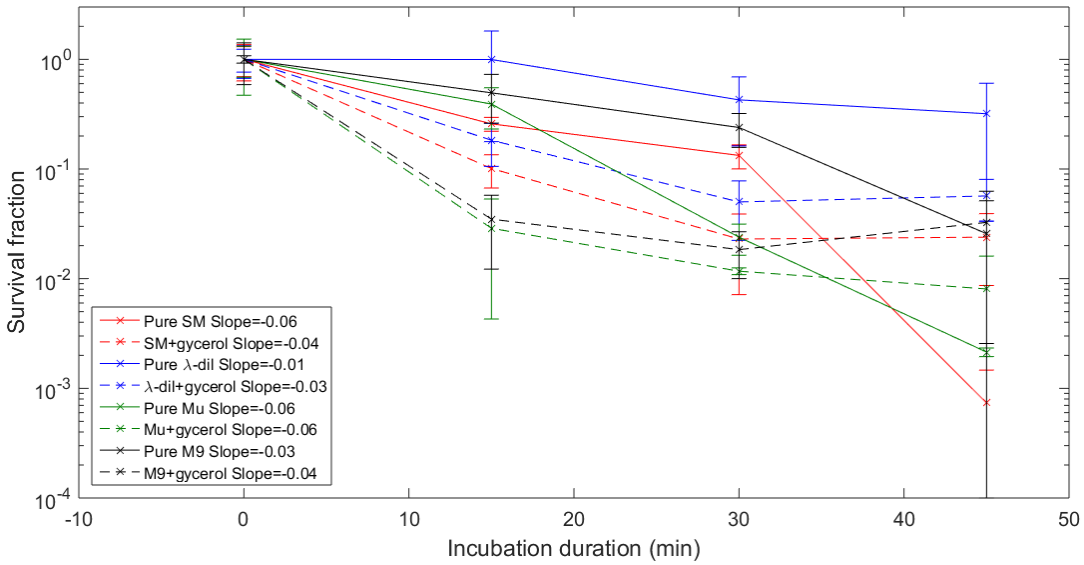

Figure 4.11 Survival fraction of T4 phage diluted in SM, λ-dil, Mu and M9 buffer solutions at 4°C with and without 10%Vol. glycerol admixture.

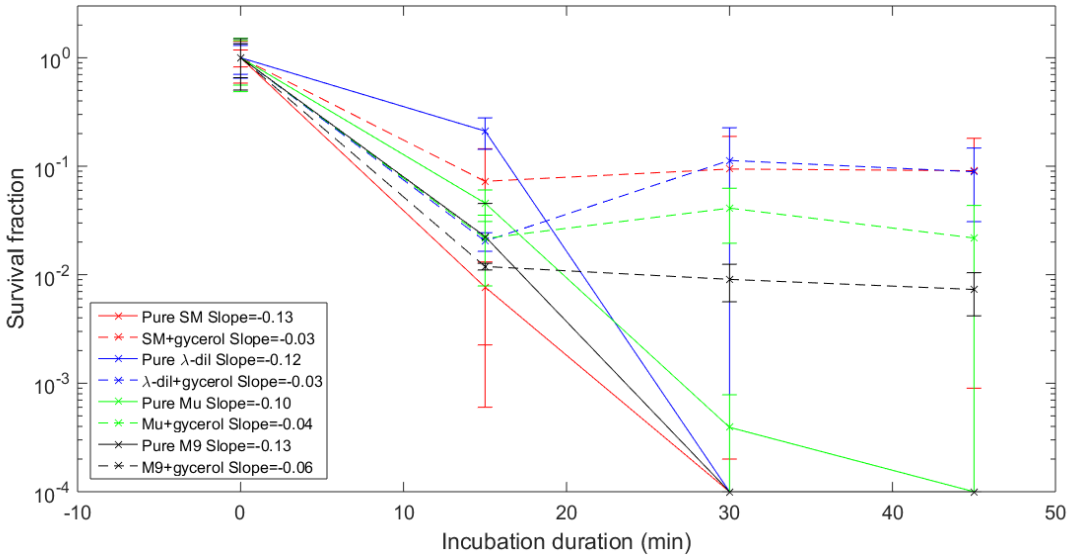

Figure 4.12 Survival fraction of T4 phage diluted in SM, λ-dil, Mu and M9 buffer solutions at room temperature with and without 10%Vol. glycerol admixture.

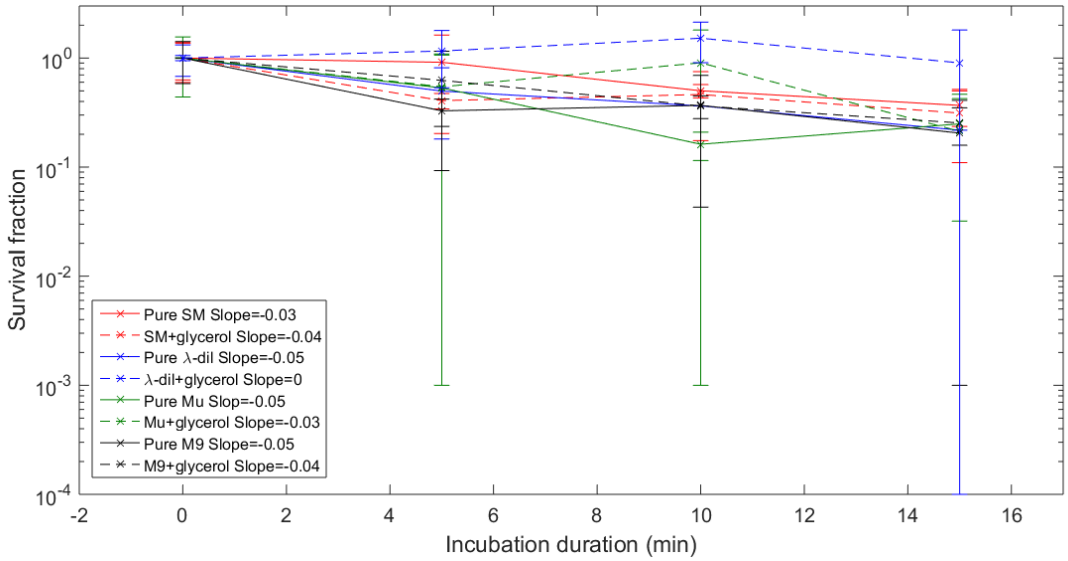

Figure 4.13 Survival fraction of MS2 phage diluted in SM, λ-dil, Mu and M9 buffer solutions at room temperature with and without 10%Vol. glycerol admixture.

As a result, λ-dil with or without 10%Vol. glycerol admixture was chosen as a buffer solution for the plasmas treatment experiments.

4.3.2 Exposure to plasma treatment

T4 and MS2 bacteriophage stock diluted in λ-dil buffer solution with or without glycerol addition were spotted (1 µL) on water-soluble paper and submitted to different treatment conditions.

As a first step, four operating conditions (detailed in Table 4.1) were examined on MS2 bacteriophage suspension (pure λ-dil buffer) for a 3-minute exposure time. In the case of argon plasma, PFU counting was under detection limit (less than 3 plaques on Petri dish) in dry conditions (plasma plume) for the 3 replicates, and in humid conditions (water vapor saturated argon at room temperature) for 2 of the 3 replicates. These promising results have not been further investigated in this work because we have chosen to focus on the most direct application of plasma using air as a plasma feed-gas, and in particular humid air (saturated with water vapor at room temperature and atmospheric pressure). In this situation, HNO_3 formation in gas phase is promoted, and dissolution of nitric acid in water solution leads to the formation of NO_3^-, which was considered as one of the main RONS species responsible for inactivation of endospores [260] and viruses [254].

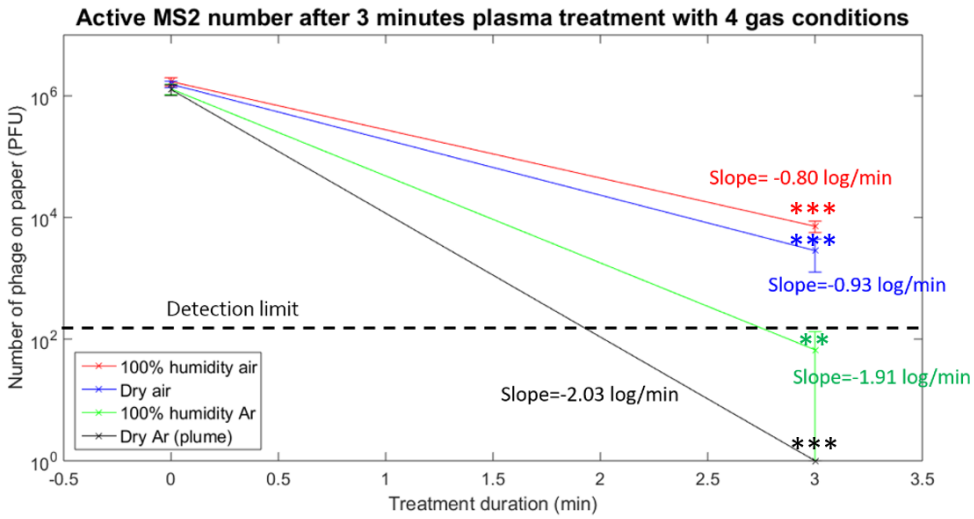

Figure 4.14 MS2 phage (λ-dil buffer solution) PFU on paper vs. exposure time to air (dry and humid) and argon (dry and humid) plasma treatment. (Student test **<0.01 and ***<0.001)

Gas analysis of the downstream flow at the tube outlet was done with air as feed gas in dry and humid conditions. The reactor tube outlet was directly connected through a perfluoroalkoxy (PFA) tubing to a 20 cm optical pathway gas cell (CaF_2 windows) for Fourier Transform Infrared (FTIR) absorption spectroscopy analysis (Tensor 27 from Bruker). Measurements were performed on a 950-4000 cm^{-1} wavenumber range. Examples of FTIR absorption spectra obtained in both conditions (dry and humid air) are presented in Figure 4.15.

Identified stable species were ozone (O_3), nitrous oxide (N_2O), dinitrogen pentoxide (N_2O_5), nitrogen dioxide (NO_2) and nitric acid (HNO_3). Ozone concentration was simultaneously measured using near UV absorption spectroscopy at 254 nm (10 cm optical pathway gas cell with quartz windows – Lambda 15 UV-Visible absorption spectrophotometer from Perkin Elmer) in the same gas line. Species concentration was quantified using reference FTIR spectra from Bruker. Corresponding results are presented in Table 4.2.

Table 4.2 concentration (ppm) of identified species in dry and humid air (95%RH à room temperature and atmospheric pressure) using UV and FTIR absorption spectroscopy. 2 L/min gas flow rate, 3 W input power.

	O_3 (UV)	O_3 (FTIR)	N_2O	N_2O_5	NO_2	HNO_3
Dry air (ppm)	497.0 ± 9.6	467.9 ± 9.8	6.4 ± 0.2	23.5 ± 0.4	1.4 ± 0.4	traces*
Humid air (ppm)	205.0 ± 3.3	208.0 ± 5.0	6.6 ± 0.5	10.5 ± 1.0	8.4 ± 4.7	65.4 ± 10.0

*under limit of quantification (2 ppm)

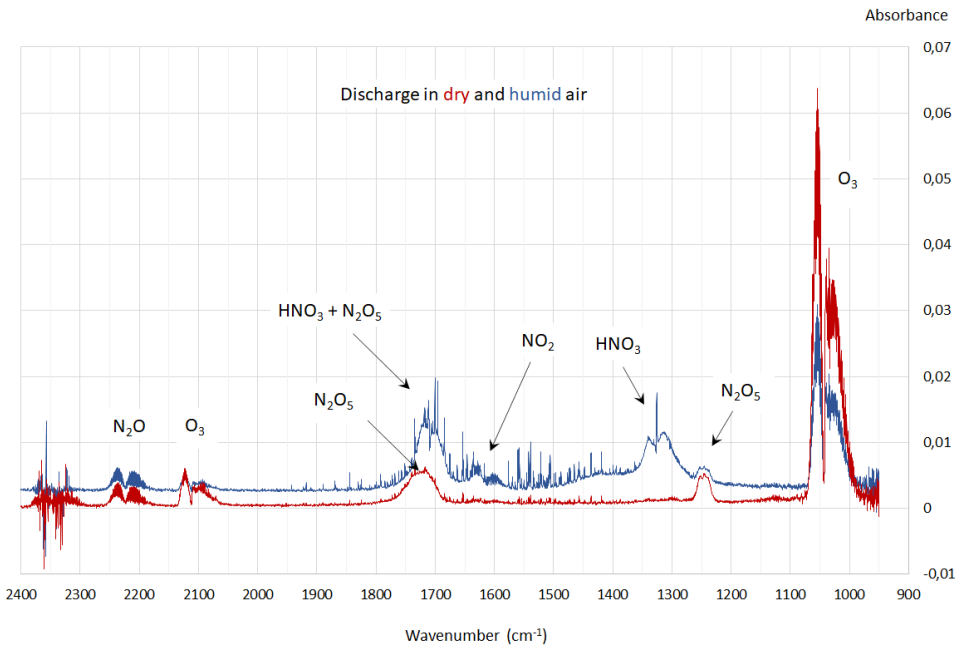

Figure 4.15 FTIR absorption spectra obtained in both conditions dry and humid air (95%RH at room temperature and atmospheric pressure). 2 L/min gas flow rate, 3 W input power.

Ozone concentration was lower in humid conditions due to destruction reactions with water vapor dissociation products:

$O_3 + H \rightarrow OH + O_2$ $\quad k = 11 \cdot 10^{-11} \cdot \exp(-480/T)$ $cm^3 \cdot molecule^{-1} \cdot s^{-1}$

$O_3 + H \rightarrow HO_2 + O$ $\quad k = 10^{-11} \cdot \exp(-480/T)$ $cm^3 \cdot molecule^{-1} \cdot s^{-1}$

$O_3 + HO_2 \rightarrow 2\ O_2 + OH$ $\quad k = 1.4 \cdot 10^{-14} \cdot \exp(-600/T)$ $cm^3 \cdot molecule^{-1} \cdot s^{-1}$

$O_3 + OH \rightarrow HO_2 + O_2$ $\quad k = 1.9 \cdot 10^{-12} \cdot \exp(-1000/T)$ $cm^3 \cdot molecule^{-1} \cdot s^{-1}$

N_2O_5 concentration is significantly lower in humid air compared to dry air. Its main formation reaction:

$NO_3 + NO_2 + M \rightarrow N_2O_5 + M$ $\quad k = 5.3 \cdot 10^{-20} T^{-4.1}$ $cm^6 \cdot molecule^{-2} \cdot s^{-1}$

is disadvantaged due to the consumption of NO_3 by the reactions with the dissociation products of water vapor:

$NO_3 + OH \rightarrow NO_2 + HO_2$ $\quad k = 2.3 \cdot 10^{-11}$ $cm^3 \cdot molecule^{-1} \cdot s^{-1}$

$NO_3 + HO_2 \rightarrow NO_2 + O_2 + OH$ $\quad k = 4.3 \cdot 10^{-12}$ $cm^3 \cdot molecule^{-1} \cdot s^{-1}$

In addition, N_2O_5 produced is converted to HNO_3:

$N_2O_5 + H_2O \rightarrow 2\ HNO_3$ $\quad k = 5.10^{-21}$ $cm^3.molecule^{-1}.s^{-1}$

HNO_3 is also produced in gas phase though oxidation of NO_2 by OH radical:

$NO_2(g) + OH(g) \rightarrow HNO_3(g)$ $\quad k = 4.1.10^{-11}$ $cm^3.molecule^{-1}.s^{-1}$

During plasma treatment, this gas mixture was spread on WSP surface on which

aqueous suspension of phages was previously spotted. Nitrogen dioxide and nitric acid dissolve into aqueous solution according to their Henry constant k_H (from NIST):

$$2\ NO_2(g) + H_2O(l) \rightarrow HNO_2(aq) + HNO_3\ (aq)$$

$$k_H = 0.012\ mol \cdot kg^{-1} \cdot bar^{-1} \text{ for } NO_2(g)$$

$$HNO_3(g) \rightarrow HNO_3\ (aq)$$

$$k_H \text{ in the range of } 10^6\ mol \cdot kg^{-1} \cdot bar^{-1} \text{ for } HNO_3(g)$$

Dissolution (and reaction) of these gases in liquid phase results in an acidification of the solution [261].

In the same operating conditions, a 50 µL distilled water volume was exposed for 4 min. to the downstream flow at the tube outlet (2 cm from the tube outlet). The same experiment was done with pure λ-dil buffer solution and λ-dil buffer solution with 10%Vol. glycerol admixture. Results are presented in Table 4.3.

Table 4.3 Solution pH value for 4 min. exposure time to plasma treatment. 2 L/min gas flow rate, 3 W input power.

	Distilled water	Pure λ-dil buffer sol.	λ-dil + 10% Vol. glycerol buffer sol.
Non-treated	6	6 - 6.5	6 - 6.5
Dry air	2.9	4.6	5.3
Humid air	1.1	1.6	2.1

Acidification of the solution during air plasma is evidenced even with buffer solution. In agreement with the results of the gas analysis at the reactor outlet, the acidification of the solution is more advanced in the case of the humid air plasma (higher concentration of nitric acid).

Note that formation of $ONOO^-$ in liquid phase was invoked as a major contributor to virus inactivation [254]. Nevertheless, this species was not mentioned in our measurement.

T4 phage treatment by humid air plasma

In the case of T4 phage diluted in pure λ-dil buffer, the stability on paper was confirmed on the bench and under humid air flow with inactivation rates of 0.03 and 0.05 log/min respectively (red and blue lines in Figure 4.17). On the other

hand, under humid air flow at 34°C, the detection limit was reached after 2 minutes of treatment. A comparable result was observed with the humid air plasma treatment (black and green lines in Figure 4.16).

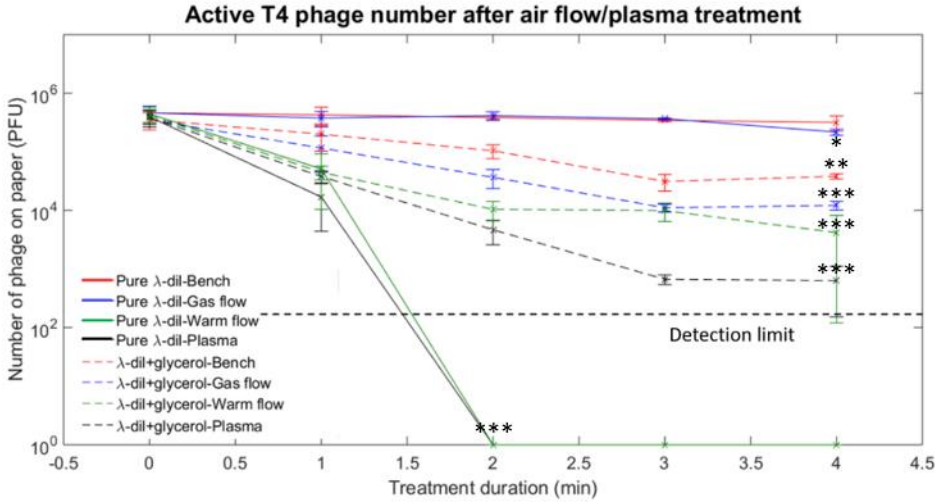

Figure 4.16 T4 phage (λ-dil buffer solution w/wo glycerol admixture) PFU on paper vs. exposure time on the bench, to gas flow-only, to warm gas flow-only, to humid air plasma treatment. (Student's test: 0.025*, 0.01**, and 0.005***)

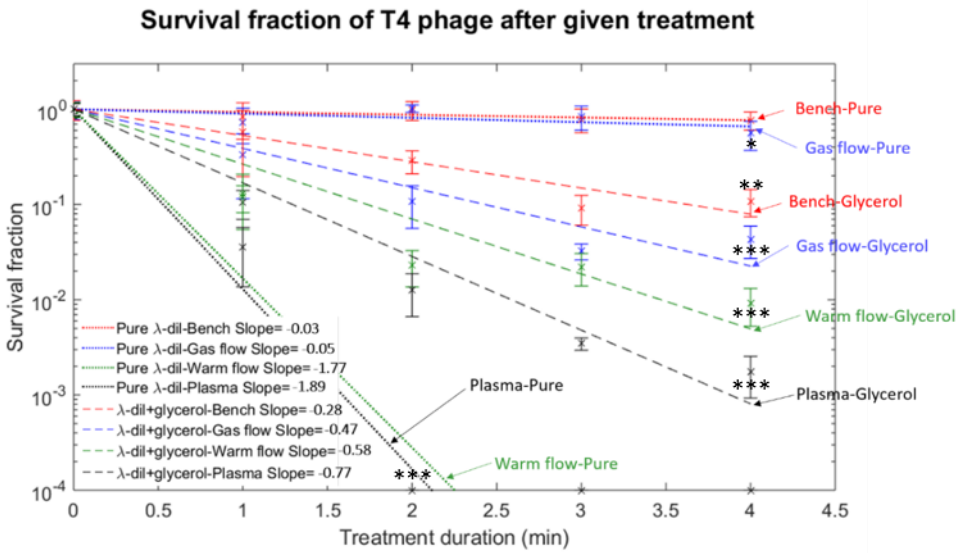

Figure 4.17 Survival fraction of T4 phage (λ-dil buffer solution w/wo glycerol admixture) after different treatments: on the bench, exposed to gas flow-only, exposed to warm gas flow-only, exposed to humid air plasma treatment. (Student's test: 0.025*, 0.01**, and 0.005***)

In the case of T4 phage diluted in λ-dil buffer with the addition of 10%Vol. glycerol, the results of the stability tests were also confirmed: the stability dropped initially and then stabilized (dotted red and blue lines in Figure 4.16). It is remarkable that the presence of glycerol reduces the inactivation under humid air flow at 34°C and under humid air plasma treatment. The hygroscopic function of glycerol thus seems to protect the phages. In contrast to the

experiments without glycerol addition, the results obtained by thermal treatment and by plasma treatment are clearly discernable (dashed green and black lines in Figure 4.16). In the latter case, the detection limit was approached after 4 minutes of treatment.

MS2 phage treatment by humid air plasma

Inactivation of MS2 by exposure in liquid suspension to ozone gas with 55% RH was previously studied: a 2 log PFU decrease after less than 20 s (18.4 s exactly) exposure time was observed [262]. In our experiments, ozone concentration produced by humid air plasma was over 200 ppm (shown in Table 4.2) in gas phase. The 2 log PFU decrease was achieved with 2 min exposure time to the post-discharge. This shows that MS2 is much more resistant to ozone exposure when spotted on a highly absorbent solid surface than suspended in an aerosol phase.

In MS2 phage experiments, the glycerol had less impact on the phage inactivation. Up to 4 minutes, a high stability of MS2 was observed for samples on the bench and submitted to gas flow only: respectively 0.03 and 0.07 log/min inactivation rates for sample diluted in pure λ-dil (red and blue dot lines in Figure 4.19), and 0.06 and 0.02 log/min for samples diluted in λ-dil with 10% Vol. glycerol (red and blue dashed lines in Figure 4.19). Exposure to warm humid air flow induced less than 0.5 log/min inactivation rate (0.47 log/min for pure λ-dil sample and 0.38 log/min for glycerol λ-dil sample).

However, the inactivation induced by exposure to humid air post-discharge was influenced by the addition of glycerol in the buffer solution. For the 1-minute exposure time, inactivation rates were high: 1.56 log/min and 1.25 log/min for pure λ-dil and λ-dil with glycerol buffer solutions respectively. From 1 to 2 min exposure time, inactivation rates decreased for both buffer solutions (0.5 log/min). After 2 minutes of exposure (up to 4 minutes), a 0.12 log/min inactivation rate of was observed for pure λ-dil buffer solution (2nd black dot line in Figure 4.19) while a 0.25 log/min inactivation rate was still present for λ-dil with glycerol buffer solution (2nd black dashed line in Figure 4.19). In other words, starting with high inactivation rates (higher for pure λ-dil), inactivation rate decreased with time for both buffer solutions; but this decrease was more pronounced without glycerol than with glycerol admixture.

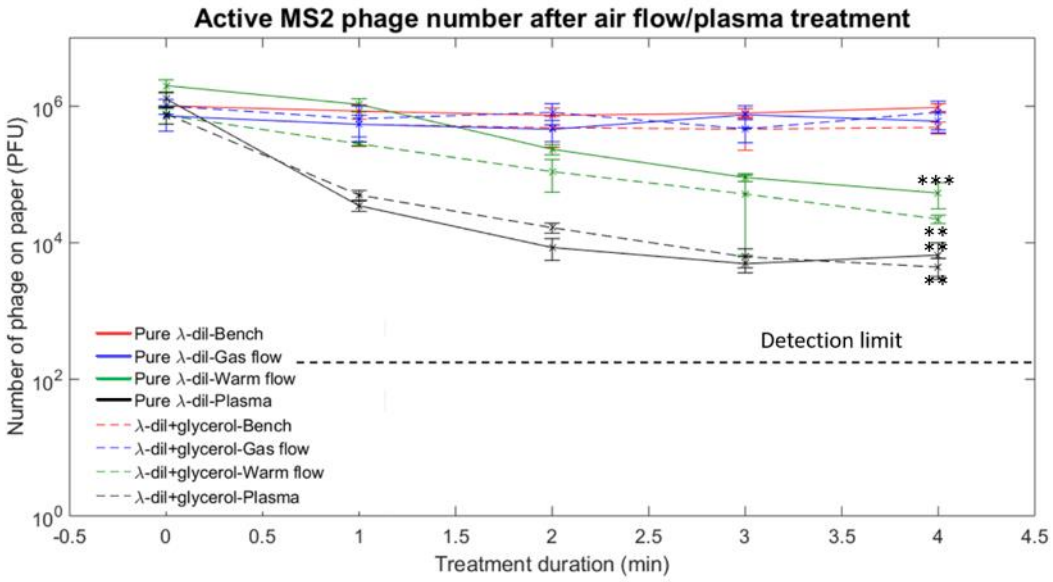

Figure 4.18 MS2 phage (λ-dil buffer solution w/wo glycerol admixture) PFU on paper vs. exposure time on the bench, to gas flow-only, to warm gas flow-only, to humid air plasma treatment. (Student's test: 0.005** and 0.001***)

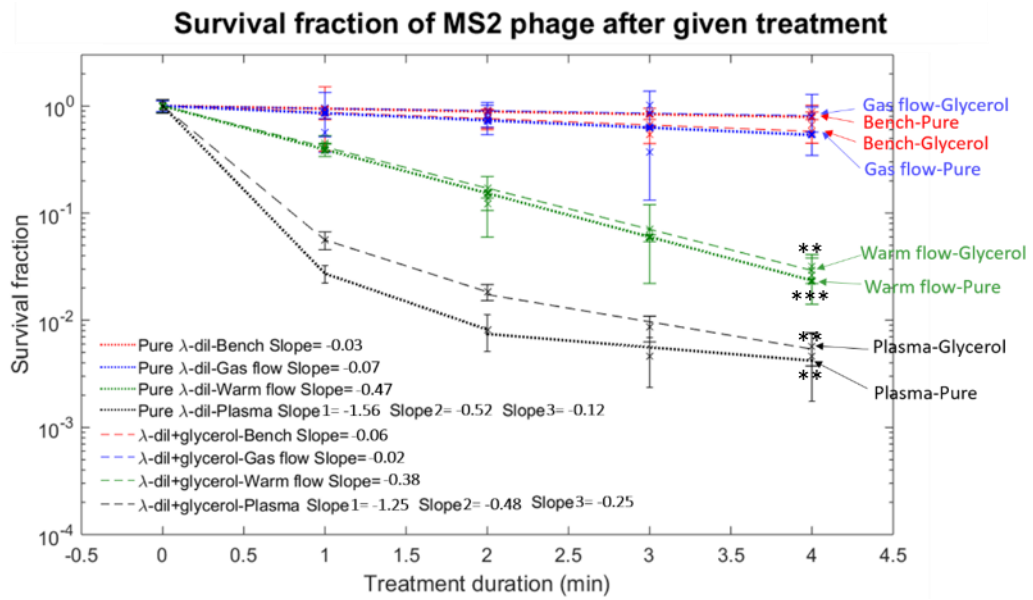

Figure 4.19 Survival fraction of MS2 phage (λ-dil buffer solution w/wo glycerol admixture) after different treatments: on the bench, exposed to gas flow-only, exposed to warm gas flow-only, exposed to humid air plasma treatment. (Student's test: 0.005** and 0.001***)

Previous work showed that the impact of temperature on T4 [263] and MS2 [264] viability and activity in the 20°-35°C range was low. Therefore, different inactivation rates (Table 4.4) observed for T4 and MS2 gas flow-only treatments at room temperature and at 34°C could be discussed rather on to the relative humidity of the environment than on temperature by itself. As a matter of fact,

in our experiments, the relative humidity at sample location was measured 87% when submitted to water saturated air flow at room temperature and 37% when submitted to warm air flow at 34°C. A study established that the viability of MS2 suspended in liquid phase was dependent on the relative humidity of the experimental chamber in which suspensions were stored. A U shape tendency of viability of MS2 with RH was observed: maximum of viability was obtained at 20% RH and 80% RH, while minimum viability was obtained at 50% RH [265]. In our experiments, under air flow-only (warm flow at 34°C), relative humidity was shifted to values (37% RH) corresponding to lower viability conditions for MS2.

Another study on viability of viruses in aerosol phase as a function of RH (10%, 35%, and 90% RH) showed that T3 (icosahedral capsid and phage tail – similar to T4) was more sensitive to RH change (for all cases, inactivation rate was maximum at 35% RH) than Newcastle disease virus (round-shaped capsid), vesicular stomatitis Indiana virus (bullet-shaped capsid), and Infectious bovine rhinotracheitis virus (round-shaped). This suggests that the difference in structure between T4 and MS2, the T4 tail in particular, would make phage more sensitive to RH variations [266]. In addition, possible aggregation of phages during buffer solution evaporation could, if significant, results in large aggregates and thus could affect PFU quantification (underestimation) [267]. This mechanism could be promoted by an increase in viscosity due to glycerol admixture (compared to pure pure λ-dil), especially for large sized bacteriophage such as T4. This may explain the drop in PFU for T4 suspended in buffer solution with glycerol admixture on the bench or submitted to gas flow only.

In addition, partial desiccation of the WSP sample led to an increase in electrolytes (NaCl) so resulting to a loss of viability [265].

Back to Figure 4.18 and Figure 4.19, a first interpretation of the results is hereafter presented. During post-discharge exposure, for the first minute of treatment, RONS accumulate in liquid phase and increase in concentration. This increase in concentration, promoted by buffer solution evaporation, results in high inactivation rate. Presence of glycerol in the buffer solution (due to the hygroscopic properties of glycerol [268]) tends to limit evaporation rate. For a given exposure time, RONS concentration in pure λ-dil solution will thus be higher (higher inactivation rate) than in λ-dil 10% Glycerol buffer solution. After 1 minute-exposure, inactivation rate was decreasing with time. Between 2 and

4 minutes, inactivation rate was again lower (than during the 1-2 min. period); but for glycerol-containing buffer solution, inactivation rate was twice than one for pure buffer solution. A possible mechanism lies on progressive desiccation of the WSP sample. Liquid phase chemistry cannot longer take place in dried locations of the substrate. In this situation, gaseous RONS would not efficiently react with phages supported by dried fibers. Note that viability of MS2 phages suspended in SM solution and sprayed on a solid surface was previously studied. Viability was asserted in fully dried droplets 14 hours after deposition [267]. In the case of phages suspended in buffer solution with glycerol (hygroscopic properties), WSP keeps moisture for a longer time, so allowing liquid phase chemistry to take place over a longer period, and resulting in a higher inactivation rate.

It should be noticed that a stable (over 4 min.) 0.4-0.5 log/min inactivation rate was obtained by submitted sample to warm flow-only whereas smaller inactivation rates (about 0.2 log/min) were observed for post-discharge treated samples after 2 min exposure time. This result suggests that desiccation rates were different in these two situations. Desiccation is influenced by the change in wettability of fibers exposed to air plasma (as studied for cotton fibers [269] for instance). In addition, acidification of the buffer solution was observed during plasma treatment. Water evaporation rate is also influenced by the pH of the solution (increased or decreased according to pH value) as reported for hydrochloric acid [270]. Therefore, from a mechanistic point of view, a direct comparison of MS2 viability / activity when spotted on WSP and submitted the warm gas flow-only or to air post-discharge is very complex.

Another interpretation could be based on aggregation of phages during treatment (and buffer solution evaporation). As mentioned above, phages aggregation could lead to underestimate PFU evaluation. MS2 aggregates were previously reported, and their formation was seen to be promoted by pH low value (pH 3). It is also interesting to note that phages aggregates were seen to be more resistant than dispersed phages to oxidative stress (peracetic acid treatment [271]). This situation could correspond to our experimental conditions: acidification of phage suspension (pH 1.6-2.1) and exposure to ROS. Nevertheless, it should be here mentioned that we did not observe large aggregates even after 4 min treatment time (see TEM examination of treated phage suspension in next section).

Finally, a possible hypothesis would invoke an inhomogeneous distribution of resistance to oxidative stress in phage population (possibly due to mutation). Several papers report on observation of different plaque size from a single virus stock. Authors suggest that phenotype difference could be due to mutant genome [272, 273]. This kind of phenotype difference was observed during MS2 plaque assay (not for DNA phage T4) as illustrated in Figure 4.6(b) where small and large plaques are visible. Even if the existence of a mutant population were confirmed, there is no evidence that it is more resistant to oxidative stress. It would then be necessary to select this population and expose it specifically to the treatment in order to assess its possible resistance.

Table 4.4 Bacteriophage inactivation rates (log/min) for different treatments.

T4 phage (log/min)				
	Bench	Gas flow only	Warm flow	Plasma
Pure λ-dil	-0.03	-0.05	-1.77** (-0.88*)	-1.89** (-1.44*)
λ-dil+ glycerol	-0.28	-0.47	-0.58	-0.77
MS2 phage (log/min)				
	Bench	Gas flow only	Warm flow	Plasma
Pure λ-dil	-0.03	-0.07	-0.47	-1.56*, -0.52***, -0.12****
λ-dil+ glycerol	-0.06	-0.02	-0.38	-1.25*, -0.48***, -0.25****

* inactivation rate for 0-1 min exposure time

** inactivation rate for 0-2 min exposure time

*** inactivation rate for 1-2 min exposure time

**** inactivation rate for 2-4 min exposure time

Transmission electron microscopy (TEM) technique was used for observation of MS2 samples in different situations (Figure 4.20). Intact capsids (containing RNA) and damaged capsids (RNA loss) distinction was difficult because of difference in contrast between phages (from one picture to the other or in a same picture). It was thus impossible to quantify the phage integrity from TEM imaging. But specific morphologic modifications could be observed. In the micro-figures of MS2 stock (Figure 4.20(a)), on the bench sample (Figure 4.20(b)), and gas flow-

only treated sample (Figure 4.20(c)), the capsids of phages had the similar round shapes. However, after 4 min. exposure to humid air post-discharge, significant proportion of phages showed capsid breaks (lost fraction of the circle indicated by yellow arrows in Figure 4.20(d)) and the magnified imagination of a capsid broken in Figure 4.20(f)). Previous studies showed that ROS species produced by plasma could induce bond-breaking of peptidoglycan (i.e. C-O, C-N, and C-C)- a structure on bacteria wall [274]. It is also worth noting that SARS-CoV-2 capsid break was previously observed for direct surface treatment by argon plasma plume [254].

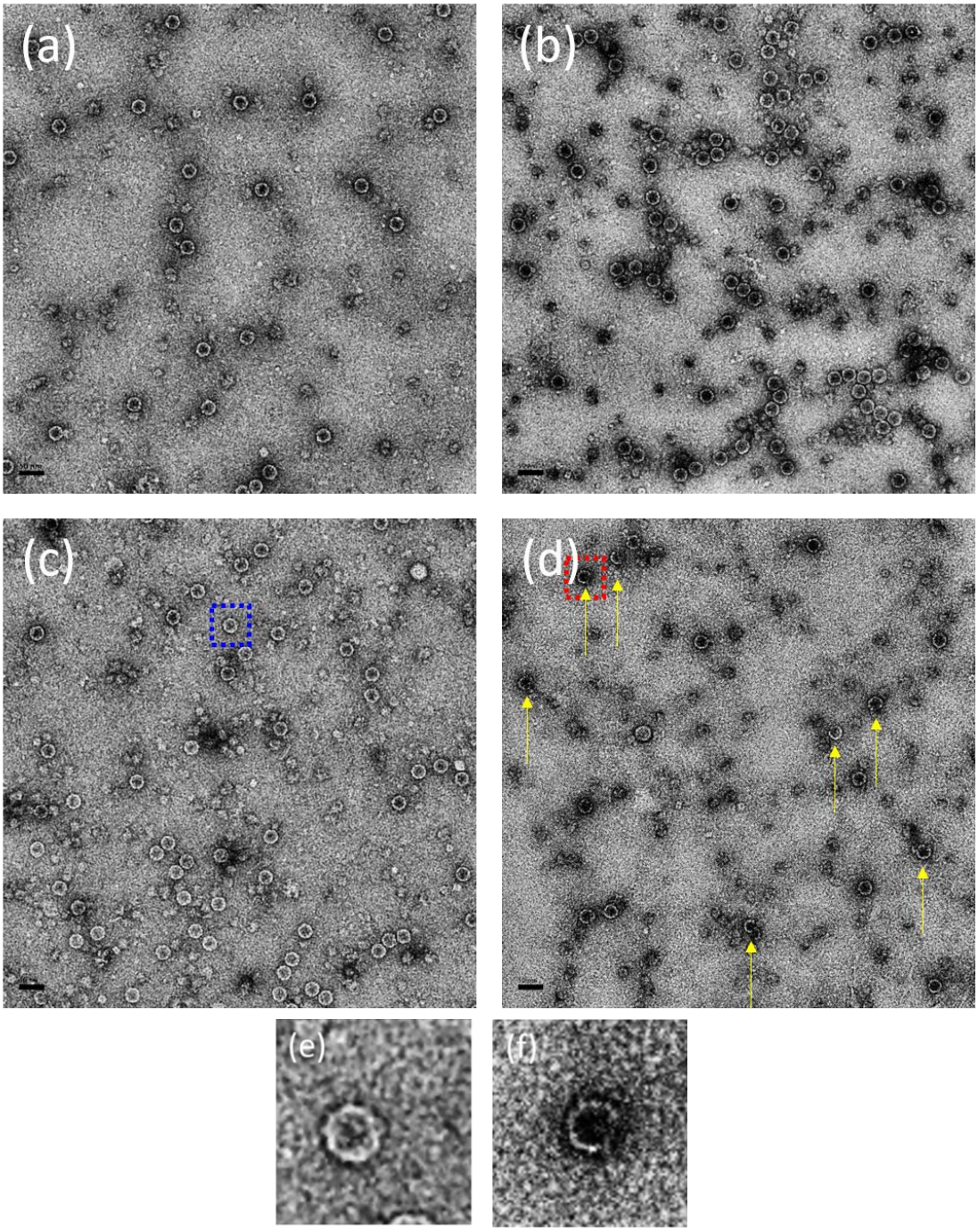

Figure 4.20 TEM micro-figures of MS2 (a) stock, (b) on bench for 4 min, (c) 4 min. humid air flow exposure, and (d) 4 min humid air post-discharge exposure. (e) and (f) are the magnification of blue block in (c) and red block in (d). The yellow arrows point the broken capsids. MS2 concentration: ~10^{12} PFU/mL. Scale bars: 50 nm.

4.4 Summary

Our goal was to study an alternative plasma-based indoor virus control strategy for domestic and biomedical applications. In this objective, we selected two bacteriophages as surrogate models to human viruses: T4 (DNA phage) and MS2 (RNA phage). Bacteriophage suspension was spotted on highly absorbent surface: a 35 µm thick paper made of cellulose and wood pulp. Previous work considered virus treatment by means of plasma process in liquid phase or exposed on a smooth surface, but to our knowledge, not on such a complex surface. However, this type of case seems more representative of a real surface contamination. In addition, admixture of glycerol in buffer solution was also chosen as an additional experimental parameter in order to study the impact of viscosity (as for saliva for instance).

Plaque assay technique (with Gratia method) was systematically used (triplicate experiments) for bacteriophage viability / activity.

As a first step, λ-dil solution was chosen among four buffer solutions in which phages were suspended. Selection was based on the stability of the phage on the paper surface.

As a second step, surface plasma decontamination tests (MS2 phage) were realized using four different feed-gases: dry and humid air, dry and humid argon. In all conditions, electrical parameters were chosen to impose a 34°C temperature on the paper sample. Argon plasma was found to be the most effective in direct exposure (dry argon plasma plume) and in remote exposure (humid argon) with minimum 5.7 log PFU reduction in 3 min. treatment time. Air (remote exposure only) was much less effective with 2.7 log PFU reduction for the same exposure time. Nevertheless, we chose to focus on the most direct application of plasma using air as a plasma feed-gas, and in particular humid air.

It is therefore clear that the experimental conditions chosen were not favorable,

both from the point of view of substrate choice and plasma type, to promote the virucidal efficacy of a plasma treatment. These conditions were chosen instead to represent a realistic decontamination situation and attempt to identify the mechanisms at taking place in such situation.

Gas analysis of the flowing air post-discharge (FTIR and UV absorption spectroscopy) was performed for identification and quantification of stable RONS impacting paper sample. Acidification of liquid phase (buffer solution) exposed to post-discharge was also measured.

T4 phage suspended in pure λ-dil buffer solution was seen to be inactivated (below detection limit, i.e. 4 log PFU reduction in this case) when exposed to humid 34°C air flow-only treatment for 2 minutes. As for most of tailed phages, T4 viability is known to be dependent on relative humidity changes (induced by temperature increase which cannot by itself result in such an inactivation rate at 34°C). For a same plasma exposure time, detection limit was also reached. It is probable that inactivation rate was higher, but intermediate exposure time (e.g. 90 s) was not investigated. When T4 was suspended in λ-dil buffer with the addition of 10%Vol. glycerol, the stability untreated samples (on the bench) was surprisingly decreased by 1 log during the first 3 minutes and then stabilized for more than 40 minutes. Exposure to humid air flow at 34°C had much less impact, leading to a 2.3 log PFU reduction in 4 min. Plasma treatment induced a 3 log PFU reduction for the same exposure time. Presence of glycerol in the buffer solution was thus protecting T4 against relative humidity change effects and RONS induced reactions.

MS2 was seen to be more resistant to environmental stress. Impact of glycerol admixture was observable but in a much lesser extent than in the case of T4. Exposure to humid air post-discharge first induced high inactivation rate (1.5 log PFU reduction in 1 min.) which decreased with time. We suggest that this decrease of inactivation rate was due to the desiccation of WSP sample. In presence of liquid phase, RONS can dissolve, accumulate (concentration increase and pH decrease), and directly or indirectly (by-products) react with MS2 capsid. When part of the contaminated paper is dried, the liquid phase chemistry can no longer take place, and MS2 capsids are only submitted to gaseous oxidative stress which is much less efficient. Note that change in pH, and surface wettability modification induced by plasma treatment affect evaporation rate. Hygroscopic and moisture retention effect of glycerol

postpones this mechanism. As a results, inactivation rate was higher for the first minute of exposure (lower evaporation and consequently lower liquid phase RONS concentration). But water retention allows liquid chemistry to take place for longer exposure time, finally resulting in higher inactivation rate than without glycerol addition for the last 2 minutes of treatment.

Formation of capsid aggregates could also contribute to the decrease in activation rate with time. Aggregates were reported to be more resistant to environmental stress and their formation is promoted by pH decrease.

The possibility of phenotype difference in MS2 population cannot be excluded and was suggested by the diversity of plaque size in MS2 plaque assays. This population could exhibit higher resistance properties to oxidative stress. This could explain the decrease in inactivation rate with time, which may correspond to the specific resistance of the 0,5% last phages. Future work could consist in selecting this specific population and test its resistance to plasma exposure.

Finally, broken MS2 capsids could be observed using TEM imaging after 4 min exposure to post-discharge (never observed for on the bench samples nor for air flow-only exposure) Such a morphological modification was previously reported for direct argon plume treatment.

5 HUMAN ADENOCARCINOMA CELLS TREATMENT

5.1 Introduction

According to the open data of the Ministry of Health and Welfare in Taiwan, cancer was ranked as the number one cause of death for 29% of total deaths in 2020 [275]. Among all kinds of cancer, the most patients died due to suffering from lung cancer.

In this work, non-thermal plasma was applied for the treatment of lung tumor cells in vitro. One plasma generation configuration with two kinds of feeding gas (dry and humid argon) resulted in different impacts on the cancer cells. Dry argon plasma was found to result in local inactivation of the cells and to inhibit the migration of tumor cells; on the other hand, humid argon plasma reduced the proliferation of the cancer cells and induced cell apoptosis in not only the directly treated region but also up to 40 mm away, but did not inhibit subsequent migration of cancer cells. This chapter will first present the experimental materials and methods for both the plasma systems and the biological measurements and then the experimental results and discussion.

5.2 Materials and methods

The plasma generation system, tumor cell sample preparation, experimental process, and tumor cell assays are introduced in this section. The plasma generator used for these experiments was very similar to the rod system (RS) DBD system which has already been introduced in previous chapters; it is reintroduced here for completeness and so that this chapter may be read without referring back to previous chapters.

5.2.1 Plasma generation

Dielectric barrier discharge (DBD) atmospheric non-thermal plasma was applied for the treatment of human lung cancer cells. The DBD configuration consisted of a borosilicate tube (outer diameter 6mm and inner diameter 3mm) and a stainless steel rod (2mm in diameter). The rod was used as a high voltage electrode connected to a 15kHz AC power supply. A 24mm long strip of copper tape was attached on the external surface of the borosilicate tube 10mm from the tube outlet and connected to ground to serve as a counter electrode. The feeding gas was argon, which was made to flow at a rate of 2 L/min. Water

vapor could be added to the argon gas flow, and two operating conditions were tested: (i) dry argon condition, with 8 kV peak to peak applied voltage; for this case, a 10mm long plasma jet propagated from the tube outlet (1 W mean input power); (ii) humid argon condition (saturated water vapor content in argon flow at room temperature and atmospheric pressure), in which the plasma was confined within the 0.5mm inter-electrode gap with an applied voltage of 13.5 kV (1.7 W mean input power). The input power for the two cases was not the same because the criterion used to determine the operating point was an applied voltage just under the voltage for which sparking was observed to occur between the HV and counter electrodes.

5.2.2 Tumor cell culture

The Gustave Roussy Cancer Campus provided human adenocarcinoma (lung cancer) cells from 5 patients - for experiments. Cells were grown in RPMI media (Gibco-Invitrogen) supplemented with 10% fetal calf serum (FCS) in Petri dishes for 48 hours in an incubator at 37°C with 5% CO_2.

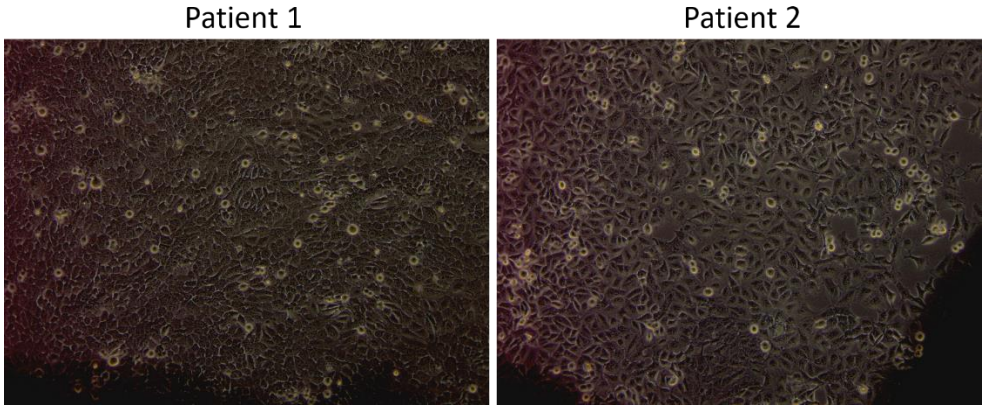

Figure 5.1 Images of the lung cancer cell cultures from two patients after 48 hours of incubation; the images were taken by charge-coupled device camera (CCD-IRIS; Sony, Paris, France) under an inverted microscope (Zeiss, Rueil-Malmaison, France).

5.2.3 Treatment process

Before treatments, the cell culture medium (including the suspended dead cells) was replaced by 3mL of HBSS (Hanks' Balanced Salt Solution). Cells were observed by microscope and the treatment location was marked using a marker on the bottom of the Petri dishes. A Petri dish containing the cell culture was placed at 10 mm downstream from the tube outlet. The tube outlet, Petri dish, and sample holder were enclosed within a treatment chamber with from which the argon or argon/H_2O gas exited via an outlet tube leading from the treatment chamber wall to the outside environment in order to prevent ambient

air backflow (thus avoiding air entering the plasma region and ozone production). A schematic representation of the experimental set-up is given in Figure 5.2. Samples were directly exposed to the plasma process in Petri dishes for 5 min after a 5-min purging phase of the treatment chamber for given argon gas condition (dry or saturated with water vapor) at 2 L/min. Cells from the same patients used for control runs were exposed to the same argon condition for 10 min. After exposure (either plasma treated samples or control samples), cell cultures were scraped from a 2 cm^2 area from two different zones on the Petri dishes with trypsin solution and by cell scrapers. The two zones symmetrical to the center of the Petri dish are detailed in Figure 5.3: the center of Zone 1 was directly below the tube outlet and thus had greater exposure to the plasma treatment than the Zone 2, for which the center was 40 mm away from the center of Zone 1. Images of treated samples were obtained with the use of a charge-coupled device camera (CCD-IRIS; Sony, Paris, France) under an inverted microscope (Zeiss, Rueil-Malmaison, France).

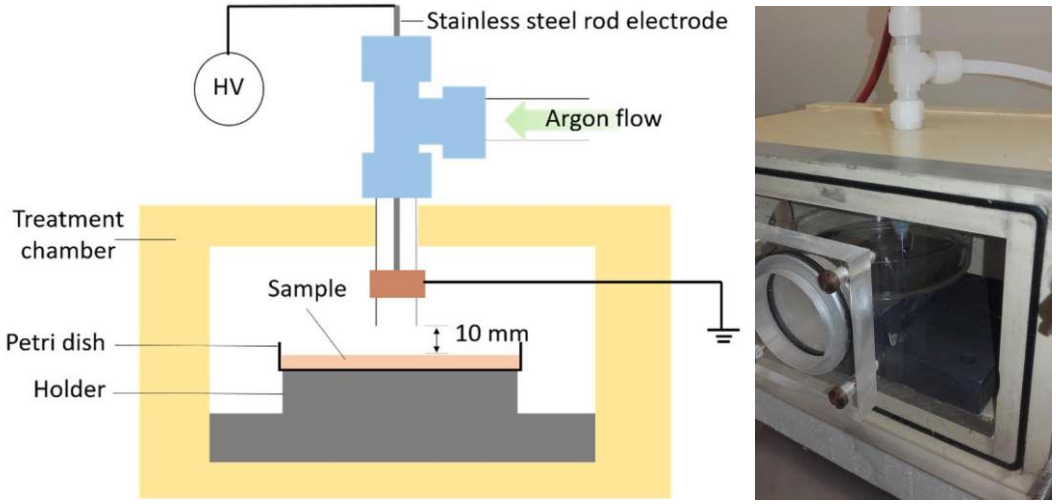

Figure 5.2 Schematic description and photograph of the experimental set-up.

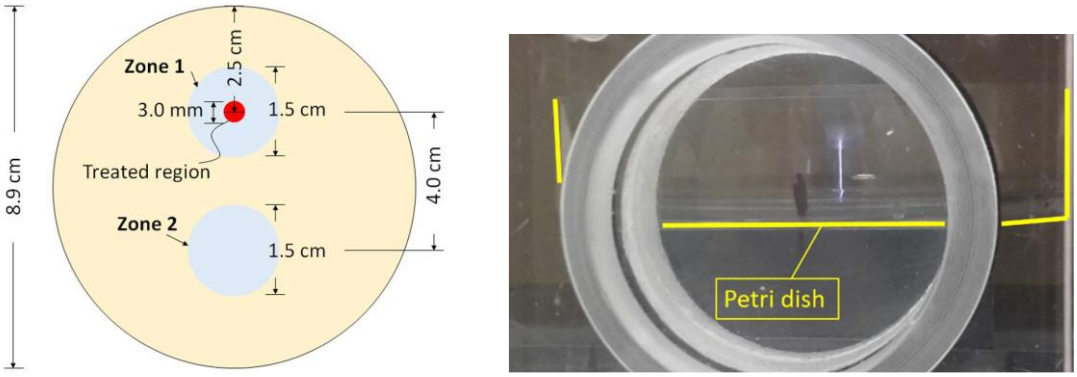

Figure 5.3 Treatment zones in Petri dish sample (left) and photograph of a sample being treated by dry argon plasma plume (right).

5.2.4 Assays

Proliferation

After treatment, the liquid medium including the detached cells (most of these were dead [276]) above the layer of attached cells in the Petri dishes was removed. Attached cells in Zone 1 and Zone 2 were collected and counted either immediately after exposure or 30 min after exposure. Control experiment and plasma-treated cells from 5 patients were seeded in 96-well plates at a density of 5000 cells per well and allowed to adhere and grow for 24 hours. Cells were then serum starved in MCDB131 medium for the next 24 hours. After that, cell growth was measured by using the Cell Proliferation measurement instrument Delfia (Perkin Elmer) according to manufacturer's instructions. Each measurement was performed in triplicate.

Apoptosis and necrosis

After treatment, as in the proliferation assay, the medium including the detached cells (most of them being dead [276]) in the Petri dishes was removed. Cells in Zone 1 and Zone 2 were collected by scraper immediately after exposure or 30 min after exposure for apoptosis assay after a 24-hour period. The annexin V-FITC assay was used to validate the presence of apoptosis. Adherent cells were harvested by trypsin/EDTA treatment and stained with annexin V–FITC (BD Biosciences), and then analyzed by flow cytometry MACSQuant (Miltenyi Biotec). In each sample, at least 10,000 cells were counted by Fluorescence activated cell sorting (FACS) analysis.

Migration

Images of samples were taken by a charge-coupled device camera immediately, 2, 4, 6, 24, 48, and 72 hours after treatment under an inverted microscope. The regrowth of cells may be discerned in the photos by using the marks made on the bottom side of the Petri dishes as reference positions.

5.3 Results and discussions

In this section, the impacts of plasma on tumor cells are presented and discussed, including proliferation, apoptosis, and migration.

5.3.1 Proliferation

Proliferation assay measures the viability of human adenocarcinoma tumor cells

after treatment *in vitro*. Cell growth was assessed (from 5 patients) after 24 hours had elapsed after the plasma treatment, and the results are presented in Figure 5.4. The experimental results showed that the impact on the proliferation of this type of cancer cell was negligible for the case of plasma treatment using dry argon gas (part (a) of the Figure).

In the results of humid argon treatment (part (b) of the Figure), the number of reproducing tumor cells was approximately 10% less in the treatment group than in control group when the assay was done immediately after treatment in not only Zone 1 but also in Zone 2, which was at a greater distance from the plasma source than Zone 1. Furthermore, if the collection of tumor cells was done at 30 minutes after treatment, the treatment group has over 30% decrease in proliferation for both zones.

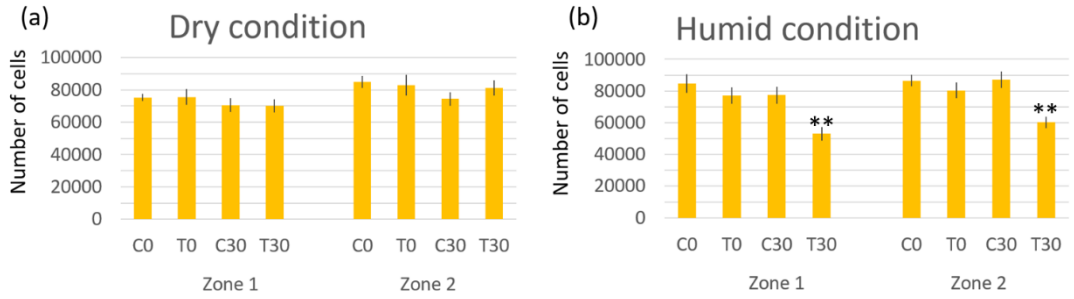

Figure 5.4 The plasma treatment result of proliferation with feeding gas: (a) dry argon and (b) humid argon. C0: control groups sampled immediately after the end of plasma treatment; C30: control groups sampled 30 minutes after treatment. T0 and T30 are experimental groups. (Student's test: 0.01**)

Possible mechanisms for the effects of dry argon plasma for the inactivation of cancer cells are interactions of the cells with charged and/or excited argon atoms, local gas heating and heat transfer to the cells, and the impact of UV light emitted by the plasma on the cells. However, from the results, these mechanisms had very little to no effect on tumor cell proliferation. When the water vapor was added into the argon flow, UV emissions were reduced to the sample (because the plasma was only present within the tube and did not propagate to the cells location on the Petri dish as for the case of dry argon plasma). However, with humid argon plasma, reactive oxygen species (ROS), such as OH radical and H_2O_2, were produced and were presumably responsible for the increased inactivation of tumor cells. These ROS species were transported to the tumor cells either directly via the gas or indirectly (by first dissolving in the medium with subsequent transport to the target cells).

A sufficient dose of ROS may induce tumor cells to go into apoptosis (meaning that the cells cannot proliferate anymore) [213]. It is worth mentioning that there was also a decrease in cell proliferation in Zone 2, further supporting the idea that ROS were responsible for the tumor cell inactivation because they may easily be transported to Zone 2 via the gas flow combined with diffusion in the medium. UV light and/or elevated temperatures would clearly not be able to have any effect in the Zone 2 since they were not able to affect proliferation even in Zone 1 for the dry case. It may therefore reasonably be concluded that ROS may then impact the tumor cells in Zone 2 at 4 cm away from the treated point, albeit with slightly less efficiency than in Zone 1 due to the greater distance needed for the transport of these species and the resulting lower concentration of them due to losses from diffusion along the way.

5.3.2 Apoptosis

In the apoptosis assay, human adenocarcinoma tumor cell death ratios *in vitro* were measured and are here presented. After a period of 24 hours after plasma treatment and sample collection, cell apoptosis and necrosis were assessed (on tumor samples from all 5 patients) and the results are presented in Figure 5.5. The results, much as in the case of the proliferation assay, show that humid argon treatment exhibits higher efficacy than dry argon treatment in inducing cell apoptosis and necrosis. While the effect of dry argon plasma appears negligible, humid argon plasma induces over 40% and 65% of total cell death in Zone 1 and Zone 2, respectively. Comparable results were obtained whether cells collected immediately or after a 30-min delay subsequent to plasma treatment.

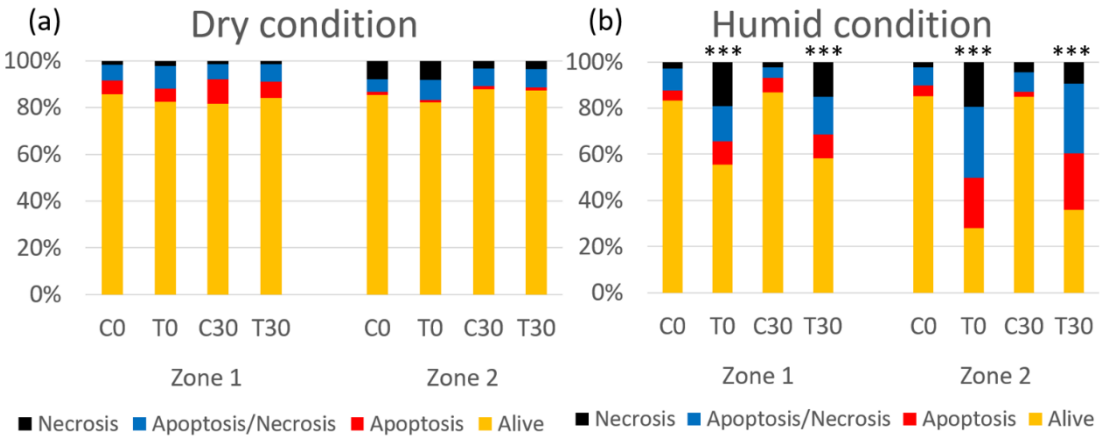

Figure 5.5 The plasma treatment result of apoptosis with feeding gas: (a) dry or (b) humid argon. (Student's test: 0.001***)

In the apoptosis assay, only the attached cells were scraped and collected. This meant that some of the cells which had died during the treatment and become detached from the surface were not quantified in the assay. These detached cells could have been removed from the two zones either during the treatment by diffusion or by the removal of the medium prior to the apoptosis assay. Of the remaining cells, which were by definition attached cells, it was observed that the ratio of the sum of apoptosis and necrosis to the total cell count in Zone 2 was higher than Zone 1 for humid argon plasma treatment. It showed that over 40% of tumor cells in Zone 1 and over 65% of tumor cells in Zone 2 went into the necrosis or apoptosis process because of action, presumably by the plasma produced ROS species according to the same reasoning made in the previous section on proliferation. The fact that a greater effect was observed in Zone 2 than in Zone 1, while counter-intuitive, may be explained if it is assumed that a much greater portion of the cells in Zone 1 became detached as compared to Zone 2.

In contrast, in dry conditions, the impact of plasma treatment on tumor cell apoptosis was negligible as may be seen by inspection of Figure 5.5(a). However, the treated spot could be seen visually using microscopy (for the dry condition as well as humid). It was thus observed that dry argon plasma had very local effect in a small (about 2-3mm diameter spot) spot, located just under the tube outlet. The surface area of this spot is of course quite inferior to the overall scraped area and did not contain any cells (according to visual observation). These two observations are in agreement with the results shown in the Figure 5.5. As shall be further discussed in the following section, even in control experiments, a spot devoid of cells was observed directly under the tube outlet, due to the mechanical action of the gas flow, and perhaps related to a local desiccation effect on the substrate. The question of whether the tumor cells may be able to recolonize, or migrate into this region directly under the tube outlet naturally led to the experiments presented in the following section.

5.3.3 Migration

For all of the treated Petri dishes, including control (humid or dry gas flow only) and plasma treatment samples, a spot was visually observed just at the center of Zone 1 under the tube outlet as previously discussed. The regrowth, or migration, of cells into these treated spots, which may be seen to be analogous to the process of wound healing, were quantified. Micrographs of the spot in Zone 1 immediately after treatment and for 24 and 48 hour periods after

exposure (Petri dishes were incubated at 37°C during these periods of time) are sequentially presented in Figure 5.6. The spots of the control group were formed by the dynamics of gas flow, and the spot size decreases over time by a migration/proliferation mechanism after 48 hours of incubation (Figure 5.6 bottom row). Healing also took place for the case of humid argon plasma treatment after 24 and 48 hours (Figure 5.6 top row). In contrast, the spot (Figure 5.6 middle row) treated by dry argon plasma maintained its size for the 48 hours, this indicating a lack of tumor cell migration back into Zone 1.

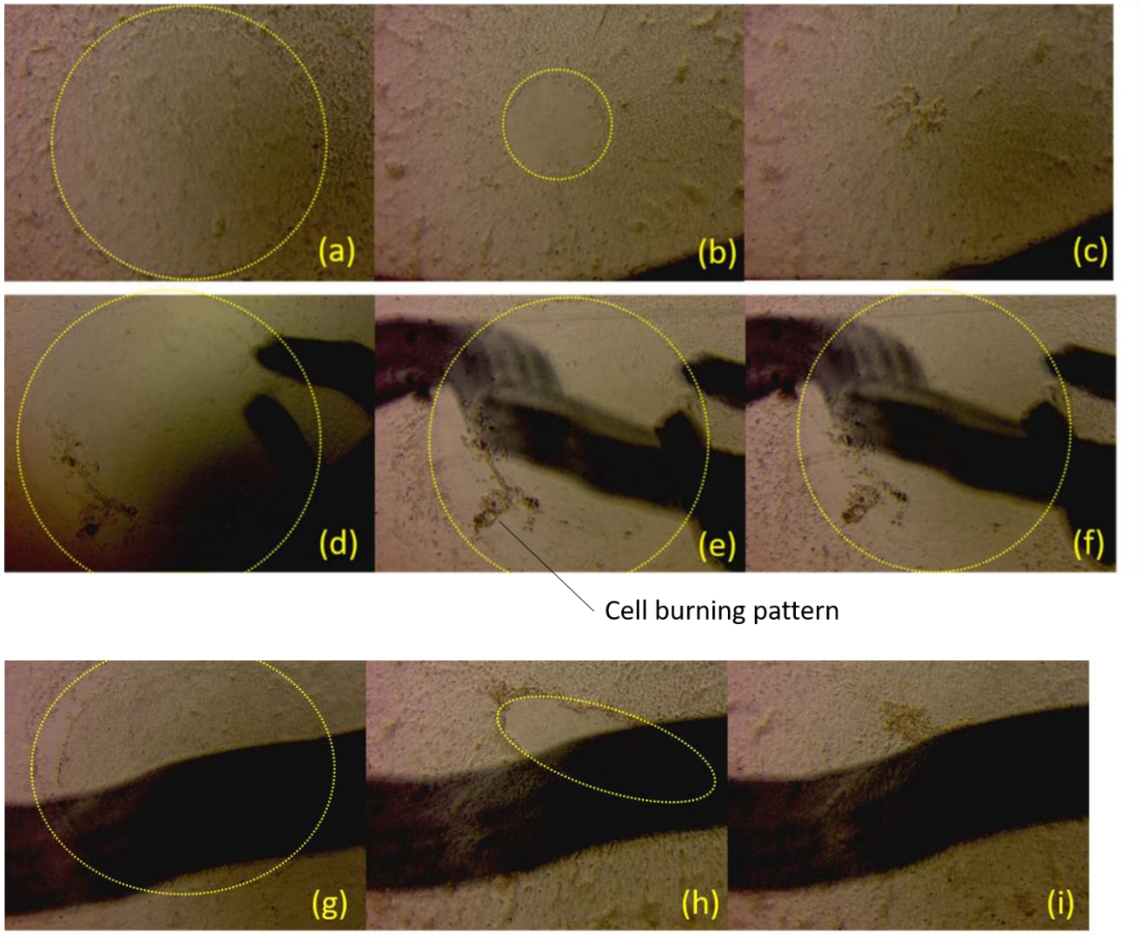

Figure 5.6 Micrographs of the treatment zone. First row: humid argon treatment. Second row: dry argon treatment. Third row: dry argon control. For all the three rows, the first column is for imagery made immediately after treatment, second column for 24 h delay after treatment and third column for 48 h delay after treatment.

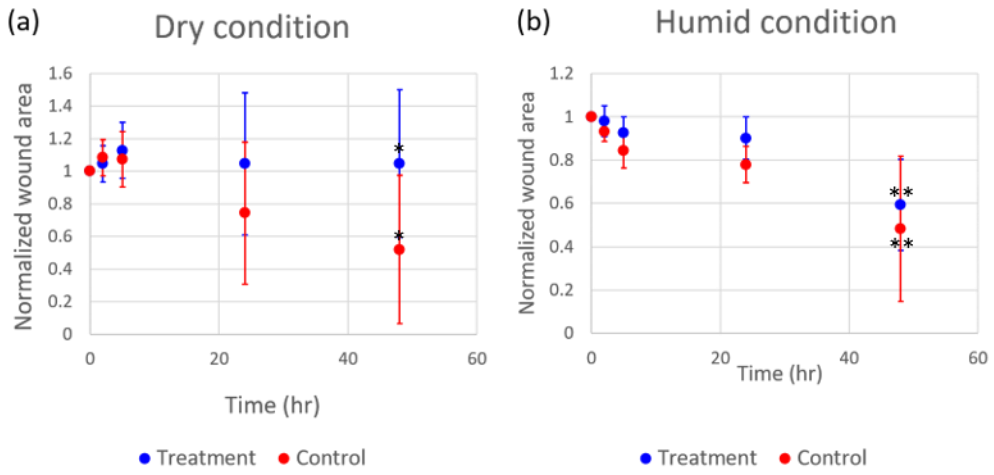

Figure 5.7 Statistics Quantification of the normalized (to the initial surface area) area of treated spots measured immediately and 2, 5, 24, and 48 hours after (a) dry or (b) humid argon plasma treatment. The error bar presents the standard deviation of 4 patient results. (Student's test: >0.1* and 0.05**)

Discussion of possible mechanisms apoptosis and migration

When tumor cells are exposed to reactive oxygenating species (ROS), a protein called p53 is an important agent for the induction of tumor cell response, including the activation of the apoptosis process. Under the action of the plasma, and especially for the case of the humid argon plasma, which contains far higher concentrations of ROS than the dry argon plasma, p53 would likely be stimulated (phosphorylation) and induce the apoptosis process as seen in the literature [12, 243]. In the humid argon plasma treatment results presented in section 3.2.1, the apoptosis assay showed significant apoptosis activity even though the assay was done 24 hours after treatment. The amounts of phosphorylation-p53 measured by Weiss *et al* was high 4 hours after plasma treatment and was significantly reduced after 24 hours [243]. Therefore, it is proposed that higher levels of stimulated p53 were likely present in the case of the humid argon plasma treatment in this work when compared to dry argon plasma treatment even at 24 hours after the treatment. Measurement of stimulated p53 levels are thus recommended for future work on this subject.

On the other hand, in the dry argon plasma treatment, the ROS species production was much less than humid argon plasma, and the impact of dry argon plasma on proliferation or apoptosis was negligible. In addition, very little cell migration was observed for this case even 48 hours after the treatment. If it is postulated that, during the dry argon plasma process, on a very local scale

withing the spot directly under the tube outlet, a large number of tumor cells went into necrosis locally (this idea is promoted by the observation of dark spots, the cell "burning pattern" indicated in Figure 5.6(d)(e)(f)).

The migration behavior which was observed in the case of the control samples indicated that this was the normal way for these cells to react under such conditions. In the case of the post-treatment for the humid plasma sample, the migration also occurred in the treated spot and full closure occurred after 48 hours, much as for the control experiment. In previous studies reported by Wang *et al*, the migration capability of the breast tumor cells was much reduced after 90s of helium plasma jet exposure [277]. The inhibition of migration of lung tumor cell for up to 48 hours was also observed in this work after 5 min exposure with a less costly plasma source: argon plasma jet. The role that the plasma jet played on the treated spot edge is still unknown. Further investigation should focus on physical or chemical changes in the edge cells.

These results indicate that further work should be done to measure the amounts of p53 to confirm or deny the proposed mechanisms of humid and dry argon plasma. Also, physical or chemical changes in the spot edge cells should be investigated. In addition, it will be important to extend experimentation to the case of non-cancerous cell to see whether there may be a selective effect (the goal being to tune the process to ideally promote apoptosis in cancer cells while minimizing impacts on healthy cells).

5.4 Summary

This work has demonstrated that non-thermal plasma can have significant effects on human cancer cells in vitro but that these effects can be strongly influenced by the presence of water in the plasma working gas. For example, significant decreases in cell proliferation and increases in tumor cell apoptosis were measured for the case of the treatment of those cells when using humid argon as the plasma working gas, while little change in cell proliferation and negligible levels of apoptosis was observed for the dry argon plasma treatment. In addition, nearly the same reduction in cell proliferation and increased levels of apoptosis were observed at a distance of 40 mm away from the tube outlet for the case of humid argon treatment, indicating the likelihood of the dominant mechanism for the induction of the apoptosis process being the production of reactive oxygen species (ROS), which are produced in much

higher quantities for the case of humid argon working gas. The mechanism for this action may have involved the production by the tumor cells of the protein p-53, which was not measured here but is recommended to be investigated in future work.

Experiments investigating the migration of the tumor cells in the hours and days subsequent to the plasma treatments also showed stark differences between the two cases of dry and humid argon plasma treatment. The level of migration of tumor cells into the location directly under the plasma reactor tube outlet was measured. This zone was initially rendered devoid of cells for all cases, even in the case of the control experiment with only gas flow and the associated mechanical action on the layer of tumor cells. However, the migration of the cells into this zone was only observed for the case of the control experiment and for the humid argon plasma treatment. The inhibition of migration by plasma jet can be found in previous studies using higher cost plasma sources (helium plasma) [277] even though the mechanism for the inhibition is still unclear according to our knowledge.

Other future work which is merited are combined treatments with alternating dry and humid conditions to tailor the system to a given application. Investigation of the increase of ROS within tumor cells would also be interesting, the mechanisms of inhibition of migration by plasma jet, and critically, the effect of these treatments on healthy cells must be investigated in view of having a process which ideally would selectively eliminate cancerous cells while minimizing negative effects on healthy cells.

6 CONCLUSION

In this work, physical and chemical properties of non-thermal plasma (NTP) generated by dielectric barrier discharges (DBD) at atmospheric pressure were investigated in the perspective of biological applications: surface decontamination and plasma medicine. Two DBD plasma sources – rod-to-cylinder system and two-ring system – were designed and characterized. Discharge propagation in long thin insulating (silicone) tube, direct interaction of plasma with surface and exposure of surface to post-discharge were examined for different feed-gases. Selected configurations of plasma source were implemented for bacteriophage inactivation and cancer cell treatment. The inactivation of DNA (T4) and RNA (MS2) bacteriophage by exposure to plasma processes was studied. Potential application motivated the choice of realistic operating conditions: feed-gas, exposure mode, choice of the contaminated substrate. In the field of plasma medicine, *in-vitro* treatment of human lung adenocarcinoma cells by humid and dry argon plasma source was examined. Local and global effects were investigated.

6.1 Investigation of DBD non-thermal plasma

The characteristics of NTP generated in argon gas by rod-to-cylinder system (RS) (applied to surface contamination (Chapter 4) and plasma medicine (Chapter 5)) and two-ring system (TR) were studied. As a first step, electrical characteristics were examined: discharge onset voltage for TR system was more than twice higher than for RS plasma; with increasing applied voltage, RS system's mean discharge power exhibited an exponential increase, while TR system's mean discharge power increased linearly. As a second step, chemical reactivity was examined through the production of hydrogen peroxide. H_2O_2 production efficiency of TR system (0.63 g/kW·h) was higher than that of RS plasma (0.34 g/kW·h). This difference in H_2O_2 production efficiency was suggested to be related to the difference in plasma plume / liquid surface interaction cross-section.

Finally, the discharge propagation along the inner surface of a quartz tube where dry argon was flowing was studied with the TR system. An external downstream wire was inserted in the tube to measure the discharge current, the voltage gradient was measured and the plasma conductivity was deduced from the Ohm's law. As expected, the conductivity of the plasma channel was found

to increase with discharge current. The same configuration was used to measure the streamer velocity which was seen to decrease along with propagation distance. Using oscillograms of the current in three different locations in the system, an effort was made to study and identify the different phases of discharge development including discharge ignition, propagation, charge deposit, and "return" or "back" discharge. However, more investigation is needed, and this study should be completed in future work by optical emission spectroscopy measurements.

In addition, RS and TR systems were connected to a small diameter silicon tube for the further investigation of argon plasma propagation with different pulse voltage parameters as well as gas flow rate. The small silicon tube was imaged as an endoscope duct. Using the RS system, discharges can propagate over 100 cm in the silicon tube, while with the TR system, a maximum propagation length of only 50 cm in silicone tube was observed. The experimental conditions leading to the maximum propagation length with both systems were very different. For instance, optimum gas flow rate was 0.41 L/min for RS system while it was more than 2 L/min for TR system. An increase in voltage pulse width resulted in a longer propagation length until saturation of its effect was reached. The saturation pulse width was 900 ns for RS system and 2000ns for TR system. These different behaviors result from the actual electric field in the streamer head which is, for given external parameters, strongly dependent on the electrode arrangement of the system.

6.2 Surface decontamination

The rod system was applied for surface decontamination. T4 (DNA phage) and MS2 (RNA phage) were chosen as surrogate models to human viruses. Bacteriophages were suspended in buffer solution with or without 10% Vol. glycerol (glycerol admixture to approach the viscosity of saliva) and spotted on a water soluble paper (complex microstructure The viability of bacteriophage was assessed by plaque assay technique with Gratia method.

The buffer solution in which bacteriophages were suspended (λ-dil) was chosen according to their highest viability at room temperature. First tests were conducted using four different feed-gases for the plasma (RS system) source. Among these conditions, the least efficient was the one using humid air. However, it is this condition that we have chosen for the rest of the study, for

reasons of feasibility of the application. Using humid air as a plasma feed-gas, four treatment conditions (on the bench, room temperature gas flow-only (20˚ C), warm flow-only (34˚ C), and plasma) with two different buffer solutions (pure λ-dil and λ-dil +10% glycerol) and two different phage types (T4 and MS2) were compared.

With T4 phage, bench and gas flow-only samples suspended in pure λ-dil had high stability on paper, but the phage number after warm flow-only and plasma treatments was lower than detection limit after 2 min. exposure time. However, admixture of glycerol decreased the survival fraction of on the bench and of gas flow-only samples. In contrast, glycerol helped phages survival over 4 min treatment of warm flow-only and plasma treatments. With MS2 phage, glycerol admixture had minor effect on phage inactivation for on the bench and gas flow-only treatments (room temperature and warm air). On the bench and gas flow-only treated samples kept high survival fraction for 4 min whereas warm flow-only treated samples had about 0.4 log/min inactivation rate. In the case of humid air plasma treatment, transmission electron microscopy images revealed the presence of ruptured capsids (absent in other treatments). This type of morphological modification had already been reported for treatments using an argon plasma plume. Plasma treatment inactivation curves exhibited three different phases: for 1 min. exposure time, plasma treatment induced strong inactivation rate (over 1.2 log/min). Then, the inactivation rate decreased with exposure duration from about 0.5 log/min in 1-2 min to 0.25 or less in 2-4 min.

Partial desiccation of the sample can explain the decrease in inactivation rate for MS2 plasma-treated samples. At the beginning of treatment, RONS dissolve and concentrate in liquid phase, so resulting in a high inactivation rate. Then, partial desiccation takes place and only the wet parts of the sample undergo effective inactivation of bacteriophages. For longer exposure time, and consequently for advanced desiccation of paper sample, phages are only exposed to gas phase RONS, so resulting in a much lower inactivation rate. Furthermore, phenomena of phage aggregation or phenotypic selection that could lead to increased resistance cannot be excluded. These aspects will be studied in future work.

6.3 *In-vitro* human adenocarcinoma (lung cancer) cell treatment

In cancer cell treatment, the rod system fed with dry or humid argon (water vapor saturated at room temperature and atmospheric pressure) was applied to generate plasma.

For a 5 min. humid argon plasma treatment, significant decrease in cell proliferation (10% for immediate assay after treatment and 30% for a 30 min. delayed assay after treatment) and increases in tumor cell apoptosis (up to 65%) were measured. It is important to note that these results could be obtained both in the area under direct post-discharge exposure and in an area 40 mm away from it. This implies that the dominant mechanism responsible for the induction of the apoptosis process is based on the production of ROS. This mechanism may involve the production of the protein p-53 by the tumor cells, which was not measured here but is recommended to be investigated in future work.

For a 5 min. dry argon plasma treatment, little change in cell proliferation and negligible levels of apoptosis were obtained. But unlike wet argon plasma treatments, the spot treated by dry argon plasma maintained its size for the 48 hours, this indicating a lack of tumor cell migration. This observation was previously reported for studies with helium plasma jet.

It is worth noting that a same plasma source can be used to promote strongly different effects on cancer cell according to water vapor content of the argon feed-gas. This result could be of interest for a combined treatment aiming on the one hand to initiate the apoptosis mechanism of the cells and on the other hand to locally prevent the migration of the cancer cells. For future work, it will be important to extend experimentation to the case of non-cancerous cell to examine the selectivity of the plasma treatment (ideally promote apoptosis in cancer cells while minimizing impacts on healthy cells).

6.4 Perspectives for future work

In this work, we have addressed many scientific questions, many of which are still unresolved. The first one concerns the study of the propagation of discharges over long distance on the surface of a solid insulator. Our approach has been to make electrical measurements only, with in some cases the risk of disturbing the phenomenon by the measurement. It would therefore be

appropriate to complete this study with emission spectroscopy measurements. Secondly, regarding the inactivation of bacteriophages on a surface, the role of liquid water will have to be specifically studied to confirm the cause of the drop in the inactivation rate with exposure time. Moreover, the resistance mechanisms of the phages themselves will have to be studied, in particular the possible aggregation and phenotypic resistances. Finally, in lung cancer cell treatment, the selectivity of the treatment on healthy and cancer cells will have to be evaluated. In addition, before moving on to an *in-vivo* model, more representative *in-vitro* models should be considered, such as spheroids or even organoids.

REFERENCE

[1] Hannah Ritchie and Max Roser, Our World in Data, "Causes of Death," 2019. [Online]. Available: https://ourworldindata.org/causes-of-death. [Accessed 19 May 2020].

[2] Tohme, S., Simmons, R. L. & Tsung A., "Surgery for cancer: a trigger for metastases," *Cancer Res,* p. 1548 – 1552, 2017.

[3] Dracham CB, Shankar A, Madan R. , "Radiation induced secondary malignancies: a review article," *Radiat Oncol J.,* p. 85 – 94, 2018.

[4] Cancer.Net, "Side Effects of Chemotherapy," 2019. [Online]. Available: https://www.cancer.net/navigating-cancer-care/how-cancer-treated/chemotherapy/side-effects-chemotherapy. [Accessed 27 May 2020].

[5] N.P. Tipnis, D.J. Burgess, "Sterilization of implantable polymer-based medical devices: a review," *Int J Pharm,* pp. 455-460, 2018.

[6] M.J. Kirkpatrick, B. Dodet, E. Odic, "Atmospheric Pressure Humid Argon DBD Plasma for the Application of Sterilization - Measurement and Simulation of Hydrogen, Oxygen, and Hydrogen Peroxide Formation," *Int. J. Plasma Environ. Sci. Technol.,* pp. 96-101, 2007.

[7] Xia T, Kleinheksel A, Lee EM, Qiao Z, Wigginton KR, Clack HL., "Inactivation of airborne viruses using a packed bed non-thermal plasma reactor," *J Phys D-Appl Phys.,* p. 12, 2019.

[8] Y. Wu, Y. Liang, K. Wei, W. Li, M. Yao, J. Zhang, S.A. Grinshpun, "MS2 virus inactivation by atmospheric-pressure cold plasma using different gas carriers and power levels," *Appl. Environ. Microbiol.,* pp. 996-1002, 2015.

[9] Guo L, Xu R, Gou L, Liu Z, Zhao Y, Liu D, Zhang L, Chen H and Kong M G, "Mechanism of Virus Inactivation by Cold Atmospheric-Pressure Plasma and Plasma Activated Water," *Appl. Environ. Microbiol,* 84, 2018.

[10] N. Alshraiedeh, M. Alkawareek, S. Gorman, W. Graham, B. Gilmore, "Atmospheric pressure, nonthermal plasma inactivation of MS2 bacteriophage: effect of oxygen concentration on virucidal activity," *J Appl Microbiol,* pp. 1420-1426, 2013.

[11] G. Nayak, A. J. Andrews, I. Marabella, H. A. Aboubakr, S. M. Goyal, B. A. Olson, M. Torremorell, P. J. Bruggeman, "Rapid inactivation of airborne

porcine reproductive and respiratory syndrome virus using an atmospheric pressure air plasma," *Plasma Process and Polymers,* 17, 10, p. 1900269, 2020.

[12] Yan D, Sherman JH, Keidar M., "Cold atmospheric plasma, a novel promising anti-cancer treatment modality," *Oncotarget,* pp. 15977-15995, 2016.

[13] M. Laroussi, "Low-temperature plasmas for medicine?," *Plasma Science, IEEE Transactionson,* p. 714 – 725, 2009.

[14] Kimura, H., Lee, C., Hayashi, K., Yamauchi, K., Yamamoto, N., Tsuchiya, H., Tomita, K., Bouvet, M., and Hoffman, R. M., "UV light killing efficacy of fluorescent protein-expressing cancer cells in vitro and in vivo," *J. Cell Biochem.,* p. 1439 – 1446, 2010.

[15] Hannah Ritchie, Our World in Data, "How many people in the world die from cancer?," 2018. [Online]. Available: https://ourworldindata.org/how-many-people-in-the-world-die-from-cancer#licence. [Accessed 10 May 2020].

[16] Ministry of Health and Welfare in Taiwan, "107 年國人死因統計結果," 2019. [Online]. Available: https://www.mohw.gov.tw/cp-16-48057-1.html. [Accessed 24 April 2020].

[17] Riihimaki, M. et al., "Metastatic sites and survival in lung cancer," *Lung Cancer,* p. 78 – 84, 2014.

[18] Guan, X., "Cancer metastases: Challenges and opportunities," *Acta Pharm. Sin,* p. 402 – 418, 2015.

[19] Chiodoni C, Colombo MP, Sangaletti S, "Matricellular proteins: from homeostasis to inflammation, cancer, and metastasis," *Cancer Metastasis Rev,* p. 295 – 307, 2010.

[20] Siva, S., MacManus, M. P., Martin, R. F. & Martin, O. A, "Abscopal effects of radiation therapy: a clinical review for the radiobiologist," *Cancer Lett,* p. 82 – 90, 2015.

[21] Yuzbasioglu E, Sarac D, Canbaz S, Sarac YS, Cengiz S, "A survey of cross-infection control procedures: knowledge and attitudes of Turkish dentists," *J Appl Oral Sci,* p. 565 – 569, 2009.

[22] Khan HA, Baig FK, Mehboob R., "Nosocomial infections: Epidemiology, prevention, control and surveillance," *Asian Pac J Trop Biomed,* p. 478 – 482, 2017.

[23] AL-Aali KY, "Microbial Profile of Burn Wound Infections in Burn

Patients," 於 *Arch Clin Microbiol*, Taif, Saudi Arabia, 2016.

[24] Death number of Covid-19,, "Death number of Covid-19".

[25] G., Garber, "An overview of fungal infections," *Drugs,* p. 1 – 12, 2001.

[26] Ulger F, Esen S, Dilek A, Yanik K, Gunaydin M, Leblebicioglu H, "Are we aware how contaminated our mobile phones with nosocomial pathogens?," *Ann Clin Microbiol Antimicrob,* 2009.

[27] Scott GM, Thomson R, Malone-Lee J et al., "Cross-infection between animals and man: possible feline transmission of Staphylococcus aureus infection in humans?," *J Hosp Infect,* p. 29 – 34, 1988.

[28] A. S. Breathnach, "Nosocomial infections and infection control," *Medicine,* p. 649 – 653, 2013.

[29] C. Huang, Y. Wang, X. Li, L. Ren, J. Zhao, Y. Hu, L. Zhang, G. Fan, J. Xu, X. Gu, Z. Cheng, T. Yu, J. Xia, Y. Wei, W. Wu, X. Xie, W. Yin, H. Li, M. Liu, Y. Xiao, H. Gao, L., "Clinical features of patients infected with 2019 novel Coronavirus in Wuhan," *Lancet,* pp. 497-506, 2020.

[30] Juffermans NP, Prins DJ, Vlaar AP, Nieuwland R, Binnekade JM., "Transfusion-related risk of secondary bacterial infections in sepsis patients: a retrospective cohort study," *Shock,* pp. 355-359, 2011.

[31] J. Kovaleva, F.T.M. Peters, H.C. van der Mei, J.E. Degener, "Transmission of infection by flexible gastrointestinal endoscopy and bronchoscopy," *Clin. Microbiol Rev,* pp. 231-254, 2013.

[32] Wingender, J. & Flemming, H.-C., "Biofilms in drinking water and their role as reservoir for pathogens," *Int. J. Hyg. Environ. Health,* p. 417 – 423, 2011.

[33] Rabin BS, Cohen S, Ganguli R, Lysle DT, Cunnick JE, "Bidirectional interaction between the central nervous system and the immune system," *Crit Rev Immunol,* p. 279 – 312, 1989.

[34] H. Khan, A. Ahmad, R. Mehboob, "Nosocomial infections and their control strategies," *Asian Pac J Trop Biomed,* pp. 509-514, 2015.

[35] Chow, EJ, Mermel, LA, "Hospital-acquired respiratory viral infections: incidence, morbidity, and mortality in pediatric and adult patients," *Open Forum Infect Dis,* 2017.

[36] Perlroth J, Choi B, Spellberg B., "Nosocomial fungal infections: epidemiology, diagnosis, and treatment," *Med Mycol,* p. 321 – 346, 2007.

[37] Y.-C. Jang, C. Lee, O.-S. Yoon, H. Kim, "Medical waste management in

Korea, Journal of Environmental Management," pp. 107-115, 2006.

[38] C. Spry, "Understanding current steam sterilisation recommendations and guidelines," *AORN J,* pp. 537-550, 2008.

[39] TRANSCAT, "Steam Sterilizer Validation Services," [Online]. Available: https://www.transcat.com/calibration-services/validation/steam-sterilization-protocols-validation-services. [Accessed 19 May 2020].

[40] Dondelinger, R. M., Sterilizers, part I: Heat sterilization, 2008, pp. 459-462.

[41] Despatch, "Thermal processing technology," [Online]. Available: https://www.despatch.com/electronics.html. [Accessed 13 May 2020].

[42] GETINGE, "GEE Ethylene Oxide (EO) Sterilizers," [Online]. Available: https://www.getinge.com/me/product-catalog/gee-ethylene-oxide-eo-sterilizers/. [Accessed 15 May 2020].

[43] Chou, J. W., Skornicki, M., & Cohen, J. T., "Unintended consequences of the potential phase-out of gamma irradiation," p. 348, 2018.

[44] Y.C. Chien, H.H. Liu, Y.C. Lin, P.C. Su, L.H. Li, C.P. Chang, et al., "Ethylene oxide sterilization in the medical-supply manufacturing industry: assessment and control of worker exposure," *J Biomed Mater Res B Appl Biomater,* pp. 527-537, 2007.

[45] Shintani H., "Ethylene Oxide Gas Sterilization of Medical Devices," *Biocontrol Sci,* p. 1 – 16, 2017.

[46] STERIS, "Ethylene Oxide Sterilization Process," [Online]. Available: https://www.steris-ast.com/techtip/anatomy-ethylene-oxide-sterilization-process/. [Accessed 14 May 2020].

[47] STERIS, "VHP VICTORY™ Biodecontamination Unit," [Online]. Available: https://www.sterislifesciences.com/products/equipment/vhp-sterilization-and-biodecontamination/vhp-victory-biodecontamination-unit. [Accessed 15 May 2020].

[48] M. Vano, D.G. Barone, A. Genovesi, A.U. Covani, "Tooth bleaching with hydrogen peroxide and nano-hydroxyapatite: a 9-month follow-up randomized clinical trial," *International Journal of Dental Hygiene,* 2015.

[49] Andersen, BM, Rasch, M, Hochlin, K, Jensen, FH, Wismar, P, Fredriksen, JE. , "Decontamination of rooms, medical equipment and ambulances using an aerosol of hydrogen peroxide disinfectant," *J Hosp Infect,* p. 149 – 155, 2006.

[50] Health Care Purchasing News, "Keys to success with vaporized hydrogen peroxide sterilization," 2020. [Online]. Available:

https://www.hpnonline.com/continuing-education/article/21129765/keys-to-success-with-vaporized-hydrogen-peroxide-steril. [Accessed 15 May 2020].

[51] STERIS, "Hydrogen Peroxide Sterilization," [Online]. Available: https://www.steris.com/healthcare/knowledge-center/sterile-processing/hydrogen-peroxide-sterilization. [Accessed 15 May 2020].

[52] Reed, N.G., "The history of ultraviolet germicidal irradiation for air disinfection," *Public Health Rep.,* p. 15 – 27, 2010.

[53] Missouri S&T,, "Center for single nanoparticle, single cell, and single molecule monitoring, General instrumentation," [Online]. Available: https://cs3m.mst.edu/facilities/instrumentation/. [Accessed 13 May 2020].

[54] Chao-Yun Liu, Chao-Heng Tseng, Huang-Chin Wang, Chuan-Fa Dai, and Yi-Hsuan Shih, "The Study of an Ultraviolet Radiation Technique for Removal of the Indoor Air Volatile Organic Compounds and Bioaerosol," *Int J Environ Res Public Health,* p. 2557, 2019.

[55] American Cancer Society, "Ultraviolet (UV) Radiation," 2019. [Online]. Available: https://www.cancer.org/cancer/cancer-causes/radiation-exposure/uv-radiation.html. [Accessed 8 May 2019].

[56] R. Brandenburg, H. Lange, T. von Woedtke, M. Stieber, E. Kindel, J. Ehlbeck, K.D. Weltmann, "Antimicrobial effects of UV and VUV radiation of nonthermal plasma jets," *IEEE Trans. Plasma Sci.,* pp. 877-883, 2009.

[57] N. Munakata, M. Saito, and K. Hieda, "Inactivation action spectra of Bacillus subtilis spores in extended ultraviolet wavelengths (50-300 nm) obtained with synchrotron radiation," *Photochem. Photobiol,* 1991.

[58] K.A. Da Silva Aquino, "Sterilization by gamma irradiation," 2012. [Online].

[59] Silindir, M, Ozer, AY. , "Sterilization methods and the comparison of E-Beam sterilization with gamma radiation sterilization," *FABAD J Pharm Sci,* p. 43 – 53, 2009.

[60] E-BEAM, "Can e-beam really penetrate my product – I mean, isn't it just a surface treatment?, " 2014. [Online]. Available: https://ebeamservices.com/blog/can-e-beam-really-penetrate-product-mean-isnt-just-surface-treatment/. [Accessed 13 May 2020].

[61] bbsteriXpert, "Irradiation service," [Online]. Available: https://www.sterixpert.de/en/irradiation-service.html. [Accessed 19 May 2020].

[62] Centers for Disease Control and Prevention, "Other Sterilization Methods," 2010. [Online]. Available: https://www.cdc.gov/infectioncontrol/guidelines/disinfection/sterilization/othe. [Accessed 4 May 2020].

[63] C.F. Rediguieri, T. de Jesus Andreoli Pinto, N.A. Bou-Chacra, R. Galante, G.L. de Araujo, T. do Nascimento Pedrosa, S.S. Maria-Engler, P.A. De Bank, "Ozone gas as a benign sterilization treatment for PLGA nanofiber scaffolds," *Tissue Eng,* p. 22.

[64] Singh B, Sharma N, "Mechanistic implications of plastic degradation," *Polym Degrad Stab,* pp. 561-584., 2008.

[65] Saccucci M., Bruni E., Uccelletti D., Bregnocchi A., Sarto M. S., Bossù M., and Polimeni A., "Surface Disinfections: Present and Future," *Journal Of Nanomaterials,* pp. 1-9, 2018.

[66] Bregnocchi A, Zanni E, Uccelletti D. et al. , "Graphene-based dental adhesive with anti-biofilm activity," *J Nanobiotechnology,* p. 89, 2017.

[67] Wesgate, R., Grasha, P., and Maillard, J.-Y., "Use of a predictive protocol to measure the antimicrobial resistance risks associated with biocidal product usage," *Am. J. Infect. Control,* p. 458 – 464, 2016.

[68] E. Zanni, S. DePalma, C.R. Chandraiahgari, G. DeBellis, S. Cialfi, C. Talora, C. Palleschi, M.R. Sarto, D. Uccelletti, P. Mancini, "In vitro toxicity studies of zinc oxide nano- and micro rods on mammalian cells: a comparative analysis," *Mater. Lett.,* pp. 90-94, 2016.

[69] Nanogloss, "Advantages and Disadvantages of Nanotechnology," 2010. [Online]. Available: http://nanogloss.com/nanotechnology/advantages-and-disadvantages-of-nanotechnology/. [Accessed 4 May 2020].

[70] C. Buzea, I.I. Pacheco, K. Robbie, "Nanomaterials and nanoparticles: sources and toxicity.," *Biointerphases,* 2007.

[71] S. Sato, C. Shibata, M. Yazu, "Nonthermal killing effect of microwave irradiation," *Biotechnol. Tech.,* pp. 145-150, 1996.

[72] E.A. Oliveira, N.G. Nogueira, M.D. Innocentini, R. Pisani Jr., "Microwave inactivation of Bacillus atrophaeus spores in healthcare waste," *Waste Manag,* pp. 2327-2335, 2010.

[73] Zimmermann K., "Microwave as an emerging technology for the treatment of biohazardous waste: a mini-review," *Waste Manage Res,* p. 471 – 479, 2017.

[74] G. Sadler, W. Chappas, D.E. Pierce , "Evaluation of e-beam, gamma- and X-ray treatment on the chemistry and safety of polymers used with pre-packaged irradiated foods: a review," *Food Additives and Contaminants,* pp. 475-501, 2001.

[75] A. M. Hernandez and J. M. Boone, "Tungsten anode spectral model using interpolating cubic splines: Unfiltered x-ray spectra from 20 to 640 kV," *Med. Phys.,* p. 15, 2014.

[76] International Atomic Energy Agency, "Trends in Radiation Sterilization of Health Care Products," 2008. [Online].

[77] B.S.M. Mahmoud, S. Chang, Y. Wu, R. Nannapaneni, C.S. Sharma, R. Coker, "Effect of X-ray treatments on Salmonella enterica and spoilage bacteria on skin-on chicken breast fillets and shell eggs, Food Control," pp. 110-114, 2015.

[78] Ha TM, Yong D, Lee EM, Kumar P, Lee YK, Zhou W, et al., "Activation and inactivation of Bacillus pumilus spores by kiloelectron volt X-ray irradiation," *PLoS One,* 2017.

[79] Qiu, QQ, Sun, WQ, Connor, J., "Sterilization of biomaterials of synthetic and biological origin," *Comprehensive biomaterials,* p. 127 – 144.

[80] E.O. Morente, M.A. Fernandez-Fuentes, M.J.G. Burgos, H. Abriouel, R.P. Pulido, A. Galvez, , "Biocide tolerance in bacteria," *Int J Food Microbiol,* pp. 13-25, 2013.

[81] Sakudo, A., Yagyu, Y., Onodera, T., "Disinfection and sterilization using plasma technology: fundamentals and future perspectives for biological applications," *Int. J. Mol. Sci,* p. 5216, 2019.

[82] rotalab, "Low-Pressure Plasma Systems," [Online]. Available: http://www.rotalab.com/en/products/surface-treatment-systems/low-pressure-plasma-cleaner.html. [Accessed 20 May 2020].

[83] Al-rawaf A F, Fuliful F K, Khalaf M K and Oudah H K, "Studying the non-thermal plasma jet characteristics and application on bacterial decontamination," *J. Theor. Appl. Phys.* , p. 45 – 51, 2018.

[84] National Cancer Institute, "Symptoms of Cancer," 2019. [Online]. Available: https://www.cancer.gov/about-cancer/diagnosis-staging/symptoms. [Accessed 23 May 2020].

[85] National Cancer Institute, "NCI Dictionary of Cancer Terms," [Online]. Available: https://www.cancer.gov/publications/dictionaries/cancer-terms/def/tumor. [Accessed 24 May 2020].

[86] Verywellhealth, "Differences Between a Malignant and Benign Tumor," 2020. [Online]. Available: https://www.verywellhealth.com/what-does-malignant-and-benign-mean-514240. [Accessed 24 May 2020].

[87] A. Dellwo, "Lipomas and Fibromyalgia," verywellhealth, 24 8 2021. [Online]. Available: https://www.verywellhealth.com/lumps-bumps-fibromyalgia-lipomas-3972970. [Accessed 23 11 2021].

[88] IQWiG (Institute for Quality and Efficiency in Health Care), "How do cancer cells grow and spread?," 2019. [Online]. Available: https://www.ncbi.nlm.nih.gov/books/NBK279410/. [Accessed 24 May 2020].

[89] Verywellhealth, "Understanding "Liquid Tumors",," 2020. [Online]. Available: https://www.verywellhealth.com/understanding-the-liquid-tumors-514444. [Accessed 23 May 2020].

[90] Clinic, Cleveland, "What is Cancer?," [Online]. Available: https://my.clevelandclinic.org/departments/cancer/patient-education/wellness-prevention/what-is-cancer. [Accessed 23 May 2020].

[91] Frangioni, J. V., "New technologies for human cancer imaging," *J. Clin. Oncol.,* pp. 4012-4021, 2008.

[92] World Health Organization (WHO), "Cancer," 2018. [Online]. Available: https://www.who.int/news-room/fact-sheets/detail/cancer. [Accessed 24 May 2020].

[93] A.J. Cohen, "Outdoor air pollution and lung cancer," *Environ Health Perspect,* pp. 743-750, 2000.

[94] Hilakivi-Clarke, L., "Estrogens, BRCA1, and breast cancer," *Cancer Res,* pp. 4993-5001, 2000.

[95] M. Ghoussaini, P.D. Pharoah, D.F. Easton, " Inherited genetic susceptibility to breast cancer: the beginning of the end or the end of the beginning?," *Am J Pathol,* pp. 1038-1051, 2013.

[96] Boyle P, Leon ME, "Epidemiology of colorectal cancer," *Br Med Bull,* pp. 1-25, 2002.

[97] A. Chao, M. J. Thun, C. J. Connell, M. L. McCullough, E. J. Jacobs, W. D. Flanders, C. Rodriguez, R. Sinha, and E. E. Calle, "Meat consumption and risk of colorectal cancer".

[98] American Cancer Society, "Prostate Cancer Risk Factors," 2019. [Online]. Available: https://www.cancer.org/cancer/prostate-cancer/causes-risks-prevention/risk-factors.html.

[99] D.L. Narayanan, R.N. Saladi, J.L. Fox, "Ultraviolet radiation and skin cancer," *Int. J. Dermatol,* pp. 978-986, 2010.

[100] H. Brenner, et al., "Epidemiology of stomach cancer," *Methods Mol. Biol.,* pp. 467-477, 2009.

[101] World Health Organization, "Human papillomavirus (HPV) and cervical cancer," 2019. [Online]. Available: https://www.who.int/news-room/fact-sheets/detail/human-papillomavirus-(hpv)-and-cervical-cancer. [Accessed 4 June 2020].

[102] B., Bartosch, "Hepatitis B and C viruses and hepatocellular carcinoma," *Viruses,* p. 1504 – 1509, 2010.

[103] Łukasiewicz K, Fol M, "Microorganisms in the treatment of cancer: advantages and limitations," *J Immunol Res,* 2018.

[104] MAYO CLINIC, "Cancer surgery: Physically removing cancer," 2019. [Online]. Available: https://www.mayoclinic.org/diseases-conditions/cancer/in-depth/cancer-surgery/art-20044171. [Accessed 25 May 2020].

[105] National Cancer Institute, "Radiation Therapy to Treat Cancer," 2019. [Online]. Available: https://www.cancer.gov/about-cancer/treatment/types/radiation-therapy. [Accessed 25 May 2020].

[106] R. Baskar, K.A. Lee, R. Yeo, K.-W. Yeoh, "Cancer and radiation therapy: current advances and future directions," *Int. J. Med. Sci,* pp. 193-199, 2012.

[107] S. Kry, M. Salehpour, D.S. Followill, et al., "The calculated risk of fatal secondary malignancies from intensity-modulated radiation therapy," *Int J Radiat Oncol Biol Phys,* pp. 1195-1203, 2005.

[108] Center, Central Florida Cancer Care, "Gynecologic Cancers," [Online]. Available: https://www.cancercarecenter.md/gynecologic-cancers/. [Accessed 25 May 2020].

[109] EUROMEDICA, "Prostate Brachytherapy," [Online]. Available: http://kianous-stavros.gr/en/prostate-brachytherapy/. [Accessed 4 June 2020].

[110] J., Skowronek, "Current status of brachytherapy in cancer treatment – short overview," *J Contemp Brachytherapy,* p. 581 – 589, 2017.

[111] J., Burger, "Radioactive sources in brachytherapy," *Radiology and Oncology,* p. 127 – 13, 2013.

[112] National Cancer Institute, "Brachytherapy to Treat Cancer," 2019. [Online].

Available: https://www.cancer.gov/about-cancer/treatment/types/radiation-therapy/brachytherapy. [Accessed 4 June 2020].

[113] E.B. Holliday, S.J. Frank, "Proton radiation therapy for head and neck cancer: a review of the clinical experience to date," *Int. J. Radiat. Oncol. Biol. Phys,* pp. 292-302, 2014.

[114] Levin, W. P. et al., "Proton beam therapy," *Br. J. Cancer,* p. 849 – 854, 2005.

[115] B. Furlow, OncologyNurseAdvisor, "Cost vs Benefits: The Controversy Over Proton Beam Radiotherapy," 2018. [Online]. Available: https://www.oncologynurseadvisor.com/home/cancer-types/general-oncology/cost-vs-benefits-the-controversy-over-proton-beam-radiotherapy/. [Accessed 26 May 2020].

[116] American Cancer Society, "Treatment of Breast Cancer Stages I-III," 2019. [Online]. Available: https://www.cancer.org/cancer/breast-cancer/treatment/treatment-of-breast-cancer-by-stage/treatment-of-breast-cancer-stages-i-iii.html. [Accessed 27 May 2020].

[117] Cancer.Net, "Understanding Chemotherapy," 2019. [Online]. Available: https://www.cancer.net/navigating-cancer-care/how-cancer-treated/chemotherapy/understanding-chemotherapy. [Accessed 27 May 2020].

[118] American Cancer Society, "Treatment of Inflammatory Breast Cancer," 2019. [Online]. Available: https://www.cancer.org/cancer/breast-cancer/treatment/treatment-of-inflammatory-breast-cancer.html. [Accessed 27 May 2020].

[119] LUNGEVITY, "Chemotherapy," 2019. [Online]. Available: https://lungevity.org/for-patients-caregivers/lung-cancer-101/treatment-options/chemotherapy#2. [Accessed 3 June 2020].

[120] Cancer.Net, "Understanding Targeted Therapy," 2020. [Online]. Available: https://www.cancer.net/navigating-cancer-care/how-cancer-treated/personalized-and-targeted-therapies/understanding-targeted-therapy. [Accessed 27 May 2020].

[121] National Cancer Institute, "Targeted Therapy to Treat Cancer," 2020. [Online]. Available: https://www.cancer.gov/about-cancer/treatment/types/targeted-therapies. [Accessed 27 May 2020].

[122] National Cancer Institute, "Hormone Therapy to Treat Cancer," 2015.

[Online]. Available: https://www.cancer.gov/about-cancer/treatment/types/hormone-therapy. [Accessed 27 May 2020].

[123] National Cancer Institute, "Immunotherapy to Treat Cancer," 2019. [Online]. Available: https://www.cancer.gov/about-cancer/treatment/types/immunotherapy. [Accessed 30 May 2020].

[124] We, Ms Cher Boon Meng and Khor Ing, "Immune System Unplugged: Releasing Cancer's Grip on Immune Cells with Checkpoint Inhibitors," [Online]. Available: http://nusmedicine.nus.edu.sg/newsletter/issue21/science-of-life/cancer-immunotherapy. [Accessed 3 June 2020].

[125] National Cancer Institute, "Immunotherapy Side Effects," 2019. [Online]. Available: https://www.cancer.gov/about-cancer/treatment/types/immunotherapy/side-effects. [Accessed 31 May 2020].

[126] Yolanda Smith, "What is Intravesical Therapy?," 2018. [Online]. Available: https://www.news-medical.net/health/What-is-Intravesical-Therapy.aspx. [Accessed 1 June 2020].

[127] Osama Rahma, "What Types of Cancer Can Be Treated With Immunotherapy?," 2020. [Online]. Available: https://blog.dana-farber.org/insight/2020/04/what-types-of-cancer-can-be-treated-with-immunotherapy/. [Accessed 1 June 2020].

[128] Bolhassani A, Khavari A, Orafa Z, " "Electroporation-Advantages and Drawbacks for Delivery of Drug, Gene and Vaccine," in Application of Nanotechnology in Drug Delivery," *Application of Nanotechnology in Drug Delivery, InTech,* p. 369 – 398, 2014.

[129] Cadossi, R., " Locally enhanced chemotherapy by electroporation: Clinical experiences and perspective of use of electrochemotherapy," *Future Oncol,* pp. 877-890, 2014.

[130] Sersa G, Stabuc B, Cemazar M, Miklavcic D, Rudolf Z, "Electrochemotherapy with cisplatin: clinical experience in malignant melanoma patients," *Cancer Res,* p. 863 – 867, 2000.

[131] Quaglino P, Mortera C, Marenco F, " Electrochemotherapy in the treatment of cutaneous melanoma metastases: long-term follow-up results and response-," Madrid, 2010.

[132] Kenneth N. Aycock and Rafael V. Davalos, "Irreversible Electroporation: Background, Theory, and Review of Recent Developments in Clinical

Oncology," *Bioelectricity,* pp. 214-234, 2019.

[133] Al-Sakere B, André F, Bernat C, et al., "Tumor ablation with irreversible electroporation," *PLoS One,* 2007.

[134] Lee EW, Wong D, Tafti BA, et al., "Irreversible electroporation in eradication of rabbit VX2 liver tumor," *J Vasc Interv Radiol,* p. 833 – 840, 2012.

[135] Lopez-Alonso, B., A. Hernaez, H. Sarnago, A. Naval, A. Guemes, C. Junquera, J. M. Burdıo, T. Castiella, E. Monleon, J. Gracia-Llanes, F. Burdio, E. Mejıa, and O. Lucıa, "Histopathological and ultrastructural changes after electroporation in pig liver using parallel-plate electrodes and high-performance generator," *Sci. Rep.,* 2019.

[136] Walther W, Schlag PM., "Current status of gene therapy for cancer," *Curr Opin Oncol,* p. 659 – 664, 2013.

[137] Lu C, Stewart DJ, Lee JJ, et al, "Phase I clinical trial of systemically administered TUSC2(FUS1)- nanoparticles mediating functional gene transfer in humans," *PLoS One,* 2012.

[138] Senzer N, Nemunaitis J, Meninaitis D, et al., "Phase I study of a systemically delivered p53 nanoparticle in advanced solid tumors," *Mol Ther,* p. 1096 – 1103, 2013.

[139] EPFL, "New vectors for Gene Therapy," 2011. [Online]. Available: https://actu.epfl.ch/news/new-vectors-for-gene-therapy/. [Accessed 8 June 2020].

[140] Gopisankar, M. G., & Surendiran, A., "Oncolytic virotherapy – A novel strategy for cancer therapy," *Egyptian Journal of Medical Human Genetics,* p. 165 – 169, 2018.

[141] Russell SJ, Peng KW., "Oncolytic virotherapy: a contest between apples and," *Mol Ther,* pp. 1107-1116, 2017.

[142] Fridman G, Shereshevsky A, Jost MM, Brooks AD, "Electrode Dielectric Barrier Discharge Plasma in Air Promoting Apoptotic Behavior in Melanoma Skin Cancer Cell Lines," *Plasma Chemistry and Plasma Processing,* pp. 163-176, 2007.

[143] Lieberman, Michael A.; Lichtenberg, Allan J., Principles of plasma discharges and materials processing, 2nd 編者, Hoboken, N.J.: Wiley-Interscience, 2005, p. 546.

[144] E. Vitz, J. W. Moore, J. Shorb, X. Prat-Resina, T. Wendorff, & A. Hahn, "6.6: Ionization Energies," Libretexts, 22 July 2021. [Online]. Available:

https://chem.libretexts.org/Bookshelves/General_Chemistry/Book%3A_ChemPRIME_(Moore_et_al.)/06%3A_Chemical_Bonding_-_Electron_Pairs_and_Octets/6.06%3A_Ionization_Energies. [Accessed 17 Dec. 2021].

[145] A. Bogaerts, "The glow discharge: an exciting plasma!," *J. Anal. At. Spectrom.,* p. 1375 – 1384, 1999,.

[146] E.M. van Veldhuizen, W.R. Rutgers, "Corona discharges: fundamentals and diagnostics," *Proc. Frontiers in Low Temp. Plasma Diagn. IV,* pp. 40-49, March 2001..

[147] Ryu, J., Wakida, T., and Takagishi, T., "Effect of corona discharge on the surface of wool and its application to printing," *Textile Res. J.,* pp. 595-601, 1991.

[148] F. Pontiga, C. Soria, A. Castellanos, and J. Skalny, "A study of ozone generation by negative corona discharge through different plasma chemistry," *Ozone, Sci. Eng.,,* pp. 447-462, 2002.

[149] Vogtlin G.E., Penetrante B.M., Pulsed Corona Discharge for Removal of NOx from Flue Gas., S. S. Penetrante B.M., 編者, Berlin, Heidelberg: Springer, 1993.

[150] Kovalova, Z., Leroy, M., Kirkpatrick, M. J., Odic, E., and, "Corona discharges with water electrospray for Escherichia coli biofilm eradication on a surface.," *Bioelectrochemistry,* p. 91–99, 2016.

[151] V. I. Grinevich, E. Y. Kvitkova, N. A. Plastinina, and V. V. Rybkin, "Application of dielectric barrier discharge for waste water purification," *Plasma Chem. Plasma Process,* 31, 4, p. 573 – 583, 2011.

[152] X. Lu, M. Laroussi, V. Puech, "On atmospheric-pressure non-equilibrium plasma jets and plasma bullets," *Plasma Sources Sci. Technol.,* 2010.

[153] R. Wang, Y. Gao, C. Zhang, P. Yan, and T. Shao, "Dynamics of Plasma Bullets in a Microsecond-Pulse-Driven Atmospheric-Pressure He Plasma Jet," *IEEE Trans. Plasma Sci.,* pp. 393-397, 2016.

[154] J.P. Boeuf, L.L. Yang, L.C. Pitchford, "Dynamics of a guided streamer ('plasma bullet') in a helium jet in air at atmospheric pressure," *J. Phys. D: Appl. Phys.,* 2013.

[155] Raizer Y P, Gas Discharge Physics, Berlin: Springer, 1991.

[156] M. Dang Van Sung Mussard, O. Guaitella, and A. Rousseau, "Propagation of plasma bullets in helium within a dielectric capillary—influence of the interaction with surfaces," *J. Phys. D: Appl. Phys.,* 2013.

[157] S. V. Vladimirov and M. Y. Yu, "Solitary ionizing surface waves on low-temperature plasmas," *IEEE Trans. Plasma Sci.,* pp. 250-253, 1993.

[158] Zhengshi Chang , Ni Zhao, Guoqiang Li, and Guanjun Zhang, "Plasma "bullet" with hollow structure: formation and evolution," *Scientific Report,* 2018.

[159] L. W. Chen, P Zhao, X. S. Shu, J. Shen and Y. D. Meng, "On the mechanism of atmospheric pressure plasma plume," *Phys. Plasmas,* 2010.

[160] N. Mericam-Bourdet, M. Laroussi, A. Begum and E. Karakas, "Experimental investigations of plasma bullets," *J. Phys. D: Appl. Phys.,* 2009.

[161] S. Wu, H. Xu, X. Lu, Y. Pan, "Effect of pulse rising time of pulse DC voltage on atmospheric pressure non-equilibrium plasma," *Plasma Process. Polym.,* pp. 136-140, 2013.

[162] Rossi F, Kylián O and Hasiwa M, "Decontamination of surfaces by low pressure plasma discharges," *Plasma Process. Polym.,* pp. 431-42, 2006.

[163] A. Filipić, et al., "Cold atmospheric plasma as a novel method for inactivation of potato virus Y in water samples," *Food Environ. Virol.,* pp. 220-228, 2019.

[164] Cao Yingguang et al, "Efficacy of Atmospheric Pressure Plasma as an Antibacterial Agent Against Enterococcus Faecalis in vitro," *Plasma Sci. Technol.,* pp. 93-98, 2011.

[165] S. Choi, P. Puligundla, C. Mok, "Corona discharge plasma jet for inactivation of Escherichia coli O157:H7 and Listeria monocytogenes on inoculated pork and its impact on meat quality attributes," *Annals of Microbiology,* pp. 685-694, 2015.

[166] Sladek R E J, Stoffels E, Walraven R, Tielbeek P J A and Koolhoven R A, "Plasma treatment of dental cavities: a feasibility study," *IEEE Trans. Plasma Sci.,* 32, 4, pp. 1540-1543, 2004.

[167] H.I. Yong, H.-J. Kim, S. Park, K. Kim, W. Choe, S.J. Yoo, C. Jo, "Pathogen inactivation and quality changes in sliced cheddar cheese treated using flexible thin-layer dielectric barrier discharge plasma," *Food Research International,* pp. 57-63, 2015.

[168] Marchal F, Robert H, Merbahi N, Fontagne-Faucher C, Yousfi M, Romain C E, Eichwald O, Rondel C and Gabriel B, "Inactivation of Gram-positive biofilms by low-temperature plasma jet at atmospheric pressure," *J.*

Phys. D: Appl. Phys., 2012.

[169] Liang Y, Li Y, Sun K, Zhang Q, Li W, Zhu W, Zhang J, Fang J, "Plasma Thorns: Atmospheric Pressure Non-Thermal Plasma Source for Dentistry Applications," *Plasma Processes and Polymers,* p. 1069 – 1074, 2015.

[170] M. Vleugels, G. Shama, X.T. Deng, E. Greenacre, T. Brocklehurst, M.G. Kong, "Atmospheric plasma inactivation of biofilm-forming bacteria for food safety control," *IEEE Trans. Plasma Sci.,* pp. 824-828, 2005.

[171] K. Fricke, I. Koban, H. Tresp, L. Jablonowski, K. Schröder, A. Kramer, K.-D. Weltmann, T. von Woedtke, T. Kocher, "Atmospheric pressure plasma: a high-performance tool for the efficient removal of biofilms," *PLoS One,* p. e42539, 2012.

[172] I. Koban, R. Matthes, N.-O. Hübner, A. Welk, P. Meisel, B. Holtfreter, R. Sietmann, E. Kindel, K.-D. Weltmann, A. Kramer, T. Kocher, "Treatment of Candida albicans biofilms with low-temperature plasma induced by dielectric barrier discharge and atmospheric pressure plasma jet," *New J. Phys.,* p. 073039, 2010.

[173] Z.M. Xu, J. Shen, C. Cheng, S.H. Hu, Y. Lan, P.K. Chu, "In vitro antimicrobial effects and mechanism of atmospheric-pressure He/O2 plasma jet on Staphylococcus aureus biofilm," *J. Phys. D. Appl. Phys.,* p. 105201, 2017.

[174] B. Niemira, G. Boyd, J. Sites, "Cold plasma rapid decontamination of food contact surfaces contaminated with Salmonella biofilms," *J Food Sci,* pp. M917-M922, 2014.

[175] S.A. Ermolaeva et al, "Bactericidal effects of non-thermal argon plasma in vitro, in biofilms and in the animal model of infected wounds," *J. Med. Microbiol.,* pp. 75-83, 2011.

[176] S. Roth, J. Feichtinger, C. Hertel, "Characterization of Bacillus subtilis spore inactivation in low-pressure, low-temperature gas plasma sterilization processes," *J Appl Microbiol,* pp. 521-531, 2010.

[177] A. I. Al-Shamma'a, I. Pandithas and J. Lucas, "Low Pressure Microwave plasma UV lamp for water purification and ozone production," *IEEE,* 2001.

[178] S Lerouge, A.C Fozza, M.R Wertheimer, R Marchand, L'H Yahia, "Sterilization by low-pressure plasma: the role of vacuum-ultraviolet radiation," *Plasmas and Polymers,* pp. 31-46, 2000.

[179] N Hayashi, W Guan, S Tsutsui, T Tomari, Y Hanada, "Sterilization of

medical equipment using radicals produced by oxygen/water vapor RF plasma," *Jpn J Appl Phys,* pp. 8358-8363, 2006.

[180] A.H. Sari, F. Fadaee, "Effect of corona discharge on decontamination of Pseudomonas aeruginosa and E. coli," *Surf. Coat. Technol.,* pp. S385-S390, 2010.

[181] Z. Kovaľová, M. Leroy, M. J. Kirkpatrick, E. Odic, & Z. Machala, "Corona discharges with water electrospray for Escherichia coli biofilm eradication on a surface.," *Bioelectrochem.,* p. 91 – 99, 2016.

[182] V Scholtz, J Julák, V. Kříha, "Comparison of point-to-plane, point-to-point and cometary corona discharges for decontamination of surfaces," *Acta Technica,* pp. 395-399, 2010.

[183] Z. Kovalóvá, M. Zahoran, A. Zahoranová, Z. Machala, "Streptococci biofilm decontamination on teeth by low-temperature air plasma of dc corona discharges," *J Phys D Appl Phys,* p. 2014.

[184] K. Bujacek, V. Fantova, V. Kriha, "Decontamination effects of the corona discharge with plane to bent needle configuration," *Probl. At. Sci. Technol.,* pp. 187-189, 2012.

[185] Stocks, S. M., "Mechanism and use of the commercially available viability stain, BacLight," *Cytometry A,* 61, p. 189 – 195, 2004.

[186] Negri M Gonçalves V Silva S Henriques M Azeredo J Oliveira R, "Crystal violet staining to quantify Candida adhesion to epithelial cells," *Brit J Biomed Sci,* 67, p. 120 – 125, 2010.

[187] A. Gratia, "Numerical Relationships between Lysogenic Bacteria and Particles of Bacteriophage," *Ann Inst Pasteur,* 57, p. 652, 1936.

[188] Winey, M., Meehl, J. B., O'Toole, E. T. & Giddings, T. H. Jr., "Conventional transmission electron microscopy," *Mol. Biol. Cell,* 25, p. 319 – 323, 2014.

[189] Olson, M. E., H. Ceri, D. W. Morck, A. G. Buret, and R. R. Read, "Biofilm bacteria: formation and comparative susceptibility to antibiotics," *Can. J. Vet. Res.,* 66, pp. 86-92, 2002.

[190] O. Choi, C.Y. Yu, E. Fernández, Z. Hu, "Interactions of nanosilver with Escherichia coli cells in planktonic and biofilm cultures".*Water Res.*.

[191] M.O. Elasri, R.V. Miller, "Study of the response of a biofilm bacterial community to UV radiation," *Appl. Environ. Microbiol.,* 65, pp. 2025-2031, 1999.

[192] T.-F. Mah, B. Pitts, B. Pellock, G.C. Walker, P.S. Stewart, G.A. O'Toole, "A

genetic basis for Pseudomonas aeruginosa biofilm antibiotic resistance," *Nature,* 426, pp. 306-310, 2003.

[193] Xu Z, Cheng C, Shen J, Lan Y, Hu S, Han W, Chu PK, "In vitro antimicrobial effects and mechanisms of direct current air-liquid discharge plasma on planktonic Staphylococcus aureus and Escherichia coli in liquids," *Bioelectrochemistry,* 121, p. 125–134, 2018.

[194] Charles Patrick Davis, "DEFINITION OF DNA VIRUS," RxList, 29 March 2021. [Online]. Available: https://www.rxlist.com/dna_virus/definition.htm. [Accessed 3 January 2022].

[195] Poltronieri, P.; Sun, B.; Mallardo, M., "RNA Viruses: RNA Roles in Pathogenesis, Coreplication and Viral Load.," *Curr. Genomics,* 6, 5, p. 327– 335, 2015.

[196] Chaitanya, K. V., Structure and Organization of Virus Genomes,1, Springer, 2019, p. 1–30.

[197] A.M. Gall, B.J. Mariñas, Y. Lu, J.L. Shisler, "Waterborne viruses: a barrier to safe drinking water," *PLoS Pathog.,* p. e1004867, 2015.

[198] L.D. Simon, T.F. Anderson, "The infection of Escherichia coli by T2 and T4 bacteriophages as seen in the electron microscope. I. Attachment and penetration," *Virology,* 32, pp. 279-297, 1967.

[199] E.R. Donley, J.W. Loyd, "Hemorrhage control," *StatPearls. Treasure. Island,* 2020.

[200] M. Blaise, D. Pateron, J.C. Trinchet, S. Levacher, M. Beaugrand, J.L. Pourriat, "Systemic antibiotic therapy prevents bacterial infection in cirrhotic patients with gastrointestinal haemorrhage," *Hepatology,* 20, pp. 34-38, 1994.

[201] S.U. Kalghatgi, G. Fridman, M. Cooper, G. Nagaraj, M. Peddinghaus, M. Balasubramanian, V.N. Vasilets, A.F. Gutsol, A. Fridman, G. Friedman, "Mechanism of blood coagulation by nonthermal atmospheric pressure dielectric barrier discharge plasma," *IEEE Trans. Plasma Sci.,* 35, 5, pp. 1559-1566, 2007.

[202] G. Fridman, M. Peddinghaus, M. Balasubramanian, H. Ayan, A. Fridman, A. Gutsol, A. Brooks, "Blood coagulation and living tissue sterilization by floating-electrode dielectric barrier discharge in air," *Plasma Chem. Plasma Process.,* 26, 4, pp. 425-442, 2006.

[203] G. Fridman, G. Friedman, A. Gutsol, A.B. Shekhter, V.N. Vasilets, A. Fridman, "Applied Plasma Medicine," *Plasma Processes Polym.,* 5, 6,

pp. 503-533, 2008.

[204] H.W., I. Henins, J. Park, G.S. Selwyn, "Decontamination of chemical and biological warfare (CBW) agents using an atmospheric pressure plasma jet (APPJ)," *Phys. Plasmas,* 6, 5, pp. 2284-2291, 1999.

[205] Z. Machala, L. Chl á dekov á , M. Pelach, " Plasma agents in bio-decontamination by dc discharges in atmospheric air," *J. Phys. D: Appl. Phys.,* 43, p. 222001, 2010.

[206] Fathollah, S. et al., "Investigation on the effects of the atmospheric pressure plasma on wound healing in diabetic rats, *Sci Rep.,* 6, p. 19144, 2016.

[207] F. A. Misyn, V. A. Gostev, ' 'Cold' ' Plasma Application in Eyelid Phlegmon Curing'' in Diagnostics and treatment of infectious diseases, Petrozavodsk, Russia, 2000.

[208] R. Ranjan, P.V. Krishnamraju, T. Shankar, S. Gowd, "Nonthermal plasma in dentistry: An update," *Journal of International Society of Preventive and Community Dentistry,* 7, pp. 71-75, 2017.

[209] S. Rupf, A. Lehmann, M. Hannig, B. Schafer, A. Schubert, U. Feldmann, A. Schindler, " Killing of adherent oral microbes by a non-thermal atmospheric plasma jet," *J. Med. Microbiol.,* 59, pp. 206-212, 2010.

[210] Yan D, Sherman JH, Keidar M., "Cold atmospheric plasma, a novel promising anti-cancer treatment modality.," *Oncotarget,* 8, pp. 15977-15995, 2016.

[211] N. Barekzi, M. Laroussi, "Dose-dependent killing of leukemia cells by low-temperature plasma," *J. Phys. D: Appl. Phys.,* 2012.

[212] J. Teissie, M. Golzio, and M. P. Rols, "Mechanisms of cell membrane electropermeabilization: A minireview of our present (lack of ?) knowledge," *Biochimica et Biophysica Acta – General Subjects,* p. 270 – 280, 2005.

[213] Wang, J. & Yi, J., "Cancer cell killing via ROS: to increase or decrease, that is the question," *Cancer Biol. Ther.,* p. 1875 – 1884, 2008.

[214] Ishaq M, Evans MDM and Ostrikov K, "Atmospheric pressure gas plasma-induced colorectal cancer cell death is mediated by Nox2 – ASK1 apoptosis pathways and oxidative stress is mitigated by Srx – Nrf2 anti-oxidant system.," *Biochimica et Biophysica Acta (BBA) - Molecular Cell Research,* pp. 2827-2837, 2014.

[215] Duan, J., Lu, X. & He, G., "The selective effect of plasma activated

medium in an in vitro co-culture of liver cancer and normal cells," *J. Appl. Phys.,* 2017.

[216] Z. Chen, L. Lin, E. Gjika, X. Cheng, J. Canady, and M. Keidar, "Selective treatment of pancreatic cancer cells by plasma-activated saline solutions," *IEEE Trans. Radiat. Plasma Med. Sci.,* p. 116 – 120, 2018.

[217] Nakamura, K., Peng, Y., Utsumi, F., Tanaka, H., Mizuno, M., Toyokuni, M., Hori, M., Kikkawa, F., and Kajiyama, H. , " Novel intraperitoneal treatment with non-thermal plasma-activated medium inhibits metastatic potential of ovarian cancer cells.," *Sci. Rep.,* 2017.

[218] Kurake N, Tanaka H, Ishikawa K, Kondo T, Sekine M, Nakamura K, Kajiyama H, Kikkawa F, Mizuno M, Hori M., "Cell survival of glioblastoma grown in medium containing hydrogen peroxide and/or nitrite, or in plasma-activated medium," *Arch Biochem Biophys.,* p. 102 – 108, 2016.

[219] Papadopoulos MC and Saadoun S. , "Key roles of aquaporins in tumor biology," *Biochimica et Biophysica Acta (BBA)-Biomembranes,* pp. 2576-2583, 2015.

[220] Trachootham D, Alexandre J and Huang P., "Targeting cancer cells by ROS-mediated mechanisms: a radical therapeutic approach? Nature reviews Drug discovery," pp. 579-591, 2009.

[221] A.G. Lin, B. Xiang, D.J. Merlino, T.R. Baybutt, J. Sahu, A. Fridman, A.E. Snook, V. Miller, "Non-thermal plasma induces immunogenic cell death in vivo in murine CT26 colorectal tumors," *OncoImmunology,* 2018.

[222] Creative Proteomics, "Cell Proliferation Assay," [Online]. Available: https://www.creative-proteomics.com/cell/services/cell-proliferation-assay.htm. [Accessed 18 June 2020].

[223] Riss TL, Moravec RA, Niles AL, Duellman S, Benink HA, Worzella TJ, Minor L, Cell viability assays, Assay guidance manual., Bethesda: Sittampalam GS, Coussens NP, Brimacombe K et al. (eds), 2004.

[224] Ö.S. Aslantürk, "In Vitro Cytotoxicity and Cell Viability Assays: Principles, Advantages, and Disadvantages," *InTech,* 2018.

[225] Saikumar P, Dong Z, Mikhailov V, Denton M, Weinberg JM, Venkatachalam MA, "Apoptosis: definition, mechanisms, and relevance to disease," *Am J Med,* p. 489 – 506, 1999.

[226] Labclinics, "IDENTIFYING THE STAGES OF APOPTOSIS," 14 10 2015. [Online]. Available: https://www.labclinics.com/en/identifying-stages-apoptosis/. [Accessed 19 6 2019].

[227] H. Yamaguchi, J. Wyckoff, J. Condeelis, "Cell migration in tumors," *Curr. Opin. Cell Biol.,* pp. 559-564, 2005.

[228] Azzariti, A.; Iacobazzi, R.M.; Di Fonte, R.; Porcelli, L.; Gristina, R.; Favia, P.; Fracassi, F.; Trizio, I.; Silvestris, N.; Guida, G.; et al., "Plasma-Activated Medium Triggers Cell Death and the Presentation of Immune Activating Danger Signals in Melanoma and Pancreatic Cancer Cells," *Sci. Rep.,* 2019.

[229] Utsumi, F. et al. , "Variable susceptibility of ovarian cancer cells to non-thermal plasma-activated medium," *Oncol. Rep.,* p. 3169 – 3177, 2016.

[230] Sersenová et al, "Selective Apoptotic Effect of Plasma Activated Liquids on Human Cancer Cell Lines," *Molecules,* 26, 14, p. 4254, 2021.

[231] S. Takeda, S. Yamada, N. Hattori, K. Nakamura, H. Tanaka, H. Kajiyama, M. Kanda, D. Kobayashi, C. Tanaka, T. Fujii et al., " Intraperitoneal administration of plasma-activated medium: proposal of a novel treatment option for peritoneal metastasis from gastric cancer.," *Ann Surg Oncol.,* 2017.

[232] Freund, E. et al. , " Physical plasma-treated saline promotes an immunogenic phenotype in CT26 colon cancer cells in vitro and in vivo.," *Sci. Rep.,* p. 634 – 634, 2019.

[233] Liedtke, K.R.; Bekeschus, S.; Kaeding, A.; Hackbarth, C.; Kuehn, J.-P.; Heidecke, C.-D.; von Bernstorff, W.; von Woedtke, T.; Partecke, L.I., "Non-thermal plasma-treated solution demonstrates antitumor activity against pancreatic cancer cells in vitro and in vivo," *Sci. Rep. ,* 2017.

[234] Sato, Y. et al., "Effect of Plasma-Activated Lactated Ringer's Solution on Pancreatic Cancer Cells In Vitro and In Vivo," *Ann. Surg. Oncol.,* p. 299 – 307, 2018.

[235] S. B. Karki, E. Yildirim-Ayan, K. M. Eisenmann, and H. Ayan, "Miniature dielectric barrier discharge nonthermal plasma induces apoptosis in lung cancer cells and inhibits cell migration," *BioMed Research International,* 2017.

[236] Choi, J.-S.; Kim, J.; Hong, Y.-J.; Bae, W.-Y.; Choi, E.H.; Jeong, J.-W.; Park, H.-K. , "Evaluation of non-thermal plasma-induced anticancer effects on human colon cancer cells," *Biomed. Opt. Express,* p. 2649 – 2659, 2017.

[237] Kim JY, Kim S-O, Wei Y, Li J. , "A flexible cold microplasma jet using biocompatible dielectric tubes for cancer therapy.," *Applied Physics Letters.,* 2010.

[238] Z. Chen, L. Lin, Q. Zheng, J.H. Sherman, J. Canady, B. Trink, M. Keidar, "Micro-sized cold atmospheric plasma source for brain and breast cancer treatment," *Plasma Med.,* pp. 203-215, 2018.

[239] Vandamme M et al, "ROS implication in a new antitumor strategy based on non-thermal plasma," *Int. J. Cancer,* 2012.

[240] Binenbaum, Y. et al. , "Cold atmospheric plasma, created at the tip of an elongated flexible capillary uusing low electric current, can slow the progression of melanoma," *PLoS ONE,* 2017.

[241] F. Lin, G. Xu, J. Liu, H. Mu, X. Shi and Z. Guan-Jun,, "Characteristics of three-electrode plasma Jet and its influence on melanoma cells," 於 *12th International Conference on the Properties and Applications of Dielectric Materials (ICPADM)*, Xi'an, 2018.

[242] K. Mine, Y. Miyamaru, N. Hayashi, R. Aijima, and Y. Yamashita, "Mechanism of inactivation of oral cancer cells irradiated by active oxygen species from DBD plasma," *Plasma Med.,* p. 201 – 213, 2017.

[243] Weiss, M. et al., " Inhibition of Cell Growth of the Prostate Cancer Cell Model LNCaP by Cold Atmospheric Plasma.," *In vivo,* p. 611 – 616, 2015.

[244] M. Fofana, J. Buñay, F. Judée, S. Baron, S. Menecier, M. Nivoix, F. Perisse, A. Vacavant, X. Balandraud, "Selective treatments of prostate tumor cells with a cold atmospheric plasma jet," *Clinical Plasma Medicine,* 2020.

[245] Mirpour, S. et al., "Utilizing the micron sized non-thermal atmospheric pressure plasma inside the animal body for the tumor treatment application," *Scientific reports,* 2016.

[246] Karki, S.B.; Gupta, T.T.; Yildirim-Ayan, E.; Eisenmann, K.M.; Ayan, H., "Investigation of non-thermal plasma effects on lung cancer cells within 3D collagen matrices," *J. Phys. D Appl. Phys.* , 2017.

[247] Metelmann H-R et al., "Clinical experience with cold plasma in the treatment of locally advanced head and neck cancer," *Clin. Plasma Med.,* p. 6 – 13, 2018 .

[248] B. Dodet, E. Odic, A. Goldman, M. Goldman, and D. Renard, "Hydrogen peroxide formation by discharges in argon/water vapor mixtures at atmospheric pressure," *Journal of Advanced Oxidation Technologies,* 8, 1, p. 91 – 97, 2005.

[249] Z. Kovalová, "Bio-decontamination of biofilms on surfaces by cold plasma," Gif-sur-Yvette, 2016.

[250] Z. Kovalova, M. Leroy, C. Jacobs, M.J. Kirkpatrick, Z. Machala, F. Lopes, C.O. Laux, M.S. DuBow, E. Odic, "Atmospheric pressure argon surface discharges propagated in long tubes: physical," *Journal of Physics D: Applied Physics,* 48, 46, 2015.

[251] A. Sharma, D. Levko, and L. L. Raja, "Effect of oxygen impurities on atmospheric-pressure surface streamer discharge in argon for large gap arc breakdown," *Phys. Plasmas,* 23, 10, p. 103501, 2016.

[252] World Health Organization, "WHO Coronavirus (COVID-19) Dashboard," WHO, [Online]. Available: https://covid19.who.int/. [Accessed 20th Feb. 2022].

[253] Z. Chen, G. Garcia, V. Arumugaswami, and R. E. Wirz, "Cold atmospheric plasma for SARS-CoV-2 inactivation," *Phys. Fluids,* 32, p. 111702, 2020.

[254] H. Qin, H. Qiu, S. He, B. Hong, K.Liu, F. Lou, M. Li, P. Hu, X. Kong, Y. Song, Y. Liu, M. Pu, P. Han, M.e Li, X. An, L. Song, Y. Tong, H. Fan, R. Wang, "Efficient disinfection of SARS-CoV-2-like coronavirus, pseudotyped SARS-CoV-2 and other coronaviruses using cold plasma induces spike protein damage," *Journal of Hazardous Materials,* 430, p. 128414, 2022.

[255] Olson MR, Axler RP, Hicks RE, "Effects of freezing and storage temperature on MS2 viability," *J Virol Meth.* , 122, p. 147–152, 2004.

[256] S.P. Humphrey, R.T. Williamson, "A review of saliva: normal composition, flow, and function," *J. Prosthet. Dent.,* 85, pp. 162-169, 2001.

[257] G. Sethuraman, D. M. Jonathan, V. S. Subramanian, K. J. Vannathan, "Changes in salivary flow rate, pH, and viscosity among working men and women," *Dent. Med. Res.,* 7, 2, pp. 56-59, 2019.

[258] K. Takamura, H. Fischer, N.R. Morrow, "Physical properties of aqueous glycerol solutions," *J. Pet. Sci. Eng.,* 98, 99, pp. 50-60, 2012.

[259] Gratia A., "Numerical Relationships between Lysogenic Bacteria and Particles of Bacteriophage," *Ann Inst Pasteur,* 57, p. 652, 1936.

[260] J. Shen, Y. Tian, Y. Li, R. Ma, Q. Zhang, J. Zhang, et al., "Bactericidal effects against S. aureus and physicochemical properties of plasma activated water stored at different temperatures," *Scientific Reports,* 6, 2016.

[261] Odic E. et al, "Biological Applications of Atmospheric Pressure Dielectric Barrier Discharges," in *Proc. HAKONE 10 Conf.*, Saga, Japan , September 4-8 2006.

[262] Chun-Chieh Tseng & Chih-Shan Li, "Ozone for Inactivation of Aerosolized Bacteriophages, Aerosol Science and Technology," 40, 9, pp. 683-689, 2006.

[263] Pollard, E. C., Solosko, W., "The thermal inactivation of T4 and λ bacteriophages," *Biophys. J.,* 11, p. 66 – 74, 1971.

[264] Feng YY, Ong SL, Hu JY, Tan XL, Ng WJ, "Effects of pH and temperature on the survival of coliphages MS2 and Qbeta," *J Ind Microbiol Biotechnol,* 30, p. 549 – 552, 2003.

[265] K. Lin, C.R. Schulte, L.C. Marr, "Survival of MS2 and Φ6 viruses in droplets as a function of relative humidity, pH, and salt, protein, and surfactant concentrations," *PloS One,* 15, 12, 2020.

[266] Songer J. R., "Influence of relative humidity on the survival of some airborne viruses.," *Ecology,* 15, p. 35 – 42, 1967.

[267] A. Fedorenko, M. Grinberg, T. Orevi, N. Kashtan, "Survival of the enveloped bacteriophage Phi6 (a surrogate for SARS-CoV-2) in evaporated saliva microdroplets deposited on glass surfaces," *Sci. Rep.,* 10, p. 22419, 2020.

[268] J.W. Fluhr, R. Darlenski, C. Surber, "Glycerol and the skin: holistic approach to its origin and functions," *Br. J. Dermatol.,* 159, pp. 23-34, 2008.

[269] Kramar, A. D., Obradović, B. M., Schiehser, S., Potthast, A., Kuraica, M. M., & Kostić, M. M., "Enhanced Antimicrobial Activity of Atmospheric Pressure Plasma Treated and Aged Cotton Fibers," *Journal of Natural Fibers,* pp. 1-15, 2021.

[270] Rizzuto, A. M., Cheng, E. S., Lam, R. K., & Saykally, R. J., "Surprising effects of hydrochloric acid on the water evaporation coefficient observed by Raman thermometry.," *The Journal of Physical Chemistry C,* 121, 8, pp. 4420-4425, 2017.

[271] Gerba, C. P., & Betancourt, W. Q., "Viral aggregation: impact on virus behavior in the environment.," *Environmental science & technology,* 51, 13, pp. 7318-7325, 2017.

[272] .Domingo E, Sheldon J, Perales C, "Viral quasispecies evolution," *Microbiol Mol Biol Rev,* 76, 2, p. 159 – 216., 2012.

[273] Pourcel, C., Midoux, C., Vergnaud, G., and Latino, L. , "A carrier state is established in Pseudomonas aeruginosa by phage LeviOr01, a newly isolated ssRNA levivirus," *J. Gen. Virol.,* 98, p. 2181 – 2189, 2017.

[274] Yusupov, M. et al., “Plasma-Induced Destruction of Bacterial Cell Wall Components: A Reactive Molecular Dynamics Simulation.,” *The Journal of Physical Chemistry C,* 117, p. 5993 – 5998, 2013.

[275] 衛生福利部, “109 年國人死因統計結果,” Ministry of Health and Welfare in Taiwan, 19 August 2021. [Online]. Available: https://www.mohw.gov.tw/cp-5017-61533-1.html. [Accessed 17 November 2021].

[276] O. Fromigue, L. Lagneaux, J.J. Body, “Bisphosphonates Induce Breast Cancer Cell Death In Vitro,” *J. Bone Miner. Res.,* 15, pp. 2211-2221, 2000.

[277] Wang, M., Holmes, B., Cheng, X., Zhu, W., Keidar, M., & Zhang, L. G., “Cold atmospheric plasma for selectively ablating metastatic breast cancer cells,” *PloS one,* 8, 9, p. e73741, 2013.

Résumé

L'objectif de ces travaux était d'étudier l'interaction entre des plasmas froids à pression atmosphérique et des milieux biologiques en vue d'application de ce type de technologie au secteur biomédical.

Dans un premier temps, des sources plasma ont été conçues, réalisées et caractérisées. Il s'agissait de réacteurs mettant en œuvre des décharges sur barrière diélectrique (DBD) dans différents gaz en flux (air synthétique, argon, avec ou sans apport de vapeur d'eau). L'utilisation de l'argon a permis de sélectionner des conditions dans lesquelles le plasma demeurait confiné dans la zone inter-électrodes (humidité relative supérieure à 95% à température ambiante) ou au contraire se propageait soit en atmosphère libre, soit guidé dans un tube isolant dans lequel circulait le gaz (argon sec). Dans ce dernier cas, deux dispositifs ont été étudiés, tous deux permettant d'imposer un champ électrique intense aux bornes d'un volume gazeux en circulation dans un tube au moyen d'un jeu de deux électrodes : (a) annulaires disposées sur la face externe du tube pour le « two-ring system » (TR), (b) annulaire sur la face externe du tube associée à une tige centrée à l'intérieur du tube pour le « rod (cylinder) system » (RS).

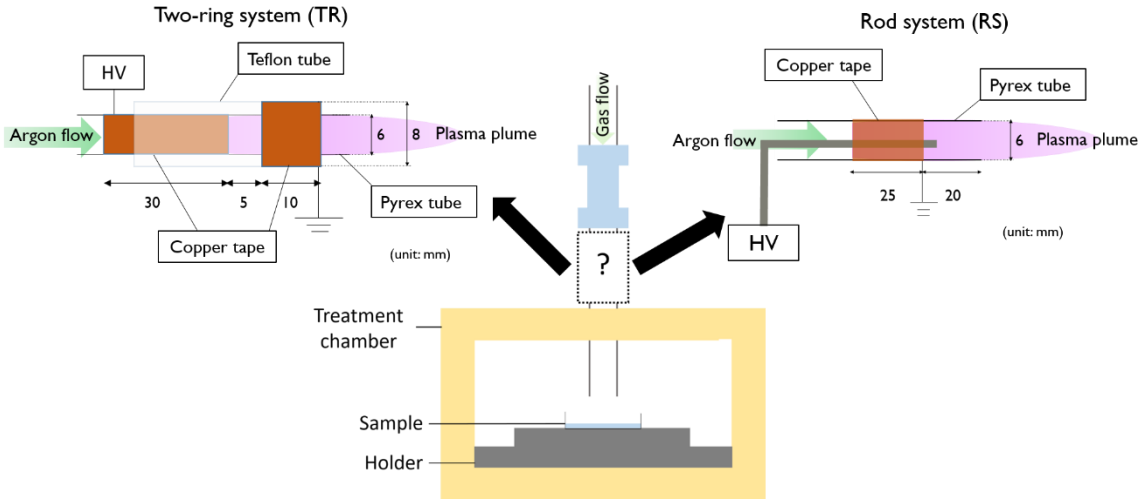

Figure 1 Configurations du « two-ring system » (a) à gauche et du« rod (cylinder) system » (b) à droite.

Les deux dispositifs destinés à produire une plume plasma ont été caractérisés en termes de tension-seuil d'amorçage de décharge, de tension-seuil de propagation du plasma hors de l'espace inter-électrodes, de puissance moyenne dissipée dans le plasma, et de production de peroxyde d'hydrogène. De plus, la propagation du plasma dans un tube fin isolant (silicone) dans lequel un débit d'argon sec était imposé a été étudiée. Dans le cas du dispositif RS, le plasma a pu être propagé sur une distance de 90 cm sous un débit d'argon inférieur à 1 L/min. Une propagation maximale bien inférieure (30 cm) a été observée pour le dispositif TR, avec une forte dépendance avec le débit d'argon. Dans ce dernier cas, le phénomène de propagation dans un tube de quartz (Figure 2) a été examiné par des mesures électriques synchronisées et résolues

dans le temps : mesure de la tension appliquée (V), mesures de courant au niveau de l'anneau connecté à la source haute tension (A_1), au niveau de l'anneau connecté à la terre (A_2), et enfin au niveau d'un conducteur disposé en sortie de tube et connecté à la terre (A_3).

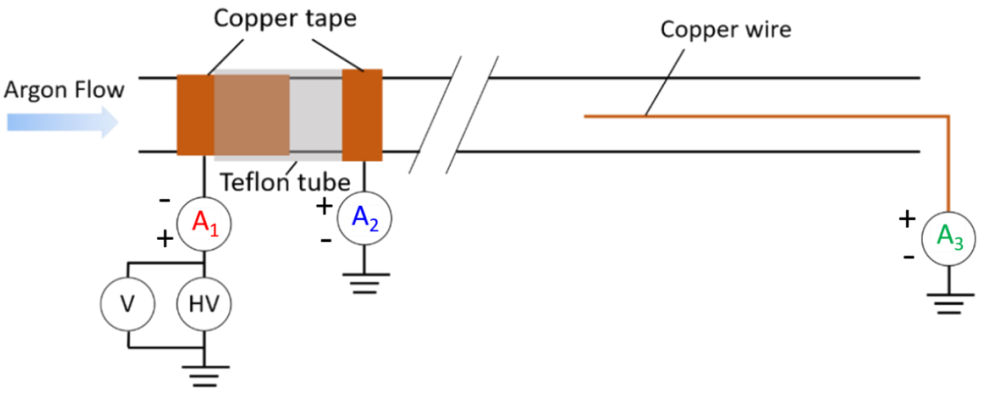

Figure 2 Dispositif « two-ring system » (TR) dédié à l'étude de la propagation du plasma dans un tube de quartz par analyse des signaux électriques.

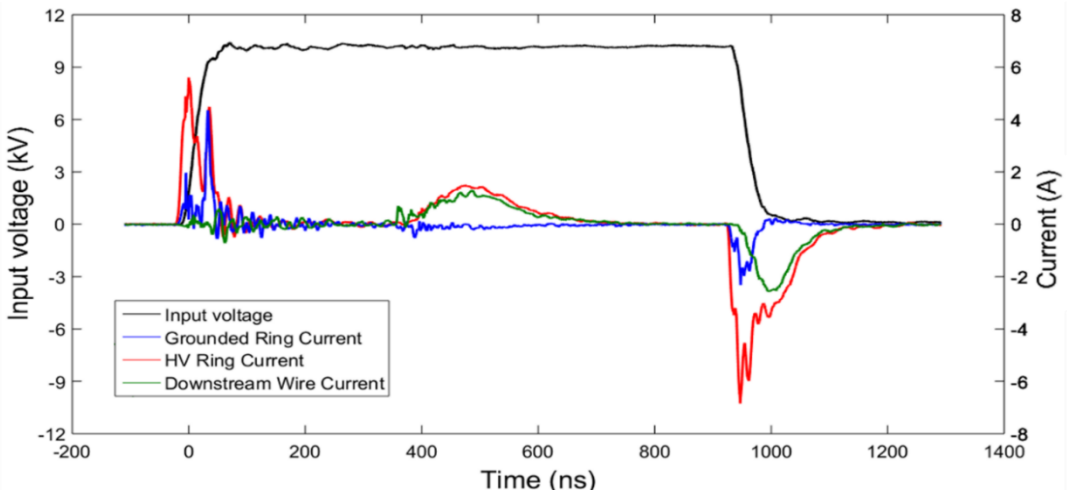

Figure 3 Formes d'onde de tension appliquée et de courant lors de la propagation du plasma.

Un exemple est donné en (Figure 3). Un pic de courant capacitif (5,5 A) est clairement observable (t~0 s) sur le front montant de tension. Ce pic est suivi par une impulsion de courant (4,5 A à t~50 ns) associée à l'amorçage de la décharge dans le volume gazeux délimité par les électrodes annulaires. La décharge se propage sur les parois internes du tube isolant pour atteindre le conducteur disposé en sortie de tube. Cet événement, signalé par une impulsion de courant de 800 mA à t~375 ns, est immédiatement suivi par un signal de courant beaucoup plus lent et ample (1,5 A), pouvant être associé un phénomène de relaxation des charges stockées en surface de l'isolant lors de la phase de propagation du plasma. Enfin, la chute de tension est accompagnée par un courant capacitif négatif et par l'amorçage d'une décharge résultant du champ électrique intense apparaissant dans l'espace inter-électrodes à

l'annulation rapide de la tension alors que le diélectrique est chargé. Il conviendra par la suite de réaliser des mesures optiques rapides afin de confirmer ces interprétations. Ces mesures ont également permis d'estimer par le calcul (i) la vitesse de propagation du front d'ionisation (2-6·10^5 m/s) – confirmant ainsi un mécanisme de « streamer », (ii) la conductivité du plasma (~ 150 $(\Omega \cdot m)^{-1}$) - cohérente avec les résultats issus de la littérature.

Deux études spécifiques ont alors été conduites, l'une susceptible de trouver des applications dans le domaine de la « plasma médecine », l'autre dans le domaine de la lutte contre les épidémies virales. Dans ce dernier cas, les travaux ont porté sur l'inactivation de virus bactériens, ou bactériophages, infectant *Escherichia coli*. Il s'agissait du phage T4, phage à ADN double brin, et du phage MS2, phage à ARN simple brin.

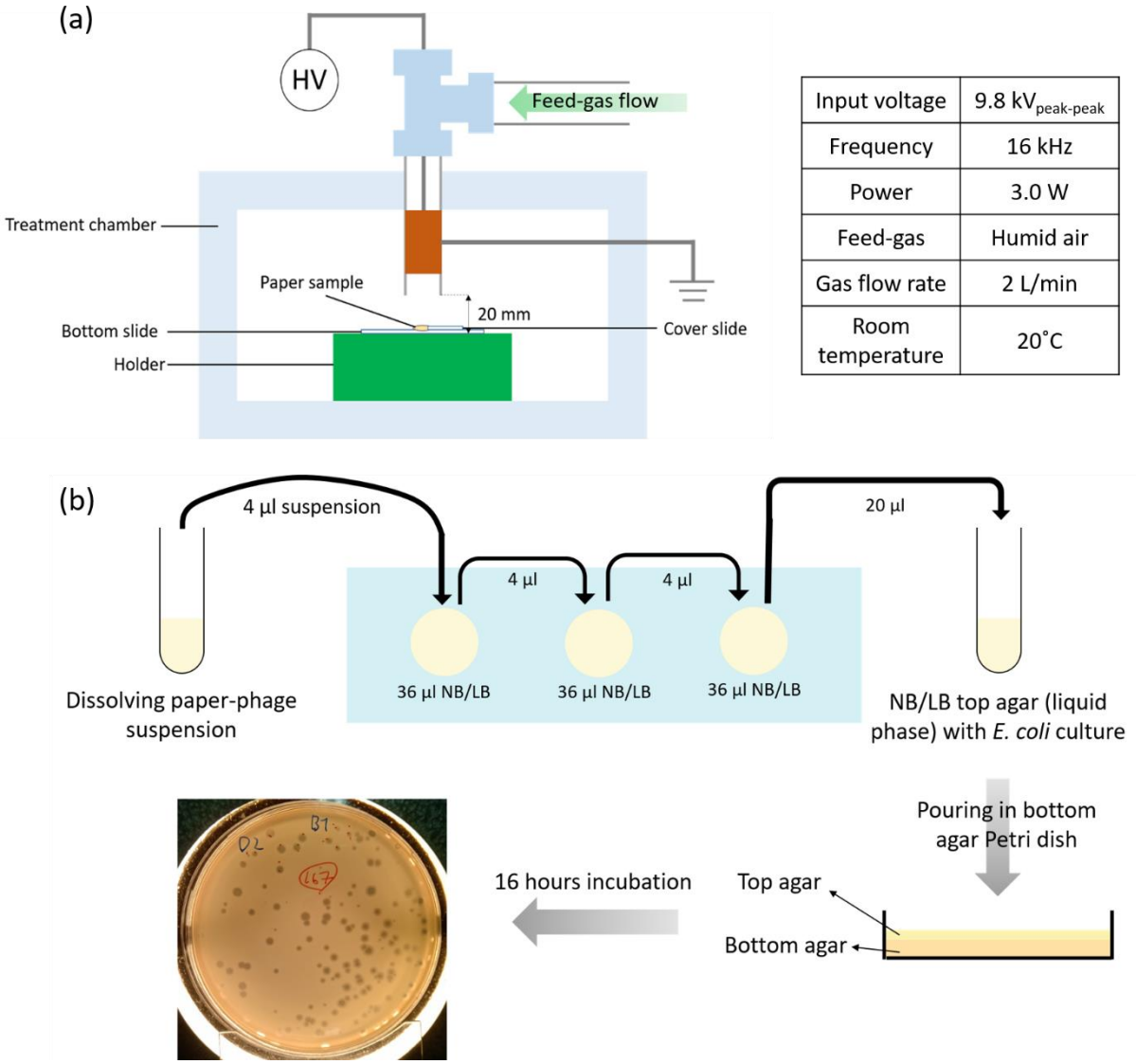

Input voltage	9.8 $kV_{peak-peak}$
Frequency	16 kHz
Power	3.0 W
Feed-gas	Humid air
Gas flow rate	2 L/min
Room temperature	20°C

Figure 4 (a) Dispositif de traitement de surface contaminée par des bactériophages avec paramètres expérimentaux pour l'utilisation de l'air humide comme gaz plasmagène, (b) protocole d'essai sur plaque mettant en œuvre la méthode de Gratia.

Les suspensions de phages ont été diluées dans différentes solutions tampons et déposées sur un substrat de papier hydrosoluble pour être exposées aux différents traitements par plasma froid avec le dispositif RS. L'utilisation originale de ce substrat a permis de résoudre le problème difficile de la récupération des particules de phage après traitement. Ce substrat correspond également à une situation d'application défavorable à ce type de traitement (surface complexe avec diffusion en volume de la suspension, au contraire d'une surface lisse non absorbante telle qu'une lamelle de verre), conduisant à obtenir des résultats plus réalistes et transposables à une application réelle. De plus, du glycérol a été ajouté (10% Vol.) à la solution tampon de suspension pour obtenir une viscosité comparable à celle de la salive. L'inactivation des phages a été quantifiée par comptage de plages de lyse sur culture d'*Escherichia coli* (Figure 4). Ainsi, des taux d'inactivation compris entre 0,7 log/min et 2 log/min ont été mesurés suivant le type de phage, la nature de la solution tampon et le type de gaz plasmagène (Figure 5). Le choix de l'air comme gaz plasmagène a également été considéré en raison des contraintes d'application ne permettant pas systématiquement l'utilisation d'un autre gaz. L'influence de la température imposée au substrat a également été examinée. Ces résultats montrent que l'inactivation de virus (ici un modèle de virus bactérien) sur surface complexe par procédé plasma froid est efficace et que la transposition vers des applications est réaliste. D'un point de vue mécanistique, il a été montré que le phage T4 était très sensible aux changements d'humidité. Il est par ailleurs suggéré que les réactions conduisant à l'inactivation des bactériophages doivent avoir lieu en phase aqueuse, et que par conséquent, le séchage du substrat constitue facteur défavorable au procédé, en particulier pour MS2. Enfin, la rupture de la capside de MS2 après traitement par plasma froid a été mise en évidence par microscopie électronique à transmission.

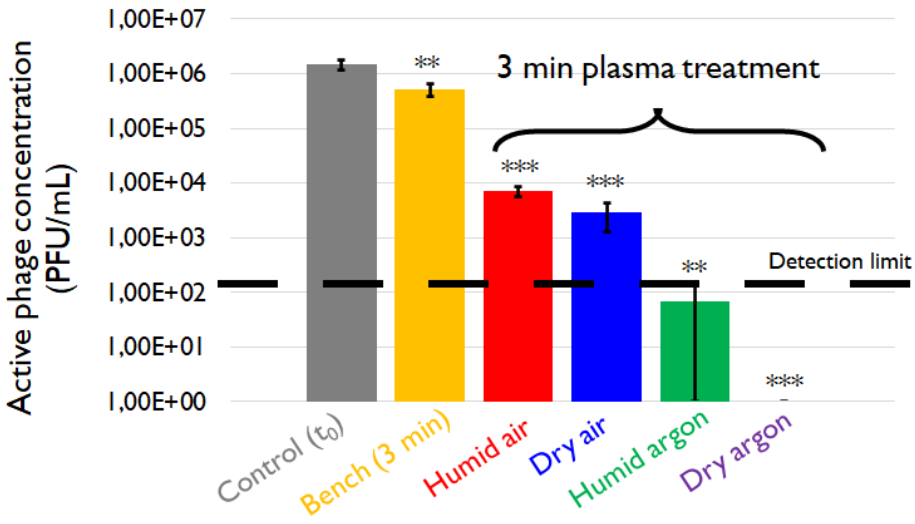

Figure 5 Inactivation du bactériophage MS2 soumis sur papier absorbant à une exposition de 3 minutes au traitement plasma (P=3 W ; Q=2 L/min) pour 4 gaz plasmagènes différents : air sec ou humide, argon sec ou humide. Tets de Student : 0,01** et 0,001***.

Dans le cadre de l'application en plasma médecine, des cellules d'adénocarcinome humain (cancer du poumon) provenant de cinq patients ont été traitées *in-vitro* à l'aide du dispositif RS dans deux conditions de fonctionnement déterminées par la composition du gaz d'alimentation : jet de plasma avec de l'argon sec et source d'espèces oxydantes avec de l'argon saturé en vapeur d'eau à température ambiante.

A l'issue d'une exposition de 5 minutes au traitement par décharge d'argon humide, 65% des cellules étaient dans un état apoptotique/nécrotique. Pour le traitement par plasma d'argon sec, les tests globaux de prolifération et d'apoptose n'ont pas montré une grande efficacité.

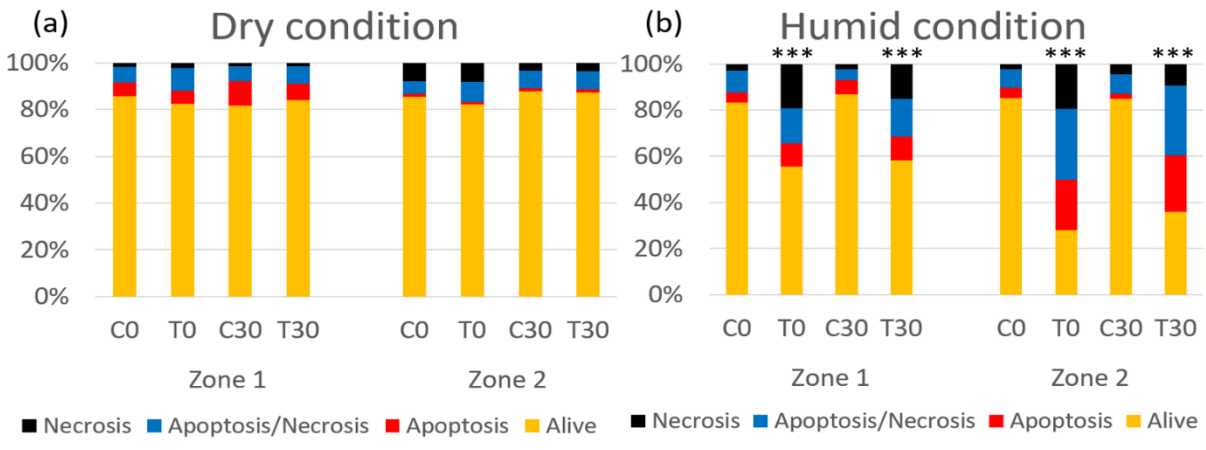

Figure 6 Test d'apoptose après traitement au plasma d'argon (a) sec ou (b) humide (C0 : échantillon témoin prélevé immédiatement, C30 : échantillon témoin prélevé avec après un délai de 30 minutes, T0 : échantillon traité prélevé immédiatement, T30 : échantillon traité prélevé après un délai de 30 min) (Zone 1 : emplacement traité, Zone 2 : emplacement situé à 4 cm de la Zone 1)

Toutefois, le jet de plasma d'argon sec a présenté un effet rapide et localisé sur les cellules cancéreuses, induisant une inhibition de la capacité des cellules à proliférer et à migrer.

Ces deux conditions de fonctionnement sont d'intérêt pour l'application clinique, permettant d'avoir un seul dispositif plasma capable de délivrer un traitement très localisé des cellules (jet plasma) ou de transférer des espèces oxydantes sur une plus grande surface conduisant à des mécanismes d'apoptose (décharge d'argon humide).

Mots-clés : plasma froid, décharge sur barrière diélectrique, plasma médecine, cellules cancéreuses, décontamination de surface, bactériophage